UNIVERSITAT DE BARCELONA

The motion sensing problema in spherical gravitational wave detectors

Mª Ángeles Serrano Moral

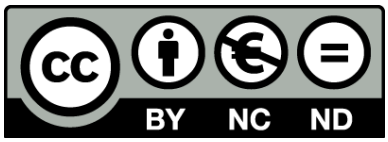

Universitat de Barcelona
Departament de Física Fonamental
Facultat de Física

The Motion Sensing Problem in Spherical Gravitational Wave Detectors

Mª Angeles Serrano Moral

Programa de doctorado: *Métodos Estadísticos de la Física*

Bienio 1994–1996

Memoria presentada per Mª Angeles Serrano Moral para optar al título de Doctora en Ciencias Físicas.

Certifico que la presente tesis doctoral ha sido realizada bajo mi dirección.
Barcelona, Abril de 1999.

José Alberto Lobo Gutiérrez
Profesor Titular
Departament de Física Fonamental
Universitat de Barcelona

A la Suerte y a la Casualidad, y también a la Ironía
que a veces las acompaña.

Agradecimientos

Quiero hacer constar mi agradecimiento a todas las personas que de forma directa o indirecta han estado relacionadas con este trabajo:

Gracias justas al profesor José Albeto Lobo por la dirección de esta tesis, su colaboración y sus sugerencias. Su voluntad ha sido clave en la consecución de la beca FPI que disfruto, la cuál además exige mi gratitud para el MEC.

Gracias cordiales a Stephen Merkowitz por dos colaboraciones puntuales: la facilitacion de los datos de la antena prototipo TIGA en la Tabla 5.6 del Capítulo 5 y el intercambio de ideas y trabajo en común con respecto al tema de deconvolución de señales ruidosas en el Capítulo 6.

Gracias rigurosamente atentas a todos los miembros del tribunal por su interés y su tiempo.

Mil gracias a mis colegas de Materia Condensada y Física Teórica, y extensivamente al resto del Departamento, por su disposición siempre que los he requerido para resolver cualquier asunto científico y técnico.

Doblemente a mis colegas-amigos. Los motivos de mi gratitud son tantos y tan intrincados que podría incluir aquí otra tesis, seguramente mucho más divertida que ésta.

Muchísimas gracias a mis amigos-amigos, alimentadores del ánimo, viajeros y fluctuantes.

Gracias naranjas y lilas sentidas desde el no pensamiento a la trayectoria especular largo tiempo paralela, por su constancia en acabar complicándome la vida y sobretodo por mostrarme cómo es de ridícula nuestra capacidad actual de predicción.

Gracias merecidísimas hasta categoría de deuda a mi familia tan incondicional.

Gracias últimas a los que haya podido haber olvidado.

Summary

Chapter 1

PRELIMINARIES

1.1 Historical Introduction

1.1.1 Confirming Einstein's General Relativity

Half a century before Albert Einstein arrived to his geometric account of gravity, Georg Friedrich Bernhard Riemann had already marked the way to a new conception of space. Riemann [115], who generalized the concepts of his master Carl Friedrich Gauss, not only realized that space, telling mass how to move, could itself –by the newtonian principle of action and reaction– be curved by mass becoming not a mere spectator but a participant in the world of physics, but also achieved a great mathematical description for this space curvature. Later on, the indissoluble character of space and time was revealed by the Special Relativity of Einstein which also restored the physical equivalence between all of the inertial frames. Einstein fruitlessly attempted at first to formulate a field law for gravitation consistent with the spacetime structure given by this theory. However, the Equivalence Principle, and in a much less precise sense Ernst Mach's principle [89], made him suspect that a new theory was unavoidable and necessary for a correct description of space and gravitation, a theory which extended the principle of relativity to the non inertial coordinate systems and where the structure of spacetime, and not just space, was influenced by the presence of matter.

This theory was formulated on the mathematical basis of the absolute differential calculus of Ricci and Levi-Cività and was called Einstein's General Relativity [43, 44]. It is based on a central idea: gravity is a manifestation of the curvature of spacetime, which basically arises from the fundamental principle in any metric theory: the Principle of

Equivalence of Gravitation and Inertia, which rests on the equality of gravitational and inertial mass to tell us how an arbitrary physical system responds to an external gravitational field. It states that the intrinsic, observer-independent, properties of spacetime are given as functions of a spacetime metric $g_{\mu\nu}$ which need not have the flat form $\eta_{\mu\nu}$ it has in Special Relativity. Indeed, its curvature accounts for the gravitational effects usually ascribed to a gravitational field, locally equivalent to an accelerated reference system. What distinguishes one metric theory from other metric theories of gravity is its particular field equations, which are necessary to determine the gravitational fields themselves. In General Relativity, Einstein postulated them by way of relating the curvature of spacetime to the stress-energy-momentum tensor of the matter $T_{\mu\nu}$ in that very spacetime.

Since its publication in 1916, impressive confirmations of the foundations of Einstein's theory and also of some of its new predictions and implications have been obtained. From the beginning, the well-known three classical tests, proposed by Einstein himself in 1916, –explanation of the anomalies in the motion of the perihelion of Mercury, prediction of bending of light rays confirmed by Eddington [38, 107], and the partially proved effect of red shift of spectral lines [107]– soon conformed a successful basis for General Relativity. However, experimental gravitation lay nearly dormant during a number of years, as much as the theory itself, partly because, although being considered as a beautiful theory leading to even revolutionary implications in particular areas such as Cosmology, its potential relevance to the rest of physics had not been universally acknowledged, partly because Einstein's and Newton's theories led to the same predictions when dealing with weak gravitational fields as in the case of laboratory experimental conditions.

Nevertheless, strong interest began to be revived in the late 1950s, particularly by the Princeton group led by John Wheeler and the London group led by Herman Bondi. Two discoveries greatly contributed to the sustained interest which has continued since then. The first refers to the astronomical discoveries of the existence of a cosmic microwave background radiation and of highly energetic compact objects involving strong gravitational fields, i.e., quasars and compact X-ray sources. The second is the realization that a quantum theory of gravitation will help to further understanding laws of nature. Even aside from this potential impact on other branches of physics, the theory of General Relativity on its own also attracted more attention and this renewed interest, along with the development of great technical advances, led to more accurate versions of the older

astronomical tests as well as observations of previously inaccessible effects[1], from which Einstein's General Relativity stands as the classical theory of gravitation.

So, the third effect predicted by Einstein was neatly verified by Pound and Rebka [112] in the sixties and soon other experiments concerning the foundations of the theory were also performed and repeated again. In particular, important features of Einstein theory that are consequences or parts of the Equivalence Principle in its various forms -from the uniqueness of free fall for test particles, or Galilei equivalence principle, to the very strong form- have been tested, among them the gravitational time dilation or gravitational redshift, the constancy in time and space of constants as the gravitational constant G, the local Lorentz invariance of physical laws in the freely falling frames or the equal contribution of the gravitational binding energy to the inertial mass of celestial bodies in agreement with the very strong form. It is also worth noting that there exists experimental support for another basic assumption of GR. For instance, space curvature is supported by the confirmation of the de Sitter effect (or geodesic precession), or by solar system measurements of the deflection of photons and of the Shapiro time delay in the propagation of radio waves travelling near the sun. And certain other effects which confirm more than one single aspect of General Relativity have also been observed. Thus, experimetal verifications of the equations of motion and of the solution of the Einstein field equation are obtained from the outcomes of studies dealing with the pericentre advance of a test body, the dynamics of planets, spacecraft or even the moon motion, or observations of some astrophysical binary systems such as the paradigmatic case of the binary pulsar PSR $1913+16$, which deserves special attention since it also stands as the observational test confirming the existence of another fundamental prediction of General Relativity: Gravitational Waves.

1.1.2 An Early Prediction: Gravitational Waves

Gravitational Waves were one of the new physical phenomena not ensuing from newtonian gravitation but naturally predicted by Einstein's General Relativity, and also by any metric theory of gravity [135, 66, 67, 54]. As Einstein soon indicated, the gravitational field became a dynamical entity making possible curvature perturbations propagating in spacetime with a finite speed, analogously to what happens when one goes from Coulomb's electrostatics to Maxwell's theory of electromagnetism. He showed [41, 42] that his equations for the gravitational field admitted in the linear approximation radia-

[1] See [28, 120, 142] for further references.

tive solutions that represented plane GWs and that divided into *real waves*, which carry energy, and *apparent waves*, which do not and can be eliminated by a coordinate transformation. Eddington [40] first gave an invariant criterion valid in any coordinate system to distinguish *real* from *apparent waves*. Like electromagnetic waves, in GR gravitational waves are transverse plane waves with two states of polarization propagating in vacuum with the velocity of light.

In his paper on linearized gravitation theory, Einstein also investigated the generation of GW by the sources of the field, being able to compute the power radiated by non-self-gravitating masses by the derivation in this case of the quadrupole moment formula relating the intensity of the radiation field to the second time derivative of the quadrupole moment of the stress-energy tensor of the sources. However, in most astrophysical applications, such as gravitationally bound binary star systems, it is just the self-gravitational field that is crucial. Consequently, during the 1940s and the 1950s there was considerable controversy over the applicability of the quadrupole formula and indeed over whether self-gravitating systems emit gravitational radiation at all. Thus, for may years the subject became exclusively a matter of theoretical discussion focussed on the attempt to extend the quadrupole formula to self-gravitating systems, which was acquired by the notably methods of Landau-Lifshitz in 1941 [77] and Fock in 1955 [46], later further developed and improved in response to criticisms. Despite these advances, it was not until the work by Bondi in 1957 [12] that Gravitational Waves were generally accepted as a potentially measurable physical phenomenon implying energy transport, instead of the mere coordinate effect suggested by other authors (Infeld in [65]).

Testing GW

It was J. Weber who pioneered the work of measuring GW in the 1960s. His method was based on the fact that free particles moving through a gravitational field experience relative accelerations as expressed by the equation of geodesic deviation. If the particles are not free to move but are connected by a rigid solid piece of material, the gravitational tidal forces will stress it whence the whole system will be set into oscillation. Weber's technique [136, 137] consisted in measuring these deformations in large aluminium cylinders at room temperature, presumably triggered up by incident gravitational radiation impulses. After working with a single detector during the period 1963-1968, Weber built a second cylinder at the Argonne National Laboratory of Chicago to undertake coordinate experiments between the opposite ends of a 1000 Km baseline, searching for coincidences

in their outputs within the maximum delay in respective times of arrival of the events.

Indeed, strong gravitational waves cannot be produced on Earth, so he had to look for the events producing them in the sky. His work was soon backed up by the discovery in the same decade of a wealth of new astrophysical objects such as quasars, pulsars and binary X-ray sources [110]. It was then possible to conceive highly relativistic events such as pulsating, accreating or colliding black holes, collapsing stars or merging neutron stars binaries which could be strong sources of gravitational radiation [109]. In this period of enthusiasm for the physics and astrophysics of collapsed objects, Weber announced the detection of radiation emanating from the centre of our galaxy [138, 139]. He assured that he had detected several signals per day, although this assertion was not supported by other contrasting observations as those of optical telescopes. However, the news led to a wave of work on the gravitational radiation from astrophysical sources and also to the construction of a *first generation* of room temperature detectors. All this happened despite the considerable controversy that surrounded Weber's claims, since the sensitivity of the bar antennæ was considered to be only enough to detect radiation emanating from supernovæ explosions in our galaxy, what in accordance to Weber's results implied that several of these events ocurred each day in the Milky Way, an incredible circumstance. Moreover, there was also dispute over the way the results were analysed and the consensus is that the equipment was probably not detecting GW. Nevertheless, Weber is recognized as the pioneer who promoted this area of investigation with the invention of the resonant antenna able to reach revolutionary –although not sufficient– precision of order $\frac{\delta l}{l} = 10^{-16}$, under one nuclear radius in a length of 1m. Not only this, but he also played the important role of alerting the experimentalists to the possibility of undertaking this investigation and hence, in the late seventies, other researchers got involved in building a *second generation* of gravitational antennæ [10], which offered better perfomance by means of important technological improvements in their design, such as cryogenics, more careful isolation or improved readout systems with resonant transducers and low-noise quantum-effect based amplifiers.

It was at the period of the growing of resonant antennæ that other methods of detecting gravitational radiation, such as spacecraft Doppler tracking or interferometry, also initiated –for instance, in 1972 Forward [48] constructed the first small-scale prototype of a laser interferometric detector. Nevertheless, the general realization was that the detection of GW was a much more difficult task than was originally expected. It also became clear that in order to study strong sources of GW more elaborate models had to be worked out. This meant that new experimental, as well as theoretical, tools had to be

developed in order to succeed. As a result, both resonant and interferometric detectors, and also other techniques, were perfected in the eighties and nowadays a continued major effort is being pursued as is reflected by the several ambitious projects under planning or even operating [28, 111, 45][2].

In spite of all this outstanding technological effort, Weber's observations have received no confirmation from other experiments. But fortunately, the existence of Gravitational Waves, as well as some of the predictions of gravitational wave physics, was confirmed by the discovery by Hulse and Taylor [64] of the binary pulsar PSR $1913+16$ in 1974[3]. This stellar object consists of a 59 milisecond periodic pulsar drawing an elliptical orbit, of period 2.79×10^4 seconds, around the centre of mass of the system and a second neutron star with a maximum separation of only 10^{11} cm ($\approx$ 1 solar radius). After five years of continuous data analysis, secular changes in the orbit of the pulsar, which were expected to correspond to gravitational radiation damping effects according to the quadrupole radiation formula, were observed [126]. More concretely, analysis of the arrival times of the signals from the pulsar have shown that the observed value of the decay of the system's orbital period is in convincing agreement with that predicted by General Relativity, with less than a 1% error[4] [127, 128].

This strong experimental evidence suggests that negative results of present gravitational antennæ ensue from not having enough sensitivity. The fact is that the expected signals are extremely weak and can be easily swamped by the noise emanating from different disturbing sources: brownian motion of the atoms of the detector due to its temperature above the absolute zero, seismic perturbations, rudimentary readout systems... Therefore, further improvements are needed to increase it. For interferometers, the future seems to relay in projects of large magnitude. For resonant detection, the sensitivity threshold is expected to be pushed forward with the aid of technological improvements -ultracryogenics and SQUID low noise amplifiers-, but there is a different way of making a further step: the introduction of spherical geometry. Indeed, it was long ago recognized by Forward [47] that a sphere is a very natural shape for a resonant mass detector of gravitational waves offering better detection capabilities than cylindrical bars. Soon after, other authors were also interested in the topic. Thus, in 1975, Ashby and Dreitlein [4] studied the response of an elastic sphere to gravitational radiation and in

[2] See section 2.2 in next chapter for more detailed references.

[3] In 1993, Taylor and Hulse were awarded the Nobel Prize in Physics for the discovery of and work on this system.

[4] In [72] calculations yield $\dot{\tau}_{predicted} = -2.4032 \times 10^{-12}$, while $\dot{\tau}_{observed} = -2.409 \times 10^{-12}$.

1977 Wagoner and Paik [133] found a set of equations to determine the source direction in the celestial hemisphere and wave polarizations from their modes, and also showed that sphere's sensitivity per unit mass is slightly better than that of cylinders. These results were ignored by experimentalists until the beginning of the present decade, when several research groups have appeared worldwide developing spherical detectors from both theoretical [80, 32, 84, 103] and experimental [49, 69, 97] points of view. With the prospects of success improving significantly at each step, they face the challenging but promising task of detecting GW, which seems an actual possibility not so far in the future.

1.2 Motivation

In view of this short account of the evolution of gravitational radiation research, it is not possible to avoid the following question: which is in fact the final objective pursued by these scientific investigators involved in the detection of gravitational waves? Is it the mere resolution, defiant on the other hand, of quantitatively measuring those extremely weak travelling spacetime perturbations, or possibly is it the search for a *concluding and direct* experimental proof of their reality?

It seems that after the discovery of the binary pulsar PSR 1913+16 and the subsequent related analyses and conclusions, the existence of GW in Nature *must be* no longer a polemical subject. However, these results are sometimes referred to as providing an *indirect proof*, and so the interest in designing and constructing an operative GW antenna is explained by the aim of obtaining a *direct* evidence.

Nevertheless, it would be not exact to restrict the answer to such a concrete short-term motivation. It is not at all unwise to state that the ultimate purpose resides in an attempt to lay down the basis for a new *gravitational-wave astronomy*. If cosmic gravitational waves can be detected and studied, they will become a new source of information for astrophysics and cosmology. Furthermore, it is believed that they will create a revolution in our knowledge about the Universe, comparable to or greater than that which resulted from the discovery of radio waves and radio astronomy, which changed our view from a serene Universe where stars and planets wheel smoothly in their orbits as viewed by light to a violent scenario where galaxies in collision, jets ejected from galactic nuclei, or quasars with luminosities varying on timescales of hours occurred as viewed by radio waves. This spectacular revolution was possible due to the fact that the information carried by radio waves is so different from that carried by light. It happens that the

differences are even more important in the comparison between electromagnetic and gravitational radiation, which makes it likely that the advent of *gravitational astronomy* will deeply impact, allowing direct investigation of the gravitational interaction under extreme conditions and creating again a new and more trustworthy image of the Universe.

The development of such a new gravitationally based astronomy demands not only experimental effort but also theoretical contributions. On one hand, *realistic* sources of GW have to be further studied so that more appropriate models determine with greater accuracy the values of gravitational radiation emitted by astrophysical systems, what kind of sources actually occur and how frequently. On the other hand, it is obvious that a complete understanding of the physical characteristics and the dynamical behaviour of detectors is absolutely essential for the correct interpretation of their readout information.

In the case of resonant antennæ, existing dynamical models are based on oversimplified assumptions which neglect important effects. In particular for spherical detectors, the main oversight –leaving aside the noise question– refers to the consideration of the resonator problem. The philosophy of using resonant transducers for motion sensing began with cylindrical bars. They are used as mechanical-impedance matching devices of the primary vibrational modes of the antenna, producing an essential increase in the mechanical coupling when their resonance frequency is accurately tuned to that of the cylinder. This idea is transplanted to spherically shaped antennæ under the proviso that a multiple set rather than a single resonator is needed to exploit its better potential capabilities as a multimode system, i.e., if information on the GW amplitudes and incidence direction is required. Thus, the coupled dynamics of the whole system has to be studied to give an adequate theoretical interpretation of its readout, or, in other words, the resonator problem has to be solved. Currently, the predicted behaviour of this coupled sphere is just an extrapolation from the results that hold for the free sphere, what, for example, amounts to producing an invalid implementation of second order corrections on the accuracy of experimental data. And this situation becomes highly undesirable under the reasonable expectation that future spherical GW antennæ will make use of extremely precise measurement techniques, likely to demand more refined analyses.

Hence, our particular aim in this work is devoted to construct such a sophisticated theoretical model depending on, as far as possible, not unwarranted hypotheses, with the objective of determining the system response to any interesting signal with unlimited precision. The mathematics we develop are based on perturbative expansions of the solutions to our general equations describing the antenna in ascending powers of the small coupling constant η –given by the ratio of the transducers' average mass to

the sphere's mass–, but also on the simple and powerful algebraic scheme emerging from Green function formalism and Laplace transformation. The analysis reveals with remarkable transparency the general structure of the resonant mode splitting and coupling, providing results which account, in a systematic way, for the dynamical effects of the coupled device for completely general resonator distributions over the sphere's surface. Beyond this. unprecedented new considerations are allowed, such as that of the second resonance frequency –making possible to exploit the already demonstrated potentially good sensitivity of spherical detectors at two frequencies–, or the question of how the system characteristics are affected by slight departures from perfect spherical symmetry or identity of resonators, what constitutes the foundations for the analysis of more realistic instances. Furthermore, we will see that within this study we are able to confirm and generalize other previous implementations, and even to evaluate any existent particular proposal for spherical detector or transducers layout. It enables the discussion of several interesting alternatives, such as the truncated icosahedral layout TIGA or our specific PHCA proposal for a rather complete monopole-quadrupole GW antenna.

1.3 Overview

Summing up, this thesis presents an accurate, both mathematical and physical, description of the dynamical behaviour of GW spherical antennæ when excited by incoming gravitational radiation and also by calibration signals[5], making special attention to the resonator problem and developing a general procedure applicable to any proposal for a spherical detector.

It has been structured in three major parts.

The first part, which includes chapters 1 and 2, stands as an introduction. After the historical background set in this chapter of *Preliminaries*, Chapter 2 begins with a brief survey of the theory of Gravitational Radiation within the weak field limit of General Relativity, although it has been pointed out that the main arguments also apply to any other metric theory of gravity. We derive the wave equation in the linear approximation and discuss its vacuum solutions, characterized as plane waves, their polarizations and their action on extended bodies. what will become of major interest for the study of resonant detectors. General solutions of the retarded potential type for the complete

[5] It will lie somewhat out of the thesis' main line of development, but represents also an interesting case from both experimental and theoretical points of view.

Einstein equation will be considered in connection to the subject of generation of gravitational waves and quadrupole radiation, where we also enumerate some of its possible sources.

Then, in the second part of the chapter, attention is centred in another important, already classical, topic referring Gravitational Radiation: the detection of gravitational waves, the frame subject of this essay. So to establish a general perspective, we firstly describe the present status revising the several developed detection techniques. After a short description of Doppler Tracking in Space and Interferometry including comments on the last experimental projects, we restrict to resonant antennæ providing some more technical details. We briefly review how the present bars work and how a suitable readout system –composed of a resonant transducer, dynamically described as an harmonic-oscillator, and an electromagnetic amplifier– must be added to the body in order to monitor the effects and quantitatively assess their magnitude and physical significance; which are the operative detectors nowadays and what are their already reached sensitivities to the several possible sources of gravitational radiation and that expected for the future detectors of spherical shape. Finally, we conclude by revising theoretically the advantages of those spherical antennæ, which offer better detection capabilities and possibly will be the *next generation* of GW detectors of the resonant type. For the remainder of this thesis, parts two and three, emphasis exclusively focuses on them.

Chapter 3 opens the second part of the work. It is centered on the mathematical description of the dynamical behaviour of a spherical GW antenna under the action of a gravitational wave or also a calibration signal. The core of the device, the detector, is modelled as a perfect homogeneous spherical elastic solid. As a necessary introduction, we will first review some well known derivations about its free performance when it is acted upon by an external force, and will see how its monopole and quadrupole normal modes of vibration are the only possibly excited ones by an incoming GW. Practicality requires also a readout system for motion sensing. Thus, the detector is endowed with a multiple set of identical resonant transducers attached at fixed but arbitrary positions on its surface. The resonators will be treated as linear harmonic oscillators with a natural resonance frequency accurately tuned to a specific frequency of the free sphere spectrum, logically a monopole or a quadrupole one.

The analysis of the coupled device begins by laying out the differential set of equations, called the GRD equations, describing the system under several most general assumptions: the detector is a solid elastic body of any shape, the resonators are modelized to behave as linear harmonic oscillators moving radially, they could be non-identical and are cou-

pled at arbitrary locations. Immediately after, the set is transformed into an algebraic system in the Laplace domain, which of course will be constricted to perfect spherical detectors, identical resonators, and forces of the GW –or calibration– type. The resolution provides the new coupled device resonances from the splitting of the uncoupled sphere's frequencies, as well as the vibrational amplitudes at the resonators' positions, although exact solutions are not available and all the results are obtained as perturbative series expansions in ascending powers of the small dimensionless coupling constant $\eta^{\frac{1}{2}}$ ($\eta \equiv \frac{m_{resonators}}{M_{sphere}}$). We will restrict to first order calculations. Finally, we discuss the possibility of construction of mode channels –fixed linear combinations of the measured resonators' motions directly proportional to the GW amplitudes at single specific coupled frequency pairs– and find the mathematical property which characterizes their existence.

Our PHCA proposal or the TIGA antenna of Jonhson and Merkowitz, which are examined in Chapter 4 as applications of our theoretical developments in Chapter 3. present minimal distributions of transducers which allow the implementation of mode channels. For experimental exigencies, they both adopt the substitution of a true sphere by a regular polyhedron which approximates it, and suggest specific configurations of resonators, according to axial symmetry or maximum isotropy respectively. Hence, their associated GW responses differ obviously not in the basic structures arising from the general model, but in particular although relevant peculiarities, also contrastable in the simpler case of the detector being set into vibration by a calibration signal.

After this exposition of the core of our theory and its most outstanding derivations in the most ideal situation, we undertake in the third part of the essay two essential and further steps: the question of how the system characteristics are affected by slight departures from ideality, and the problem of the signal deconvolution also in the noisy situation.

The first subject is specially interesting for increasing the degree of applicability of the ideal model to real systems –it is important to remind that we meant to describe the behaviour of experimental devices–, so that special attention is devoted to non-identity of resonators, to the existence of a *second* resonance frequency (URF effect), or to the breaking of spherical symmetry by suspension. These two last failures lead to significant changes with respect to the ideal perfect device perfomance. Furthermore, for the suspended antenna our model's predictions have been confronted with the reported experimental data obtained in the TIGA prototype experiment, and they both have been found to satisfactorily agree.

Signal deconvolution is the last topic treated in the essay. We will begin by finding the

incidence direction of the GW signal, its amplitudes and polarization –i.e., by solving the inverse problem– in the noiseless case, and next we will address for the first time in this work the important question of the presence of noise in the system. We restrict to treat this key problem just for deconvolution, and study how noise affects the determination of the GW parameters, with associated errors which are expected to be isotropic.

The memory is closed with a brief final discussion which summarizes our results and some comments on proposals for future work.

1.4 Notation

- Latin indices i, j, k and so run over three spatial coordinate labels, usually $1, 2, 3$ or x, y, z.
- Greek indices μ, ν and so range from 0 to 3, the four coordinate labels in a general coordinate system.
- Repeated indices are summed following Einstein's summation convention.
- The metric tensor of the spacetime $g_{\mu\nu}$ has signature $-+++$; the metric tensor $\eta_{\mu\nu}$ in an inertial coordinate system has diagonal elements $-1+1+1+1$.
- Boldface letters denote three-dimension Cartesian vectors.
- A dot over any quantity denotes the time derivative of that quantity.
- Partial derivatives with respect to x appear in the text in the form of $\frac{\partial}{\partial x}$.
- Partial derivatives with respect to x^μ appear in the form of a colon$_{,\mu}$.
- Laplace transform of a function $F(t)$ is denoted by $\hat{f}(s)$ or by $\mathcal{L}\{F(t)\}$.
- The speed of light is taken to be unity.
- G is the Newtonian gravitational constant and K_B is the Boltzmann's constant.
- Acronyms:

GR	General Relativity,
GW	Gravitational Wave,
TT gauge	Transverse Traceless gauge,
SQUID	Superconducting QUantum Interference Device,
SNR	Signal to Noise Ratio,
GRD equations	General Resonant Detector equations,
PHC	Pentagonal HexaContahedron,
PHCA	Pentagonal HexaContahedral gravitational wave Antenna,
TI	Truncated Icosahedron,
TIGA	Truncated Icosahedral Gravitational wave Antenna,
URF	Unisolated Resonance Frequency,
IRF	Isolated Resonance Frequency,
scS,wcS	strongly coupled Singlet, weakly coupled Singlet,
scD,wcD	strongly coupled Doublet, weakly coupled Doublet,
scT,wcT	strongly coupled Triplet, weakly coupled Triplet,
L-F	Laboratory reference Frame,
W-F	Wave reference Frame,
D-F	Diagonal reference Frame.

Chapter 2

THEORY AND DETECTION OF GRAVITATIONAL WAVES

In this chapter, we shall centre our attention on Gravitational Wave Detection and more specifically on Resonant Spherical Antennæ. Our main aim is to briefly present a general panorama of the current status of gravitational-wave research. Secondly, we would like to confine the scope going into some more technical details referring Resonant Detectors and looking with a major interest to the case of Spherical Antennæ.

But before, let us give an overview of the standard theory of Gravitational Radiation itself, focusing on the basic ideas that conform it and that will help us in a better understanding of subsequent discussions. Of course, more complete and thorough presentations may be found in standard textbooks, such as Kenyon [72], Wald [134] or Weinberg [140].

2.1 Generalities on Gravitational Radiation Theory

As we have already pointed out, Gravitational Waves are not unique to Einstein's theory of gravity. Among the alternative theories, there is a wide class –the so-called metric theories[1]– whose members are very similar to General Relativity, which is in fact a metric theory of gravity itself, as much as Dicke-Brans-Jordan's theory or Rosen's theory [141]. Any metric theory of gravity predicts curvature perturbations propagating in spacetime carrying energy, thus responsible for changes in geometric quantities and

[1] A metric theory of gravity is characterized by a 4-dimensional, symmetric spacetime metric $g_{\alpha\beta}$ of signature +2, and by satisfying the Einstein's Equivalence Principle, i.e., all the nongravitational laws of physics take on their standard special relativistic forms in the local Lorentz frames of $g_{\alpha\beta}$ [100].

for tidal forces in material systems. Here, we will restrict ourselves to a discussion of GW in General Relativity, although the perspective and general arguments –such as the existence and validity of the geodesic deviation equation derived from the Einstein's Equivalence Principle– also holds for any other metric theory of gravity.

Our specific purpose is to see how it is possible to find weak radiative solutions of Einstein equations describing waves carrying not enough energy and momentum to affect their own propagation, and how they, that are described by a symmetric matrix with, in principle, ten independent terms, can be fully locally characterized by just two functions due to gauge invariance. We shall also try to briefly describe some important gravity waves topics[2]: the produced effects on spacetime depending on the polarization properties of the waves, their action as tidal driving forces on material physical systems, and their generation and approximate strain magnitude derived through the quadrupole formalism, which is highly accurate for many sources and is accurate at least in order of magnitude for most. Finally a few words are written on possible sources.

2.1.1 Gravitational Radiation in the Weak Field Limit

A weak gravitational field is one in which the spacetime is *nearly* flat. Except for phenomena dealing with the large scale structure of the universe, this gravitational field limit is in practice an excellent approximation in nature very appropriate for the waves likely to reach the Earth.

In this situation, and in a properly chosen coordinate system, the metric can be considered

$$g_{\mu\nu}(x) = \eta_{\mu\nu} + h_{\mu\nu}(x) \qquad |h_{\mu\nu}(x)| \ll 1, \tag{2.1}$$

where $\eta_{\mu\nu}$ represents the flat Minkowski metric and $h_{\mu\nu}(x)$ is a small perturbation.

Substituting this particular decomposition in Einstein's equations

$$R_{\mu\nu} - \frac{1}{2} g_{\mu\nu} R^{\alpha}_{\alpha} = 8\pi G T_{\mu\nu}, \tag{2.2}$$

and retaining only the linear terms in $h_{\mu\nu}(x)$, a new set of equations is achieved:

[2] There remain some other aspects laying somewhat out of the scope of this work but which are of importance in some specific areas of gravitational waves theory –and more concretely of gravitational wave detection– not treated in this essay. For instance, a complete description of the GW received on Earth distorted by the Doppler effect[70, 101] is essential for data analysis. For a general catalogue of effects, see [130].

$$\Box h_{\mu\nu}(x) - h^{\lambda}_{\nu,\lambda\mu} - h^{\lambda}_{\mu,\lambda\nu} - h^{\lambda}_{\lambda,\mu\nu} = -16\pi G S_{\mu\nu} \tag{2.3}$$

$$S_{\mu\nu} \equiv T_{\mu\nu} - \frac{1}{2}\eta_{\mu\nu} T^{\lambda}_{\lambda}. \tag{2.4}$$

Here, the energy-momentum tensor $T_{\mu\nu}$ is taken to lowest order in $h_{\mu\nu}(x)$, so it is in fact independent of those quantities and satisfies the ordinary conservation condition $T^{\mu}_{\nu,\mu} = 0$ implying

$$S^{\mu}_{\nu,\mu} = \frac{1}{2} S^{\lambda}_{\lambda,\nu}. \tag{2.5}$$

Due to the gauge invariance of the field equation, from any of its solutions it is possible to generate equivalent ones by performing coordinate transformations. The most general transformation that leaves the field weak is

$$x'^{\mu} = x^{\mu} + \epsilon^{\mu}(x), \tag{2.6}$$

with $\epsilon^{\mu}(x)$ four arbitrary functions only subject to the condition of being of the same order of magnitude as $h_{\mu\nu}$. We can certainly benefit from this and fix the gauge by choosing those coordinates which simplify most the equations. In particular, we can work with harmonic coordinates such that

$$h^{\mu}_{\nu,\mu} = \frac{1}{2} h^{\mu}_{\mu,\nu} \tag{2.7}$$

and then

$$\Box \epsilon^{\mu}(x) = 0. \tag{2.8}$$

In this case, the linearized Einstein's equation reduces to

$$\Box h_{\mu\nu} = -16\pi G S_{\mu\nu}, \tag{2.9}$$

with solutions of the retarded type that can be formally expressed by

$$h_{\mu\nu}(x) = 4G \int S_{\mu\nu}\left(\mathbf{x}', t - |\mathbf{x} - \mathbf{x}'|\right) \frac{d^3x'}{|\mathbf{x} - \mathbf{x}'|}, \tag{2.10}$$

to which we can add any solution of the homogeneous equation

$$\Box h_{\mu\nu} = 0. \tag{2.11}$$

We interpret the retarded potential (2.10) as the gravitational radiation propagating with the speed of light produced by the sources $S_{\mu\nu}$, whereas any additional term satisfying the homogeneous equation (2.11) represents the gravitational radiation coming in from infinity.

Since eventual detection of GW will take place far from their source, $S_{\mu\nu} = 0$, we centre our attention on the vacuum Eisntein equation which will clearly provide plane-wave solutions of the form:

$$h_{\mu\nu}(x) = e_{\mu\nu} \exp(ik_\lambda x^\lambda) + e^*_{\mu\nu} \exp(-ik_\lambda x^\lambda) \tag{2.12}$$

provided that

$$k_\mu k^\mu = 0 \tag{2.13}$$

$$k_\mu e^\mu_\nu = \frac{1}{2} k_\nu e^\mu_\mu, \tag{2.14}$$

being k_μ the constant four-dimensional wave vector.

At first sight, it may seem that the symmetric polarization tensor $e_{\mu\nu}$, and so $h_{\mu\nu}$, has ten independent components, but the four relations (2.13) would lower this number to six, although in fact only two of them are actually relevant since four more constraints can be imposed by fixing gauge degrees of freedom. Indeed, we still are able to perform any first order change of coordinates preserving equation (2.8), it is their harmonic character. If one chooses a suitable harmonic system of coordinates such as the transverse-traceless or TT gauge, one has the canonical form of $h_{\mu\nu}$

$$h_{\mu\nu}(x) = \begin{pmatrix} 0 & 0 & 0 & 0 \\ 0 & h_+ & h_\times & 0 \\ 0 & h_\times & -h_+ & 0 \\ 0 & 0 & 0 & 0 \end{pmatrix} = h_+ \begin{pmatrix} 0 & 0 & 0 & 0 \\ 0 & 1 & 0 & 0 \\ 0 & 0 & -1 & 0 \\ 0 & 0 & 0 & 0 \end{pmatrix} + h_\times \begin{pmatrix} 0 & 0 & 0 & 0 \\ 0 & 0 & 1 & 0 \\ 0 & 1 & 0 & 0 \\ 0 & 0 & 0 & 0 \end{pmatrix} \tag{2.15}$$

for a wave orthogonal to its direction z of propagation, which effectively is traceless and transverse (the vibration of the wave is orthogonal to its propagation). Here,

$$h_+ = A_+ \exp(-i\omega(t-z))$$

$$h_\times = A_\times \exp(-i\omega(t-z+\varphi)) \tag{2.16}$$

with φ an arbitrary phase angle and A_+ and $A_\times$ the wave amplitudes. Thus, the general solution can be expressed by superposition of plane waves as a linear combination of two polarization states.

2.1.2 Plane-Wave Polarizations

The distinction between the different components of the polarization tensor $e_{\mu\nu}$ is clarified by the study of its behaviour under a rotation R of angle θ about the direction of propagation of the wave, say the z axis.

This is just a Lorentz transformation of the form

$$\begin{aligned} \mathcal{R}_1^1 = \mathcal{R}_2^2 &= \cos\theta \\ \mathcal{R}_1^2 = -\mathcal{R}_2^1 &= \sin\theta \\ \mathcal{R}_3^3 = \mathcal{R}_0^0 = 1 \qquad & \text{other } \mathcal{R}_\mu^\nu = 0, \end{aligned}$$

that takes $e_{\mu\nu}$ into:

$$e'_{\mu\nu} = \mathcal{R}_\mu^\rho \mathcal{R}_\nu^\sigma e_{\rho\sigma}. \tag{2.17}$$

Taking into account relations (2.14), it happens that

$$e'_\pm = e^{\pm 2i\theta} e_\pm \tag{2.18}$$

$$f'_\pm = e^{\pm 1i\theta} f_\pm \tag{2.19}$$

$$e'_{33} = e_{33} \tag{2.20}$$

$$e'_{00} = e_{00} \tag{2.21}$$

where

$$e_\pm \equiv e_{11} \mp i e_{12} = -e_{22} \mp i e_{12} \tag{2.22}$$

$$f_\pm \equiv e_{31} \mp i e_{32} = -e_{01} \pm i e_{02}. \tag{2.23}$$

Any plane wave ϕ which transforms into

$$\phi' = e^{ih\theta}\phi \tag{2.24}$$

after a rotation of angle θ about its direction of propagation is said to have helicity h. Hence, it has been shown that a gravitational plane wave can be generally decomposed

into six different polarization contributions: two parts (2.20) and (2.21), with just one polarization state each corresponding to helicity 0; and parts (2.19) and (2.18) each having two polarization states with associated helicities ± 1 and ± 2 respectively (see [39] for further details).

In General Relativity, as has already been seen, parts with helicities 0 and ± 1 can be made to vanish by a suitable choice of coordinates, and so the physically significant components are just spin 2 waves, said of the T2 type (waves-transverse, spin-two). This is not the case for other metric theories of gravity. For instance, Brans-Dicke-Jordan's theory has both spin 2 waves and spin 0 waves, T2 and T0 waves [19].

These characteristic polarization properties would allow experimental investigation to discriminate among the competing theories of GW physics. The discerning fact is that different polarization states produce different deformation patterns in spacetime. In order to construct a picture of these effects one can consider a cloud of nearby test particles surrounding a central, fiducial one, all of them in the $x - y$ plane. Initially, the cloud resides in flat spacetime, all its particles are at rest with respect to each other and its shape is precisely that of a circumference. Then, a GW travelling along the z axis hits and deforms the cloud. The deformations can be analysed using the equation of geodesic deviation, which describes the relative motion that any pair of nearby freely falling particles exhibits to an observer that falls with them under the presence of a gravitational field,

$$\frac{D^2\xi^\mu}{D\tau^2} = R^\mu_{\nu\rho\sigma} u^\nu u^\sigma \xi^\rho, \tag{2.25}$$

being D the covariant derivative applied to ξ^μ, the relative four-vector called geodesic deviation connecting the two test particles, and u^ν the four-velocity of any of them, with proper time τ.

Whenever the separation between particles is much less than the characteristic dimensions of the field, and taking the particles at rest before the passage of the wave, the geodesic deviation equation can be written

$$\frac{d^2\xi^k_i}{dt^2} = R^k_{0j0}(t)\xi^j_i; \tag{2.26}$$

ξ^k_i represents the k component of the i-particle location in the local inertial frame associated to the fiducial particle at the center of the circumference, where the Riemann tensor is evaluated.

In the weak field limit, and for General Relativity, the Riemann tensor is seen to be

$$R_{k0j0} = -\frac{1}{2}h_{kj,00} \tag{2.27}$$

and then the only non-zero components in the TT-gauge are

$$R_{x0x0} = -R_{y0y0} = -\frac{1}{2}h_{+,00} \tag{2.28}$$

$$R_{x0y0} = R_{y0x0} = -\frac{1}{2}h_{\times,00} \tag{2.29}$$

since (2.15) holds. In this case, (2.26) can be integrated to give the components $x_i(t)$ and $y_i(t)$ of $\xi_i(t) \equiv (x_i(t), y_i(t), 0)$:

$$\begin{aligned} x_i(t) &= l_0 \cos\phi_i + \frac{l_0}{2}\left(h_+(t)\cos\phi_i + h_\times(t)\sin\phi_i\right) \\ y_i(t) &= l_0 \sin\phi_i + \frac{l_0}{2}\left(h_\times(t)\cos\phi_i - h_+(t)\sin\phi_i\right), \end{aligned} \tag{2.30}$$

where we have used first that the particles were originally at rest at a distance l_0 respect to the center of the circle being ϕ_i the angular variable that locates them in the $x-y$ plane, and secondly that the deformations in the distance l are always small: $\frac{\delta l}{l} << 1$.

If one restricts to $T2+$, which means that $h_\times = 0$, or to $T2\times$, and so $h_+ = 0$, those deformations are respectively

$$\left(\frac{\delta l}{l}\right)_{+,i} \approx -\frac{1}{2}h_+(t)\cos 2\phi_i \tag{2.31}$$

$$\left(\frac{\delta l}{l}\right)_{\times,i} \approx \frac{1}{2}h_\times(t)\sin 2\phi_i. \tag{2.32}$$

If we assume h_+ and $h_\times$ having a sinusoidal behaviour of the form given in (2.16), we find that $T2+$ and $T2\times$ deform the circumference to elliptical shape with patterns rotated an angle of 45° from one another and both of them exhibiting invariance under a 180° rotation about the propagation direction at any moment.

Analogously, calculations for the spin 0 radiation appearing in Brans-Dicke-Jordan's theory show that it will set the cloud into alternating expansions and compressions in the transverse plane, while leaving it transversely circular (see Figure 2.1, taking into account that the displacements introduced in the graph have been enhanced for the sake of clarity).

Remarkably, these T0, $T2+$ and $T2\times$ waves maintain their polarization character in any Lorentz frame, what arises from these particular spins being Lorentz invariant [129].

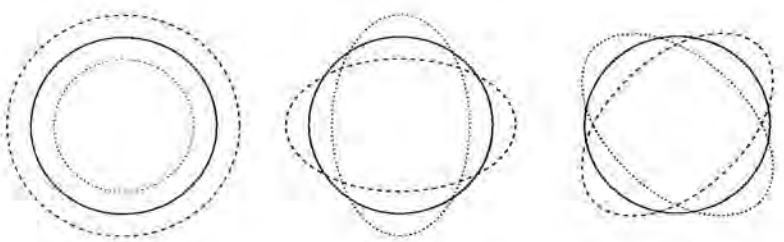

Figure 2.1. *The effect of a GW on a cloud of test particles arranged on a circular layout before its propagation out of the page. In (a), the T0 wave present in Brans-Dicke-Jordan's theory. In (b) and (c), the spin-2 T2+ and T2× waves of General Relativity. As the wave oscillates, the solid circumference gets deformed in the manner shown dashed after one-quarter of its cycle; after half a cycle, the ring returns to its circular shape, and after three-quarters the cloud is distorted in the manner shown dotted. As can be seen, T2+ and T2× cause the same sequence of distortions, with the pattern rotated 45° from one another. A general wave of the Brans-Dicke-Jordan's theory causes a superposition of the three distortions, and of the two shown in (b) and (c) in General Relativity.*

2.1.3 Gravitational Waves as Tidal Driving Forces

Up to this point we have reviewed how curvature perturbations travelling in spacetime change geometric quantities such as proper distances. But, and as a consequence of, they can also act as tidal driving forces to modify the shape and dimensions of material objects, that eventually could become detectors of gravitational waves [129]. This driving density of force reads:

$$\mathbf{f}_j(\mathbf{x},t) = \varrho R_{0j0k}(t)\mathbf{x}^k \tag{2.33}$$

which arises from the geodesic deviation equation (2.26) after multiplying its both sides by the density ϱ of the material, and considering $\mathbf{x}^k$ the cartesian coordinates of a point of the solid relative to a coordinate system with origin in its centre of mass, in relation to which the *electric* components of the Riemann tensor $R_{0j0k}(t)$ are also evaluated.

Assuming as always General Relativity and a TT-coordinate reference system, the previous equation simplifies to just:

$$\mathbf{f}_j(\mathbf{x},t) = -\frac{1}{2}\varrho h_{jk,00}(t)\mathbf{x}^k. \tag{2.34}$$

However, one could be interested in calculating the solid's response to other metric GWs. So, we consider $R_{0j0k}(t)$ more generally:

$$R_{0j0k}(t) = -\frac{1}{2}(h_{jk,00}(t) - h_{0j,0k}(t) - h_{0k,0j}(t) + h_{00,jk}(t)) \tag{2.35}$$

and

$$\mathbf{f}_j(\mathbf{x},t) = -\frac{1}{2}\varrho(h_{jk,00} - h_{0j,0k} - h_{0k,0j} + h_{00,jk})\mathbf{x}^k. \tag{2.36}$$

By the study of the form of the Riemann tensor spatial components $R_{0j0k}(t)$, it can be shown that the structure of this tidal force follows a monopole-quadrupole pattern. It happens that $R_{0j0k}(t)$ is a three-dimensional symmetric tensor, whereby it and therefore $\mathbf{f}(\mathbf{x},t)$ consequently admit the decomposition into a non traceless and a traceless contribution, the latter expressed in a suitable basis:

$$\begin{aligned}\mathbf{f}(\mathbf{x},t) &= \sum_{\alpha}\mathbf{f}^{(\alpha)}(\mathbf{x})g^{(\alpha)}(t) \\ &= \underbrace{\mathbf{f}^{(00)}(\mathbf{x})g^{(00)}(t)}_{non-traceless} + \underbrace{\sum_{m=-2}^{m=2}\mathbf{f}^{(2m)}(\mathbf{x})g^{(2m)}(t)}_{traceless},\end{aligned} \tag{2.37}$$

where $g^{(00)}(t)$ and $g^{(2m)}(t)$ are the monopole and the quadrupole amplitudes of the Riemann tensor carrying all the dynamical GW information, while $\mathbf{f}^{(00)}$ and $\mathbf{f}^{(2m)}$ are pure tidal form factors with explicit expressions [80]

$$\begin{aligned} g^{00}(t) &= \tfrac{4\pi}{3}E_{ij}^{*(00)}R_{0i0j}(t) & g^{2m}(t) &= \frac{8\pi}{15}E_{ij}^{*(2m)}R_{0i0j}(t) \\ \mathbf{f}_i^{00}(\mathbf{x}) &= \varrho E_{ij}^{(00)}\mathbf{x}_j & \mathbf{f}_i^{2m}(\mathbf{x}) &= \varrho E_{ij}^{(2m)}\mathbf{x}_j, \end{aligned} \tag{2.38}$$

provided that the following choice is made:

$$E_{ij}^{(00)} = (\frac{1}{4\pi})^{\frac{1}{2}} \begin{pmatrix} 1 & 0 & 0 \\ 0 & 1 & 0 \\ 0 & 0 & 1 \end{pmatrix} \quad E_{ij}^{(20)} = (\tfrac{5}{16\pi})^{\frac{1}{2}} \begin{pmatrix} -1 & 0 & 0 \\ 0 & -1 & 0 \\ 0 & 0 & 2 \end{pmatrix}$$

$$E_{ij}^{(2\pm1)} = (\frac{15}{32\pi})^{\frac{1}{2}} \begin{pmatrix} 0 & 0 & \mp 1 \\ 0 & 0 & -i \\ \mp 1 & -i & 0 \end{pmatrix} \quad E_{ij}^{(2\pm2)} = (\tfrac{15}{32\pi})^{\frac{1}{2}} \begin{pmatrix} 1 & \pm i & 0 \\ \pm i & -1 & 0 \\ 0 & 0 & 0 \end{pmatrix} \tag{2.39}$$

which is the one bringing out the monopole-quadrupole structure of the Riemann tensor for a general metric.

We see that $E_{ij}^{(00)}$is a matrix proportional to the identity, while $\{E_{ij}^{(20)}, E_{ij}^{(2\pm1)}, E_{ij}^{(2\pm2)}\}$ constitutes an orthogonal set of linearly independent matrices, which is a basis for the five-dimensional vector space of three-dimensional, symmetric and traceless matrices. They obey the orthogonality relations

$$E_{jk}^{*(2m)} E_{jk}^{(2m')} = \frac{15}{8\pi}\delta_{mm'} \tag{2.40}$$

and satisfy the following properties

$$E_{jk}^{(2m)} n_j n_k = Y_{2m}(\theta, \phi), \tag{2.41}$$

where $\mathbf{n}$ is the radial unit vector $\frac{\mathbf{x}}{|\mathbf{x}|}$ and $Y_{2m}(\theta, \varphi)$ denotes spherical harmonics.

Of course, a decomposition analogous to (2.37) also holds for $h_{jk}(t)$:

$$h_{jk}(t) = \frac{1}{3}h(t)\delta_{jk} + \sum_{m=-2}^{m=2} E_{jk}^{(2m)} h^{(m)}(t) \tag{2.42}$$

with

$$h(t) = \delta_{jk} h_{jk}(t) \qquad\qquad h^{(m)}(t) = \tfrac{8\pi}{15} E_{jk}^{*(2m)} h_{jk}(t) .$$

Once again, as expected and already described in section 2.1.2., we see the structure of gravitational waves emerging from the analysis of their effects. Again, they separate into a monopole (00) contribution corresponding to spin 0 transversal waves –the T0 waves of Brans-Dicke-Jordan theory–, and the quadrupole $(2m)$ terms of helicity 2 in General Relativity.

2.1.4 Quadrupole Radiation

We centre now our attention on equation (2.10) in section 2.1.1. So, we turn now to wave generation. We wish to study the energy that a given physical system emits in the form of gravitational radiation. If we consider it far from the source, i.e., in the wave zone as realistically occurs in GW observations,

$$|\mathbf{x}| \gg |\mathbf{x}'|, \tag{2.43}$$

it happens that $r \equiv |\mathbf{x}-\mathbf{x}'| \approx |\mathbf{x}|$ is the distance between that source and the observation point and

$$h_{\mu\nu}(x) \approx \frac{4G}{r} \int T_{\mu\nu}\left(\mathbf{x}', t-r\right) d^3x'. \tag{2.44}$$

Beyond the basic assumption that the fields are weak, we make a further approximation and accept that the source radius R is much smaller than the wavelength of the radiation, which is equivalent to assume that the typical velocity within the source is very much less than the velocity of light (nonrelativistic systems). The absence of dipole radiation in the gravitational field because of the conservation of the total momentum and the angular momentum –what amounts to be a revealing difference between gravitational and electromagnetic radiation– makes the contribution due to the quadrupole motion of the source to be the relevant term in the computation of the metric. In these circumstances, equation (2.44) can be rewritten in a useful way according to the approximations by using the conservation laws $T^{\mu\nu}_{\ ,\nu} = 0$ for the energy-momentum tensor, so that the only nonvanishing contributions in the TT gauge are:

$$h_{ij}(x) = \frac{2G}{r}\ddot{Q}_{ij}(t-r). \tag{2.45}$$

Q_{ij} is the trace-free part of the second moment of the source's mass density ρ evaluated at the retarded time $(t-r)$:

$$Q_{ij}(t) = \int \left(x_i x_j - \frac{1}{3}|\mathbf{x}|^2\delta_{ij}\right) T_{00} d^3x', \tag{2.46}$$

as computed in a Cartesian coordinate system centred on the source, and taking into account that the energy density T_{00} can be substituted by the rest-mass density $\rho(t)$ of the system, which is dominant in slow motion.

Equivalently, Q_{ij} could also be read off the coefficient of the $\frac{1}{r^3}$ part of the Newtonian gravitational potential of the source of mass M:

$$\phi = -\frac{M}{r} - \frac{3}{2}\frac{Q_{ij}(t)}{r^3}\frac{x_i}{r}\frac{x_j}{r} - \frac{5}{2}\frac{Q_{ijk}(t)}{r^5}\frac{x_i}{r}\frac{x_j}{r}\frac{x_k}{r} - \cdots, \tag{2.47}$$

since under the assumed hypotheses of slow internal motions and even if the source has strong internal gravity, it can be described with high accuracy as Newtonian at least in a region of space far enough from the source to be in vacuum and far enough from gravity to be weak, yet near enough for retardation and wave behaviour to be unimportant.

It seems that, in principle, one could compute Qij and therefore have the values of h_{ij} for several different emitters, or even the energy loss rate due to the emission of gravitational radiation:

$$\dot{E} = -\frac{G}{5}\dddot{Q}_{ij}\dddot{Q}_{ij} . \tag{2.48}$$

However, it is not an easy task in most cases of interest, and so it would be convenient to find, in the basis of these equations and for a more general understanding, an order of magnitude estimation for (2.45). It can be given by the product [81]

$$\frac{R_0}{r} \times \frac{v^2}{c^2}, \tag{2.49}$$

for a typical source of Schwarzschild radius $R_0 = \frac{2GM}{c^2}$ and typical velocity v. Hence, in the case of Earth-based sources such as ordinary mechanical oscillators, the two terms of (2.49) are very small, what means that vastly more of its energy will always be given out, for instance, to heat than to gravitational radiation. Thus, appreciable generation of gravitational waves must imply enormous masses undergoing not uniform highly swift motions and for this reason potentially measurable GWs have to be searched in the outer Universe.

Sources

Likely astrophysical sources of gravitational radiation [130, 81, 118] can be classified according to the emission duration in short signals, long signals, and a permanent stochastic background.

The most intense are bursts of brief duration related with astrophysical catastrophic events: collapsing stars, supernovæ, coalescencing binaries, or the fall of stars and small holes into supermassive holes. Other candidates, such as pulsars, produce periodic waves which are superpositions of sinusoids with frequencies that are more or less constant over times long compared to an observation run. And finally, a stochastic background

of gravitational waves produced by binary stars in the low frequency range, Population III stars, or relic waves from string cosmology and phase transitions associated with quantum cromodynamics and with electroweak interactions, is predicted to be always present with a continuous frequency spectrum.

Although several models have been developed for describing the physics of such systems and processes, detailed knowledge about them is hardly available, specially if relativistic effects are relevant for their dynamics, what precisely amounts to be the most interesting case. What is commonly done is to assume simplifications which enable at least to calculate order of magnitude estimations.

These estimations for the outgoing flux of gravitational energy of periodic sources producing monochromatic waves give results several orders of magnitude smaller than the typical burst amplitudes [130]. So, the events [50] more easily detectable by most of the cryogenic resonant antennæ are of this kind: massive star collapses or gamma-ray bursters [116], because of their relative large intensity, but also because of their short duration when compared with the characteristic time-scales (the decay time of the mechanical oscillations) of the resonant detectors. Then, it can be done on-line data analyses [83, 13] with the explicit aim of detecting those impulses, or subsequent studies, for instance for timing information [33] or more generally for an optimal reconstruction of the input signal [104].

Among this type of events, one finds that stellar collapses in our Galaxy would produce the most energetic waves likely to be observed on Earth, estimated to produce stresses in spacetime of amplitude about $h \approx 10^{-18}$, which represents tiny strains comparable to a displacement of under one nuclear diameter in a length of 1 m. Unfortunately, their rate of occurrence is fairly well determined observationally to be roughly one type I supernova each 40 years and one type II also each 40 years. If one wants to increase this rate of potentially observable events in a given period of time, it is unavoidable to look for them in more distant places, say in the Virgo cluster at about 10 Mpc, where a few events per year could be detected, but then the strain sensitivity must be appreciably increased to a smaller value around 10^{-21}.

2.2 Detection of Gravitational Waves

As we have seen, gravitational waves received on Earth show a breathtaking weakness that has always handicapped the attempt to measure Gravitational Radiation. However,

experimentalists and theoreticians working on this subject have always vigorously responded to this difficult task.

They have thought up several different methods for measuring gravity waves, what has given place to an important number of suggested different possible detectors which can be classified in accordance to their operational frequency regime: those that work in the high-frequency spectrum, $f \geq 10Hz$, all of them earth-based; and those for low frequencies, $10Hz \geq f \geq 10^{-5}Hz$, and for very low frequencies, $f \leq 10^{-5}Hz$ which must be space-based in order to maximally avoid seismic, acoustic and gravity-gradient noise.

The first kind of receivers includes resonant massive detectors and laser-interferometers of the Michelson type. In addition, other possibilities have been conceived of, although none of these have been taken into practice: other electromagnetically coupled detectors [53] –large microwave cavities in which wall motion driven by GWs upconverts microwave quanta from one mode to another mode of slightly higher frequency, or where GWs interact with a resonating electromagnetic field to change the mode of these quanta or even to create them, etc.–; superfluid interferometers and superconducting circuits based on the direct interaction of a GW and a magnetic field in superconducting solenoids, with the resulting current change monitored by a SQUID [117, 2]...

For low frequencies. Doppler tracking of spacecraft and ambitious interferometers have been proposed, as well as some other less successful techniques and experimental devices. Suggestions refer to measuring the normal modes of the Earth and the Sun [15], the vibrations of blocks of the Earth's crust [16], or to study an Earth-orbiting skyhook consisting of two masses one on each end of a long thin cable with a spring at its centre [18].

At frequencies below about $10^{-5}Hz$, the only sources of gravitational waves are probably stochastic background from the early Universe, and detection involves the use of distant astronomical bodies as *astronomical detectors* of gravity waves [35, 143]: pulsar timing or orbital motions timing of lunar or planetary or binary systems, the search of anisotropies in the temperature of the cosmic microwave radiation, among other astronomical observations that can be used as probes of low-frequency gravitational waves, such as deviations from Hubble flow of galaxies and clusters or peculiarities in primordial nucleosynthesis. Resonant-mass GW detectors are also interesting [132].

All these planned techniques have not had, of course, equal success and had not been pursued in a serious experimental way with the same intensity. Up to this moment, the only actually developed detectors that have been taking data for years are bars of the resonant type, although some prototypes of earth-based laser-interferometers have been

constructed, all of them working at high frequencies above $10Hz$. For the following years, it seems that these detectors will be joined respectively by spherical resonant antennæ, as yet under experimental and theoretical consideration, and space-based interferometers, but also Doppler tracking of spacecraft is foreseen to attract an increasing interest.

2.2.1 Doppler Tracking in Space and Interferometry

One of the two most general procedures to detect gravitational radiation is based on the analysis of the perceptible influence that gravitational waves have on the propagation of light. The main experiments investigating this effect develop two different methods: Doppler tracking of spacecraft and interferometry.

Doppler Tracking in Space

Doppler tracking of spacecraft are the best present gravity wave detectors working at low frequencies at periods between a few minutes and a few hours. These devices are thought to measure variations in h_{ij} due to a gravitational signal, which will produce oscillations in the Doppler shift of electromagnetic radiation. This phenomenon could be observed when an electromagnetic signal travels between two faraway points, say the Earth and a spacecraft orbiting in the Solar System, and coincides in the same region with a GW having a wavelength of the order of the Earth-spacecraft distance. Then, oscillations in the Doppler shift would be produced having a relative magnitude of $\frac{\delta\nu}{\nu} \approx h$, where the metric perturbation is computed in the TT gauge and ν is the frequency of the electromagnetic wave which in practice is controlled by an hydrogen-maser clock with a high stability standard frequency.

The use of Doppler data for gravity-wave searches was first proposed by Braginsky and Gertsenshtein in 1967 [17] and later other author have discussed the subject. Preliminary measurements have already been done with the VIKING, the VOYAGER, the PIONEER 10 and 11, the GALILEO and the ULYSSES spacecraft and will be performed with the CASSINI mission (see [28] and references therein). It is believed that with this last project it should be possible to reach a sensitivity to bursts better than $\approx 10^{-15}$ in the range of frequencies between 10^{-2} and $10^{-4}Hz$, and in the future it is expected to be of order $\approx 10^{-17}$.

However, interferometers can improve these values.

Interferometry

Schematically, interferometers consist of one or more receivers that are operated simultaneously with cross-correlated outputs –the cross-correlation is always necessary to remove spurious noise–. Each receiver works in a very similar way to an interferometer of the Michelson type, with a system of masses and mirrors where a laser beam is sent back to its origin and recombined after travelling a distance along two different paths drawing the so-called arms. Oscillations in the arm-lengths difference $\delta l(t)$ induced by a passing GW produce oscillations in the relative phases of the recombined light which goes to a photodetector. This equipment, by monitoring the changes in intensity, is in effect monitoring the oscillation of $\delta l(t)$ and thence the gravity-wave oscillations $h_{ij}(t)$.

Since the 1970s, when a number of small-scale prototypes were set up using laser interferometers with arm lengths of 3 to 40 m to measure the separation of suspended test masses, important progress has been made. Earth-based prototypes, like those in Glasgow and Garching [102], were considered a previous step to earth-based detectors with kilometric arms and able to work in the frequency range of $10 - 10^3 Hz$ at best strain sensitivity $h < 10^{-23} Hz^{-1/2}$. They are now in construction: TAMA300 [71], GEO600 [88], LIGO [1] and VIRGO [23]. At the same time, the ideas for carrying out interferometer experiments in space began to be developed. They offer the possibility of escaping from the low background noise that is present on Earth and besides of a very long path length which relaxes the requirements on position measurement noise. These experiments are thought to work in the range of $10^{-4} - 1 Hz$, with expected strain sensitivity around $h < 10^{-23} Hz^{-1/2}$. One of these projects is the ambitious LISA [34] of the European Space Agency. It aims for low-frequency sensitivity by employing laser interferometric distance measurements over a very long baseline of $\approx 5 \times 10^6 Km$. Three of these baselines form an equilateral triangle with spacecraft at each vertex in an Earth-like orbit around the Sun.

2.2.2 Resonant Detectors I. Present Status

The other main method, and historically the first, for the detection of gravitational waves makes use of antennæ of the resonant type.

As known, Weber was the first building a detector of these characteristics [136, 137]. He constructed large, heavy, solid cylindrical aluminium bars of $M = 1.4 \times 10^3$ Kgr, length $L_0 = 1.5$ m, first resonant frequency $\Omega = 10^4 s^{-1}$ and a quality factor Q about 10^5 (the quality factor is given by $Q = \pi \Omega \tau$, where τ is the time that the amplitudes

of oscillations in the bars take to drop by a factor of e –i.e., it is the decay time of the mode– so that Q is a measure of the energy losses of the cylinders when they vibrate). It has been this Weber's experimental philosophy and practice of using bars that has prevailed and developed up to present day.

Bars [130] become operative when undergoing mechanical oscillations that are thought to be potentially driven by gravitational waves, with a maximum efficiency if the antenna is tuned so that its resonant frequency Ω is equal to the frequency of the incident wave and its axis is perpendicular to the direction of propagation of the gravitational perturbation –what is just a reflection of the fact that GW, like electromagnetic waves, are transverse.

A transducer converts the information about the bar's oscillations into an electrical signal, and an amplifier and a recording system are also needed. The transducer is formed by the coupled system of a resonator and an amplifier. It is very much lighter than the cylinder and is designed to couple mechanically to the bar and is typically mounted on one of its ends, producing an output voltage or current proportional to the displacement $x(t)$ of the bar's end from equilibrium. As a consequence of the fact that this transducer has also a main resonant frequency very close to the fundamental one of the detector –ideally it would be the same–, a pre-electronics mechanical magnification of the amplitude is acquired by this particular tuning that makes the vibrational energy to be resonantly transferred between the bar and the transducer.

By the application of the elasticity theory to the bar ends, approximating its behaviour to that of a one-dimensional finite medium described with a harmonic-oscillator model to derive and solve the corresponding dynamical equations for the displacement $x(t)$, it is found that the response of the antenna at the frequency associated to its fundamental mode can be expressed in the form

$$x(t) = X\, e^{-2\pi i \Omega t}, \tag{2.50}$$

so that an impinging gravitational wave will produce length changes in the cylinder.

After the first Weber's experiments, other room-temperature resonant antennæ like GEOGRAV [21] were designed and built. However, a second generation of technically enhanced cryogenic detectors appeared in the late seventies with the development of the ALTAIR [14] detector. Since 1990, these cryogenic resonant antennæ have been the only detectors in continuous operation and data have been recorded by EXPLORER [101, 7], ALLEGRO [93] or NIOBE [59]. More recently, the ultracryogenic AURIGA [26] antenna at Legnaro in Padua and the NAUTILUS [9] detector of the INFN laboratories

currently work with continuity at such low temperature as $0.1K$ and have entered into coincident operation for the search of wave bursts and for the measurement of stochastic background. Finally, in Tokyo a resonant antenna of a particular shape, which has lower natural frequencies for a given size than bars, has been planned resonating at about 60 Hz to detect gravitational waves possibly emitted by the Crab pulsar [125].

EXPERIMENT	LOCATION	START	MASS (Kgr)	T(K)	SENSITIVITY
ALLEGRO (LSU)	Louisiana	June 1991	2300	4	6×10^{-19}
AURIGA (INFN)	Legnaro	1995	2300	0.1	6×10^{-19}
EXPLORER (CERN)	Geneva	July 1990	2270	2.6	6×10^{-19}
NAUTILUS (INFN)	Frascati	94-95	2300	0.1	6×10^{-19}
NIOBE	Perth	June 1993	1500	6	6×10^{-19}
CRAB	Tokyo	1991	1200	4.2	2×10^{-22}

Table 2.1. *Present-day cryogenic resonant bars in different world places, operating since indicated dates. Sensitivity is given is terms of the minimum detectable GW amplitude for a 1ms burst, except for CRAB highest sensitivity, which is attained only for monochromatic sources. All of them are bars, except CRAB.*

The detector burst sensitivity h depends on the time duration of the event τ_b and on the noise temperature T_{eff} of the system, defined such that $K_B T_{eff}$ is the minimum energy increase that can be detected (with a value of the signal to noise ratio, SNR. equal to 1) [51]:

$$h \approx \frac{L}{\tau_b v^2} \sqrt{\frac{K_B T_{eff}}{M}}. \tag{2.51}$$

For monochromatic waves [8], the expression for h is

$$h = \frac{\pi K_B T_t}{MQ\Omega v^2} {\tau_m}^{-\frac{1}{2}} \equiv h_{sa} \times {\tau_m}^{-\frac{1}{2}}, \tag{2.52}$$

where h_{sa} is the so-called spectral amplitude sensitivity and τ_m is the duration of the measurement. This idea of spectral strain amplitude also holds for stochastic background measurements, although the sensitivity is also usually given by the estimation of the energy density per unit logaritmic frequency depending on the closure density of the Universe [132].

Numerical results referring these calculations over current parameters' values [8, 132] show that resonant bars have reached a burst sensitivity of the order of $h \approx 10^{-19}$ – corresponding to a total energy of less than 0.001 solar masses for a source in the Galactic Center. Their spectral amplitude sensitivity would be of less than $1 \times 10^{-21} Hz^{-1/2}$ –with such a value they can detect monochromatic waves with an amplitude of $h \approx 2 \times 10^{-25}$ for one year of integration–, and about $h \approx 7 \times 10^{-22} Hz^{-1/2}$ for stochastic background radiation.

In addition to bars, other new projects for resonant detectors are beginning. Most of the groups referred above as well as others are considering the possibility of new resonant detectors with spherical shape. Spherical detectors have basically two advantages with respect to bars: it is possible to use much heavier antennæ and the spherical detector is omnidirectional. In fact, one sphere is equivalent to six bars properly oriented each one with a mass $\frac{3}{4}$ of the mass of the sphere [27, 29]. Estimations of the sensitivity for a 3m sphere resonating at $1KHz$ and cooled down to $20mK$ give, for $1ms$ bursts, an approximate strain of $h \approx 3 \times 10^{-22}$; the spectral amplitude sensitivity would be of $h \approx 7 \times 10^{-24} Hz^{-1/2}$ and the sensitivity for monochromatic waves should approach $h \approx 10^{-27}$; and finally, the cross-correlation of two such large detectors for one year can give a sensitivity for stochastic background of the order of $h \approx 10^{-26} Hz^{-1/2}$ [108, 132].

2.2.3 Resonant Detectors II. Future Spherical Antennæ

We would like to emphasize the motivation for changing from bars to spherical detectors. In a few words, the aim is to optimize the capabilities of resonant antennæ.

One possibility for reaching this objective with present cylindrical detectors is to control noise in bars. Detectors respond not only to the influence of an impinging wave but also to any external or internal perturbation. Two important sources of such kind are the thermal noise in the cylinders and the noise in the sensors of the readout system. Both of them combine to determine the so-called noise temperature of the antennæ T_n. It is clear that by lowering down this T_n by the use of cryogenic and ultracryogenic techniques and by including low noise quantum-based amplifiers of the SQUID type. the sensitivity of bars could be increased. One needs also to increase the bandwidth of transducers and enhance their matching to the amplifiers and to the bar; it would also be advantageous to maximize the fundamental bar mode's quality factor Q, since larger is its value, more time the oscillation induced by a perturbation will remain increasing the chance of detection.

Nevertheless, there are other possibilities to improve resonant massive antennæ that are independent of the noise temperature. The cross section of the antennæ could be optimized, or one could construct many of them, each aimed in a different direction, so every source direction and polarization, which could be determined, will be in the most sensitive part of at least one device pattern. However, there already exists one more way of making a further step that will provide all these advantages: the introduction of a more adequate geometry, the spherical geometry.

From a strictly theoretical point of view, a solid elastic sphere is the best resonant mass GW antenna, obviously omnidirectional, that one can possibly think of, yet practical difficulties have prevented their construction so far.

One requirement for practicality is the use of a multiple transducer set, since the single sensor used for bars would be insufficient to take advantage of *the perfect matching between the structure of the Riemann tensor of a general metric and the sphere's vibration modes* [80]. The GW radiation patterns were already presented in section 2.1.3., where we saw how a general metric generates a tidal field of forces in elastic bodies which is given in terms of equation (2.37) reproduced here:

$$\begin{aligned} \mathbf{f}(\mathbf{x},t) &= \sum_{\alpha} \mathbf{f}^{(\alpha)}(\mathbf{x}) g^{(\alpha)}(t) \\ &= \mathbf{f}^{(00)}(\mathbf{x}) g^{(00)}(t) + \sum_{m=-2}^{m=2} \mathbf{f}^{(2m)}(\mathbf{x}) g^{(2m)}(t), \end{aligned} \tag{2.53}$$

where we recall that $g^{(\alpha)}(t)$ are suitable combinations of the Riemann tensor components $R_{0i0j}(t)$ which carry all the dynamical information on the GW's monopole (00) and quadrupole ($2m$) amplitudes. On the other hand, the high degree of symmetry in a free elastic sphere results in a simple mathematical structure of its vibration eigenmodes divided into two families: toroidal and spheroidal modes, ordered into ascending series of l-pole harmonics, being their frequencies $(2l+1)$-fold degenerate. It happens that only monopole, $l = 0$, and quadrupole, $l = 2$, spheroidal modes can possibly be excited by an incoming metric GW [11] (see section 3.1. in Chapter 3), and their driven amplitudes are directly proportional to the GW amplitudes $g^{(\alpha)}(t)$ of equation (2.53), so that these are the quantities to be determined by a GW detector on the basis of suitable measurements of its vibrations.

Consequently, a spherical antenna is particularly well adapted to sense metric tidal GW excitations and, when suitably monitored, can generate knowledge on the gravi-

tational wave amplitudes, including the associated to monopole gravitational radiation, and on the incidence direction and wave polarizations [133, 90]. In other words, up to this moment, it is the only existing possibility for an ***individual multimode device.*** Even wave form information could be obtained by the construction of a set of spherical detectors with decreasing sizes so that their fundamental frequencies form an ascending series, which would constitute a wideband detector or ***xylophone*** with a further improved sensitivity, even better than planned for interferometers in the range of frequencies over $750Hz$ [32].

Furthermore, they present *good sensitivity not only at the first but also at the second quadrupole harmonics* [32], and besides *it has a higher absorption cross section than a cylinder* [133]. The absorption cross section is the ratio of the fraction of energy $E_A(\omega)$ carried by the incoming radiation that will be absorbed by the antenna, to the incoming flux $F(\omega)$ of GWs of angular frequency ω impinging on it:

$$\sigma_{ab}(\omega) = \frac{E_A(\omega)}{F(\omega)}. \tag{2.54}$$

According to calculations comparing a sphere to a cylindrical bar of the same material and same resonance frequency (for this being accomplished, cylinder's length must be roughly equal to sphere's diameter), the sphere has a larger cross section because of its larger mass and because it is omnidirectional, thus avoiding the severe problem of the non-optimal orientation of the bar antennæ at signal's arrival time since cylinder's amplitude sensitivity is direction dependent, dropping as much as $\sin^2(\theta)$ for an angle θ between the detector's axis and the incoming radiation direction.

We present a realistic[3] example in table 2.2, to emphasize some of these relevant results, where we see that the sphere has an energy sensitivity over 20 times that of a cylinder at the first mode. Even more, and in contrast to bars whose fundamental mode is the only one showing a significant cross section value, the second sphere's mode still shows a rather large cross section, only about half the maximum for the fundamental mode and still over 15 times bigger than that associated to the cylinder for its first mode. So, a spherical antenna is potentially sensitive at two frequencies, this being a new advantage of this kind of detectors over cylindrical ones.

Cautiously, one may expect that these presumed advantages of a sphere could be lost if the practical requirement of a clear understanding of its dynamical behaviour is not

[3]The quoted numbers for cylinder correspond to the existing detectors EXPLORER, NAUTILUS, AURIGA and ALLEGRO.

Characteristic magnitudes	CYLINDER	SPHERE
Resonant frequencies (Hz)	$\nu_1 = 910$	$\nu_1 = 910$ $\nu_2 = 1747$
Dimensions (m)	$D = 0.6$ $L = 3.1$	$D = 3$
Mass (tons)	$M = 2.3$	$M = 42$
Cross Sections (cm^2 Hz)	$\sigma_1 = 4.3 \times 10^{-21}$	$\sigma_1 = 9.2 \times 10^{-20}$ $\sigma_2 = 3.5 \times 10^{-20}$
Other	Optimal Orientation	Omnidirectional

Table 2.2. *Integrated cross sections for a standard cylinder in its first longitudinal mode and optimal orientation and for a sphere in its two quadrupole modes.*

achieved. That is why, in what follows, we are going to proceed with the development of a rigorous theoretical model describing its performance.

Chapter 3

SPHERICAL ANTENNÆ

As a multimode antenna, a spherical GW detector requires for motion sensing a set of transducers attached to its surface at suitable locations. These transducers will amplify the extremely tiny oscillations of the antenna's surface potentially induced by a passing GW, converting them into readable information. If they are of the resonant type, their motion couples to that of the sphere bringing about desirable advantages, such as that of a pre-electronics amplification of the measured quantities, but also new complexities due to the back action effects which are non negligible in the study of fine structure details of the system, whose significance grows along with the control improvement of the various antenna experimental parameters. Thus, a complete dynamical analysis of the coupled device, or in other words, the resolution of the *resonator problem*, is essential for the correct interpretation of the detector's readout.

In this chapter we present in full theoretical rigour this analysis. It results in an elegant description of the physical perfomance of spherical resonant GW antennæ, arising from a powerful mathematical scheme founded on Green function formalism, Laplace transformation and perturbative developments. More specifically, we will see how this perturbative approach will provide, to any desired order of precision. the frequency spectrum of the antenna and the amplitude readouts in the resonators locations. Summing up, we are going to obtain the solutions of the general equations of motion for the coupled system formed by the perfect sphere and the set of identical resonators, when influenced by an external force which can be a GW signal, of course, but also a calibration signal, for example. In both cases. it will be shown that under certain specific requirements there exist certain suitable linear combinations of the resonators' readouts which directly yield the quadrupole amplitudes for GW inputs, or the hitting point position for calibration

signals of the point-like impulse type. This fact is really advantageous because signal and direction deconvolution methods can take benefit from directly working with these arrangements called mode channels.

As a preliminary step, we shall review some derivations concerning the dynamical behaviour of the free uncoupled sphere in order to recover some results that become indispensable in our subsequent treatment of the resonator problem. Also, some remarks about the structural components, functioning and modelling of resonators themselves will be briefly pointed out.

3.1 The Bare Sphere

A GW antenna, spherical or not, is considered as a coupled device formed by an elastic solid of a given shape and a set of resonators (or just one for bars). A general outline of the way in which it works will require the study of the system as a whole. However, this analysis is in fact constructed on the basis of the outcomes obtained from the investigation of the dynamical behaviour of the uncoupled elastic solid constituting the detector.

Thus, before undertaking the task of describing mathematically and physically the complete spherical antenna, it is unavoidable to previously know some essential features concerning the uncoupled sphere. So, in subsection 3.1.1 we first look at the idealized case of a free, elastic, spherical solid exhibiting time-dependent, periodic vibrations when subject to neither external forces nor surface tractions. These motions are known as normal modes of vibration, and provide the basis for building and understanding the induced small deformations that the detector undergoes when influenced by a general driving force, or more concretely by a tidal driving force $\mathbf{f}(\mathbf{x}, t)$ derived from the Riemann tensor of a metric theory of gravity. The basic features referring this situation are collected in subsection 3.1.2.

Analyses of normal modes of vibration of elastic bodies, also of spherical shape, can be found in classical works on elasticity theory [68, 75, 87, 78], but also in more modern papers [4, 133, 80, 97, 95] being to our knowledge [103] the most complete survey. For the study of the problem of how an impinging gravitational wave interacts with solid homogeneous elastic bodies within the framework of a generalization of the classical theory of elastic media emerging from General Relativity, see [103, 24, 25, 60, 94, 106, 122].

We are going to summarize some of these results.

3.1.1 Normal Modes of Vibration

Normal modes of vibration of homogeneous, isotropic, elastic bodies with constant density ϱ and Lamé coefficients λ and μ describing their elastic properties are solutions of the homogeneous equation

$$\varrho\frac{\partial^2\mathbf{u}}{\partial t^2} - \mu\nabla^2\mathbf{u} - (\lambda+\mu)\,\nabla(\nabla\cdot\mathbf{u}) = 0, \tag{3.1}$$

satisfying suitable boundary conditions on the body's surface. The above equation is derived from the Classical Theory of Elasticity [78], and $\mathbf{u} \equiv \mathbf{u}(\mathbf{x}, t)$ stands for the vector field of elastic displacements in the solid.

Equation (3.1) is of the separable type for $\mathbf{x}$ and t; in consequence, the general form for its homogeneous periodic solutions is also separable and expressable as the following product of a function $\mathbf{u}(\mathbf{x})$ of the space coordinates times an exponential function of the time coordinate:

$$\mathbf{u}(\mathbf{x}, t) = \mathbf{u}(\mathbf{x})\, e^{i\omega t}, \tag{3.2}$$

where the spatial part $\mathbf{u}(\mathbf{x})$ satisfies the equation

$$(\lambda+\mu)\,\nabla(\nabla\cdot\mathbf{u}) + \mu\nabla^2\mathbf{u} = -\varrho\omega^2\mathbf{u} \tag{3.3}$$

as well as homogeneous boundary conditions.

Due to its vectorial character, $\mathbf{u}(\mathbf{x})$ splits up into its irrotational and divergence-free components, or respectively longitudinal and transversal components:

$$\mathbf{u} = \mathbf{u}_t + \mathbf{u}_l, \tag{3.4}$$

with

$$\nabla\cdot\mathbf{u}_t = 0, \quad \nabla\times\mathbf{u}_l = 0. \tag{3.5}$$

Introducing this splitting into (3.3), one finds that both $\mathbf{u}_t$ and $\mathbf{u}_l$ obey differential equations of the Helmholtz type:

$$\nabla^2\mathbf{u}_t + k^2\mathbf{u}_t = 0, \qquad k^2 \equiv \frac{\varrho\omega^2}{\mu}, \tag{3.6}$$

$$\nabla^2\mathbf{u}_l + q^2\mathbf{u}_l = 0, \qquad q^2 \equiv \frac{\varrho\omega^2}{\lambda+2\mu}. \tag{3.7}$$

In fact, we are dealing with an eigenvalue problem in a Hilbert space –clearly, equations (3.3), (3.6) or (3.7) are eigenvalue equations. Solutions $\mathbf{u}(\mathbf{x})$ will form a denumerably infinite set, each of its components labelled $\mathbf{u}_I(\mathbf{x})$ with associated eigenfrequency ω_I. They are known as normal modes of vibration, describe the unforced oscillations of the elastic body and are bound to satisfy the homogeneous conditions:

$$\lambda(\nabla \mathbf{u}_I)\mathbf{n} + 2\mu \mathbf{u}_I \nabla \mathbf{u}_I + \mu \mathbf{n} \times (\nabla \times \mathbf{u}_I) = 0 \quad \text{at } r = R, \tag{3.8}$$

which ensure the absence of tractions on the body's surface, with normal vector $\mathbf{n}$. From (3.3) and (3.8), these normal modes are orthogonal and admit only real eigenfrequencies.

In the case of solids with spherical symmetry, the resolution of the former equations in spherical coordinates (r, θ, φ) leads to expressions depending on the Bessel functions of the first kind, $j_l(qr)$ [56], plus the spherical harmonics, $Y_{lm}(\theta, \varphi)$ [61]. After rather lengthy algebra, two families of independent normal modes arise: spheroidal modes $\mathbf{u}_I^S(\mathbf{x})$ showing longitudinal distortions $\mathbf{u}_l$ as well as transverse displacements contributing to $\mathbf{u}_t$, and the purely tangential toroidal modes $\mathbf{u}_I^T(\mathbf{x})$, depending only on $\mathbf{u}_t$. We are not going to give the details of the computation here, since this is a highly complicated and sophisticated task published and presented with clarity in [103, 80]. We simply quote here the final results:

$$\begin{aligned} \mathbf{u}_I^S(\mathbf{x}) \equiv \mathbf{u}_{nlm}^S(\mathbf{x}) &= A_{nl}(r) Y_{lm}(\theta, \varphi)\mathbf{n} - B_{nl}(r)\mathbf{n} \times i\mathbf{L}Y_{lm}(\theta, \varphi) \\ \mathbf{u}_I^T(\mathbf{x}) \equiv \mathbf{u}_{nlm}^T(\mathbf{x}) &= C_{nl}(r) i\mathbf{L}Y_{lm}(\theta, \varphi), \end{aligned} \tag{3.9}$$

where $\mathbf{L} = -i\mathbf{x} \times \nabla$ is the angular momentum operator and $A_{nl}(r)$, $B_{nl}(r)$ and $C_{nl}(r)$ are complicated functions given in Appendix A, which contain the spherical Bessel functions and give the relative amplitudes of the r-independent fields $Y_{lm}\mathbf{n}$, $\mathbf{n} \times i\mathbf{L}Y_{lm}$ and $i\mathbf{L}Y_{lm}$.

As we see, I is an abbreviation for a multiple index $\{nlm\}$, n running from 1 to infinity and, as usual, l denoting a multiple integer index from zero to infinity while m can take any integer value from $-l$ to l.

In a perfect sphere each n-fixed set of $l = 2$ quadrupole eigenmodes –just the interesting for GW interaction, along with $l = 0$ monopole ones– has five normal modes of vibration distinguished only by their angular dependence. All of them are degenerate in frequency. In [103] one can find not only an accurate derivation of the related analytical expressions but also detailed numerical tables showing the values of the first eigenfrequencies for a realistic aluminium spheric prototype, according to the parameters and

data given in [31]. We reproduce the spheroidal spectrum in Figure A.1 of Appendix A.

3.1.2 Response to Specific Signals

The nice mathematical structure of the sphere oscillation normal modes shown above allows its perfect coupling to that of the Riemann tensor of any metric theory which enters the equations of motion as a tidal driving force $\mathbf{f}(\mathbf{x},t)$ if measurements taken in a normal coordinate system, the locally newtonian one, are considered. Normal coordinates are those attached to a freely falling object and valid at distances which are small compared to the radius of curvature, what amounts to saying that the detector's size is small compared to the wavelength of the signal, which shall always be the case for realistic resonant detectors. Also admitting that relativistic motions will not occur at expected GW typical frequencies ($\approx$ in the range of 1 KHz), the equation of motion reads

$$\varrho\frac{\partial^2\mathbf{u}}{\partial t^2} - \mu\nabla^2\mathbf{u} - (\lambda+\mu)\,\nabla(\nabla\cdot\mathbf{u}) = \mathbf{f}(\mathbf{x},t). \tag{3.10}$$

Green Function Formalism

Equation (3.10) applies to any driving force. It is in fact very general, and for the moment we are going to avoid constriction to particular cases. The only proviso will be that $\mathbf{f}(\mathbf{x},t)$ be of the separable type, i.e., it must have the form of a product of a function of the space variable $\mathbf{x}$ times a function of the time variable t, when properly written:

$$\mathbf{f}(\mathbf{x},t) = \mathbf{f}(\mathbf{x})\,g(t), \tag{3.11}$$

or linear combinations of similar terms.

One can formally represent the solution by the application of a Green function formalism [123], which introduces a Green's operator $G(\mathbf{x};t,t')$ defined by the impulse equation

$$\left[\varrho\frac{\partial^2}{\partial t^2} - \mu\nabla^2 - (\lambda+\mu)\,\nabla(\nabla)\right] G(\mathbf{x};t,t') = \mathbf{f}(\mathbf{x})\,\delta(t-t'). \tag{3.12}$$

The Green's function is therefore a solution for the case which is –here, inhomogeneous in space but– homogeneous in time, except at one point $t = t'$ representing the precise instant when the signal hits the body.

Multiplying both sides of (3.12) by $g(t')$ and integrating over the same variable t', it is easy to see that the formal solution to (3.10) can be written down in terms of the Green function integral

$$\mathbf{u}(\mathbf{x},t) = \int_0^\infty G(\mathbf{x};t,t')\, g(t')\, dt'. \tag{3.13}$$

$G(\mathbf{x};t,t')$ satisfies the initial condition

$$G(\mathbf{x};0,t') = \dot{G}(\mathbf{x};0,t') = 0, \tag{3.14}$$

necessary if we want that at the initial time and previously the solid be at rest and undeformed:

$$\mathbf{u}(\mathbf{x},0) = \dot{\mathbf{u}}(\mathbf{x},0) = 0. \tag{3.15}$$

The following matching conditions also hold

$$\begin{aligned} G(\mathbf{x};t'+0,t') - G(\mathbf{x};t'-0,t') &= 0 \\ \dot{G}(\mathbf{x};t'+0,t') - \dot{G}(\mathbf{x};t'-0,t') &= \frac{1}{\varrho}\mathbf{f}(\mathbf{x}), \end{aligned} \tag{3.16}$$

stating that the Green function is a regular continuous solution for t', except at the point $t = t'$ where it has a singularity as a consequence of the presence of the unit point inhomogeneous time term in the right hand side of (3.12).

Since $\mathbf{u}_I(\mathbf{x},t)$, of the form in (3.2), are just the orthogonal solutions of the eigenvalue problem associated to the homogeneous counterpart of equation (3.10), they form a complete set whereby $G(\mathbf{x};t,t')$, as any other piecewise continuous function, can be expanded as a superposition of eigenfunctions

$$G(\mathbf{x};t,t') = \sum_I \mathbf{u}_I(\mathbf{x}) \left[A_I(t') e^{-i\omega_I t} + B_I(t') e^{i\omega_I t} \right] \qquad t > t'. \tag{3.17}$$

Obviously, $G(\mathbf{x};t,t')$ is null in the time range $t < t'$ for the period before the action of the impinging force.

After determining the complex functions $A_I(t')$ and $B_I(t')$ from the matching conditions (3.16),

$$\begin{aligned} A_I(t') &= \frac{1}{2i\omega_I} f_I\, e^{i\omega_I t'} \\ B_I(t') &= -\frac{1}{2i\omega_I} f_I\, e^{-i\omega_I t'}, \end{aligned} \tag{3.18}$$

where the spatial contribution to the gravitational effective force for mode I of the sphere is

$$f_I = \frac{1}{M}\int \mathbf{u}_I^*(\mathbf{x})\,\mathbf{f}(\mathbf{x})\,d\mathbf{x}, \tag{3.19}$$

the final Green function can be written

$$G(\mathbf{x};t,t') = \begin{cases} 0 & t \le t' \\ \sum_I \frac{f_I}{\omega_I}\mathbf{u}_I(\mathbf{x})\sin\omega_I(t-t') & t \ge t'. \end{cases} \tag{3.20}$$

Consequently, the formal solution (3.13) to the non-homogeneous equation (3.10) is the orthogonal expansion

$$\mathbf{u}(\mathbf{x},t) = \sum_I \frac{f_I}{\omega_I}\mathbf{u}_I(\mathbf{x})\,g_I(t), \tag{3.21}$$

with

$$g_I(t) = \int_0^t g(t')\sin\omega_I(t-t')\,dt'. \tag{3.22}$$

These expressions are valid for a solid of any shape, whenever its normal modes of vibration are $\mathbf{u}_I(\mathbf{x})$, when driven by *any* separable force like (3.11). We must begin to get down to cases.

Interaction with a Tidal Driving Force

If $\mathbf{f}(\mathbf{x},t)$ is in fact a tidal driving force associated to an incoming GW, it reads

$$\begin{aligned} \mathbf{f}(\mathbf{x},t) &= \sum_\alpha \mathbf{f}^{(\alpha)}(\mathbf{x})g^{(\alpha)}(t) \\ &= \mathbf{f}^{(00)}(\mathbf{x})g^{(00)}(t) + \sum_{m=-2}^{m=2}\mathbf{f}^{(2m)}(\mathbf{x})g^{(2m)}(t), \end{aligned} \tag{3.23}$$

as we saw in section 2.1.3 of chapter 2, being $g^{(00)}(t)$ and $g^{(2m)}(t)$ the monopole and the quadrupole amplitudes of the Riemann tensor carrying all the dynamical GW information, while $\mathbf{f}^{(00)}$ and $\mathbf{f}^{(2m)}$ were pure tidal form factors.

In this case, and for spherically shaped solids, the solution (3.21) is found to be a combination of normal modes $\mathbf{u}_{nlm}(\mathbf{x})$ in equation (3.9):

$$\begin{aligned}\mathbf{u}(\mathbf{x},t) &= \sum_{\alpha}\mathbf{u}_{\alpha}(\mathbf{x},t)\\ &= \sum_{nlm,\alpha}\frac{f^{(\alpha)}_{nlm}}{\omega_{nl}}\,\mathbf{u}_{nlm}(\mathbf{x})\,g^{(\alpha)}_{nl}(t)\end{aligned} \tag{3.24}$$

with

$$g^{(\alpha)}_{nl}(t)=\int_0^t g^{(\alpha)}(t')\sin\omega_{nl}(t-t')dt' \tag{3.25}$$

as in (3.22), and

$$f^{(\alpha)}_{nlm}=\frac{1}{M}\int \mathbf{u}_{nlm}(\mathbf{x})^{*}\mathbf{f}^{(\alpha)}(\mathbf{x})\,d\mathbf{x}. \tag{3.26}$$

as in (3.19).

Taking into account the explicit expressions (2.38) for $f^{(\alpha)}(\mathbf{x})$ in section 2.1.3 of Chapter 2, calculations of the spatial gravitational effective forces $f^{(\alpha)}_{nlm}$ for a sphere of radius R and mass M give [80]

$$f^{(\alpha),T}_{nlm} = 0 \qquad \forall\,\alpha, nlm \tag{3.27}$$

$$\begin{aligned}f^{(00),S}_{nlm} &= -\frac{1}{M}\delta_{l0}\delta_{m0}\int_0^R r^3 A_{n0}(r)\varrho dr\\ &= a_{n0}(R)\delta_{l0}\delta_{m0}\\ f^{(2m),S}_{nlm'} &= -\frac{1}{2M}\delta_{l2}\delta_{mm'}\int_0^R r^3\left[A_{n2}(r)+3B_{n2}(r)\right]\varrho dr\\ &= a_{n2}(R)\delta_{l2}\delta_{mm'}\end{aligned} \tag{3.28}$$

for toroidal, superscript T, and spheroidal, superscript S, eigenmodes.

Therefore, the final expression for the dynamical response of spherically shaped perfect elastic bodies when excited by incoming GWs [80, 103] is:

$$\mathbf{u}(\mathbf{x},t)=\sum_{n=1}^{\infty}\frac{a_{n0}(R)}{\omega_{n0}}\mathbf{u}^{S}_{n00}(\mathbf{x})g^{(00)}_{n0}(t)+\sum_{n=1}^{\infty}\frac{a_{n2}(R)}{\omega_{n2}}\left[\sum_{m=-2}^{m=2}\mathbf{u}^{S}_{n2m}(\mathbf{x})g^{(2m)}_{n2}(t)\right] \tag{3.29}$$

As we can see, it remarkably happens that spheres become particularly convenient GW observatories, since only monopole ($l=0$) and quadrupole ($l=2$) spheroidal modes can be excited by any impinging GW, and their amplitudes are directly proportional to the monopole and quadrupole wave amplitudes $g^{(\alpha)}(t)$ of equation (3.24).

Interaction with a Calibration Signal

Taking into account results from (3.10) to (3.22) in the preceding subsection and proceeding analogously, it is now very easy to find the response of the bare sphere to a calibration signal consisting in an impulse of intensity f_0 and delivered perpendicular to the sphere's surface at point $\mathbf{x}_0$ and time $t_0 = 0$:

$$\mathbf{f}_{calibration}(\mathbf{x}, t) = \mathbf{f}_0 \, \delta^{(3)}(\mathbf{x} - \mathbf{x}_0) \, \delta(t). \tag{3.30}$$

We quote the results associated to (3.19), (3.21) and (3.22) in this case. A trivial calculation yields

$$\begin{aligned} f_I \equiv \; f_{nlm} &= \frac{1}{M} \mathbf{f}_0 \, \mathbf{u}^*_{nlm}(\mathbf{x}_0) \\ g_I \equiv \; g_{nlm} &= \sin \omega_{nl} t \qquad \forall m, \end{aligned} \tag{3.31}$$

and

$$\mathbf{u}(\mathbf{x}, t) = \sum_{nlm} \frac{\mathbf{f}_0}{M} \, \mathbf{u}^*_{nlm}(\mathbf{x}_0) \, \mathbf{u}_{nlm}(\mathbf{x}) \, \sin \omega_{nl} t \tag{3.32}$$

is the dynamical response of the uncoupled detector when driven by an impulse calibration signal [80]. Clearly, it excites all of the sphere's vibration eigenmodes except those perpendicular to $\mathbf{f}_0$, with amplitudes which are inversely proportional to the mode's frequency, what is seen to be a rather general result in the theory of sound waves in isotropic elastic solids.

3.2 The Resonators

The previous results not only show that the uncoupled sphere can be used as the core of a GW antenna, but also that its particular geometry offers advantageous detection capabilities. However, for completeness and practicality, a readout device is required for motion sensing and data acquisition.

Motion sensors in current bar antennæ are made up of two essential separate parts: a resonator fastened to one end of the detector and interacting only with the vector component of the antenna motion normal to the surface on which they are mounted[1], and an electromagnetic amplifier.

[1] Interaction with transverse components has also been under theoretical consideration [144].

The last technological advances have led to the use of transducers of the resonant type and d.c. SQUIDs, a quantum-effect based electromagnetic amplifier. A resonant transducer [113, 114, 105, 6, 5] consists in a small, relative to the detector, mechanical device. To get the idea of how small it is in fact, we give here the data of a presently working cryogenic cylindrical antenna: the Explorer detector [7, 101] installed at CERN. It consists on an aluminium bar of $2270Kgr$, in contrast to the light $0.4Kgr$ in weight of the only resonator attached to its surface, so that their ratio is

$$\eta \equiv \frac{m_{transducer}}{M_{bar}} \approx 1.76 \times 10^{-4}. \tag{3.33}$$

Such resonator is usually a mushroom-shaped solid, designed to mechanically couple to the cylinder: it possesses a resonance frequency, associated to one mode of its flexural vibrations, ideally equal to the main resonance frequency of the cylinder. The bar surface motion excites this mode causing a back-and-forth resonant energy transfer between the resonator and the bar, which results in turn in amplified oscillations of the smaller body when compared to the bar ones, the amplification factor depending on η.

This effect of pre-electronics mechanical amplification –small motions of the large antenna turn into large motions of the small resonator– is not the only purpose of resonant transducers. The second task they carry out consists in efficiently turning the cylinder vibrations into electric voltages and currents, for instance by the use of capacitors[2] (Explorer). The transducer has a disk-like part that acts as a constitutive component of a two-plate capacitor connected to other electric elements, so that distances are first turned into voltages and then into currents, ultimately induced by the relative motion between the transducer and the bar end.

Those electric signals are finally fed into a d.c. SQUID –the d.c. Superconducting QUantum Interference Device [22] is nowadays the most sensitive detector of magnetic flux and capable of transforming it into voltages afterwards– for electronics amplification.

Going back to spherical antennæ, it seems natural to restrict our considerations to resonant transducers like the one described in this section, so that one of their own normal modes could be tuned to be resonant with one frequency of the bare sphere's spectrum and they could be considered to move normal to the surface to which they are linked, that is, to move radially.

It is clear that, also, we have to assume a simplified model for calculations, and the first step is to leave aside the electric parts of resonators and just restrict to the mechanical

[2] Inductive transducers (Allegro) or microwave transducers (Niobe) are also commonly used.

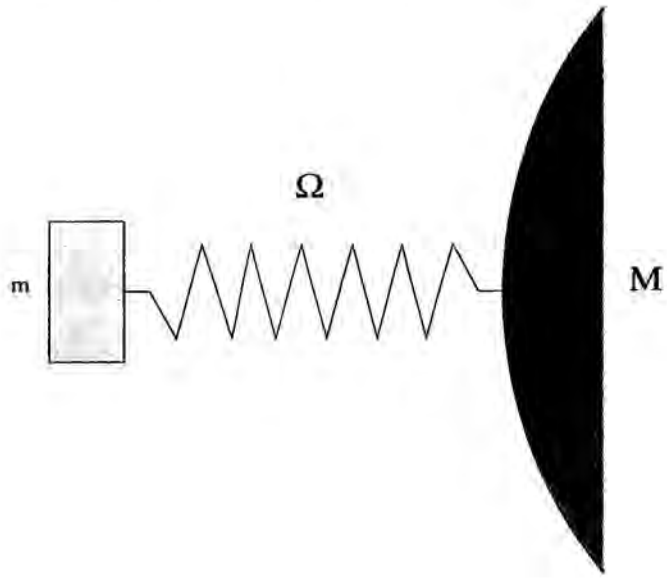

Figure 3.1. *Linear spring coupling model for a resonator attached to the sphere's surface. For clarity, dimensions in this sketch are out of proportion to reality. Actually, the resonator is much smaller than the sphere, over an approximate factor in mass of the order of thousands.*

ones. Then, we shall treat them as point masses attached to one end of a linear spring, whose other end is rigidly linked to the sphere at defined positions. Therefore, each resonator in our model will obey a one-dimensional harmonic oscillator equation.

3.3 Spherical Detectors and the Resonator Problem

Now we are ready to commence the central part of our work undertaking the task of understanding the dynamics of spherical GW antennæ. We are going to study in full theoretical rigor the problem of the coupled motion of a solid elastic perfect sphere and a set of resonators attached to its surface at arbitrary locations [82, 84, 85, 86].

For this purpose, we develop a mathematical scheme that transforms the differential equations of motion associated to the device, as usual derived from elasticity theory, into an algebraic system in the Laplace domain through the application of the powerful

Green function formalism method and Laplace transformation. Finally, by using theory of singularities and calculus of residues for functions of complex variables, we find the frequency spectrum of the system, the resonators' readouts, and when existing their advantageous linear combinations called mode channels, as ascending series in powers of the small coupling constant η, the ratio of the resonators' average mass to the sphere's large mass.

This procedure lead to predictions of all the major system characteristics and response to different incoming signals –calibrational inputs or gravitational waves–, in principle with arbitrary mathematical precision, and, of great importance, lay down a sound basis for further considerations and more realistic practical instances developed in next chapters.

3.3.1 GRD Equations for the Coupled Resonant System

We shall assume that our detector is an elastic isotropic solid perfect sphere of mass M, radius R, uniform density ϱ and Lamé coefficients λ and μ. It behaves in accordance with the Classical Theory of Elasticity, since we recall that relativistic motions in the extremely small displacements that the particles of the elastic body undergo as a result of a impinging gravitational wave at typical frequencies in the range of 1 KHz are not expected.

In these circumstances, equation (3.10) is valid

$$\varrho\frac{\partial^2\mathbf{u}}{\partial t^2} - \mu\nabla^2\mathbf{u} - (\lambda+\mu)\,\nabla(\nabla\cdot\mathbf{u}) = \mathbf{f}(\mathbf{x},t), \tag{3.34}$$

being $\mathbf{u} \equiv \mathbf{u}(\mathbf{x},t)$ as usual the field of elastic displacements in the sphere, and $\mathbf{f}(\mathbf{x},t)$ in this case the density of *all* non-inertial forces acting on it.

As already discussed, this sphere needs a set of J electromechanical transducers of masses $m_a \equiv \eta_a M$ much lighter than the sphere's ($\eta_a \ll 1$), and resonance frequencies Ω_a, being a the subscript that denotes a given resonator and so $a = 1, \ldots, J$. We restrict our considerations to radial motion resonators and quantitatively model them as point masses attached to one end of a linear spring whose other end is rigidly linked to the sphere at locations $\mathbf{x}_a$. So, the quantities describing resonators motion will be their radial displacements $z_a(t)$ relative to the sphere's undeformed surface, which will obey the simplest classical Hooke's law, with a spring deformation given by

$$q_a(t) \equiv z_a(t) - \mathbf{n}_a\mathbf{u}(\mathbf{x}_a,t), \tag{3.35}$$

being $\mathbf{n}_a \equiv \mathbf{x}_a/R$ the outward pointing normal at the a-th resonator's attachement point and consequently $\mathbf{n}_a\mathbf{u}(\mathbf{x}_a,t) \equiv u_a(t)$ the radial deformation of the sphere's surface at $\mathbf{x}_a$.

Thus, the dynamical behaviour of the coupled system is given by the set of $1+J$ differential equations

$$\varrho\frac{\partial^2\mathbf{u}}{\partial t^2} - \mu\nabla^2\mathbf{u} - (\lambda+\mu)\nabla(\nabla\cdot\mathbf{u}) = \mathbf{f}(\mathbf{x},t) \tag{3.36}$$

$$\ddot{z}_a(t) + \Omega_a^2\left[z_a(t) - u_a(t)\right] = \zeta_a(t) \qquad a = 1,\ldots,J. \tag{3.37}$$

with $\zeta_a(t)$ possible external forces affecting the resonators.

External Forces on the Sphere

Equation (3.36) describes, as (3.10), the sphere's motion and contains, in its left hand side, the inertia due to the internal strain forces, whereas $\mathbf{f}(\mathbf{x},t)$ in its right hand side represents all the *external* density forces acting on the solid.

$\mathbf{f}(\mathbf{x},t)$ expediently split into a component due to the resonators back action and an external action *proper*, be it a GW signal or a calibration signal, for example. Thus,

$$\mathbf{f}(\mathbf{x},t) = \mathbf{f}_{resonators}(\mathbf{x},t) + \mathbf{f}_{external}(\mathbf{x},t) \tag{3.38}$$

Since we are making the hypothesis that the resonators are point masses behaving as one-dimensional harmonic oscillators following Hook's law and moving radially, their back action on the sphere will be perpendicular to its surface and will have the locations of resonators' attachement positions as direct hit points:

$$\mathbf{f}_{resonators}(\mathbf{x},t) = \sum_{a=1}^{J} m_a\Omega_a^2\delta^{(3)}(\mathbf{x}-\mathbf{x}_a)\left[z_a(t)-u_a(t)\right]\mathbf{n}_a \tag{3.39}$$

where $\delta^{(3)}$ is the three dimensional Dirac density function. This term of force concentrates all the information about the interaction between sphere and resonators and, as we shall see, it causes a certain level of intercommunication between different vibration eigenmodes of the sphere and is responsible for the fine structure characteristics of the system.

On the other hand, external forces will be *par excellence* gravitational wave signals described as tidal driving forces of the separable type in section 2.1.2. of chapter 2.

$$\begin{aligned} \mathbf{f}_{GW}(\mathbf{x},t) &= \sum_{\alpha} \mathbf{f}^{(\alpha)}(\mathbf{x}) g^{(\alpha)}(t) \\ &= \mathbf{f}^{(00)}(\mathbf{x}) g^{(00)}(t) + \sum_{m=-2}^{m=2} \mathbf{f}^{(2m)}(\mathbf{x}) g^{(2m)}(t), \end{aligned} \tag{3.40}$$

where the explicit form of the several components is given there.

Besides, we shall consider in this work, although as a side subject, the response of the system to a particular calibration signal. We recall it consists in an impulse of intensity f_0 and delivered perpendicular to the sphere's surface at point $\mathbf{x}_0$ and time $t_0 = 0$:

$$\mathbf{f}_{calibration}(\mathbf{x},t) = \mathbf{f}_0 \delta^{(3)}(\mathbf{x} - \mathbf{x}_0)\delta(t). \tag{3.41}$$

External forces for resonators

Resonators themselves could also be affected by external forces $\zeta_a(t)$.

If a GW sweeps the antenna, they will be driven by a tidal acceleration $\zeta_{GW,a}(t)$ relative to the sphere's centre, as well as the spherical detector itself. As always, it can be derived from the geodesic deviation equation (2.26):

$$\frac{\mathbf{f}_j(t)}{m} = R_{0i0j}(t)\, x_i\,, \tag{3.42}$$

and since resonators only move radially,

$$\zeta_{GW,a}(t) \equiv \frac{\mathbf{f}_j(t)}{m}\, n_{a,j} = R_{0i0j}\, R\, n_{a,i}\, n_{a,j} \qquad a = 1, \ldots, J. \tag{3.43}$$

Like in the case of extended bodies, it may now be used the monopole-quadrupole decomposition of the *electric* components of the Riemann tensor:

$$R_{0i0j}(t) = \sum_{\substack{l=0 \text{ and } 2 \\ m=-l,\ldots,l}} E_{ij}^{(lm)}\, g^{(lm)}(t), \tag{3.44}$$

where we recall $E_{ij}^{(lm)}$ verify

$$E_{ij}^{(lm)} n_i n_j = Y_{lm}(\mathbf{n}), \qquad l = 0, 2, \quad m = -l, \ldots, l, \tag{3.45}$$

so that

$$\zeta_{GW,a}(t) = \left(\sum_{\substack{l=0 \text{ and } 2 \\ m=-l,\ldots,l}} E_{ij}^{(lm)}\, g^{(lm)}(t) \right) x_{a,i}\, n_{a,j}$$
$$= R \sum_{\substack{l=0 \text{ and } 2 \\ m=-l,\ldots,l}} Y_{lm}(\mathbf{n}_a) g^{(lm)}(t), \qquad a = 1, \ldots, J. \tag{3.46}$$

In return, we are just going to consider impulse calibration signals always delivered just on the sphere's surface, so not having a *direct* effect on the resonators, and hence

$$\zeta_{calibration,a}(t) = 0 \qquad a = 1, \ldots, J. \tag{3.47}$$

GRD Equations

Our equations for the general resonant detector, named GRD equations, can be rewritten as:

$$\varrho \frac{\partial^2 \mathbf{u}}{\partial t^2} - \mu \nabla^2 \mathbf{u} - (\lambda + \mu)\, \nabla(\nabla \cdot \mathbf{u}) = \sum_{a=1}^{J} m_a \Omega_a^2 \delta^{(3)}(\mathbf{x} - \mathbf{x}_a)\, [z_a(t) - u_a(t)]\, \mathbf{n}_a$$
$$+ \mathbf{f}_{external}(\mathbf{x}, t) \tag{3.48}$$

$$\ddot{z}_a(t) + \Omega_a^2\, [z_a(t) - u_a(t)] = \zeta_a(t) \qquad a = 1, \ldots, J \tag{3.49}$$

where $\mathbf{f}_{external}(\mathbf{x}, t)$ will be given by either (3.40) or (3.41) as the case may be, and likewise $\zeta_a(t)$ respectively by (3.46) or (3.47).

At this point, it is important to emphasize that although these equations have been reported as those for the *sphere* plus resonators, in fact they are completely general, valid for any solid body and boundary conditions, and so valid for *any detector shape* and also for *any configuration of resonant transducers.*

3.3.2 Mathematical Framework

The remainder of this chapter will be concerned with finding the solutions to the GRD equations of motion, but before proceeding to make further hypotheses utterly necessary to completely solve them, we shall deal first with the procedure's general guidelines that will establish the suitable mathematical framework. This procedure comes in two essential stages:

- the use of the *Green function theory* to obtain from the GRD equations the corresponding integro-differential system;
- the application of *Laplace transforms* to reduce the former system to a linear one of algebraic equations.

Green Function Formalism

We first look at equation (3.48). The general procedure of subsection 3.2.1. is also applicable to it, which indeed is a particular version of (3.10) where $\mathbf{f}(\mathbf{x},t)$ can be considered as the back action of resonators, $\mathbf{f}_{resonators}$, plus a component due to external forces, $\mathbf{f}_{external}$. It is always the case that all terms in $\mathbf{f}(\mathbf{x},t)$ are of the separable type:

$$\mathbf{f}^{(a)}_{resonators}(\mathbf{x}) = m_a\Omega_a^2\delta(\mathbf{x}-\mathbf{x}_a)\mathbf{n}_a \tag{3.50}$$

$$g^{(a)}_{resonators}(t) = z_a(t)-u_a(t) \qquad a=1,\ldots,J, \tag{3.51}$$

and generally for $\mathbf{f}_{external}$

$$\mathbf{f}_{external}(\mathbf{x},t)=\sum_{\alpha}\mathbf{f}^{(\alpha)}(\mathbf{x})g^{(\alpha)}(t). \tag{3.52}$$

In these circumstances, we recall that the formal solution reads

$$\begin{aligned}\mathbf{u}(\mathbf{x},t) &= \sum_{\alpha}\sum_{I}\frac{f_I^{(\alpha)}(\mathbf{x})}{\omega_I}\,\mathbf{u}_I(\mathbf{x})\,g_I^{(\alpha)}(t)\\ &= \sum_{\alpha}\sum_{I}\frac{f^{(\alpha)}_{I,ext}(\mathbf{x})}{\omega_I}\,\mathbf{u}_I(\mathbf{x})\,g^{(\alpha)}_{I,ext}(t)+\sum_{a=1}^{J}\sum_{I}\frac{f^{(a)}_{I,res}(\mathbf{x})}{\omega_I}\,\mathbf{u}_I(\mathbf{x})\,g^{(a)}_{I,res}(t)\\ &= \mathbf{u}_{ext}(\mathbf{x},t)+\sum_{I}\frac{\mathbf{u}_I(\mathbf{x})}{\omega_I}\sum_{a=1}^{J}f^{(a)}_{I,res}(\mathbf{x})\,g^{(a)}_{I,res}(t),\end{aligned} \tag{3.53}$$

where *ext* stands for *external*, *res* stands for *resonators*, and $\mathbf{u}_{external}(\mathbf{x},t)$ is the sphere's response to an external force in the absence of resonators, either (3.29) for impinging GWs or (3.32) for calibration signals.

Substituting

$$f^{(a)}_{I,res}(\mathbf{x}) = \frac{m_a}{M}\,\Omega_a^2\,\mathbf{n}_a\,\mathbf{u}_I^*(\mathbf{x}_a)$$

$$g^{(a)}_{I,res}(t) = \int_0^t [z_a(t') - u_a(t')] \sin\omega_I(t-t')\,dt' \qquad a = 1,\ldots,J, \tag{3.54}$$

we obtain

$$\mathbf{u}(\mathbf{x},t) = \mathbf{u}_{ext}(\mathbf{x},t) + \sum_I \frac{\mathbf{u}_I(\mathbf{x})}{\omega_I} \sum_{a=1}^J \frac{m_a}{M}\Omega_a^2 \mathbf{n}_a \mathbf{u}_I^*(\mathbf{x}_a) \int_0^t [z_a(t') - u_a(t')] \sin\omega_I(t-t')\,dt'. \tag{3.55}$$

We now specify $\mathbf{x} = \mathbf{x}_{a_i}$ since the purpose of attaching transducers to the sphere's surface is precisely to sense the sphere motion by sampling at a finite number of positions. Besides, by multiplying the both sides of expression (3.55) by $\mathbf{n}_a$, one finds an integral equation equivalent to (3.48):

$$u_a(t) = u^{(a)}_{external}(t) + \sum_{b=1}^J \eta_b \int_0^t K_{ab}(t-t')\,[z_b(t') - u_b(t')]\,dt'. \tag{3.56}$$

$u_a(t)$ is the scalar function $\mathbf{n}_a\mathbf{u}_{external}(\mathbf{x}_a,t)$, and the Kernel matrix K_{ab} stands for the following weighted sum of diadic products of the perfect sphere wavefunctions:

$$K_{ab} = \Omega_b \sum_I \frac{1}{\omega_I} [\mathbf{n}_b \mathbf{u}_I^*(\mathbf{x}_b)]\,[\mathbf{n}_a \mathbf{u}_I(\mathbf{x}_a)] \sin\omega_I t. \tag{3.57}$$

Finally, η_b are the ratios of the resonators' mass to that of the sphere

$$\eta_b = \frac{m_b}{M} \qquad b = 1,\ldots,J, \tag{3.58}$$

which actually are small dimensionless parameters since $m_b << M_{sphere}$ in a real device.

This last term in (3.56) is introduced by the small parameter η_b –what will allow perturbative developments as we shall see–, and is commanded by the Kernel matrix K_{ab} correlating all of the sphere's spheroidal eigenmodes. Therefore, attachement of resonators to the free sphere causes a cross-communication between modes so that, although initially only some of them could be excited by an incoming signal –like a GW that just couple to monopole and quadrupole spheroidal modes–, energy will be transferred from these into the others creating a flux between the different possible vibration states.

Laplace Transformations

Formula (3.56) describing sphere's deformations mathematically corresponds to an integral equation of the Volterra type [131]. The equations belonging to this category accept a series solution in ascending powers of the small coupling constants η_b by iterative subsitutions of $u_b(t)$ into the kernel integral. However, in this particular case this is not useful because this integral equation forms part of a coupled set, now transformed into the integro-differential system

$$u_a(t) = u^{(a)}_{external}(t) + \sum_{b=1}^{J} \eta_b \int_0^t K_{ab}(t-t')\,[z_b(t') - u_b(t')]\,dt' \tag{3.59}$$

$$\ddot{z}_a(t) = -\Omega_a^2\,[z_a(t) - u_a(t)] + \zeta_a(t) \qquad a = 1, \ldots, J, \tag{3.60}$$

containing the differential equations (3.60) that govern the behaviour of the dynamical contribution of $z_b(t)$ in (3.59).

Nevertheless, there is another general mathematical procedure of resolution based in the application of Laplace transforms (see Appendix B), which will convert the former integro-differential system into a set of coupled algebraic equations:

$$\hat{u}_a(s) = \hat{u}^{(a)}_{ext}(s) + \sum_{b=1}^{J} \eta_b \hat{K}_{ab}(s)\,[\hat{z}_b(s) - \hat{u}_b(s)] \tag{3.61}$$

$$s^2\hat{z}_a(s) - sz_a(0) - \dot{z}_a(0) = -\Omega_a^2\,[\hat{z}_a(s) - \hat{u}_a(s)] + \zeta_a(s). \tag{3.62}$$

Under the assumption that the system is at rest and undeformed before the instant of time $t = 0$.

$$\mathbf{u}(\mathbf{x}, 0) = \dot{\mathbf{u}}(\mathbf{x}, 0) = z_a(0) = \dot{z}_a(0) = 0, \tag{3.63}$$

we write

$$\hat{u}_a(s) = \hat{u}^{(a)}_{external}(s) + \sum_{b=1}^{J} \eta_b \hat{K}_{ab}(s)\,[\hat{z}_b(s) - \hat{u}_b(s)] \tag{3.64}$$

$$s^2\hat{z}_a(s) = -\Omega_a^2\,[\hat{z}_a(s) - \hat{u}_a(s)] + \zeta_a(s) \qquad a = 1, \ldots, J. \tag{3.65}$$

At this point, we make use of the fact that the only measurable quantities are the resonators' elastic deformations $q_a(t)$. related to the equations variables through

$$q_a(t) \equiv z_a(t) - u_a(t). \tag{3.66}$$

Therefore, these are the only quantities of our concern, so that the final step before proceeding to definitely solve the set of equations (3.64)-(3.65) is to make a further transformation and express it as a function of $q_a(t)$ rather than $z_a(t)$ or $u_a(t)$. After some algebraic rearrangement, it is readily seen that the Laplace transform of $q_a(t)$ verifies

$$\sum_{b=1}^{J} M_{ab}\, \hat{q}_b(s) = -\frac{s^2}{s^2+\Omega_a^2}\, \hat{u}_{a,external}(s) + \frac{\hat{\zeta}_a(s)}{s^2+\Omega_a^2}\,, \qquad a = 1, \ldots, J, \tag{3.67}$$

where $M_{ab}(s)$ is the following matrix in the Laplace domain:

$$M_{ab} \equiv \left[\delta_{ab} + \eta_b \frac{s^2}{s^2+\Omega_a^2}\, \hat{K}_{ab}(s)\right], \tag{3.68}$$

and the Laplace transforms of $u_{a,external}$ and K_{ab} read

$$\hat{u}_{a,external}(s) = \sum_{\alpha}\sum_{I} \frac{1}{s^2+\omega_I^2} f^{(\alpha)}_{I,external}\, [\mathbf{n}_a \mathbf{u}_I(\mathbf{x}_a)]\, \hat{g}^{(\alpha)}_{external}(s) \tag{3.69}$$

$$\hat{K}_{ab}(s) = \sum_{I} \frac{\Omega_b^2}{s^2+\omega_I^2} [\mathbf{n}_b \mathbf{u}_I^*(\mathbf{x}_b)] [\mathbf{n}_a \mathbf{u}_I(\mathbf{x}_a)]\,. \tag{3.70}$$

Thus, the process of transformation of the initial *differential GRD system* has effectively led to a set of just J *algebraic equations* (3.67), what constitutes a significant simplification of the original problem.

Now, it is possible to solve (3.67) for the unknowns $\hat{q}_a(s)$ in the Laplace domain, and then perform inverse transforms to revert to time domain (see again Appendix B). This can be done by computing the Fourier-Mellin integral through the residue theorem, for which it is necessary to determine the residues at the poles of $\hat{q}_a(s)e^{st}$.

By inspection of (3.67) and (3.68), it is seen that the poles correspond to those values of s for which the matrix M_{ab} is singular, or equivalently non-invertible, since, contrary to appearances at first sight, there are no poles at $s^2 = -\Omega^2$ or at $s^2 = -\omega_{nl}^2$ because divergences compensate each other at those points when $\hat{q}_a(s)$ is isolated in (3.67).

Thus, the only poles correspond to the zeroes of the determinant:

$$\Delta(s) \equiv \det\, M \equiv \det\left[\delta_{ab} + \eta_b \frac{s^2}{s^2+\Omega_a^2}\, \hat{K}_{ab}(s)\right] = 0. \tag{3.71}$$

As one can find in [58], the imaginary parts of these poles give the system characteristic frequencies or resonances, and residues at such poles determine the specific weight of the respectively associated modes in the system response to a given external agent.

3.4 The Ideal Approximation

The generality of assumptions in last section make the algebraic GRD equations (3.67) applicable to any shaped detector coupled to a set of J resonators in arbitrary locations and which can differ in mass and resonance frequency.

This freedom is highly desirable since then one can evaluate the response of differently shaped antennæ to any external separable force acting on them by following the given procedure's guidelines.

For instance, one could study cylindrical bar detectors, already constructed and currently working and generating data. It would be only necessary to know their normal modes of vibration and associated eigenfrequencies, and restrict to just one transducer with resonance frequency in coincidence with the most suitable frequency of the bar's spectrum. The results obtained from our scheme could in fact corroborate the conclusions drawn from other analyses or provide fine structure details.

But indeed our model has been thought up with a more interesting and complicated purpose: that of finding the dynamical performance of spherical antennæ through a non oversimplified and rigorous development.

We begin with the simplest, most idealized case, of a perfect sphere with perfectly tuned identical resonators. This situation corresponds to the acceptance of four further hypotheses concerning the set (3.67) for the resonators' elastic deformations and the characteristic frequencies.

The first assumption is obvious: the detector is perfectly spherically shaped. It means that its modes of vibration, when uncoupled, as well as its response to external forces, are those of section 3.1. There, we saw that this specific solid has two different families of eigenmodes, toroidal and spheroidal, with eigenfrequencies that can be classified as l-pole series of ascending harmonics, each frequency in a given series being $(2l+1)$-fold degenerate. Since GWs exclusively couple to spheroidal eigenmodes, results (3.27)-(3.28), and the resonators are theoretically sensitive to just radial deformations of the sphere, only spheroidal modes will be relevant:

$$\mathbf{u}_{nlm}(\mathbf{x}) \equiv \mathbf{u}^S_{nlm}(\mathbf{x}) = A_{nl}(r)Y_{lm}(\theta,\varphi)\mathbf{n} - B_{nl}(r)\mathbf{n}\times i\mathbf{L}Y_{lm}(\theta,\varphi), \tag{3.72}$$

with radial projections

$$\mathbf{n}\,\mathbf{u}_{nlm}(\mathbf{x}) = A_{nl}(r)Y_{lm}(\theta,\varphi), \tag{3.73}$$

which introduced into the kernel matrix give

$$\tilde{K}_{ab}(s) = \sum_{nlm}\frac{\Omega_b^2}{s^2+\omega_{nl}^2}|A_{nl}(R)|^2 Y^*_{lm}(\theta_b,\varphi_b)Y_{lm}(\theta_a,\varphi_a). \tag{3.74}$$

Degeneracy of eigefrequencies enables direct summation over the degeneracy index m. Spherical harmonics obey the summation formula

$$\sum_{m=-l}^{l} Y^*_{lm}(\theta_b,\varphi_b)Y_{lm}(\theta_a,\varphi_a) = \frac{2l+1}{4\pi}\mathcal{P}_l(\mathbf{n}_b\mathbf{n}_a) \qquad a,b=1,\ldots,J, \tag{3.75}$$

where $\mathbf{n}_b$ and $\mathbf{n}_a$ are unit vectors associated to directions (θ_b,φ_b) and (θ_a,φ_a) respectively, and $\mathcal{P}_l$ is the Legendre polynomial

$$\mathcal{P}_l(z) = \frac{1}{2^l l!}\frac{d^l}{dz^l}(z^l-1)^l. \tag{3.76}$$

From these results, we can construct a $J\times J$ symmetric matrix P_l for each l having as element ab the Legendre polynomial or order l $\mathcal{P}_l(\mathbf{n}_a\mathbf{n}_b)$ (see Appendix C). It is interesting to note that matrix P_l is very similar to a so-called Toeplitz matrix –that associated to a hierarchy for the autocorrelation functions of, for instance, auto-regressive models in the theory of time series–. In fact, the structure of P_l stands for a generalization of the structure of a Toeplitz matrix, and for some particular resonator layouts –as the PHCA or the TIGA proposals discussed in next chapter– the first strictly matches the second. Hence, the common sense understanding of P_l as a matrix keeping the information about the *correlations between pairs of resonators* is further supported by this characterization.

Going back to (3.74), writing

$$\chi^{(nl)}_{ab} \equiv \frac{2l+1}{4\pi}|A_{nl}(R)|^2\mathcal{P}_l(\mathbf{n}_a\mathbf{n}_b) \tag{3.77}$$

we have the condensed form

$$\tilde{K}_{ab}(s) = \sum_{nl}\frac{\Omega_b^2}{s^2+\omega_{nl}^2}\chi^{(nl)}_{ab} \tag{3.78}$$

for the kernel matrix of a perfect sphere.

Our next hypothesis is that all the resonators are identical:

$$\begin{aligned} m_b &= m \;\Rightarrow\; \eta_b = \eta \quad \forall b = 1, \ldots, J \\ \Omega_b &= \Omega \qquad\qquad\quad \forall b = 1, \ldots, J. \end{aligned} \tag{3.79}$$

We also make use of the idea that transducers are resonators mechanically designed to have a resonance frequency ideally equal to one of the eigenfrequencies of the sphere's spectrum[3]:

$$\Omega = \omega_{NL}. \tag{3.80}$$

Equation (3.67) is now

$$\sum_{b=1}^{J} M_{ab}\, \hat{q}_b(s) = -\frac{s^2}{s^2+\Omega^2}\, \hat{u}_{a,external}(s) + \frac{\hat{\zeta}_a(s)}{s^2+\Omega^2}\,, \qquad a = 1, \ldots, J \tag{3.81}$$

with

$$M_{ab} \equiv \left[\delta_{ab} + \eta \sum_{nl} \frac{s^2\Omega^2}{(s^2+\Omega^2)(s^2+\omega_{nl}^2)}\, \chi_{ab}^{(nl)} \right], \tag{3.82}$$

or distinguishing the NL term in the sum:

$$M_{ab} \equiv \left[\delta_{ab} + \eta\, \frac{s^2\Omega^2}{(s^2+\Omega^2)^2}\, \chi_{ab}^{(NL)} + \eta \sum_{nl \neq NL} \frac{s^2\Omega^2}{(s^2+\Omega^2)(s^2+\omega_{nl}^2)}\, \chi_{ab}^{(nl)} \right]. \tag{3.83}$$

And finally, we assume that ω_{NL} is an *isolated resonance frequency*: there is no other frequency ω_{nl} of the free sphere's spectrum in its *neighbourhood*. What do we mean by a neighbourhood of ω_{NL}? We advance that we already have a good indication in the parametrization assumed in general for ideality departures studied in Chapter 5, in this case

$$\omega_{nl}^2 = \omega_{NL}^2 \left(1 + r_{nl}\, \eta^{\frac{1}{2}} \right), \tag{3.84}$$

[3] At this stage, this eigenfrequency ω_{NL} is not fixed. We maintain its generic subindexes for the time being to consider any possibility, although for GWs detection only $L = 0$ and $L = 2$ will be convenient, with N tuned to the first, $N = 1$, or even the second harmonic, $N = 2$ (see section 3.4.2.).

which here reflects the fact that one of the uncoupled sphere's frequencies, ω_{nl}, is at a distance

$$\omega_{nl} - \omega_{NL} = \omega_{NL} \frac{r_{nl}}{2} \eta^{\frac{1}{2}} \tag{3.85}$$

from the resonance frequency ω_{NL}.

This distance can be calculated for any ω_{nl} of the free sphere spectrum, whereby the dimensionless parameter r_{nl} must be bounded for (3.84) to be meaningful: it seems clear that if r_{nl} is too large ω_{nl} will be placed at a sufficient distance from ω_{NL} for not interfering in the resonance but, in return, if r_{nl} is of order 1 or at least significantly larger than $\eta^{\frac{1}{2}}$, then the order $\eta^{\frac{1}{2}}$ is fully maintained in (3.84) and the dynamical behaviour of the system could be affected by the *nearness*. Eventually, if r_{nl} is too small, of order $\eta^{\frac{1}{2}}$ itself or smaller, then the device will not be able to discriminate between ω_{nl} and ω_{NL} for responses at leading order.

Therefore, we imagine that r_{nl} is of order appreciably larger than 1, so that ω_{nl}, $\forall nl \neq NL$, does not interfere in the resonance. In practice this is not always the case as we will see in section 5.2 of Chapter 5, but for the moment we limit to this most ideal situation.

3.4.1 Frequency Spectrum

First Order Calculations

Perturbation methods are particularly appropiate when the system under consideration closely resembles one which is exactly solvable, or whenever one kows the solution for the unperturbed problem, here the free sphere problem. In our case, one can consider the coupling of resonators as a source of disturbance, so that it becomes possible to develop the interesting quantities describing the change in the physical situation as a series in the small dimensionless coupling constant η,

$$\eta \equiv \frac{m_{resonators}}{M_{sphere}} << 1, \tag{3.86}$$

which precisely is the parameter introducing the term of interaction between resonators and sphere in the equations of motion.

Frequency Spectrum

For the frequencies, the interesting quantities which have to be developed as series in powers of η are the possible roots of the determinant $\Delta(s)$ giving the system resonances.

They are obtained from:

$$\Delta(s) \equiv \det\left[\delta_{ab} + \eta \frac{s^2\Omega^2}{(s^2+\Omega^2)^2}\chi_{ab}^{(NL)} + \eta \sum_{nl\neq NL} \frac{s^2\Omega^2}{(s^2+\Omega^2)(s^2+\omega_{nl}^2)}\chi_{ab}^{(nl)}\right] = 0. \tag{3.87}$$

The first remark about this determinant is that δ_{ab} is obviously a regular matrix; a second remark is that we can theoretically assign an arbitrarily small value to η. Therefore, solutions of equation (3.87) are required to be such that the denominators in the fractions are proportional to η so as to cancel the already appearing as multiplicative factors to guarantee the vanishing of $\Delta(s)$. Due to the fact that it is necessary and just sufficient only one of the two denominators being proportional to η, we distinguish two categories of roots: roots which are close to $s = \pm i\Omega = \pm i\omega_{NL}$ and roots which are close to $s = \pm i\omega_{nl}, nl \neq NL$.

For roots near Ω, it is clear that they must be of the form

$$s_0^2 = -\Omega^2\,(1 + \chi_{\frac{1}{2}}\eta^{\frac{1}{2}} + \chi_1\eta + \ldots), \tag{3.88}$$

whereas roots near $\omega_{nl}, nl \neq NL$ must be expressed as

$$s_{nl}^2 = -\omega_{nl}^2\,(1 + b_1^{(nl)}\eta + b_2^{(nl)}\eta^2 \ldots). \tag{3.89}$$

Roots near Ω: The expansion (3.88) is in powers of $\eta^{\frac{1}{2}}$. The reason is that, as explained, for arbitrarily small values of η the second term in $\Delta(s)$,

$$\eta \frac{s^2\Omega^2}{(s^2+\Omega^2)^2}\chi_{ab}^{(NL)}, \tag{3.90}$$

is required to compete with the regular matrix δ_{ab}, whence the denominator $(s^2+\Omega^2)^2$ must be proportional to η so as to cancel the one already appearing.

The coefficients $\chi_{\frac{1}{2}}$, χ_1.... can be calculated recursively. Substituting (3.88) into (3.87).

$$\begin{aligned}\Delta(s) \;\equiv\; \det\Bigg[\delta_{ab} &- \frac{(1+\chi_{\frac{1}{2}}\eta^{\frac{1}{2}}+\ldots)}{(1+\frac{\chi_1}{\chi_{\frac{1}{2}}}\eta^{\frac{1}{2}}+\ldots)^2}\frac{\chi_{ab}^{(NL)}}{\chi_{\frac{1}{2}}^2} + \\ &+ \eta^{\frac{1}{2}}\sum_{nl\neq NL}\frac{(1+\chi_{\frac{1}{2}}\eta^{\frac{1}{2}}+\ldots)}{(1+\frac{\chi_1}{\chi_{\frac{1}{2}}}\eta^{\frac{1}{2}}+\ldots)(1-\chi_{\frac{1}{2}}\frac{\Omega^2}{\omega_{nl}^2-\Omega^2})}\frac{\Omega^2}{\omega_{nl}^2-\Omega^2}\frac{\chi_{ab}^{(nl)}}{\chi_{\frac{1}{2}}}\Bigg] = 0,\end{aligned}$$

(3.91)

and operating we write down $\Delta(s)$ as

$$\Delta(s) \equiv \det\left[\delta_{ab} - \frac{\chi_{ab}^{(NL)}}{\chi_{\frac{1}{2}}^2} + \eta^{\frac{1}{2}}\left(\left(-\chi_{\frac{1}{2}} + 2\frac{\chi_1}{\chi_{\frac{1}{2}}}\right)\frac{\chi_{ab}^{(NL)}}{\chi_{\frac{1}{2}}^2} + \sum_{nl\neq NL}\frac{\Omega^2}{\omega_{nl}^2-\Omega^2}\frac{\chi_{ab}^{(nl)}}{\chi_{\frac{1}{2}}}\right) + \right.$$

$$\left. + \eta\left(\left(\chi_1 - 3\frac{\chi_1^2}{\chi_{\frac{1}{2}}^2} + 2\frac{\chi_2}{\chi_{\frac{1}{2}}}\right)\frac{\chi_{ab}^{(NL)}}{\chi_{\frac{1}{2}}^2} + \sum_{nl\neq NL}\left(\chi_{\frac{1}{2}} - \frac{\chi_1}{\chi_{\frac{1}{2}}} + \frac{\Omega^2}{\omega_{nl}^2-\Omega^2}\right)\frac{\Omega^2}{\omega_{nl}^2-\Omega^2}\frac{\chi_{ab}^{(nl)}}{\chi_{\frac{1}{2}}}\right) + \ldots\right] = 0. \tag{3.92}$$

From this expression it is readily seen that $\chi_{\frac{1}{2}}$ is a solution to the algebraic equation for the lowest order, η^0, in the development of the determinant:

$$\det\left[\delta_{ab} - \frac{1}{\chi_{\frac{1}{2}}^2}\chi_{ab}^{(NL)}\right] = 0. \tag{3.93}$$

This shows that $\chi_{\frac{1}{2}}^2$ are the J eigenvalues of the $J \times J$ square symmetric matrix $\chi_{ab}^{(NL)}$, and from (3.77) they have the form

$$\chi_{\frac{1}{2}}^2 = \frac{2l+1}{4\pi}|A_{NL}(R)|^2\xi_a^2, \tag{3.94}$$

where ξ_a^2 are the J positive or null eigenvalues of the P_L matrix. At this point, it is worth noting that the number of positive non-null eigenvalues ξ_a^2 is at most $2L+1$, independently of the number J of resonators (see Appendix C), and so there actually will exist at most $2L+1$ different pairs of poles near $s^2 = -\Omega^2$ at order $\eta^{\frac{1}{2}}$. The poles can be written

$$s_{0,\pm}^2 = -\Omega^2\left(1 \pm \sqrt{\frac{2L+1}{4\pi}}|A_{NL}(R)|\xi_a\eta^{\frac{1}{2}}\right) + O(\eta) \qquad a = 1, \ldots, J, \tag{3.95}$$

their imaginary parts giving the system resonant frequencies, the J symmetric pairs around Ω:

$$\omega_{a,\pm}^2 = \Omega^2\left(1 \pm \sqrt{\frac{2L+1}{4\pi}}|A_{NL}(R)|\xi_a\eta^{\frac{1}{2}}\right) + O(\eta) \qquad a = 1, \ldots, J \tag{3.96}$$

This result is analogous to that for bars [6], for which the attachment of one resonator causes the main resonance frequency of the bar to split up into a symmetric pair around

the original value, the amount of relative shift being proportional to $\eta^{\frac{1}{2}}$. It is precisely controlled by the geometry dependent eigenvalues ξ_a.

Roots near $\omega_{\mathbf{nl}}$, $\mathbf{nl} \neq \mathbf{NL}$: For the rest of possible roots close to other eigenfrequencies ω_{nl} different from $\Omega = \omega_{NL}$, i.e., that of non-tuned modes, an analogous analysis leads to forms in (3.89),

$$s_{nl}^2 = -\omega_{nl}^2 \left(1 + b_1^{(nl)}\eta + b_2^{(nl)}\eta^2 \ldots\right), \tag{3.97}$$

since in this case it is the term of the sum in (3.87)

$$\eta \frac{s^2\Omega^2}{(s^2+\Omega^2)(s^2+\omega_{nl}^2)} \chi_{ab}^{(nl)} \tag{3.98}$$

that has to compete with the identity matrix δ_{ab} through the denominator $(s^2+\omega_{nl}^2)$ being of order η. The finding of the coefficients b_i is absolutely analogous to that of the coefficients χ_i. Once more, the substitution of (3.97) into equation (3.87),

$$\Delta(s) \equiv \det \left[\delta_{ab} + \frac{(1 + b_1^{(nl)}\eta + \ldots)}{(1 + \frac{b_2^{(nl)}}{b_1^{(nl)}}\eta + \ldots)(1 - \frac{\omega_{nl}^2}{\Omega^2-\omega_{nl}^2} b_1^{(nl)}\eta + \ldots)} \frac{\Omega^2}{\Omega^2-\omega_{nl}^2} \frac{\chi_{ab}^{(nl)}}{b_1} - \right.$$

$$- \eta \frac{(1 + b_1^{(nl)}\eta + \ldots)}{(1 - 2\frac{\omega_{nl}^2}{\Omega^2-\omega_{nl}^2} b_1^{(nl)}\eta + \ldots)} \frac{\Omega^2\omega_{nl}^2}{(\Omega^2-\omega_{nl}^2)^2} \chi_{ab}^{(NL)} -$$

$$\left. - \eta \sum_{n'l' \neq nl, NL} \frac{(1 + b_1^{(nl)}\eta + \ldots)}{(1 - \frac{\Omega^2+\omega_{n'l'}^2-2\omega_{nl}^2}{(\Omega^2-\omega_{nl}^2)(\omega_{n'l'}^2-\omega_{nl}^2)} \omega_{nl}^2 b_1^{(nl)}\eta + \ldots)} \frac{\Omega^2\omega_{nl}^2}{(\Omega^2-\omega_{nl}^2)(\omega_{n'l'}^2-\omega_{nl}^2)} \chi_{ab}^{(n'l')} \right] = 0, \tag{3.99}$$

yields after some algebraic manipulation

$$\Delta(s) \equiv \det \left[\delta_{ab} + \frac{\Omega^2}{\Omega^2-\omega_{nl}^2} \frac{\chi_{ab}^{(nl)}}{b_1^{(nl)}} - -\eta \left(\left(b_1^{(nl)} + \frac{\omega_{nl}^2}{\Omega^2-\omega_{nl}^2} b_1^{(nl)} - \frac{b_2^{(nl)}}{b_1^{(nl)}} \right) \frac{\Omega^2}{\Omega^2-\omega_{nl}^2} \frac{\chi_{ab}^{(nl)}}{b_1^{(nl)}} - \right.\right.$$

$$\left.\left. - \frac{\Omega^2\omega_{nl}^2}{(\Omega^2-\omega_{nl}^2)^2} \chi_{ab}^{(NL)} - \sum_{n'l' \neq nl, NL} \frac{\Omega^2\omega_{nl}^2}{(\Omega^2-\omega_{nl}^2)(\omega_{n'l'}^2-\omega_{nl}^2)} \chi_{ab}^{(n'l')} \right) + \ldots \right] = 0. \tag{3.100}$$

Therefore, we find that $b_1^{(nl)}$ is obtained from the lowest order equation

$$\det \left[\frac{\Omega^2-\omega_{nl}^2}{\Omega^2} b_1^{(nl)} \delta_{ab} - \chi_{ab}^{(nl)} \right] = 0, \tag{3.101}$$

which is again an eigenvalue equation with J solutions representing downshifts for frequencies above Ω and upshifts if they are below, due to the fact that the eigenvalues of $\chi_{ab}^{(nl)}$ are always positive or null (Appendix C), and so the sign of $b_1^{(nl)}$ is that of $(\Omega^2 - \omega_{nl}^2)$.

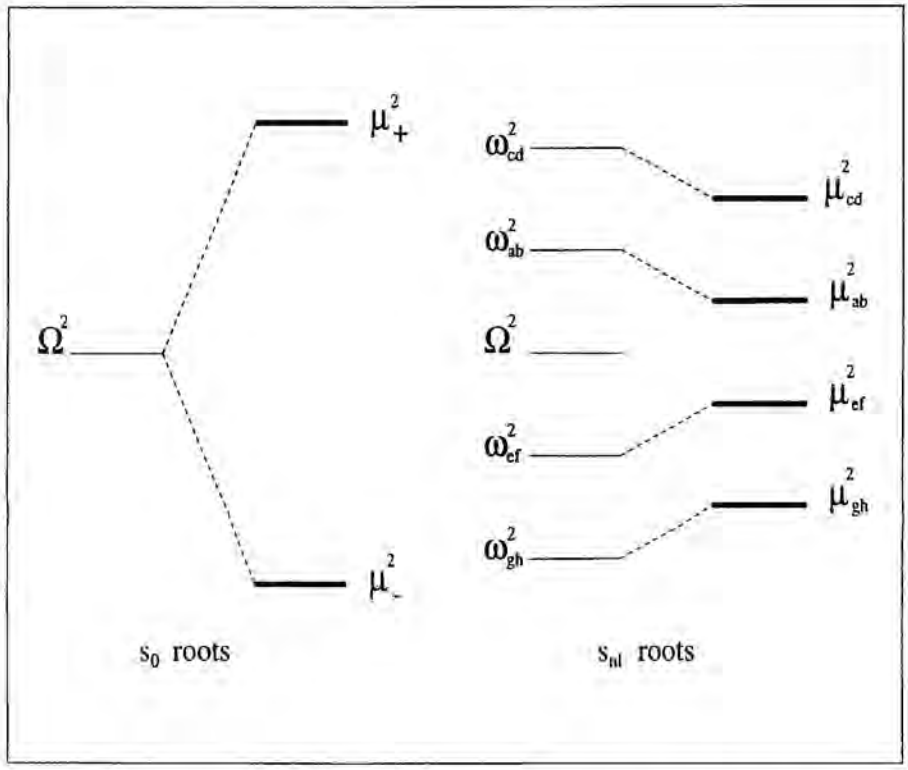

Figure 3.2. *Each thin line represents a single frequency ω_{nl}^2 of the free sphere, whereas thick lines μ^2 denote a multiple set of the coupled sphere spectrum. For the tuning frequency $\Omega^2 = \omega_{NL}^2$, the splitting happens in J pairs symmetrically distributed around it. For each of the reamining, the new multiplet contains only J frequencies, all of them downshifted in relation to the initial one if they are above Ω^2, or upshifted when below.*

Hence, we see that the presence of resonators indeed affects the whole spectrum of the free sphere being responsible for the appearance of J doublets of frequencies symmetrically distributed around the tuning frequency Ω, and J shifted singlets for the original non-tuned ones ω_{nl}, the splitting always in accordance with the number of resonators. Particularly, at order $\eta^{\frac{1}{2}}$ the accordance is in fact with the number $2L + 1$

of non-null eigenvalues ξ_a^2.

With respect to higher order corrections, they are both interesting and necessary for better accuracy, but they show complex characteristics and so will be treated with special attention in future work.

3.4.2 System Response to Specific Signals

Amplitudes

The calculation of the amplitudes of the excited modes corresponding to the frequencies that we have just estimated is an extremely laborious task, although the way to proceed is relatively simple and clear.

In fact, we have already solved the problem in the Laplace domain, since it is formally trivial to isolate $\tilde{q}_a(s)$ in (3.81):

$$\tilde{q}_a(s) = -\sum_{b=1}^{J} M_{ab}^{-1} \frac{s^2}{s^2+\Omega^2} \left(\hat{u}_{b,external}(s) - \frac{\hat{\zeta}_b(s)}{s^2} \right) \qquad a = 1, \ldots, J. \tag{3.102}$$

However, the final aim would be to find it in the time domain. For doing that, it is necessary to perform its inverse Laplace transform by computing its associated Bromwich integral (Appendix B)

$$q_a(t) = \frac{1}{2\pi i} \int_{\gamma-i\infty}^{\gamma+i\infty} e^{st} \hat{q}_a(s) ds \tag{3.103}$$

through the residue theorem

$$q_a(t) = \sum residues \ at \ the \ poles \ of \ e^{st}\tilde{q}_a(s) \ in \ the \ complex \ s-plane, \tag{3.104}$$

what amounts to be a quite bothersome work.

We recall that residues must be calculated at poles of $e^{st}\hat{q}_a(s)$, and they happen to be exclusively at the already calculated zeros of the determinant $\Delta(s)$ of matrix M_{ab}, those of equations (3.88) and (3.89). We advance that these poles are simple poles and then their associated residues are simply calculated as the limits

$$\lim_{s \to s_{pole}} (s - s_{pole}) \times e^{st}\tilde{q}_a(s). \tag{3.105}$$

These responses can not be obtained in an analytic form. But, like for the frequencies, one can fall back on perturbative expansions so that the result can be written as a series function in ascending powers of the small parameter η. However, the nature of the calculations would make it impossible to advance an *a priori* structure of the development specifying, for instance, which would be its leading order. It would rather be obtained *a posteriori*.

For further work, it is necessary to specify both the tuning frequency ω_{NL} and the expressions of $\hat{u}_{b,external}(s)$ and $\hat{\zeta}_b(s)$ in (3.102). This is what we are going to do in next subsections, where we analyse the response of the antenna to two different possible signals: the major topic of gravitational waves and the also interesting case of calibration inputs.

System Response to a Gravitational Wave

For a gravitational wave we saw, when studying the case of the isolated sphere, that the system response was

$$\begin{aligned}\mathbf{u}_{ext}(\mathbf{x},t) &= \sum_{n=1}^{\infty}\frac{a_{n0}(R)}{\omega_{n0}}\mathbf{u}^S_{n00}(\mathbf{x})g^{(00)}_{n0}(t)+\sum_{n=1}^{\infty}\frac{a_{n2}(R)}{\omega_{n2}}\left[\sum_{m=-2}^{m=2}\mathbf{u}^S_{n2m}(\mathbf{x})g^{(2m)}_{n2}(t)\right]\\ &\equiv \sum_{\substack{l=0 \text{ and } 2\\ m=-l,\ldots,l}}\sum_{n=1}^{\infty}\frac{a_{nl}}{\omega_{nl}}\mathbf{u}^S_{nlm}(\mathbf{x})g^{(lm)}_{nl}(t).\end{aligned} \tag{3.106}$$

and in the paragraph devoted to describe the possible external forces that could act on the resonators

$$\zeta_{GW,a}(t)=R\sum_{\substack{l=0 \text{ and } 2\\ m=-l,\ldots,l}}Y_{lm}(\mathbf{n}_a)g^{(lm)}(t). \qquad a=1,\ldots,J. \tag{3.107}$$

From them, and making use of the convolution theorem (Appendix B), we can find the Laplace transforms:

$$\begin{aligned}\hat{u}_{ext,b}(s) &= \mathbf{n}_b\cdot\hat{\mathbf{u}}_{ext}(\mathbf{x}_b,s)\\ &= \sum_{\substack{l=0 \text{ and } 2\\ m=-l,\ldots,l}}\sum_{n=1}^{\infty}\frac{a_{nl}A_{nl}(R)}{s^2+\omega^2_{nl}}Y_{lm}(\mathbf{n}_b)\,\hat{g}^{(lm)}(s)\end{aligned} \tag{3.108}$$

$$\tilde{\zeta}_{GW,b}(s) = R \sum_{\substack{l=0 \text{ and } 2 \\ m=-l,\dots,l}} Y_{lm}(\mathbf{n}_b)\tilde{g}^{(lm)}(s) \qquad b = 1,\dots,J. \tag{3.109}$$

Once these expressions have been inserted into the general form (3.102) for $\tilde{q}_a(s)$,

$$\tilde{q}_a(s) = -\sum_{b=1}^{J}\left[\delta_{ab} + \eta\frac{s^2\Omega^2}{(s^2+\Omega^2)^2}\chi_{ab}^{(NL)} + \eta\sum_{nl\neq NL}\frac{s^2\Omega^2}{(s^2+\Omega^2)(s^2+\omega_{nl}^2)}\chi_{ab}^{(nl)}\right]^{-1} \times$$
$$\times \frac{s^2}{s^2+\Omega^2}\sum_{\substack{l=0 \text{ and } 2 \\ m=-l,\dots,l}}\left(\sum_{n=1}^{\infty}\frac{a_{nl}A_{nl}(R)}{s^2+\omega_{nl}^2} - \frac{R}{s^2}\right)Y_{lm}(\mathbf{n}_b)\tilde{g}^{(lm)}(s), \tag{3.110}$$

it is advisable to look for further simplifications before entering residue calculation to find it in the time domain.

The amplitudes $\tilde{q}_a(s)$ has been expressed in such a way that makes explicit its summation structure, so that we can write it in a more compact form:

$$\tilde{q}_a(s) = \sum_{\substack{l=0 \text{ and } 2 \\ m=-l,\dots,l}} \tilde{\phi}_a^{(lm)}(s)\tilde{g}^{(lm)}(s) \qquad a = 1,\dots,J, \tag{3.111}$$

whereupon one just needs to compute the separate contributions

$$\tilde{\phi}_a^{(lm)}(s) = -\sum_{b=1}^{J}\left[\delta_{ab} + \eta\frac{s^2\Omega^2}{(s^2+\Omega^2)^2}\chi_{ab}^{(NL)} + \eta\sum_{nl\neq NL}\frac{s^2\Omega^2}{(s^2+\Omega^2)(s^2+\omega_{nl}^2)}\chi_{ab}^{(nl)}\right]^{-1} \times$$
$$\times \frac{s^2}{s^2+\Omega^2}\left(\sum_{n=1}^{\infty}\frac{a_{nl}A_{nl}(R)}{s^2+\omega_{nl}^2} - \frac{R}{s^2}\right)Y_{lm}(\mathbf{n}_b), \tag{3.112}$$

where $l = 0$ or $l = 2$.

It also allows the application of the convolution theorem so to differentiate and make good use of the information in the time domain depending on the gravitational waves that act on the antenna:

$$q_a(t) = \sum_{\substack{l=0 \text{ and } 2 \\ m=-l,\dots,l}} \int_0^t \phi_a^{(lm)}(t-t')\,g^{(lm)}(t')\,dt' \qquad a = 1,\dots,J. \tag{3.113}$$

Before undertaking the task of calculating $\phi_a^{(lm)}(t)$, we study the substitutions of s_{poles}, which are s_0 or s_{nl}, in place of s in (3.112). It will provide an idea about what will be the leading contributions.

s_0 poles: Let us first consider s_0 poles. From (3.88), the sum $s_0^2 + \Omega^2 = s_0^2 + \omega_{NL}^2$ around a given resonance frequency $\Omega = \omega_{NL}$ is of order $\eta^{\frac{1}{2}}$,

$$s_0^2 + \Omega^2 = s_0^2 + \omega_{NL}^2 = -\omega_{NL}^2 \left(\chi_{\frac{1}{2}} \eta^{\frac{1}{2}} + \chi_1 \eta + \dots \right), \tag{3.114}$$

while $s^2 + \omega_{nl}^2, nl \neq NL$ is proportional to η^0,

$$s_0^2 + \omega_{nl}^2 = (\omega_{nl}^2 - \omega_{NL}^2) - \omega_{NL}^2 \left(\chi_{\frac{1}{2}} \eta^{\frac{1}{2}} + \chi_1 \eta + \dots \right). \tag{3.115}$$

Then,

- beginning by the inspection of the quotient

$$\frac{s^2}{s^2 + \Omega^2} \tag{3.116}$$

it is easily understood that s_0 roots near Ω will make it to contribute at order $\eta^{-\frac{1}{2}}$.

- We also analyse the free sphere response term, the first expression of the bracket in (3.112):

$$\sum_{\substack{l=0 \text{ and } 2 \\ n}} \frac{a_{nl} A_{nl}(R)}{s^2 + \omega_{nl}^2}. \tag{3.117}$$

The first to do is the following separation:

$$\sum_{n=1}^{\infty} \frac{a_{n0} A_{n0}(R)}{s^2 + \omega_{n0}^2} + \sum_{n=1}^{\infty} \frac{a_{n2} A_{n2}(R)}{s^2 + \omega_{n2}^2}. \tag{3.118}$$

Secondly, we imagine that we are interested in roots around $\Omega = \omega_{NL}$, but $L \neq 0$ and $L \neq 2$. From (3.115), the two sums yield to η^0 contributions. In return, if $\Omega = \omega_{NL}$ is such that $L = 0$ or $L = 2$, there is a addend in the corresponding summation formula which is proportional to $\eta^{-\frac{1}{2}}$, respectively

$$\frac{a_{N0} A_{N0}(R)}{s_0^2 + \omega_{N0}^2} \quad \text{or} \quad \frac{a_{N2} A_{N2}(R)}{s_0^2 + \omega_{N2}^2}. \tag{3.119}$$

Hence, the natural link for the resonant transducers, which will take advantage of a maximum transference of energy, is their tuning to a particular ω_{N0} for monopole radiation sensing, and to a certain ω_{N2} for quadrupole radiation sensing. These are the ones associated to the eigenmodes of the free sphere excited by impinging GWs, what shows again the perfect coupling between the monopole-quadrupole structure of this radiation and the vibration patterns of the detector. Other frequencies can be chosen for tuning, but then the coupling to GW will be weaker, for the factor $\eta^{-\frac{1}{2}}$ above mentioned being substituted by higher orders.

The examination of the gravitational external force on resonators $\frac{R}{s^2}$ is trivial because it is always the case that it is proportional to η^0.

- Under the circumstance of just considering s_0 poles around the resonance frequency Ω of the form ω_{N0} or ω_{N2}, we finally examine the inverse matrix components

$$\eta \frac{s^2\Omega^2}{(s^2+\Omega^2)^2} \chi_{ab}^{(NL)} + \eta \sum_{nl \neq NL} \frac{s^2\Omega^2}{(s^2+\Omega^2)(s^2+\omega_{nl}^2)} \chi_{ab}^{(nl)}. \tag{3.120}$$

This work has been already done in the previous subsection, where the frequency spectrum was obtained. There we saw that the dominant term for s_0 roots is precisely

$$\eta \frac{s^2\Omega^2}{(s^2+\Omega^2)^2} \chi_{ab}^{(NL)}, \tag{3.121}$$

that associated to the tuning frequency, which from (3.114) is the one compensating the multiplicative factor η, while the others in (3.120) maintain $\eta^{\frac{1}{2}}$.

$s_{n_p l_p}$ poles: The evaluation of the poles around a certain non-tuning frequency, say $\omega_{n_p l_p}$, is in complete analogy to the former approach for s_0 roots. We begin by recalling from (3.89) that

$$\begin{aligned} s_{n_p l_p}^2 + \omega_{n_p l_p}^2 &= -\omega_{n_p l_p}^2 \left(b_1\eta^1 + b_2\eta^2 + \ldots\right) \\ s_{n_p l_p}^2 + \omega_{NL}^2 &= (\omega_{NL}^2 - \omega_{n_p l_p}^2) - \omega_{n_p l_p}^2 \left(b_1\eta^1 + b_2\eta^2 + \ldots\right) \\ s_{n_p l_p}^2 + \omega_{n'l'}^2 &= (\omega_{n'l'}^2 - \omega_{n_p l_p}^2) - \omega_{n_p l_p}^2 \left(b_1\eta^1 + b_2\eta^2 + \ldots\right) \\ & \quad n_p l_p \neq NL \neq n'l'. \end{aligned} \tag{3.122}$$

Hence,

- $s_{n_p l_p}$ roots will make the term

$$\frac{s^2}{s^2+\Omega^2} \tag{3.123}$$

to behave as a η^0 power.

- All the components in the sum

$$\sum_{\substack{l=0 \text{ and } 2 \\ n}} \frac{a_{nl}A_{nl}(R)}{s^2_{n_p l_p}+\omega^2_{nl}}. \tag{3.124}$$

are $O(\eta^0)$, except in the case $\omega_{n_p l_p}$ being a monopole or a quadrupole frequency $\omega_{n_p 0}$ or $\omega_{n_p 2}$; then, the term

$$\frac{a_{n_p 0}A_{n_p 0}(R)}{s^2_{n_p 0}+\omega^2_{n_p 0}} \quad \text{, or} \quad \frac{a_{n_p 2}A_{n_p 2}(R)}{s^2_{n_p 2}+\omega^2_{n_p 2}}, \tag{3.125}$$

is $O(\eta^{-1})$.

Again, the gravitational external force on resonators $\frac{R}{s^2}$ is $O(\eta^0)$.

- Eventually, the relevant inverse matrix component is just

$$\eta \frac{s^2\Omega^2}{(s^2+\Omega^2)(s^2+\omega^2_{n_p l_p})} \chi^{(nl)}_{ab}, \tag{3.126}$$

also of $O(\eta^0)$ if $s^2 \equiv s^2_{n_p l_p}$.

After all these computations, for first order calculations it will suffice to concentrate on:

- the computation of the residues of

$$\begin{aligned} \phi^{(Lm)}_a(s) &= -\sum_{b=1}^{J}\left[\delta_{ab}+\eta\frac{s^2\Omega^2}{(s^2+\Omega^2)^2}\chi^{(NL)}_{ab}\right]^{-1}\frac{s^2}{s^2+\Omega^2}\times \\ &\times \frac{a_{NL}A_{NL}(R)}{s^2+\Omega^2}Y_{Lm}(\mathbf{n}_b) \qquad a=1,\ldots,J \end{aligned} \tag{3.127}$$

when $\Omega^2=\omega^2_{NL}$, $L=0$ and $L=2$ at the, in principle J but $2L+1$ indeed, pairs of poles around the resonance frequency:

$$s^2_{0,\pm} = -\Omega^2 \left(1 \pm \sqrt{\frac{2l+1}{4\pi}} |A_{NL}(R)| \xi_a \eta^{\frac{1}{2}} \right) + O(\eta); \tag{3.128}$$

- the computation of the residues of

$$\begin{aligned} \hat{\phi}^{(lm)}_a(s) &= -\sum_{b=1}^{J} \left[\delta_{ab} + \eta \frac{s^2\Omega^2}{(s^2+\Omega^2)(s^2+\omega^2_{nl})} \chi^{(nl)}_{ab} \right]^{-1} \frac{s^2}{s^2+\Omega^2} \times \\ &\times \frac{a_{nl} A_{nl}(R)}{s^2+\omega^2_{nl}} Y_{lm}(\mathbf{n}_b) \qquad a = 1, \ldots, J \end{aligned} \tag{3.129}$$

when $l = 0$ and $l = 2$ at the J poles around any non-tuning monopole or quadrupole frequency ω_{nl}:

$$s^2_{nl} = -\omega^2_{nl} \left(1 + b_1 \eta \right) + O(\eta). \tag{3.130}$$

Although it is not at all obvious, the relevant contributions at leading order –we advance it is $\eta^{-\frac{1}{2}}$– are in fact provided by the calculation of residues at just the s_0 roots, the first item in the list above.This is proved in Appendix D, where we give a detailed exposition of the procedures.

Here we plot the final results for the two different groups of tuning frequencies: monopole frequencies ω_{N0} and quadrupole frequencies ω_{N2}.

Monopole Response

In contrast to General Relativity, some metric theories of gravitation –e.g. Brans-Dicke-Jordan theory– predict the existence of monopole radiation propagating in the weak field limit as plane waves with helicity 0, that is $T0$ waves [19].

Looking at (3.29) for the dynamical perfomance of spherically shaped antennæ when excited by incoming GWs or also at (3.127) and the discussion for s_0 poles, it is understood that they could be sensitive to this kind of radiation whenever

$$\Omega = \omega_{N0} \tag{3.131}$$

i.e., Ω is tuned to one given monopole frequency of the sphere.

For instance, for typical planned aluminium spheres of radius $R = 1.5m$, one has for the first monopolar frequency [80, 103]

$$\omega_{10} = 2\pi \cdot 1.8068 \ KHz, \tag{3.132}$$

which is the lowest in value in its category, therefore being the more easily excitable and so probably the chosen one in a practical device for monopolar tuning.

From (3.128), the coupled mode frequencies are

$$\omega_{a,\pm}^2 = \omega_{N0}^2 \left(1 \pm \frac{1}{\sqrt{4\pi}} |A_{N0}(R)| \xi_a \eta^{\frac{1}{2}}\right) + O(\eta) \qquad a = 1, \ldots, J, \tag{3.133}$$

where ξ_a^2 are the eigenvalues of the $J \times J$ symmetric matrix P_L with $L = 0$.

For this value of L, P_L contains Legendre polinomials of the form

$$\mathcal{P}_0(\mathbf{n}_a \mathbf{n}_b) = 1 \quad \forall a, b = 1, \ldots, J, \tag{3.134}$$

or in other words, P_0 is a matrix with all its components equal to 1, independently of the number J of resonators or their distribution. Its eigenvalues ξ_a^2 are (Appendix C)

$$\xi_1^2 = J, \quad \xi_a^2 = 0 \quad \forall a = 2, \ldots, J, \tag{3.135}$$

whereupon we see that the spliting in (3.133) results in a single pair

$$\omega_{\pm}^2 = \omega_{N0}^2 \left(1 \pm \sqrt{\frac{J}{4\pi}} |A_{N0}(R)| \eta^{\frac{1}{2}}\right) + O(\eta). \tag{3.136}$$

For the monopole amplitudes $\tilde{q}_a(s) = \tilde{\phi}_a^{(00)}(s)\tilde{g}^{(00)}(s)$, calculations in Appendix D yield in the Laplace domain

$$\tilde{\phi}_a^{(00)}(s) = \eta^{-\frac{1}{2}} \frac{(-1)^J}{\sqrt{J}} a_{N0} \frac{1}{2} \left[(s^2 + \omega_+^2)^{-1} - (s^2 + \omega_-^2)^{-1}\right] + O(0), \tag{3.137}$$

and so

$$\begin{aligned} \tilde{q}_a(s) \quad &= \quad \eta^{-\frac{1}{2}} \frac{(-1)^J}{\sqrt{J}} a_{N0} \frac{1}{2} \left[(s^2 + \omega_+^2)^{-1} - (s^2 + \omega_-^2)^{-1}\right] \tilde{g}^{(00)}(s) + O(0) \\ &\quad a = 1, \ldots, J, \end{aligned} \tag{3.138}$$

where for the first harmonic the overlap coefficient defined in (3.27) is [80]

$$a_{10} \approx 0.214 \, R. \tag{3.139}$$

We recall that the inverse Laplace transform of

$$\frac{1}{2}\left[(s^2+\omega_+^2)^{-1}-(s^2+\omega_-^2)^{-1}\right] \tag{3.140}$$

is

$$\frac{1}{\Omega}\sin\frac{1}{2}(\omega_+-\omega_-)t\cos\Omega t, \tag{3.141}$$

which is a beat, i.e., a sinusoid of carrier frequency Ω and amplitude modulated by another sinusoid of much smaller frequency $(\omega_+-\omega_-)$. Thus, the time domain responses, $q_a(t)$ are

$$\begin{aligned} q_a(t) &= \eta^{-\frac{1}{2}}\frac{(-1)^J}{\sqrt{J}}a_{N0}\frac{1}{2}\times \\ &\int_0^\infty\left[\frac{1}{\Omega}\sin\frac{1}{2}(\omega_+-\omega_-)(t-t')\cos\Omega(t-t')\right]g^{(00)}(t')\,dt'+O(0) \\ &a=1,\ldots,J. \end{aligned} \tag{3.142}$$

Quadrupole Response

The relevant analysis now is that referred to quadrupole sensing. In this case, the tuning frequency must be

$$\Omega=\omega_{N2}, \tag{3.143}$$

and again the chosen harmonic is the first, which is indeed the lower frequency of the whole spectrum of the sphere:

$$\omega_{12}=2\pi\cdot 0.8725\ KHz, \tag{3.144}$$

also for a typical aluminium sphere of $R=1.5m$. Due to the capability of spherical antennæ of being potentially sensitive at two frequencies because of its remarkably good sensitivity at the second mode, it would be convenient also considering

$$\Omega=\omega_{22}=2\pi\cdot 1.6781\ KHz. \tag{3.145}$$

Following the steps of the former study for monopole radiation, one has now to specify the frequencies

$$\omega_{a,\pm}^2 = \omega_{N2}^2 \left(1 \pm \sqrt{\frac{5}{4\pi}} |A_{N2}(R)| \xi_a \eta^{\frac{1}{2}}\right) + O(\eta) \tag{3.146}$$

by calculating the eigenvalues ξ_a^2 of $P_2(\mathbf{n}_a\mathbf{n}_b)$. This matrix contains the Legendre polonomials of order 2:

$$\mathcal{P}_2(\mathbf{n}_a\mathbf{n}_b) = \frac{1}{2}\left(3\left(\mathbf{n}_a\mathbf{n}_b\right)^2 - 1\right). \tag{3.147}$$

Its diagonal elements remain 1 -in fact this is a general characteristic of all P_L matrices, so that their invariant trace is always J for all L (Appendix C)-, but the non-diagonal ones depend on the locations of resonators through the $\mathbf{n}_a\mathbf{n}_b = cos\theta_{ab}$ quantities. At this stage, we want to maintain the generality of the results for any resonator layout. Thus, we postpone more particular results until the treatment of specific layouts in Chapter 4.

This situation also holds for the amplitudes, which again from the computation in Appendix D of $\tilde{\phi}_a^{(2m)}(s)$:

$$\begin{aligned}\tilde{\phi}_a^{(2m)}(s) &= (-1)^J \eta^{-\frac{1}{2}} \sqrt{\frac{4\pi}{5}} a_{N2} \sum_{b=1}^{J} \left\{ \sum_{\xi_c \neq 0} \frac{1}{2} \left[(s^2+\omega_{c+}^2)^{-1} - (s^2+\omega_{c-}^2)^{-1}\right] \right. \\ &\times \left. \frac{v_a^{(c)} v_b^{(c)*}}{\xi_c} \right\} Y_{2m}(\mathbf{n}_b),\end{aligned} \tag{3.148}$$

where $v_a^{(c)}$ is the c-th normalised eigenvector of $P_2(\mathbf{n}_a\mathbf{n}_b)$ associated to its non-null eigenvalues ξ_c^2, are

$$\begin{aligned}\tilde{q}_a(s) &= (-1)^J \eta^{-\frac{1}{2}} \sqrt{\frac{4\pi}{5}} a_{N2} \sum_{b=1}^{J} \left\{ \sum_{\xi_c \neq 0} \frac{1}{2} \left[(s^2+\omega_{c+}^2)^{-1} - (s^2+\omega_{c-}^2)^{-1}\right] \frac{v_a^{(c)} v_b^{(c)*}}{\xi_c} \right\} \\ &\times \sum_{m=-2}^{m=2} Y_{2m}(\mathbf{n}_b) \tilde{g}^{(2m)}(s) + O(0) \qquad a = 1, \ldots, J.\end{aligned} \tag{3.149}$$

Again the overlap coefficients can be calculated by means of formulas (3.28) [80]

$$a_{12} \approx 0.328R, \quad a_{22} \approx 0.106R \tag{3.150}$$

for the first and the second harmonic respectively.

Eventually, in the time domain one has

$$q_a(t) = (-1)^J \eta^{-\frac{1}{2}} \sqrt{\frac{4\pi}{5}} a_{N2} \times \sum_{b=1}^{J} \left\{ \sum_{\xi_c \neq 0} \frac{1}{2} \int_0^\infty \left[\frac{1}{\Omega} \sin \frac{1}{2}(\omega_{c+} - \omega_{c-})(t-t') \cos \Omega(t-t') \right] \frac{v_a^{(c)} v_b^{(c)*}}{\xi_c} \right\} \times \times \sum_{m=-2}^{m=2} Y_{2m}(\mathbf{n}_b) g^{(2m)}(t')\, dt' + O(0) \qquad a = 1, \ldots, J. \tag{3.151}$$

For L being 2, and since $2L+1$ is the maximum number of independent non-null eigenvalues ξ_c^2 of a general P_L matrix of arbitrary order $J \times J$ (see Appendix C), let us stress that at most there will exist five pairs of modes $\omega_{c\pm}$ in the system strongly coupling to the five quadrupole GW amplitudes.

Discussion

The first thing to notice in the last results is the general structure of $\tilde{\phi}_a^{(lm)}(s)$ at the dominant order:

$$\tilde{\phi}_a^{(lm)}(s) \propto \eta^{-\frac{1}{2}} \sum_{\xi_c \neq 0} \left[(s^2 + \omega_{c+}^2)^{-1} - (s^2 + \omega_{c-}^2)^{-1} \right], \tag{3.152}$$

where, as always, ξ_c^2 are the non-null eigenvalues of the corresponding P_L matrix and $\omega_{c\pm}$ are the symmetric pairs of coupled mode frequencies arising from the spliting of the tuning frequency $\Omega = \omega_{NL}$ as a consequence of the presence of resonators, and which dominate the spectral composition of their motions. From this expression, it is immediately seen that there exists a mechanical amplification factor $\eta^{-\frac{1}{2}}$ affecting the resonators' displacements relative to the driving GW amplitudes $\tilde{g}^{(lm)}(s)$, what amounts to be a pre-electronics amplification in the antenna highly desirable due to the extreme weakness of expected gravitational-wave signals to be detected.

It is also essential to emphasize that the only modes contributing to the amplitudes at order $\eta^{-\frac{1}{2}}$ are those associated to the tuned modes and the non-null eigenvalues ξ_c of P_L. Due to this fact, these modes and their related frequencies are said to be strongly coupled, whereas all the non-tuned modes or particular tuned modes corresponding to null eigenvalues are said to be weakly coupled, and contribute to higher order terms.

Now in particular for monopole response (3.138), besides one observes some other features, as the fact that all the components of the system response $\tilde{q}_a(s)$ have the same value independently of the label a; in other words, each resonator dynamically behaves

in the same way, as corresponds to the spherical symmetry of monopole sphere's oscillations. Even more, they are proportional to $J^{-\frac{1}{2}}$, a factor indicating that GW energy is evenly distributed among all the resonators. For these reasons, a single transducer will experimentally suffice in this case to determine the single monopole GW amplitude $\hat{g}^{(00)}(s)$, in contrast to what happens for quadrupole GW amplitudes $\hat{g}^{(2m)}(s)$ appearing in (3.149). There, the response of one resonator is, in principle, different from another so that at least we will need five resonators providing independent outputs, as expected.

Also, these expressions for $\hat{q}_a(s)$ reassure us that we have chosen the correct tuning frequency ω_{N0} or ω_{N2} for respectively measuring the scalar amplitude $\hat{g}^{(00)}(s)$ or the quadrupolar amplitudes $\hat{g}^{(2m)}(s)$: $\hat{q}_a(s)$ in (3.138) is always directly proportional to $\hat{g}^{(00)}(s)$ and analogously $\hat{q}_a(s)$ in (3.149) is always proportional to combinations of $\hat{g}^{(2m)}(s)$, reflecting the fact that the tuning of the device to a monopole frequency makes it strongly couple to just monopole wave amplitudes, while its tuning to a quadrupole frequency makes it couple to only quadrupole wave amplitudes, even if the incoming wave carries significant quadrupole energy at the monopolar duplet ω_{+}, or significant monopole energy at the quadrupolar frequencies $\omega_{c\pm}$.

Calibration Signals

Equation (3.102) is completely general, being applicable to any sort of signal exciting the detection device, with the only proviso that its associated mathematical representation is a separable function in the variables of space and time.

This requirement is accomplished by the calibration signal of the type described in (3.41), for which

$$\mathbf{u}_{a,ext}(\mathbf{x}_a,t) = \sum_{nlm} \frac{\mathbf{f}_0}{M}\,\mathbf{u}^{*}_{nlm}(\mathbf{x}_0)\,\mathbf{u}_{nlm}(\mathbf{x}_a)\,sin\omega_{nl}t \tag{3.153}$$

$$\zeta_{calibration,a}(t) = 0, \tag{3.154}$$

so that

$$\begin{aligned}\tilde{u}_{a,ext}(s) &= \mathbf{n}_a\tilde{\mathbf{u}}_{a,ext}(\mathbf{x}_a,s)\\ &= -\sum_{nl}\frac{|A_{nl}(R)|^2}{(s^2+\omega_{nl}^2)}\,\mathcal{P}_l(\mathbf{n}_a\mathbf{n}_0)f_0 \qquad (3.155)\\ \tilde{\zeta}_{calibration,a}(s) &= 0 \qquad a=1,\ldots,J, \qquad (3.156)\end{aligned}$$

where $\mathbf{n}_0$ are the coordinates of the hit point on the sphere, and $f_0 \equiv \frac{\mathbf{n}_0 \mathbf{f}_0}{M}$. Then,

$$\begin{aligned} \tilde{q}_a(s) &= \sum_{b=1}^{J} \left[\delta_{ab} + \eta \frac{s^2\Omega^2}{(s^2+\Omega^2)^2} \chi_{ab}^{(NL)} \right]^{-1} \frac{s^2}{s^2+\Omega^2} \times \\ &\times \sum_{nl} \frac{|A_{nl}(R)|^2}{(s^2+\omega_{nl}^2)} \mathcal{P}_l(\mathbf{n}_a \mathbf{n}_0) f_0 \\ & a = 1, \ldots, J. \end{aligned} \tag{3.157}$$

It would be tedious and innecesary to reproduce in this essay the whole procedure until arriving to the final expression for $\tilde{q}_a(s)$, in first place because the derivation follows step by step the developments for GW excitations, with the only proviso that one has to consider directly the amplitudes $\tilde{q}_a(s)$ instead of functions like $\tilde{\phi}_a^{(lm)}(s)$ in (3.111) and (3.112). In any case, results will be analogous, and are placed below:

$$\begin{aligned} \tilde{q}_a(s) &= (-1)^{J-1} \eta^{-\frac{1}{2}} \sqrt{\frac{2l+1}{4\pi}} |A_{NL}(R)| f_0 \times \\ &\times \sum_{b=1}^{J} \left\{ \sum_{\xi_c \neq 0} \frac{1}{2} \left[(s^2+\omega_{c+}^2)^{-1} - (s^2+\omega_{c-}^2)^{-1} \right] \frac{v_a^{(c)} v_b^{(c)*}}{\xi_c} \right\} \mathcal{P}_L(\mathbf{n}_b \mathbf{n}_0) + O(0) \\ & a = 1, \ldots, J. \end{aligned} \tag{3.158}$$

when the system is tuned to a certain arbitrary ω_{NL} spheroidal harmonic.

In particular, if ω_{NL} is a monopole frequency ω_{N0}, the system response reduces to an expression similar to (3.138):

$$\begin{aligned} \tilde{q}_a(s) &= (-1)^{J-1} \eta^{-\frac{1}{2}} \frac{f_0}{\sqrt{4\pi J}} |A_{N0}(R)| \times \\ &\times \frac{1}{2} \left[(s^2+\omega_+^2)^{-1} - (s^2+\omega_-^2)^{-1} \right] + O(0) \qquad a = 1, \ldots, J. \end{aligned} \tag{3.159}$$

and in the time domain

$$\begin{aligned} q_a(t) &= (-1)^{J-1} \eta^{-\frac{1}{2}} \frac{f_0}{\sqrt{4\pi J}} |A_{N0}(R)| \times \\ &\times \frac{1}{2} \left[\frac{1}{\Omega} \sin \frac{1}{2}(\omega_+ - \omega_-) t \cos \Omega t \right] + O(0) \qquad a = 1, \ldots, J, \end{aligned} \tag{3.160}$$

again identical for all a, independent of either the resonator layout or the hit point and showing the expected factor $J^{-\frac{1}{2}}$ and the pair of frequencies $\omega_\pm$.

For quadrupole frequencies, one can just substitute L by 2 in (3.158), but the calculations are more interesting for specific distributions of resonators, which are going to be studied immediately in Chapter 4.

3.4.3 Mode Channels

The aim of a detection experiment is not simply the mere corrobotation of the ocurrence of the physical phenomena under testing, but also the acquisition of a maximum amount of information concerning it and and its causes.

In accordance to this philosophy, one must be able to handle the results outcoming from the observation of the spherical antenna's vibrations, that referred to the resonators' outputs, to trace back the features about the causes. This is commonly called signal deconvolution [133, 80, 91] and it is expected to provide source direction, amplitudes and polarizations of gravitational waves reaching the detector from the experimental data.

It is easily recognizable that the first step of the deconvolution procedure consists in expressing the information about the signal directly appearing in the mathematical equations of the problem as a function of the measurable quantities.

For the case of a spherical GW detector endowed with a set of resonators tuned to a monopole frequency, the previous operation can trivially be put into practice. Results in (3.138) for a gravitational wave allow to experimentally determine the only monopole GW amplitude $\tilde{g}^{(00)}(s)$ as a function of any $\tilde{q}_a(s)$ since this response is the same for every resonator. Results in (3.159) for a calibration signal show that the only quantity to fix is f_0, the intensity of the impulse. Therefore, not much knowledge is eventually available from them ultimately due as a last resort to the spherical symmetry of monopole sphere's oscillations.

More interesting is the tuning to a quadrupole harmonic, although then the way to proceed is more complicated. Let us work with the Laplace transforms, although the same reasonings will be valid in the time domain. The purpose is here to decouple the quadrupole wave amplitudes $\tilde{g}^{(2m)}(s)$ in (3.149), or find the hit point position and intensity of the calibration impulse from (3.158).

First of all, we are going to establish a matrix notation for the sake of clarity and for representing at a time both cases. The resonators' elastic deformations $\tilde{q}_a(s)$ will be arranged in a J-vector $\vec{\tilde{q}}$:

$$\vec{q} \equiv \begin{pmatrix} \hat{q}_1(s) \\ \hat{q}_2(s) \\ \vdots \\ \hat{q}_J(s) \end{pmatrix}, \tag{3.161}$$

so that (3.149) or (3.158) are rewritten as

$$\vec{q} = b_n \cdot \mathbf{V} \cdot \mathbf{D} \cdot \mathbf{V}^\dagger \cdot \mathbf{H} \cdot \vec{G}, \tag{3.162}$$

if we make the following identifications:

- b_n is a function of $\eta^{-\frac{1}{2}}$ and radial contributions, and sign depending on J:

$$b_{n,GW} = (-1)^J \eta^{-\frac{1}{2}} a_{n2} \tag{3.163}$$

$$b_{n,calibration} = (-1)^{J-1} \eta^{-\frac{1}{2}} f_0 |A_{n2}(R)|. \tag{3.164}$$

- $\mathbf{V}$ is the $J \times n$ matrix of the n eigenvectors $v^{(c)}$ of $P_2(\mathbf{n}_a \mathbf{n}_b)$ corresponding to the non-null eigenvalues ξ_c^2. We are going to consider always the maximum possible value of n, i.e. $n = 5$, what amounts to assume that at least one has five resonators providing independent outputs –see Appendix C. Of course, this must be just the minimum number of transducers in independent positions of a layout to completely determine the separation of the five quantities in $\vec{G}_{GW}$ without recursing to non-fixed arbitrary parameters. Then:

$$\mathbf{V} \equiv \begin{pmatrix} \vec{v}^{(1)} & \vec{v}^{(2)} & \vec{v}^{(3)} & \vec{v}^{(4)} & \vec{v}^{(5)} \end{pmatrix}, \tag{3.165}$$

where to ease the notation each column containing the components of a given eigenvector has been represented by the name of the whole eigenvector.

$\dagger$ in (3.162) stands for complex $*$ and transposed T, so that

$$\mathbf{V}^\dagger \equiv \mathbf{V}^{*T} \tag{3.166}$$

- $\mathbf{D}$ is the $n \times n$ matrix , under our assumptions the 5×5 matrix, represented by the diagonal form

$$\mathbf{D} \equiv diag \left[\begin{array}{ccccc} c_1, & c_2, & c_3, & c_4, & c_5 \end{array} \right] \tag{3.167}$$

where the only non-null elements of $\mathbf{D}$ placed in its diagonal are the following functions depending on the eigenvalues and the split frequencies in the Laplace domain:

$$c_i = \frac{1}{2} \left[(s^2 + \omega_{i+}^2)^{-1} - (s^2 + \omega_{i-}^2)^{-1} \right] \frac{1}{\xi_i}. \tag{3.168}$$

- $\mathbf{H}$ is the $J \times 5$ matrix of spherical harmonics:

$$\mathbf{H} \equiv \sqrt{\frac{4\pi}{5}} \left(\begin{array}{ccccc} \vec{Y}_{2,-2} & \vec{Y}_{2,-1} & \vec{Y}_{2,0} & \vec{Y}_{2,1} & \vec{Y}_{2,2} \end{array} \right), \tag{3.169}$$

each vector being of the form

$$\vec{Y}_{2,m} \equiv \left(\begin{array}{c} Y_{2,m}(\theta_1, \varphi_1) \\ Y_{2,m}(\theta_2, \varphi_2) \\ \vdots \\ Y_{2,m}(\theta_J, \varphi_J) \end{array} \right), \tag{3.170}$$

with (θ_a, φ_a) the angular position of the a-resonator.

From Appendix C, we see that $\mathbf{H}$ is just the matrix from which P_L is made up since

$$P_L = \mathbf{H}\,\mathbf{H}^{\dagger}. \tag{3.171}$$

- Finally, $\vec{G}$ is the 5-vector of functions directly related to the signals and which have to be decoupled: the quadrupolar GW amplitudes $\dot{g}^{(2m)}(s)$

$$\vec{G}_{GW} \equiv \left(\begin{array}{c} \dot{g}^{(2,-2)}(s) \\ \dot{g}^{(2,-1)}(s) \\ \dot{g}^{(2,0)}(s) \\ \dot{g}^{(2,1)}(s) \\ \dot{g}^{(2,2)}(s) \end{array} \right), \tag{3.172}$$

or the vector of spherical harmonics

$$\vec{G}_{calibration} \equiv \sqrt{\frac{4\pi}{5}} \begin{pmatrix} Y^*_{2,-2}(\mathbf{n}_0) \\ Y^*_{2,-1}(\mathbf{n}_0) \\ Y^*_{2,0}(\mathbf{n}_0) \\ Y^*_{2,1}(\mathbf{n}_0) \\ Y^*_{2,2}(\mathbf{n}_0) \end{pmatrix} \tag{3.173}$$

depending on the hitting point position $\mathbf{n}_0$, and which arises from the decomposition of $\mathcal{P}_L(\mathbf{n}_b\mathbf{n}_0)$ in (3.158) for $L = 2$ giving

$$P_2(\mathbf{n}_b\mathbf{n}_0) = \mathbf{H}\,\vec{G}_{calibration}. \tag{3.174}$$

Now, to isolate $\vec{G}$ one has to eliminate matrices $\mathbf{V}$, $\mathbf{D}$, $\mathbf{V}^\dagger$ and $\mathbf{H}$ in the rhs of (3.147), taking into account that not all of them are square matrices and consequently the inverse of everyone is not defined.

Nevertheless, let us first investigate matrix $\mathbf{V}$. This is a matrix of orthonormalised eigenvectors arranged in columns. If we multiply it on the left by its complex transposed $\mathbf{V}^\dagger$, we will obtain the 5×5-identity matrix $\mathbf{I}$, since in fact we are performing scalar products between the eigenvectors which are orthogonal and normalized:

$$\mathbf{V}^\dagger \cdot \mathbf{V} = \mathbf{I}, \tag{3.175}$$

and then

$$\mathbf{V}^\dagger \cdot \vec{q} = b_n \mathbf{V}^\dagger \cdot \mathbf{V} \cdot \mathbf{D} \cdot \mathbf{V}^\dagger\mathbf{H} \cdot \vec{G} = b_n \mathbf{I} \cdot \mathbf{D} \cdot \mathbf{V}^\dagger\mathbf{H} \cdot \vec{G} = b_n \mathbf{D} \cdot \mathbf{V}^\dagger\mathbf{H} \cdot \vec{G}. \tag{3.176}$$

At this point the problem reduces to analyse just the separation of $\mathbf{D}$ and $\mathbf{V}^\dagger\mathbf{H}$ from $\vec{G}$ in the rhs of (3.176).

We are going to call $\mathbf{D}$ the frequency matrix. Clearly, $\mathbf{D}$ is invertible: it is an square matrix with an associated non-null determinant. However, when $s^2 = -\omega^2_{c\pm}$, i.e., when s is evaluated at the resonances of the system (the poles of $e^{st}\tilde{q}_a(s)$), $\mathbf{D}$ presents singular elements.

With respect to $\mathbf{V}^\dagger\mathbf{H}$, rather than considering these two matrices separately, it is more convenient to work with the whole product, which amounts to be a square 5×5 matrix invertible matrix[4]. This property can be easily verified by performing the operation

[4] We recall we are assuming a sufficient minimum number of resonators in non-parallel positions, that

$$\mathbf{V}^{\dagger}\mathbf{H}\cdot(\mathbf{V}^{\dagger}\mathbf{H})^{\dagger}=\mathbf{V}^{\dagger}\mathbf{H}\cdot\mathbf{H}^{\dagger}\mathbf{V}=\mathbf{V}^{\dagger}P_2\mathbf{V}. \tag{3.177}$$

We recall that $\mathbf{V}$ is the matrix of eigenvectors of P_2 arranged in columns, so that

$$P_2\mathbf{V}=\mathbf{V}_{\xi} \tag{3.178}$$

with

$$\mathbf{V}_{\xi}\equiv\left(\begin{array}{ccccc}\xi_1^2\vec{v}^{(1)} & \xi_2^2\vec{v}^{(2)} & \xi_3^2\vec{v}^{(3)} & \xi_4^2\vec{v}^{(4)} & \xi_5^2\vec{v}^{(5)}\end{array}\right). \tag{3.179}$$

Inserting this new result in (3.177)

$$\mathbf{V}^{\dagger}\mathbf{H}\cdot(\mathbf{V}^{\dagger}\mathbf{H})^{\dagger}=\mathbf{V}^{\dagger}\mathbf{V}_{\xi}=diag\left[\xi_1^2,\xi_2^2,\xi_3^2,\xi_4^2,\xi_5^2\right]=\mathbf{E}_{\xi}, \tag{3.180}$$

which is a regular diagonal and invertible matrix from their elements being the non-null eigenvalues of P_2.

Then, for the determinant of $\mathbf{V}^{\dagger}\mathbf{H}$ we have

$$\left[\det(\mathbf{V}^{\dagger}\mathbf{H})\right]^2=\det(\mathbf{V}^{\dagger}\mathbf{H})\cdot(\mathbf{V}^{\dagger}\mathbf{H})^{\dagger}=\det\mathbf{E}_{\xi}\neq 0, \tag{3.181}$$

and for its right-side inverse

$$(\mathbf{V}^{\dagger}\mathbf{H})^{-1}_{right}=(\mathbf{V}^{\dagger}\mathbf{H})^{\dagger}\cdot\mathbf{E}_{\xi}^{-1}. \tag{3.182}$$

In square matrix algebra [76], it is proved that when the determinant of a matrix is non-null and there exists an one-side inverse, it is unique and is indeed *the inverse matrix*, what generally holds in our case.

Thus, from (3.162) it would always be mathematically possible to find $\vec{G}$ under the only general assumption of having a layout with at least five resonators in non-parallel positions tuned to a quadrupolar frequency:

$$b_n^{-1}(\mathbf{V}^{\dagger}\mathbf{H})^{\dagger}\cdot\mathbf{E}_{\xi}^{-1}\cdot\mathbf{D}^{-1}\cdot\mathbf{V}^{\dagger}\cdot\vec{q}=\vec{G}. \tag{3.183}$$

---

is, $\mathbf{V}$ is a matrix of order $J\times n$, with number of resonators $J\geq 5$ and number of non-null eigenvectors $n=5$. If these conditions are not accomplished, matrix $\mathbf{V}^{\dagger}\mathbf{H}$ of order $n\times 5$ is not invertible. Therefore, the case $J<5$ or $n<5$ is problematic, since then (3.162) turns out to be a set of n algebraic equations insufficient for determining the 5 spinorial amplitudes in $\vec{G}$, so that $5-n$ of them would remain as arbitrary parameters to be fixed.

We have seen that the number of necessary and sufficient final equations is always 5, so that 5 must always be the number of non-null eigenvalues, degenerate or not, of P_2 with independence of the number J of resonators. It indicates that more than five of them will provide redundant information, while less than five will not lead to a complete separation of the $g^{(2m)}$'s amplitudes. Of course, these results are valid for quadrupole tuning frequencies ω_{N2}. For other non-quadrupole tuning frequencies ω_{NL}, it would be easy to implement the whole development, but then the number of required equations is maintained to be 5, as the number of spinorial amplitudes, and not $2L+1$, as the maximum number of non-null eigenfrequencies of P_L. So, also in this situation the optimum number of resonators generating independent outputs to be mounted on the sphere's surface is 5; otherwise, we would not have enough equations ($J < 5$), or we are obliged to restrict to specific layouts with only five non-null associated eigenvectors.

Note that each element of vector $\vec{G}$ obtained as a linear combination of the vibrational amplitudes depends also on the split frequencies $\omega_{i\pm}$ through the inverse frequency matrix $\mathbf{D}^{-1}$. It would be possible and interesting to demand that each linear combination of the measured $\hat{q}_a(s)$ providing the $\hat{g}^{(2m)}(s)$ comes at a single specific frequency pair $\omega^2_{m\pm}$. This specific condition is not generally supplied by every resonator configuration allowing (3.183). It is necessary a further requirement. Let us go back to (3.176). Obviously, our desired property would be immediately achieved if $\mathbf{D}$ and $\mathbf{V}^\dagger\mathbf{H}$ commute, so that

$$b_n^{-1}\mathbf{V}^\dagger\vec{q} = \mathbf{D}\cdot\mathbf{V}^\dagger\mathbf{H}\cdot\vec{G} = \mathbf{V}^\dagger\mathbf{H}\cdot\mathbf{D}\cdot\vec{G}. \tag{3.184}$$

Vector $\mathbf{D}\vec{G}$ is already of the desired form. For instance, for a GW:

$$\vec{G}_{GW} \equiv \begin{pmatrix} c_{-2}\,\hat{g}^{(2,-2)}(s) \\ c_{-1}\,\hat{g}^{(2,-1)}(s) \\ c_0\,\hat{g}^{(2,0)}(s) \\ c_1\,\hat{g}^{(2,1)}(s) \\ c_2\,\hat{g}^{(2,2)}(s) \end{pmatrix}, \tag{3.185}$$

and hence we only need to separate it in (3.162):

$$b_n^{-1}(\mathbf{V}^\dagger\mathbf{H})^\dagger\cdot\mathbf{E}_\xi^{-1}\cdot\mathbf{V}^\dagger\cdot\vec{q} = \mathbf{D}\vec{G}. \tag{3.186}$$

Therefore, configurations of at least five resonators in non-parallel positions satisfying

$$\mathbf{D}\cdot\mathbf{V}^\dagger\mathbf{H} = \mathbf{V}^\dagger\mathbf{H}\cdot\mathbf{D} \tag{3.187}$$

will be the only allowing the construction of linear combinations at single specific frequency pairs proportional to the amplitudes in $\vec{G}$. The commutativity of these matrices is exclusively possible in two non-excluding situations: **D** is proportional to the identity matrix, that is, all the eigenvalues ξ_i and so all the frequencies $\omega_{i\pm}$ are exactly equal (maximum degeneracy, maximum isotropy in the transducers distribution); or $\mathbf{V}^{\dagger}\mathbf{H}$ is diagonal.

In next chapter we will analyse the two minimum configurations in number of resonators accomplishing these requirements, although actually they are not unique [91]. These particular distributions are on the basis of the PHCA and TIGA proposals. In fact, separation of the spherical amplitudes $h_m(t)$ for gravitational waves by forming fixed linear combinations of the measured resonators' motions was first obtained by Merkowitz and Johnson [69, 97] when studying their specific proposal TIGA for a GW antenna. They named their combinations *mode channels*, to indicate that each one is coupled only to a single mode amplitude of the uncoupled sphere and hence to a single amplitude of the gravitational field, so that signal and direction deconvolution methods can be directly applied to the mode channel set very advantageously, whereupon their occurrence is an important and attractive property highly desirable. We extend their nomenclature to the linear combinations of resonators outputs prividing the decoupling of the $g^{(2m)}(t)$ amplitudes, directly related to the the spherical $h_m(t)$ amplitudes -the specific relations are given in Chapter 6.

Here we have demonstrated that such combinations are not exclusive to the distribution associated to the TIGA layout, but always exist for resonator layouts in spherical antennæ whenever the number of non-null eigenvalues of their associated P_L matrix is exactly 5, which in particular is always assured in quadrupolar tuning for layouts with at least five resonators located in non-parallel positions, and matrices **D** and $\mathbf{V}^{\dagger}\mathbf{H}$ commute. It is nevertheless true that among those, some particular transducer configurations yield to the simplest expressions for their associated mode channels, as we will see in next chapter.

Chapter 4

SPECIFIC RESONATOR LAYOUTS

In Chapter 3, we have presented an elegant approach to the question of how the coupled system formed by a solid elastic perfect sphere and a tuned set of any number of identical resonators in arbitrary locations dynamically behaves when excited by an incoming signal, *par excellence* a gravitational wave. It has been achieved through the development of a detailed and rather sophisticated mathematical scheme, although simple in structure, providing the whole spectrum of the spherical antenna as a splitting of the free sphere's frequencies, the relative displacements at the resonators' positions, and the mode channels. It has been shown how these responses are obtained as series expansions in the small coupling constant η, revealing relevant general features such as that of the pre-electronics amplitude amplifications, or the implications of the transducer attachement causing the correlation of the sphere's deformations to all of the sphere's spheroidal eigenmodes.

Based on these results, it is possible and convenient for practical situations to analyse particular proposals of spherical antennæ with resonators fixed at specific locations. The generality of our procedures ensures their capability of being applicable to any thinkable device, whenever the transducers remain identical at this stage and the core of the detector is, if not a perfect sphere, a quasi spherical elastic body with equivalent monopole and quadrupole vibrational modes.

This philosophy of substituting a true sphere by an object that approximates it is required as a solution to certain technical complications of spherical antennæ. like, for

instance, those emerging from the practical mounting and stability of resonators. Thus, practical GW-antenna devices are milled into a close-to-spherical geometry, usually a regular polyhedric shape, with a given number of ideally-identical ideally-tuned resonators linked at specific positions making a particular configuration. Then, the important question is whether there exists any favoured or optimum arrangement between those allowing mode channels.

Stephen Merkowitz and Warren Johnson were the pioneers suggesting and experimentally implementing a GW detector of these characteristics at LSU [69, 97, 95, 98]. They proposed for quadrupole sensing a highly symmetric resonator layout consisting in a set of six transducers attached to the six non-parallel faces of a truncated icosahedron. The system was called TIGA, the acronym for *Truncated Icosahedral Gravitational wave Antenna*, and will be reconsidered in section 4.2 according to our general procedures and results in the former chapter, reassessing in this new light its response.

Previously, in section 4.1, we present an alternative new proposal based on pentagonal layouts of only five resonators equidistantly distributed along a parallel of the sphere, in this case replaced by a pentagonal hexacontahedron (PHC). These pentagonal arrangements exhibit rather appealing properties and also some desirable advantages for a complete GW antenna called by us PHCA -Pentagonal Hexacontahedral Antenna-, which we are going to discuss immediately below [84, 85, 86].

4.1 PHCA Proposal

As we have discussed when analysing the concept of mode channels in subsection 3.4.3 of Chapter 3, the minimum number of resonators in a layout providing independent outputs required for the unambiguous determination of the five quadrupole GW amplitudes $\hat{g}^{(2m)}(s)$ in a deconvolution procedure is precisely five. Since having more than five sensors, even in non-parallel positions, just produces redundant information and also increases the number of mathematical equations in the GRD set describing the dynamical behaviour of the coupled system, what, in principle, makes more difficult its resolution -for instance, it would be necessary to find the eigenvalues and eigenvectors of the $J \times J$ matrix $P_2(\mathbf{n}_a \mathbf{n}_b)$, where we recall J is the number of resonators-, one may wonder whether there exist optimum transducer layouts with only five of them. The answer is affirmative: distributions having a sphere diameter as an axis of *pentagonal symmetry* show a rather interesting structure. On the basis of this feature, let us present

our PHCA proposal.

4.1.1 Description

In pursuing a search for five transducer configurations, we found that sets with resonators placed in the same plane along a parallel of the sphere every 72°, i.e., layouts exhibiting *pentagonal symmetry*, also named by us *pentagonal arrangements*, possess important distinguishing characteristics affecting the responses of the complete GW antenna: the splitting and distribution of the system's frequencies and amplitudes, the structure of the mode channels...

More explicitly, in pentagonal layouts the five resonators are located at the spherical positions on the sphere surface:

$$\theta_a = \Theta, \qquad \varphi_a = (a-1)\frac{2\pi}{5} \qquad a = 1, \ldots, 5. \tag{4.1}$$

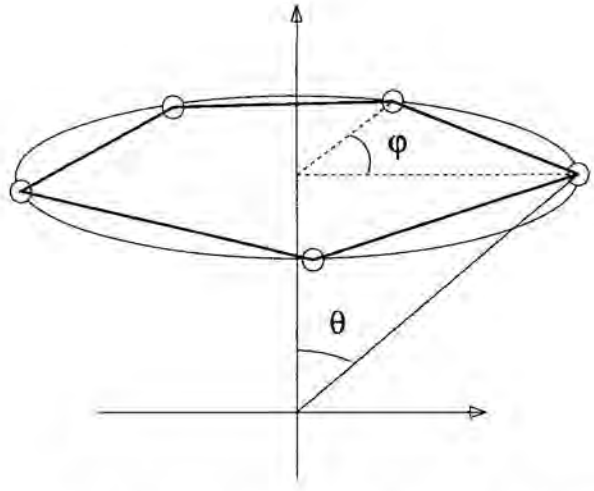

Figure 4.1. *Pentagonal layout. Resonators are positioned on the sphere surface drawing an imaginary regular pentagon on a plane including a given parallel of the sphere, denoted by angle* Θ. φ *stands for the angle of separation between any pair of neighbouring transducers, and its value is of* 72°.

As explained above, these transducers are not mounted in practice on a perfect sphere, but on a quasi spherically shaped detector so to avoid technical complications. Therefore,

shapes with axes of pentagonal symmetry facilitating such distributions must be searched.

Among the 18 quasi-regular convex polyhedra[1] [63, 57], the *pentagonal hexacontahedron*, PHC, erects into the most satisfactory candidate. This is a sixty face convex body with six different axes of pentagonal symmetry, whose faces are the identical irregular pentagons shown in Figure 4.2., but no two of them are parallel, so that we have not to worry about the matter of locating the resonators in non-parallel positions.

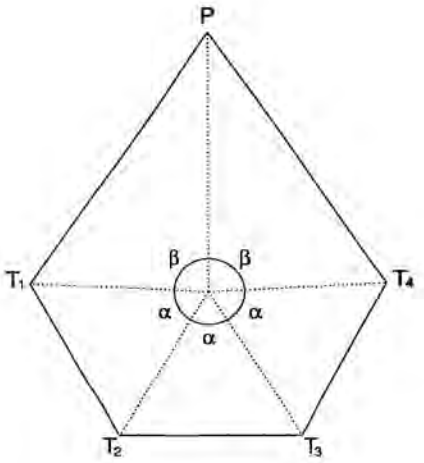

Figure 4.2. *Face of the pentagonal hexacontahedron. The confluence point of the dotted lines at the centre is the tangency point of the inscribed sphere to the polyhedron: the labeled angles have values $\alpha = 61.863°$, $\beta = 87.205°$; the angles at the T-vertices are all equal, and are $118.1366°$, while the angle at P is $67.4536°$; the ratio of a long edge (e.g. PT_1) to a short one (e.g. T_1T_2) is 1.74985, and the radius of the inscribed sphere is twice the long edge of the pentagon, $R = 2\,PT_1$.*

This polyhedron encloses an inscribed sphere which is tangent to each face at the confluence point marked in the figure. If transducers are attached to such positions, they will all be equidistant from the centre of the body, in a very good simulation of the ideal theoretical spherical situation, also supported by the fact that the ratio of the

[1] Indeed, 5 of these quasi-regular convex polyhedra actually are strictly regular, and are called the Plato's solids: the tetrahedron, the cube, the octahedron, the dodecahedron and the icosahedron. One can also count as elements of the quasi-regular convex polyhedra group the duals of the remaining 13 Archimedes' bodies, whereupon the total number of elements grows up to 31, and up to 35 if the 4 mirror images which differ from the originals are also added.

pentagonal hexacontahedron volume to that of the inscribed sphere is very close to 1, being the exact value of 1.057.

We thus propose the pentagonal hexacontahedron elastic solid coupled to a set of 5 resonant transducers attached to the centres of certain suitable faces distributed so as to preserve an axis of pentagonal symmetry as a GW antenna.

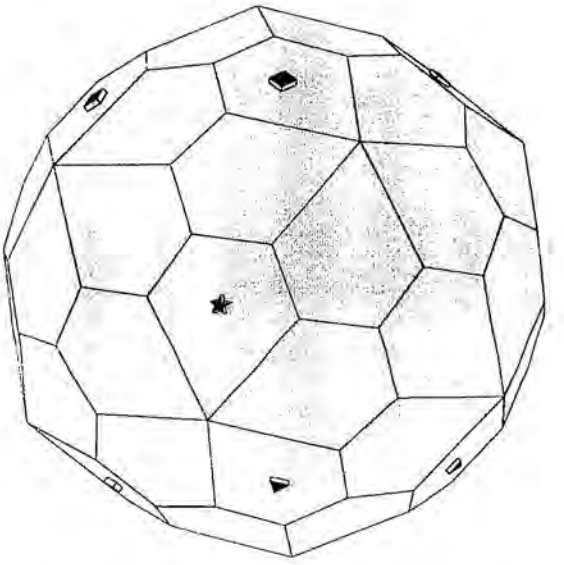

Figure 4.3. *PHC Proposal. Marked faces in the pentagonal hexacontahedron indicate resonator positions: a square for transducers tuned to the first quadrupole frequency, a triangle for that tuned to the second, and a star for the monopole sensor.*

The question of which is the most suitable transducer distribution with an axis of pentagonal symmetry, or equivalently, which must be the chosen faces for sensor mounting, is clarified by the analysis of the spherical antenna responses for generic pentagonal configurations, what will be undertook in the following subsection, before the concluding study of the capabilities of such a device as a complete multimode multifrequency individual antenna.

4.1.2 Pentagonal Arrangements Response

It is worth noting that, as already shown in subsection 3.4.2, the system response to monopole gravitational radiation does not depend on the resonators' positions on the sphere's surface, so attention here will be exclusively centred on the expressions for quadrupole gravitational radiation.

We recall that results in the precedent chapter are general and valid for spherical detectors coupled to any layout of identical resonators, so that, in particular, they also apply and can be further constrained to arrangements of the pentagonal type. It would be only necessary to evaluate the eigenvalues and eigenvectors of the 5×5 P_2 matrix of Legendre polynomials, which will read as always (see Appendix C)

$$P_2 = \mathbf{H}\mathbf{H}^{\dagger}, \tag{4.2}$$

being $\mathbf{H}$ the 5×5 matrix made up from the spherical harmonics 5-vectors $\vec{Y}_{2,m}$ having as components the values for each resonator location:

$$\mathbf{H} = \sqrt{\frac{4\pi}{5}} \left(\begin{array}{ccccc} \vec{Y}_{2,-2} & \vec{Y}_{2,-1} & \vec{Y}_{2,0} & \vec{Y}_{2,1} & \vec{Y}_{2,2} \end{array} \right), \tag{4.3}$$

$$\vec{Y}_{2,m} = \left(\begin{array}{c} Y_{2,m}(\mathbf{n}_1) \\ Y_{2,m}(\mathbf{n}_2) \\ \vdots \\ Y_{2,m}(\mathbf{n}_5) \end{array} \right), \tag{4.4}$$

Since the five pentagonal locations of the transducers are:

Resonator	Polar angle θ	Azimuthal angle φ
1	Θ	0
2	Θ	$72° \equiv \frac{2\pi}{5}$ rad
3	Θ	$144° \equiv \frac{4\pi}{5}$ rad
4	Θ	$216° \equiv \frac{6\pi}{5}$ rad
5	Θ	$288° \equiv \frac{8\pi}{5}$ rad

H can be written

$$\mathbf{H} = \begin{pmatrix} A & B & C & -B & A \\ Ae^{-2i\frac{2\pi}{5}} & Be^{-i\frac{2\pi}{5}} & C & -Be^{i\frac{2\pi}{5}} & Ae^{2i\frac{2\pi}{5}} \\ Ae^{-2i\frac{4\pi}{5}} & Be^{-i\frac{4\pi}{5}} & C & -Be^{i\frac{4\pi}{5}} & Ae^{2i\frac{4\pi}{5}} \\ Ae^{-2i\frac{6\pi}{5}} & Be^{-i\frac{6\pi}{5}} & C & -Be^{i\frac{6\pi}{5}} & Ae^{2i\frac{6\pi}{5}} \\ Ae^{-2i\frac{8\pi}{5}} & Be^{-i\frac{8\pi}{5}} & C & -Be^{i\frac{8\pi}{5}} & Ae^{2i\frac{8\pi}{5}} \end{pmatrix}, \tag{4.5}$$

with A, B and C just functions of the common polar angle α entering the spherical harmonics $Y_{2,m}^{*}$:

$$\begin{aligned} A &= \sqrt{\frac{3}{8}}\sin^2\Theta \\ B &= \sqrt{\frac{3}{2}}\sin\Theta\cos\Theta \\ C &= \frac{1}{2}(3\cos^2\Theta - 1), \end{aligned} \tag{4.6}$$

and P_2 is

$$P_2 = \begin{pmatrix} 1 & b^2 & c^2 & c^2 & b^2 \\ b^2 & 1 & b^2 & c^2 & c^2 \\ c^2 & b^2 & 1 & b^2 & c^2 \\ c^2 & c^2 & b^2 & 1 & b^2 \\ b^2 & c^2 & c^2 & b^2 & 1 \end{pmatrix}, \tag{4.7}$$

with

$$\begin{aligned} b^2 &= 2A^2 \cos\frac{4\pi}{5} + 2B^2 \cos\frac{2\pi}{5} + C^2 \\ c^2 &= 2A^2 \cos\frac{2\pi}{5} + 2B^2 \cos\frac{4\pi}{5} + C^2. \end{aligned} \tag{4.8}$$

We clearly observe, as already announced in Chapter 3, that P_2 strictly is a Toeplitz matrix for pentagonal distributions with the correlations between pairs of resonators distinguishing between *first* and *second* neighbours, being respectively b^2 and c^2 their characteristic values.

It happens that the five eigenvalues of P_2 are precisely

$$\begin{aligned} 5\,A^2 &= \xi_2^2 = \xi_{-2}^2 = \frac{15}{8}\sin^4\Theta \\ 5\,B^2 &= \xi_1^2 = \xi_{-1}^2 = \frac{15}{2}\sin^2\Theta\cos^2\Theta \\ 5\,C^2 &= \xi_0^2 = \frac{5}{4}(3\cos^2\Theta - 1)^2. \end{aligned} \tag{4.9}$$

This can be easily verified from the fact that they also are eigenvalues of $\mathbf{H}^\dagger\mathbf{H}$. The proof is given in Appendix C.

$\mathbf{H}^\dagger\mathbf{H}$ is here a diagonal matrix due to the following identity nicely fulfilled by pentagonal distributions:

$$1 + e^{in\frac{2\pi}{5}} + e^{in\frac{4\pi}{5}} + e^{in\frac{6\pi}{5}} + e^{in\frac{8\pi}{5}} = 0 \tag{4.10}$$

for any integer value of n. except multiples of 5; in this case, the result will be just 5 and not 0.

Having this into account, the multiplication of matrices $\mathbf{H}^\dagger$ and $\mathbf{H}$ is

$$\mathbf{H}^{\dagger}\mathbf{H} = \begin{pmatrix} 5A^2 & 0 & 0 & 0 & 0 \\ 0 & 5B^2 & 0 & 0 & 0 \\ 0 & 0 & 5C^2 & 0 & 0 \\ 0 & 0 & 0 & 5B^2 & 0 \\ 0 & 0 & 0 & 0 & 5A^2 \end{pmatrix} = \mathbf{E}_{\xi}, \tag{4.11}$$

and from this it is directly seen that the eigenvalues of $P_2 = \mathbf{H}\mathbf{H}^{\dagger}$ are those in (4.7).

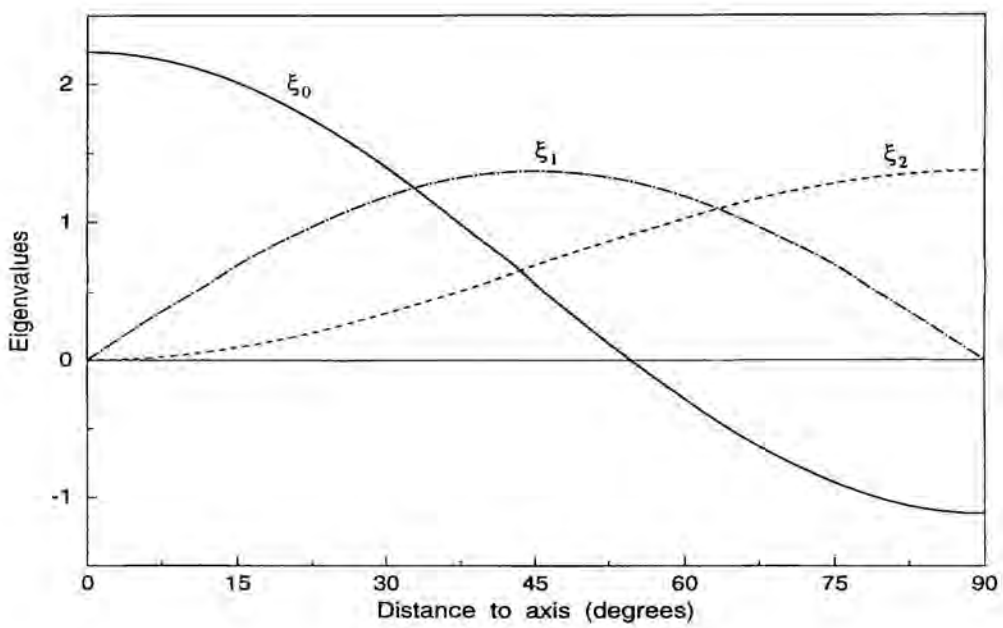

Figure 4.4. *Eigenvalues ξ_0, ξ_1 and ξ_2 for pentagonal configurations as functions of the polar angle α relative to the axis of symmetry of the distribution, in accordance to formulas 4.7.*

With respect to the eigenvectors, they are immediately inferred from (4.9) by multiplying its left hand side by matrix $\mathbf{H}$ on the left

$$\mathbf{H} \cdot \mathbf{H}^{\dagger}\mathbf{H} = (\mathbf{H}\mathbf{H}^{\dagger}) \cdot \mathbf{H} = P_2\,\mathbf{H}, \tag{4.12}$$

and its right hand side by the same matrix also on the left

$$\mathbf{H} \cdot \mathbf{H}^{\dagger}\mathbf{H} = \mathbf{H}\,\mathbf{E}_{\xi}. \tag{4.13}$$

Then,

$$P_2\,\mathbf{H} = \mathbf{H}\,\mathbf{E}_{\xi}, \tag{4.14}$$

what means that eigenvectors of P_2 corresponding to the found eigenvalues (4.7) are basically the constructing vectors of $\mathbf{H}$, from (4.3):

$$\vec{v}^{(m)} = \sqrt{\frac{4\pi}{5}}\vec{Y}_{2,m} \tag{4.15}$$

with components

$$v_a^{(m)} = \sqrt{\frac{4\pi}{5}}Y_{2,m}(\mathbf{n}_a). \tag{4.16}$$

Their normalization includes the eigenvalues as normalization constants, so that the normalized eigenvectors finally are:

$$\vec{v}^{(m)} = \sqrt{\frac{4\pi}{5}}\xi_m^{-1}\vec{Y}_{2,m}. \tag{4.17}$$

Now, the only operation one has to perform is the substitution of these pentagonal eigenvalues and eigenvectors in the expressions for the frequencies, the amplitudes and the mode channels.

- **Frequencies**

From (3.131),

$$\omega_{m,\pm}^2 = \omega_{N2}^2\left(1 \pm \sqrt{\frac{5}{4\pi}}|A_{N2}(R)|\xi_m\eta^{\frac{1}{2}}\right) + O(\eta) \qquad m = -2,\ldots,2. \tag{4.18}$$

Hence, to the lowest order one has for pentagonal configurations:

$$\omega_{0,\pm}^2 = \omega_{N2}^2\left(1 \pm \frac{5}{2}\sqrt{\frac{1}{4\pi}}|A_{N2}(R)|(3\cos^2\Theta - 1)\,\eta^{\frac{1}{2}}\right)$$

$$\omega_{1,\pm}^2 = \omega_{+1,\pm}^2 = \omega_{-1,\pm}^2 = \omega_{N2}^2 \left(1 \pm \frac{5}{2}\sqrt{\frac{3}{2\pi}}|A_{N2}(R)|\sin\Theta\cos\Theta\,\eta^{\frac{1}{2}}\right)$$
$$\omega_{2,\pm}^2 = \omega_{+2,\pm}^2 = \omega_{-2,\pm}^2 = \omega_{N2}^2 \left(1 \pm \frac{5}{2}\sqrt{\frac{3}{8\pi}}|A_{N2}(R)|\sin^2\Theta\,\eta^{\frac{1}{2}}\right). \qquad (4.19)$$

As is clearly reflected in these formulas, the five expected pairs of frequencies reduce to three different doublets $\omega_{0,\pm}^2$, $\omega_{1,\pm}^2$ and $\omega_{2,\pm}^2$, so that pentagonal distributions keep a certain degree of degeneracy.

- **Amplitudes**

The most important distinguishing characteristics of pentagonal layouts is best displayed by the explicit vibrational amplitudes measured by the transducers. From (3.134):

$$\tilde{q}_a(s) = -\eta^{-\frac{1}{2}}\sqrt{\frac{4\pi}{5}}a_{N2}\left\{\frac{1}{2\xi_0}\left[(s^2+\omega_{0+}^2)^{-1}-(s^2+\omega_{0-}^2)^{-1}\right]Y_{20}(\mathbf{n}_a)\hat{g}^{(20)}(s)\right.$$
$$+\frac{1}{2\xi_1}\left[(s^2+\omega_{1+}^2)^{-1}-(s^2+\omega_{1-}^2)^{-1}\right]\left[Y_{21}(\mathbf{n}_a)\hat{g}^{(21)}(s)+Y_{2-1}(\mathbf{n}_a)\hat{g}^{(2-1)}(s)\right]$$
$$\left.+\frac{1}{2\xi_2}\left[(s^2+\omega_{2+}^2)^{-1}-(s^2+\omega_{2-}^2)^{-1}\right]\left[Y_{22}(\mathbf{n}_a)\hat{g}^{(22)}(s)+Y_{2-2}(\mathbf{n}_a)\hat{g}^{(2-2)}(s)\right]\right\} \qquad (4.20)$$

This equation clearly indicates that different wave amplitudes selectively couple to different detector frequencies. This should be consideed a very remarkable fact, for it thence follows that simple inspection of the system readout spectrum immediately reveals whether a given wave amplitude $\hat{g}^{(2m)}(s)$ is present in the incoming signal or not.

- **Mode Channels**

Mode channels for pentagonal configurations are easily constructed. Equation (3.171) gives us the recipe in a general case:

$$\mathbf{D}\vec{G} = b_n^{-1}(\mathbf{V}^\dagger\mathbf{H})^\dagger \cdot \mathbf{E}_\xi^{-1} \cdot \mathbf{V}^\dagger \cdot \vec{q}, \qquad (4.21)$$

whenever $\mathbf{D}$ and $\mathbf{V}^\dagger\mathbf{H}$ commute (quantities, vectors and matrices entering this expression are the usual –refresh your memory in 3.4.3).

Thanks to the nice properties of the layouts we are working with, the commutativity requirement is satisfied due to the fact that $\mathbf{V}^\dagger\mathbf{H}$ is in this case a diagonal matrix, indeed *matricially proportional* to $\mathbf{E}_\xi$ in (4.9).

$$\mathbf{V}^\dagger\mathbf{H} \equiv \tilde{\mathbf{H}}^\dagger\mathbf{H} = \begin{pmatrix} \frac{1}{\xi_2} & 0 & 0 & 0 & 0 \\ 0 & \frac{1}{\xi_1} & 0 & 0 & 0 \\ 0 & 0 & \frac{1}{\xi_0} & 0 & 0 \\ 0 & 0 & 0 & \frac{1}{\xi_1} & 0 \\ 0 & 0 & 0 & 0 & \frac{1}{\xi_2} \end{pmatrix} \cdot \mathbf{E}_\xi$$

$$= \begin{pmatrix} \xi_2 & 0 & 0 & 0 & 0 \\ 0 & \xi_1 & 0 & 0 & 0 \\ 0 & 0 & \xi_0 & 0 & 0 \\ 0 & 0 & 0 & \xi_1 & 0 \\ 0 & 0 & 0 & 0 & \xi_2 \end{pmatrix}, \tag{4.22}$$

since the renamed matrix $\tilde{\mathbf{H}}^\dagger \equiv \mathbf{V}^\dagger$ is basically $\mathbf{H}^\dagger$:

$$\tilde{\mathbf{H}}^\dagger = \sqrt{\frac{4\pi}{5}} \begin{pmatrix} \frac{1}{\xi_2}\vec{Y}^*_{2-2} \\ \frac{1}{\xi_1}\vec{Y}^*_{2-1} \\ \frac{1}{\xi_0}\vec{Y}^*_{20} \\ \frac{1}{\xi_1}\vec{Y}^*_{21} \\ \frac{1}{\xi_2}\vec{Y}^*_{22} \end{pmatrix}. \tag{4.23}$$

Hence, by substitution into (4.19), it is found that

$$\mathbf{D}\vec{G} = b_n^{-1}(\mathbf{V}^\dagger\mathbf{H})^\dagger \cdot \mathbf{E}_\xi^{-1} \cdot \mathbf{V}^\dagger \cdot \vec{q} =$$

$$= b_n^{-1} \begin{pmatrix} \xi_{-2}^{-1} & 0 & 0 & 0 & 0 \\ 0 & \xi_{-1}^{-1} & 0 & 0 & 0 \\ 0 & 0 & \xi_0^{-1} & 0 & 0 \\ 0 & 0 & 0 & \xi_1^{-1} & 0 \\ 0 & 0 & 0 & 0 & \xi_2^{-1} \end{pmatrix} \mathbf{V}^\dagger\vec{q}, \tag{4.24}$$

and equivalently

$$\vec{y}(s) \equiv \mathbf{V}^\dagger\vec{q}(s) = b_n \begin{pmatrix} \xi_{-2} & 0 & 0 & 0 & 0 \\ 0 & \xi_{-1} & 0 & 0 & 0 \\ 0 & 0 & \xi_0 & 0 & 0 \\ 0 & 0 & 0 & \xi_1 & 0 \\ 0 & 0 & 0 & 0 & \xi_2 \end{pmatrix} \mathbf{D}\vec{G}, \tag{4.25}$$

or in components

$$\hat{y}^{(m)}(s) \equiv \sum_{a=1}^{5} v_a^{(m)*} \hat{q}_a(s) =$$
$$= \eta^{-\frac{1}{2}} a_{N2} \frac{1}{2} \left[(s^2 + \omega_{m+}^2)^{-1} - (s^2 + \omega_{m-}^2)^{-1} \right] \hat{g}^{(2m)}(s) + O(0). \qquad (4.26)$$

As could be expected, each mode channel comes at a single specific pair $\omega_{m,\pm}$ associated to a certain quadrupole component of the gravitational wave. It thus appears that a pentagonal transducer configuration not only immediately reflects the spinorial GW structure as seen in the laboratory frame, but at the same time enables signal observations over a somewhat richer frequency band than other recognized configurations, as will be seen in next section.

4.1.3 PHCA as a Complete GW Antenna

Among all the virtually infinite number of pentagonal configurations of resonators attachable to a sphere's surface, it is clear that that compatible with the pentagonal hexacontahedron face orientations must be selected for the construction of a PHCA antenna.

Once given a certain axis of symmetry of the polyhedron, it happens that the number of possible pentagonal distributions reduce to only twelve available layouts, which can be divided into two groups, each element of one of them having a relative in the other, so that their respective layout parallel's co-latitude angle Θ are supplementary; however, these *supplementary pentagonal distributions* are not reflections with respect to the equatorial plane, since the resonators' azimuthal angles are not the same. In any case, these spherical coordinates of course coincide with the polar and azimuthal angles locating in space the centre of the faces on which they are mounted.

These supplementary pentagonal distributions cause identical frequency splitting and hence identical system's responses, what can be inferred from the eigenvalues ξ_m only depending through trigonometric functions on angle Θ and never on φ (see (4.7) and (4.17)), whereby the actual number of pentagonal arrangements being individual candidates for finally conclude the PHCA proposal is six.

Which one would be the most favourable distribution? The answer must be searched in accordance to adequate optimization criteria on the basis of properties for the system's responses. There is not an unique criterion for the selection of a certain polar

Pentagonal Layout	Polar Angle Θ	Azimutal angles φ_1	φ_2	φ_3	φ_4	φ_5
1	23.233°	0°				
2	42.6°	36°				
3	50.05°	0°				
			+72°	+144°	+216°	+288°
4	67.617°	23.95°				
5	76.783°	69.417°				
6	86.15°	43.967°				
6'	93.85°	18.25°				
5'	103.217°	64.8°				
4'	112.383°	38.267°				
			+72°	+144°	+216°	+288°
3'	129.95°	62.217°				
2'	137.4°	26.217°				
1'	156.767°	62.217°				

Table 4.1. *Possible pentagonal distributions of resonators in a pentagonal hexacontahedron around an unique axis of pentagonal symmetry taken as the z axis of coordinates. Θ comes in pairs of supplementary angles for layouts n and n', and φ is explicitly written for one of the resonators in every pentagonal distribution. The remaining four azimuthal angles are always obtained from respectively adding to the one given the quantities* 72°, 144°, 216° *and* 288°.

angle Θ, mainly if we do not restrict to exclusively consider the pentagonal hexacontahedron [124]. For example, if the 5 faces of a regular icosahedron are selected for sensor mounting, $\Theta = 63.45°$. then a four-fold degenerate pair plus a single non-degenerate pair is obtained. Moreover. the number of choices in virtually infinite if the sphere is not milled into a polyhedral shape; if the resonator parallel is 50° or 22.6° then the three frequencies ω_{0+}, ω_{1+} and ω_{2+} are equally spaced. In analogy, and since the most relevant distinguishing characteristic of pentagonal arrangements is precisely that of causing the selective coupling of the different wave amplitudes to the different detector frequencies arising from the splitting of the resonant ω_{NL}, the assessment leading to the definite PHCA proposal will be that of maintaining the frequency pairs $\omega_{m\pm}$ as evenly spaced as possible so to maximally preserve the spectral structure far from any degree of nearness or even degeneracy of the $\omega_{0\pm}$, $\omega_{1\pm}$ and $\omega_{2\pm}$ frequencies.

Then, regarding the pentagonal hexacontahedron, there is only one pentagonal layout in the best agreement with the previous criterion, and it is that arranged at angle $\Theta = 67.617°$, whence

$$\begin{aligned} \omega_{0\pm} &= \omega_{12}\left(1 \pm 0.5756\eta^{\frac{1}{2}}\right) \\ \omega_{1\pm} &= \omega_{12}\left(1 \pm 0.8787\eta^{\frac{1}{2}}\right) \\ \omega_{2\pm} &= \omega_{12}\left(1 \pm 1.0668\eta^{\frac{1}{2}}\right) \end{aligned} \tag{4.27}$$

for instance for $\omega_{N2} \equiv \omega_{12}$, the first quadrupole harmonic.

Summing up. our PHCA proposal plans the use of a pentagonal hexacontahedral shaped detector with five resonators attached to its five faces at polar angle $\Theta = 67.617°$ *following a distribution of pentagonal geometry around an axis of symmetry.*

Even more, this proposal was made with the idea of building an as complete as possible spherical GW antenna. which amounts to making it sensitive at the first two quadrupole frequencies and at the first monopole one. This would take advantage of the good sphere cross section at the second quadrupole harmonic [32] -see Table 2.2. in Chapter 2-, and would enable measuring, or thresholding, eventual monopole GW radiation. This second quadrupole harmonic can be ω_{22}, and thanks to the fact that the system patterns have identical structure for the harmonics of a given l series, in this case $l = 2$, -see formulas for quadrupole and monopole radiation sensing, respectively (3.123) and (3.134)-, identical criteria for resonator layout design apply to either set of transducers tuned to the first harmonic ω_{12} or the second ω_{22}. Therefore, we propose that a second set of resonators

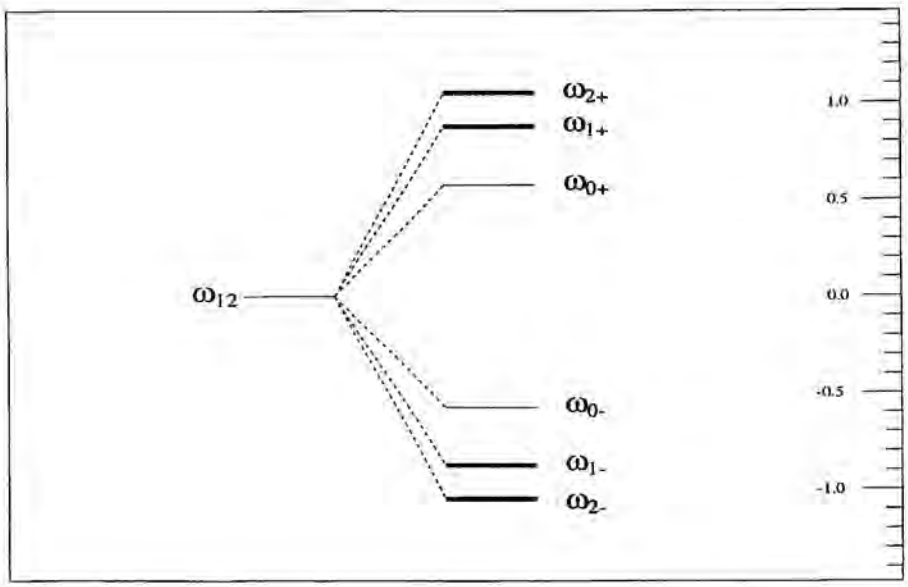

Figure 4.5. *Splitting of the resonance frequency for the first quadrupole harmonic in the PHCA proposal. The two outer pairs of the spectrum are doubly degenerate each, whereas the inner pair is non-degenerate. Distances from the new frequencies to the resonance original one are represented in the graduated vertical axis, where units are* $\omega_{12}\eta^{\frac{1}{2}}$, *and the central value, labelled 0.0, corresponds to* ω_{12}.

tuned to the second quadrupole harmonic can be placed in an equivalent position in the southern hemisphere, i.e., *we propose two sets of supplementary pentagonal layouts, each respectively tuned to the first quadrupole harmonic* ω_{12} *and the second quadrupole harmonic* ω_{22}, *so to exploit the possibility of the PHCA antenna as a multi-frequency device. Finally, an eleventh resonator tuned to the first monopole frequency* ω_{10} *can be added at another arbitrary face for monopole sensing.* It is not difficult to see, by the general methods outlined in this essay, that cross interactions between these three sets of resonators is only second order in $\eta^{\frac{1}{2}}$, therefore weak.

A spherical GW detector with such a set of altogether 11 transducers would be a very complete multi-mode multi-frequency device with an unprecedented capability as an individual antenna. Among other, it would practically enable monitoring of coales-

cencing binary chirp signals by means of a rather robust double passage method [30], a prospect which was considered so far possible only with broadband long baseline laser interferometers [73, 74], and is almost unthinkable with currently operating cylindrical bars.

4.2 The TIGA Configuration

Stephen Merkowitz and Warren Johnson of the LSU were the first suggesting a specific desing for a spherical GW antenna, which consisted in a set of six transducers attached to the six non-parallel pentagonal faces of a truncated icosahedron, as shown schematically in Figure 4.6. They called this special arrangement TIGA, for Truncated Icosahedral Gravitational wave Antenna [69, 97, 95, 98]. It will be reconsidered here as one more particularization of our general theory for spherical GW detectors.

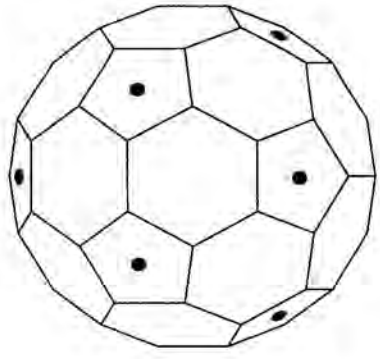

Figure 4.6. *Scheme of the Truncated Icosahedral GW Antenna, with resonator locations indicated.*

4.2.1 Description

The truncated icosahedron, TI, is a polyhedron belonging to the same point group of symmetries as the dodecahedron [63, 57], although the former better approximates a sphere: the ratio of the *circumscribed* sphere to the TI volume is of 1.153 –compare with the 1.057 for the ratio of the *inscribed* sphere to the PHC volume; clearly, the

pentagonal hexacontahedron is appreciably more spherical–. It has 32 flat surfaces – instead of the sixty of the PHC– for mounting transducers, calibrators, balancing weights and suspension attachments. 20 of them are regular hexagons, whereas the remaining 12 are pentagons forming six pairs of parallel faces. Merkowitz and Johnson precisely proposed for resonator locations the centers of six of those pentagons, being non-parallel, which were interesting for being also the positions of the centres of half the faces of a suitably oriented dodecahedron.

Resonator	Polar angle θ	Azimuthal angle φ
1	37.377°	180°
2	37.377°	60°
3	37.377°	300°
4	79.188°	120°
5	79.188°	0°
6	79.188°	240°

Table 4.2. *Resonator positions for the TIGA configuration. The transducers lie at two polar angles, and the azimuthal angles are multiples of* 60° *as shown, whenever the coordinate axes are taken so that the z axis is perpendicular to the x-y plane of Figure 4.6., passing through the centre of the central hexagon.*

They discovered that they had an arrangement that greatly simplified the frequency structure of the system's spectrum: it became two degenerate quintuplets and a singlet. It is also not difficult to see that the TIGA was the minimal configuration with so much degeneracy, as there are no 5-resonator configurations with equivalent high symmetry since there is no regular polyhedron with 10 faces. (There are however other non-minimal sets with the same degree of degeneracy, but then more than six resonators are required,

for example 10 transducers on the ten non-parallel faces of a regular icosahedron, etc. –see [91] for further analysis of this and other possibilities). This high symmetry of the TIGA arrangement became evident even when examining the *analytic* solutions for the equations of motion describing the resonator amplitudes $q_j(t)$, and from these the mode channels.

Let us now reconsider these results in accordance with our general procedures, indeed applicable to any conceivable proposal.

4.2.2 TIGA Response

The first step in the finding of the eigenvalues and the eigenvectors of the P_2 matrix of Legendre polynomials, in this case of range 6×6, which is written

$$P_2 = \mathbf{H}\mathbf{H}^\dagger, \tag{4.28}$$

with

$$\begin{aligned} \mathbf{H} &= \sqrt{\frac{4\pi}{5}} \left(\begin{array}{ccccc} \vec{Y}_{2,-2} & \vec{Y}_{2,-1} & \vec{Y}_{2,0} & \vec{Y}_{2,1} & \vec{Y}_{2,2} \end{array} \right) = \\ &= \left(\begin{array}{ccccc} Aa & -Ba & C & Ba & Aa \\ Ab & -B\bar{b} & C & B\bar{b} & A\bar{b} \\ A\bar{b} & -B\bar{b} & C & B\bar{b} & Ab \\ B\bar{b} & Ab & -C & -A\bar{b} & B\bar{b} \\ Ba & Aa & -C & -Aa & Ba \\ B\bar{b} & A\bar{b} & -C & -Ab & B\bar{b} \end{array} \right), \end{aligned} \tag{4.29}$$

where A, B and C are the real values:

$$\begin{aligned} A &= \sqrt{\tfrac{3}{8}} \sin^2\theta_1 = \sqrt{\frac{3}{2}} \sin\theta_2 \cos\theta_2; \qquad \theta_1 = 37.377^\circ \\ B &= \sqrt{\tfrac{3}{8}} \sin^2\theta_2 = \sqrt{\frac{3}{2}} \sin\theta_1 \cos\theta_1; \qquad \theta_2 = 79.188^\circ \\ C &= \tfrac{1}{2} \left(3\cos^2\theta_1 - 1\right) = -\frac{1}{2} \left(3\cos^2\theta_2 - 1\right), \end{aligned} \tag{4.30}$$

and a, b and c are the complex numbers:

$$a = 1$$
$$b = -\frac{1}{2} - \frac{\sqrt{3}}{2}i \qquad \bar{b} = -\frac{1}{2} + \frac{\sqrt{3}}{2}i. \tag{4.31}$$

P_2 is

$$P_2 = \begin{pmatrix} 1 & -b^2 & -b^2 & -b^2 & -b^2 & -b^2 \\ -b^2 & 1 & -b^2 & -b^2 & -b^2 & -b^2 \\ -b^2 & -b^2 & 1 & -b^2 & -b^2 & -b^2 \\ -b^2 & -b^2 & -b^2 & 1 & -b^2 & -b^2 \\ -b^2 & -b^2 & -b^2 & -b^2 & 1 & -b^2 \\ -b^2 & -b^2 & -b^2 & -b^2 & -b^2 & 1 \end{pmatrix}, \quad b^2 = A^2 + B^2 - C^2. \tag{4.32}$$

P_2 in this case trivially is a Toeplitz matrix like for pentagonal distributions. The correlations between any given pair of resonators is always characterized by the same value $-b^2$.

The product of $\mathbf{H}^\dagger$ and $\mathbf{H}$ immediately gives the five non-null eigenvalues (see the precedent section 4.2.1 and Appendix C):

$$\mathbf{H}^\dagger\mathbf{H} = \begin{pmatrix} 3A^2+3B^2 & 0 & 0 & 0 & 0 \\ 0 & 3A^2+3B^2 & 0 & 0 & 0 \\ 0 & 0 & 6C^2 & 0 & 0 \\ 0 & 0 & 0 & 3A^2+3B^2 & 0 \\ 0 & 0 & 0 & 0 & 3A^2+3B^2 \end{pmatrix} =$$
$$= \begin{pmatrix} \frac{6}{5} & 0 & 0 & 0 & 0 \\ 0 & \frac{6}{5} & 0 & 0 & 0 \\ 0 & 0 & \frac{6}{5} & 0 & 0 \\ 0 & 0 & 0 & \frac{6}{5} & 0 \\ 0 & 0 & 0 & 0 & \frac{6}{5} \end{pmatrix} = \frac{6}{5}\,\mathbf{I}_{5\times 5} \equiv \mathbf{E}_\xi, \tag{4.33}$$

from which we read that they are completely degenerate, and recalling that there exists a sixth null eigenvalue the whole set is:

$$\xi^2_{1,\ldots,5} = \frac{6}{5} \qquad \xi^2_6 = 0. \tag{4.34}$$

For the TIGA configuration, and due to the fact that $\mathbf{H}^{\dagger}\mathbf{H} \equiv \mathbf{E}_{\xi}$ is a diagonal matrix, indeed here proportional to the identity, it is also true that the eigenvectors of P_2 essentially are the constituting eigenvectors of matrix $\mathbf{H}$:

$$\vec{v}^{(m)} = \sqrt{\frac{4\pi}{5}}\,\xi_m^{-1}\,\vec{Y}_{2,m} = \sqrt{\frac{2\pi}{3}}\,\vec{Y}_{2,m} \qquad m = -2, \ldots, 2 \tag{4.35}$$

when normalized, with components

$$v_a^{(m)} = \sqrt{\frac{2\pi}{3}}\,Y_{2,m}(\mathbf{n}_a). \tag{4.36}$$

There remains also a single eigenvector associated to the null eigenvalue. But this mode is at the original sphere resonance frequency and does not interact at lowest order with a GW. In fact, the amplitude of this mode appears at a dominant order of η^0, smaller than that of the quintuplets, $\eta^{-\frac{1}{2}}$, by a factor of $\eta^{\frac{1}{2}}$. It is because of this that we say it is weakly coupled, and as already seen, it does not enter the explicit expressions for the system response.

- **Frequencies**

Eigenvalues in (4.31) imply that all the five pairs of strongly coupled frequencies collapse into a single, five-fold degenerate pair

$$\omega_{\pm}^2 = \omega_{N2}^2 \left(1 \pm \sqrt{\frac{3}{2\pi}}|A_{N2}(R)|\eta^{\frac{1}{2}}\right) + O(\eta), \tag{4.37}$$

and when tuning to the first quadrupolar harmonic

$$\omega_{\pm} = \omega_{12}\left(1 \pm 0.998\,\eta^{\frac{1}{2}}\right) + O(\eta). \tag{4.38}$$

Comparing with the numerical values for the PHCA spectrum in (4.25), we see that the span of both distributions is naturally comparable, yet the PHCA is slightly broader.

- **Amplitudes**

Again, from the general expression (3.134) and taking into account the calculated eigenvalues and eigenvectors:

$$\begin{aligned} q_a(s) &= \eta^{-\frac{1}{2}}\sqrt{\frac{2\pi}{3}}\,a_{N2}\,\frac{1}{2}\left[(s^2+\omega_+^2)^{-1} - (s^2+\omega_-^2)^{-1}\right] \times \\ &\times \sum_{m=-2}^{2} Y_{2m}(\mathbf{n}_a)\,\hat{g}^{(2m)}(s) + O(0) \qquad a = 1, \ldots, 6. \end{aligned} \tag{4.39}$$

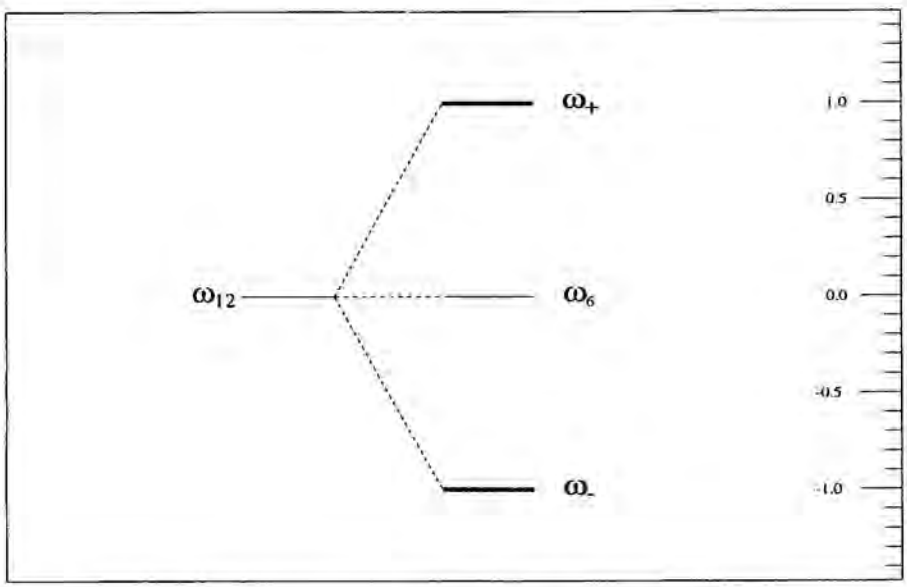

Figure 4.7. *TIGA spectrum. The weakly coupled central frequency is non-degenerated and corresponds to the null eigenvalue, whereas the thick lines represent the frequency pair five-fold degenerated. As in Figure 4.5 for the PHCA spectrum, units in the graduated vertical axis are* $\omega_{12}\eta^{\frac{1}{2}}$, *and the central value 0.0 corresponds to* ω_{12}.

This highly symmetric and remarkably simple formula was first obtained by Merkowitz and Johnson [69, 97], although its scope and range of validity are now more firmly established in the light of the present analysis.

- **Mode Channels**

Based on the above equation, Merkowitz and Johnson also were the first in defining the concept of mode channel [69]. They discovered that they could decouple each of the spherical amplitudes at the splitted frequencies by forming linear combinations of the measured amplitudes $q_a(t)$. We have demonstrated in Chapter 3 that it does not exclusively occur for the TIGA configuration; on the contrary, it is possible for any resonator layout satisfying the commutativity condition (3.187). When it is accomplished, we can write:

$$\mathbf{D}\vec{G} = b_n^{-1}(\mathbf{V}^\dagger\mathbf{H})^\dagger \cdot \mathbf{E}_\xi^{-1} \cdot \mathbf{V}^\dagger \cdot \vec{q}. \tag{4.40}$$

Nevertheless, it is true that here we face perhaps the simpler case, for the key matrix $\mathbf{V}^\dagger\mathbf{H}$ in the construction of the mode channels is not only diagonal, like for the PHC pentagonal arrangements, but furthermore proportional to the identity:

$$\mathbf{V}^\dagger\mathbf{H} = \xi\, \mathbf{I}_{5\times 5}, \tag{4.41}$$

as much as the frequency matrix itself:

$$\mathbf{D} = \frac{1}{2}\left[(s^2+\omega_+^2)^{-1} - (s^2+\omega_-^2)^{-1}\right]\frac{1}{\xi}\mathbf{I}_{5\times 5}. \tag{4.42}$$

Hence, it is simply found that:

$$\mathbf{D}\vec{G} = b_n^{-1}\,\frac{1}{\xi}\mathbf{I}_{5\times 5}\cdot\mathbf{V}^\dagger\vec{q} = b_n^{-1}\,\frac{1}{\xi}\,\mathbf{V}^\dagger\vec{q} \tag{4.43}$$

or analogously:

$$\vec{y}(s) \equiv \mathbf{V}^\dagger\vec{q}(s) = b_n\,\xi\,\mathbf{D}\vec{G} \tag{4.44}$$

and in components

$$\begin{aligned} y^{(m)}(s) &\equiv \sum_{a=1}^{6} v_a^{(m)*}\tilde{q}_a(s) = \\ &= \eta^{-\frac{1}{2}}a_{N2}\frac{1}{2}\left[(s^2+\omega_+^2)^{-1} - (s^2+\omega_-^2)^{-1}\right]\tilde{g}^{(2m)}(s) + O(0) \\ &\qquad\qquad m = -2,\ldots,2. \end{aligned} \tag{4.45}$$

There naturally are 5 rather than 6 mode channels, each giving a direct one-to-one readout of a single mode amplitude of the gravitational field.

4.3 A Simpler Example: Responses to a Calibration Signal

To contrast these results for the PHCA and the TIGA configurations we now study the responses of these devices to a particular simpler signal, a calibration signal, what will

very neatly display the most relevant features of both resonator distributions enabling a comparison of the merits of either.

We recall that in this work the calibration signals are always considered to be impulses of intensity f_0 delivered perpendicularly to the sphere's surface at point $\mathbf{x}_0$ and time $t_0 = 0$:

$$\mathbf{f}_{calibration}(\mathbf{x}, t) = \mathbf{f}_0\, \delta^3(\mathbf{x} - \mathbf{x}_0)\, \delta(t) \tag{4.46}$$

as already described in section 3.1.2 of Chapter 3. In that very chapter, the behaviour of a generic spherical GW antenna under the action of such a force density was also treated, whereby the following amplitude responses of the transducers were obtained:

$$\begin{aligned} \tilde{q}_a(s) &= (-1)^{J-1}\eta^{-\frac{1}{2}}\sqrt{\frac{2l+1}{4\pi}}|A_{NL}(R)|\mathbf{f}_0 \times \\ &\times \sum_{b=1}^{J}\left\{\sum_{\xi_m\neq 0}\frac{1}{2}\left[(s^2+\omega_{m+}^2)^{-1}-(s^2+\omega_{m-}^2)^{-1}\right]\frac{v_a^{(m)}v_b^{(m)*}}{\xi_m}\right\}\mathcal{P}_L(\mathbf{n}_b\mathbf{n}_0) \\ &+ O(0) \qquad\qquad a = 1,\ldots,J, \end{aligned} \tag{4.47}$$

for any resonator layout when the system was tuned to a certain arbitrary ω_{NL} spheroidal harmonic.

Besides, there we gave these system responses when resonators were tuned to a monopole frequency, $\omega_{NL} = \omega_{N0}$, but postponed the implementation of the quadrupole tuning, $\omega_{NL} = \omega_{N2}$, until the study of specific layouts since these are indeed the interesting considerations. Therefore, we are now ready to reach some results concerning this situation, what at this point amounts to be a very easy task, only requiring the respective substitutions in (4.44) of the already calculated eigenfrequencies and eigenvalues of matrix P_2 for the PHCA and the TIGA proposals.

In the first case, the number J of resonators was fixed to 5. The eigenvectors $\vec{v}^{(m)}$ and the eigenvalues ξ_m^2 were computed to be (section 4.1.):

$$\begin{aligned} v_a^{(m)} &= \sqrt{\frac{4\pi}{5}}\,\xi_m^{-1}\,Y_{2,m}(\mathbf{n}_a) \qquad\qquad m = -2,\ldots,2 \\ \xi_2^2 &= \frac{15}{8}\sin^4\alpha \quad \xi_1^2 = \frac{15}{2}\sin^2\alpha\cos^2\alpha \quad \xi_0^2 = \frac{5}{4}(3\cos^2-1)^2 \end{aligned} \tag{4.48}$$

for $\mathbf{n}_a$ the resonator positions in a pentagonal distribution, preferable at polar angle $\alpha = 67.617°$ on the PHC surface (see Table 4.1.).

When inserted in formula (4.44), these values directly yield

$$\hat{q}_{a,PHC}(s) = \eta^{-\frac{1}{2}}\sqrt{\frac{4\pi}{5}}|A_{N2}(R)|\mathbf{f}_0 \times$$
$$\times \sum_{m=-2}^{2} \frac{1}{2}\left[(s^2+\omega_{m+}^2)^{-1} - (s^2+\omega_{m-}^2)^{-1}\right] \frac{1}{\xi_m} Y_{2,m}(\mathbf{n}_a)Y_{2,m}^*(\mathbf{n}_0)$$
$$a = 1, \ldots, 5. \qquad (4.49)$$

For the mode channels one has:

$$\hat{y}_{PHC}^{(m)}(s) = \eta^{-\frac{1}{2}}|A_{N2}(R)|\mathbf{f}_0 \frac{1}{2}\left[(s^2+\omega_{m+}^2)^{-1} - (s^2+\omega_{m-}^2)^{-1}\right] Y_{2,m}^*(\mathbf{n}_0)$$
$$m = -2, \ldots, 2. \qquad (4.50)$$

We recall that the inverse Laplace transform of

$$\frac{1}{2}\left[(s^2+\omega_{m+}^2)^{-1} - (s^2+\omega_{m-}^2)^{-1}\right] \qquad (4.51)$$

is

$$\omega_{N2}^{-1} \sin\frac{1}{2}(\omega_{m+} - \omega_{m-})\,t \cdot \cos\omega_{N2}\,t + O(\eta^{\frac{1}{2}}) \qquad (4.52)$$

which is a beat, a sinusoid of carrier frequency ω_{N2} and amplitude modulated by another sinusoid of much smaller frequency of order $\eta^{\frac{1}{2}}\omega_{N2}$. This is illustrated in a numerical simulation for the five measurable quantities $q_a(t)$ –the resonator displacements– when the antenna is acted upon by the abovementioned calibration signal, what is displayed in graphs 4.8 for the time series and their respective spectra. Mode channels temporal and spectral evolutions are also showed. Note that while the former are not simple beats, the latter are.

In the second case for the TIGA, the number J of resonators was 6, and the completely degenerate non-null eigenvalues and associated eigenvectors read:

$$\nu_a^{(m)} = \sqrt{\frac{2\pi}{3}} Y_{2,m}(\mathbf{n}_a)$$
$$\xi_m^2 = \frac{6}{5} \qquad m = -2, \ldots, 2, \qquad (4.53)$$

for $\mathbf{n}_a$ the locations of the centers of half the pentagonal faces of the TI (Table 4.2).

In terms of these quantities, the amplitude responses are:

$$\begin{aligned} \hat{q}_{a,TIGA}(s) &= -\eta^{-\frac{1}{2}} \frac{5}{\sqrt{24\pi}} |A_{N2}(R)| f_0 \times \\ &\times \frac{1}{2} \left[(s^2+\omega_+^2)^{-1} - (s^2+\omega_-^2)^{-1} \right] \mathcal{P}_2(\mathbf{n}_a \mathbf{n}_0) \\ & \qquad a = 1, \ldots, 6. \end{aligned} \tag{4.54}$$

These equations show that the hitting point position $\mathbf{n}_0$ can be easily and *reduntlantly* determined from the readouts $\hat{q}_a(s)$.

The mode channels

$$\begin{aligned} \hat{y}^{(m)}_{TIGA}(s) &= -\eta^{-\frac{1}{2}} |A_{N2}(R)| \mathbf{f}_0 \frac{1}{2} \left[(s^2+\omega_+^2)^{-1} - (s^2+\omega_-^2)^{-1} \right] Y^*_{2,m}(\mathbf{n}_0) \\ & \qquad m = -2, \ldots, 2 \end{aligned} \tag{4.55}$$

are proportional to the sphere's quadrupole radial oscillation amplitude $|A_{N2}(R)| Y^*_{2,m}(\mathbf{n}_0)$ at the hit point [80]. The results of a numerical simulation of these TIGA responses to an impulse signal delivered to the TI solid at the same location as in the PHCA example is plotted in diagrams labelled Figure 4.9.

As clearly shown in both Figure 4.8. and Figure 4.9., the most relevant difference between the PHCA and the TIGA proposals is that the PHCA system responses $q_a(t)$ are superpositions of three different beats, from which the frequency spectrum shows three pairs of peaks as expected from (4.17), in contrast to the unique component for the TIGA. In return, the PHCA mode channels are single beats each, but with differing modulation frequencies, whereas the modulation frequencies of the single beats in the TIGA case are exactly equal.

So we see that the mode channels are always *pure beats*, whose spectra consist of the *individually separate* pairs of peaks at, of course, precisely the frequencies arising from the splitting of the resonance due to the coupling. One might interpret that the PHCA device gives rise to a sort of *Zeeman splitting* of the TIGA degenerate frequencies, which can be attributed to an axial symmetry breaking of the isotropic character of that resonator distribution; the PHCA mode channels naturally resolve the split multiplet into its components.

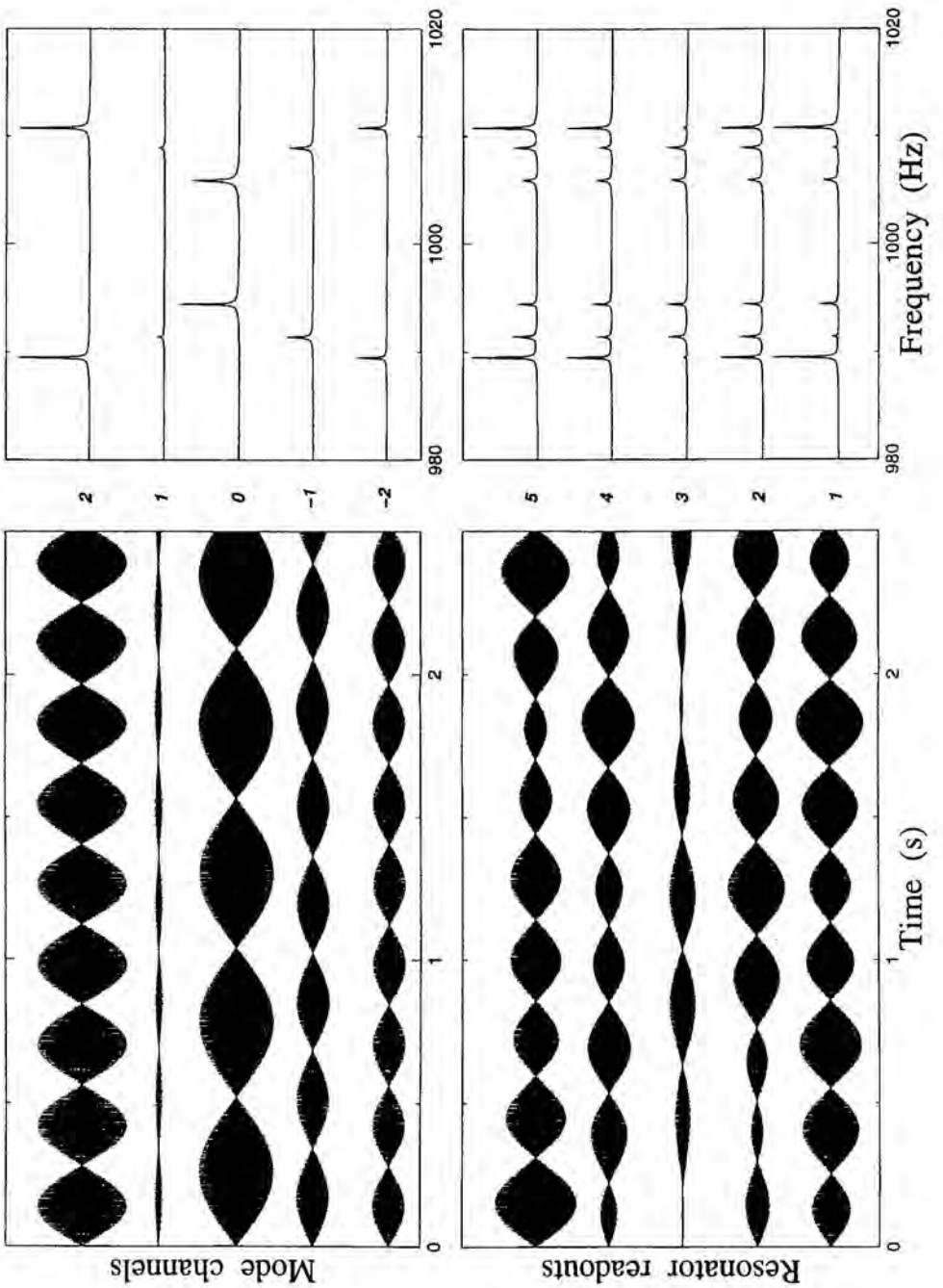

Figure 4.8. *Simulated responses of PHCA to an impulsive calibration signal, with associated spectra.*

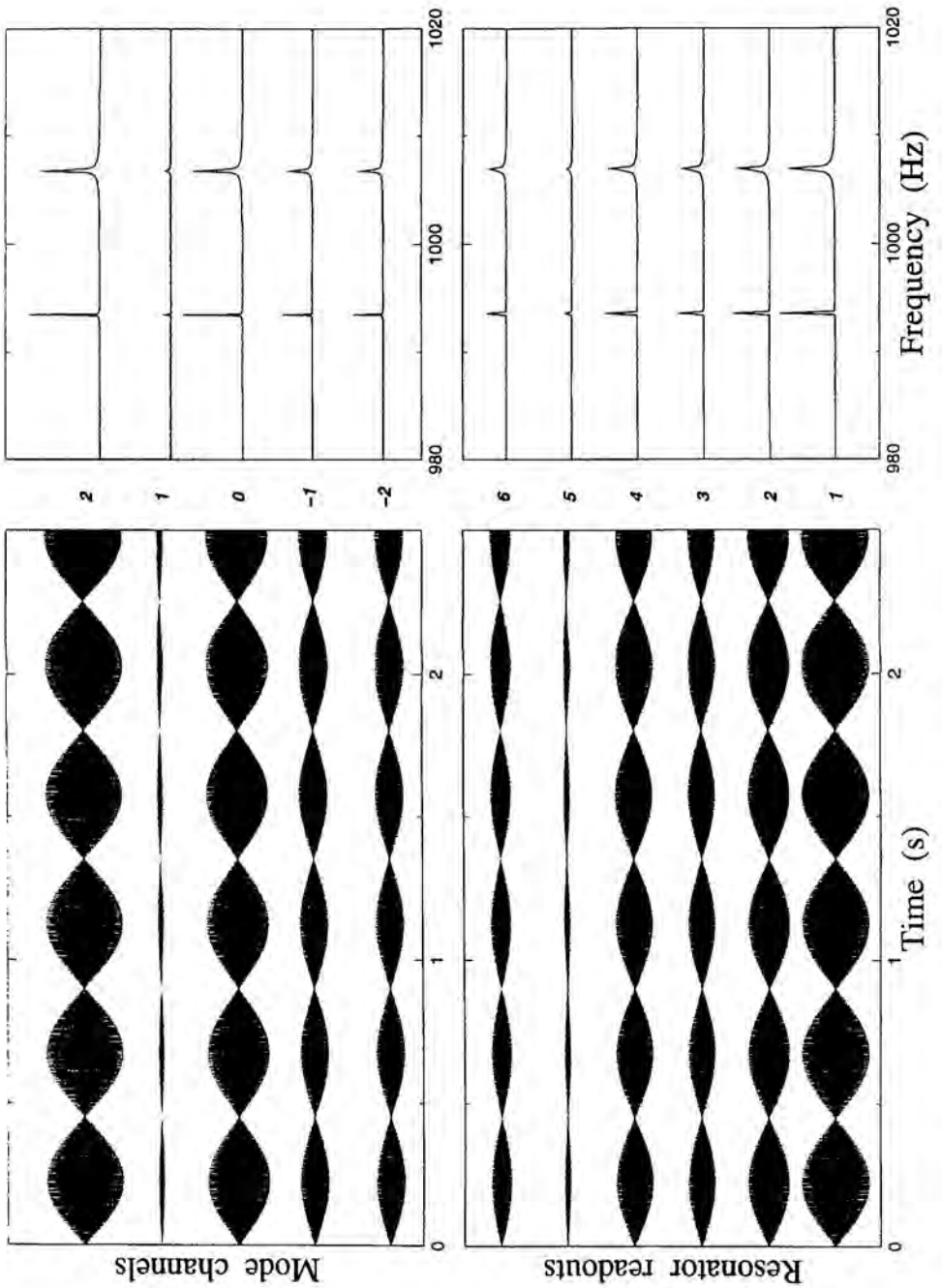

Figure 4.9. *Simulated responses of TIGA to an impulsive calibration signal, with associated spectra.*

Chapter 5

IDEALITY DEPARTURES IN SPHERICAL DETECTORS

Our model for the dynamical description of GW antennæ was constructed regarding a perfectly homogeneous and symmetric spherical detector and a set of identical resonators, which were ideally located on its surface at exact positions and were also tuned to just one given isolated resonance frequency of the free sphere spectrum.

Since these are, of course, quite unrealistic assumptions, a natural extension of this work would be the calculation of the effects produced in the antenna behaviour by small departures from those perfect matching and perfect spherical symmetry assumed so far, thereby increasing the degree of the theory applicability to real systems.

Experience with similar failures, for example in perfect matching on bar antennæ [121], suggests that the system responses should be influenced only in second order by small departures of a parameter from its nominal value, at least with respect to a certain number of those small defects. Nevertheless, a quantitative calculation for each case will be of practical interest.

As we shall see, this evaluation reveals that the system is effectively rather *robust* against some of those small imperfections. what has also been reported in reference [98]; however, there are two cases deserving special attention because they show significant changes relative to the ideal perfect device performance: the existence of a second free sphere's frequency *near* the resonator's one, and the breaking of spherical symmetry due to suspension.

- **Parametrization of Ideality Departures**

In order to quantitatively assess those ideality departures, we are going to adopt a philosophy derived from the procedure applied to the ideal system. Its key point consists in accepting that the difference between the numerical value P_{real} of a certain system parameter suffering departure from ideality –resonator masses, frequencies or locations, ...–, and its value P_{ideal} in the ideal detector, is, *a priori*, of order $\eta^{\frac{1}{2}}$:

$$P_{real} = P_{ideal}\,(\,1 + p\,\eta^{\frac{1}{2}}\,), \tag{5.1}$$

which in fact stands as a definition for p.

Hence, once P_{ideal} is thought to be known p could be readily determined, whereupon the *robustness* of the system can be tested: if the dimensionless parameter p is of order 1 or, at least, appreciably larger than $\eta^{\frac{1}{2}}$, then the device is recognized to be affected by that particular deviation from ideality, but if, in return, p happens to be too small, i.e., of order $\eta^{\frac{1}{2}}$ itself or smaller, then the system will be considered *robust* as regards the failing parameter.

This parametrization is understood from the fact that our solutions are always given as perturbative series expansions in ascending powers of the small quantity $\eta^{\frac{1}{2}}$. It is therefore appropriate to parametrize deviations in terms of its powers so as to address them consistently with the orders of accuracy of the series solutions to the equations of motion. When p is appreciably larger than $\eta^{\frac{1}{2}}$, ideality departures actually are of order $\eta^{\frac{1}{2}}$ and the above mentioned solutions will be appreciably altered in their leading order terms –contributions proportional to $\eta^{\frac{1}{2}}$ for the frequencies and those proportional to $\eta^{-\frac{1}{2}}$ for the amplitudes–; if, on the other hand, p is too small, such defects are of order η or smaller, and any modification to the responses will be swallowed into their non-dominant higher order correction terms –O(0) or O(1)...–, so that the more important ones will remain unaffected, from which the system is said to be *robust* against that ideality breaking as explained above.

Let us now quantitatively develop the procedures to study various interesting departures from ideality.

5.1 Mismatched Resonator Parameters

In this section, we are going to study ideality departures in three different parameters referred to the physical characteristics and situation of resonators. Firstly, exact

resonator positions of the ideal detector are going to be displaced to new *close* real locations. Afterwards, resonator masses and natural frequencies, both of them groups of quantities with the same value in a perfect device, would be allowed to slightly differ among them.

- **Location Tolerances**

Let $\mathbf{n}_a$, $a = 1, \ldots, J$, denote the J resonator positions relative to a pre-selected ideal distribution, for example the TIGA or the PHCA configurations. Let now $\mathbf{n'}_a$ be the real locations, not equal to the former but *close* to them. Following (5.1), we write

$$\mathbf{n'}_a = \mathbf{n}_a + \mathbf{v}_a \eta^{\frac{1}{2}} \qquad a = 1, \ldots, J. \tag{5.2}$$

As shown in Chapter 3, the system responses depend on the resonator positions through the spherical harmonics $Y_{lm}(\mathbf{n}_a)$ and through the eigenvalues ξ_m^2 and the eigenvectors $v^{(m)}$ of the $P_l(\mathbf{n}_a \mathbf{n}_b)$ matrix, explicitly entering the expressions within lowest order terms. So, it would be necessary to find out how these functions change when $\mathbf{n}_a$ is substituted by $\mathbf{n'}_a$. It can be easily found that

$$\begin{aligned} Y_{lm}(\mathbf{n'}_a) &= Y_{lm}(\mathbf{n}_a) + O(\eta^{\frac{1}{2}}) \\ \xi'_m &= \xi_m + O(\eta^{\frac{1}{2}}) \\ v^{(m)\prime} &= v^{(m)} + O(\eta^{\frac{1}{2}}). \end{aligned} \tag{5.3}$$

Hence, corrections to the coupled antenna normal frequencies, amplitudes or mode channels will be of second order.

We thus conclude that the system is robust with respect to small misplacements of resonators relative to their pre-established chosen positions.

- **Non Identical Resonators**

Non identical resonators may differ in mass or natural frequency.

For the masses, one can consider changes like

$$m'_a = m_a \left(1 + \mu_a \eta^{\frac{1}{2}}\right) \qquad a = 1, \ldots, J, \tag{5.4}$$

or

$$m'_a = \eta \mathcal{M} \left(1 + \mu_a \eta^{\frac{1}{2}} \right) \qquad a = 1, \ldots, J, \tag{5.5}$$

where η has to be defined in this situation, for instance, as the ratio of the average resonator mass to the sphere mass.

The circumstance of η appearing as a multiplicative factor in the rhs of expression (5.5) makes obvious the fact that non-uniformities in the resonator masses only affect the equations describing the dynamics of the antenna again in second order, since from this formula it can be seen that the parameter η allowing the perturbative series expansions of the system responses is corrected itself by $\eta^{\frac{1}{2}}$ terms.

Therefore, the device is also robust to resonator mass mismatches.

As regards the frequencies, they may also differ among them:

$$\Omega_a^2 = \Omega^2 \left(1 + \varrho_a \eta^{\frac{1}{2}} \right) \qquad a = 1, \ldots, J. \tag{5.6}$$

Here, continuity arguments like those used above cannot be applied due to the fact that these changes on the resonator frequencies affect calculations of the coupled sphere spectrum, and so the situation of poles and the value of their residues in the original Laplace transform expressions for the measurable $\tilde{q}_a(s)$ displacements.

Instead, one must go back to formula (3.71) in Chapter 3 for the zeroes of the $\Delta(s)$ determinant:

$$\Delta(s) = \det \left[\delta_{ab} + \eta \frac{s^2}{s^2 + \Omega_a^2} \tilde{K}_{ab}(s) \right] = 0, \tag{5.7}$$

which we recall is the equation leading to the coupled detector spectrum, and recalculate it following the procedures of section 3.4 in Chapter 3, but taking also into account the substitutions (5.6). We recall that for roots around the resonance frequency $\Omega = \omega_{NL}$,

$$s^2 = -\Omega^2 \left(1 + \gamma_{\frac{1}{2}} \eta^{\frac{1}{2}} \right) + O(\eta), \tag{5.8}$$

the dominant term in $\tilde{K}_{ab}(s)$ is

$$\frac{s^2 \Omega_b^2}{s^2 + \Omega_b^2} \chi_{ab}^{(NL)}. \tag{5.9}$$

Hence, $\Delta(s)$ is given by

$$\Delta(s) = \det \left[\delta_{ab} + \eta \frac{s^2 \Omega_b^2}{s^2 + \Omega_a^2} \frac{\chi_{ab}^{(NL)}}{s^2 + \Omega_b^2} \right] = 0, \tag{5.10}$$

and inserting (5.6) and (5.8) one finds:

$$\begin{aligned}\Delta(s) &= \det\left[\delta_{ab}+\eta\,\frac{s^2\Omega^2}{s^2+\Omega^2}\,\frac{1+\varrho_b\eta^{\frac{1}{2}}+\dots}{1+\frac{\Omega^2}{s^2+\Omega^2}\varrho_a\eta^{\frac{1}{2}}+\dots}\,\frac{\chi_{ab}^{(NL)}}{s^2+\Omega^2(1+\varrho_b\eta^{\frac{1}{2}})}\right]\\ &= \det\left[\delta_{ab}+\frac{1+\chi_{\frac{1}{2}}\eta^{\frac{1}{2}}+\dots}{\chi_{\frac{1}{2}}+\chi_1\eta^{\frac{1}{2}}+\dots}\,\frac{1+\varrho_b\eta^{\frac{1}{2}}+\dots}{1+\frac{\Omega^2}{s^2+\Omega^2}\varrho_a\eta^{\frac{1}{2}}+\dots}\,\frac{\chi_{ab}^{(NL)}}{(\varrho_b-\chi_{\frac{1}{2}})+\dots}\right]\\ &= 0.\end{aligned} \tag{5.11}$$

From here, one can easily arrive to see that the old equation (3.93) for the lowest order coefficient $\chi_{\frac{1}{2}}$ in the development (3.88) of the system frequencies around the resonant ω_{NL},

$$\det\left[\delta_{ab}-\frac{1}{\chi_{\frac{1}{2}}^2}\chi_{ab}^{(NL)}\right]=0, \tag{5.12}$$

is replaced by

$$\det\left[\delta_{ab}-\frac{\chi_{ab}^{(NL)}}{\chi_{\frac{1}{2}}(\chi_{\frac{1}{2}}-\varrho_b)}\right]=0, \tag{5.13}$$

which of course reduces to formula (5.8) when all the ϱ's vanish, i.e., when all the resonators are characterised by the same resonance frequency.

Therefore, if resonator real frequencies are actually described by (5.6), then significant effects on the results of the theory for the ideal device are expected even to lowest order in $\eta^{\frac{1}{2}}$.

But before carrying on with more complicated operations to quantitatively assess the consequences of this assertion, equation (5.6) has to be carefully reconsidered, since we are precisely concerned with realistic situations and it is possibly unrealistic to admit such large tolerances in resonator vibrational behaviour.

For example, in the TIGA experiment [95], an error of order $\eta^{\frac{1}{2}}$ would amount to around $50Hz$ of mistuning between resonators, what by all means is absurd. Besides, in a full scale sphere (≈ 40 tons, $\approx 3\ m$ in diameter, $\approx 80Hz$ fundamental quadrupole frequency and $\eta \approx 10^{-5}$) the same error would amount to between $5Hz$ and $10Hz$ in resonator mistunings for the lowest frequency, what is probably excessive for a capacitive transducer, although, on the contrary, may be realistic for an inductive one. Then, (5.9) would be the master equation providing the frequencies of the antenna.

With this exception, it is thus more appropiate to consider that resonator mistunings are at least of order η. If this is the case, once more the system happens to be insensitive at leading order to such mistunings.

5.2 Non Ideal Tuning: URF Effect

In the introduction to the chapter we announced that, in contrast to what happens for the above treated ideality failures against which the system behaviour is quite unsensitive, at least two different departures from the original assumptions can be considered to appreciably affect the device response even at leading order.

In this section, we are going to discuss the first of them, which assumes the existence of a second free sphere frequency $\omega_{N'L'}$ *near* $\omega_{NL} \equiv \Omega$, quantifying and evaluating also its substantial effects on the detector frequency spectrum.

5.2.1 Unisolated Resonance Frequency

The first question we want to address now is this: does the presence in the *neighbourhood* of ω_{NL} of a second $\omega_{N'L'}$ frequency alter in some appreciable way the results obtained for the ideal antenna?

The first thing to do is the definition of what we mean by a *neighbourhood* of ω_{NL}. We have already set out this question again in section 3.4 of Chapter 3, when supplying the hypotheses for the most idealized situation of a perfect sphere with perfectly tuned identical resonators. We recall here that the nearness between eigenfrequencies is parametrized, as any ideality departure, in the form

$$\omega^2_{N'L'} = \omega^2_{NL}\,(1 + r\,\eta^{\frac{1}{2}}). \tag{5.14}$$

If r is of order 1 or at least significantly larger than $\eta^{\frac{1}{2}}$, then the order $\eta^{\frac{1}{2}}$ is fully maintained in (5.14) and the dynamical behaviour of the system could be affected by the *nearness*, as usual.

In contrast to the discussion for mismatched resonator parameters, here r must not be determined but is in fact a known quantity, since the whole spectrum of the free sphere is known (see references in Chapter 3) and $\eta^{\frac{1}{2}}$ is a fixed quantity in a particular experiment. Hence, the key point here resides in investigating the differences between the ω_{nl} of the free sphere spectrum and the chosen resonant ω_{NL}, for bringing out to light the possible existence of a given $\omega_{N'L'}$ satisfying (5.14) with the required condition

on r. Naturally, ω_{NL} must be a quadrupole harmonic with $L = 2$ if quadrupole motion sensing is expected, and preferably the first, $N = 1$, or the second, $N = 2$, of the series in a practical system.

After a careful examination of the spectrum of a typical planned aluminium sphere [1], see graph in Figure A.1 of Appendix A, one can verify that there is a pair of candidates, with values expressed in kHz: ω_{22} and ω_{14}.

From these quantities and any sphere:

$$\omega_{14}^2 = \omega_{22}^2 (1 - 1.105 \cdot 10^{-2}). \tag{5.15}$$

Introducing a likely value for η, around the exact value in the TIGA prototype, of approximately $\eta \approx \frac{1}{1700} = 5.88 \cdot 10^{-4}$, r is found to be $r \approx -0.456$, a quantity appreciably larger by one order of magnitude in absolute value than $\eta^{\frac{1}{2}} \approx 2.42 \cdot 10^{-2}$, so that equation (5.14) is appropiate for describing the degree of *nearness* between the frequencies of that selected pair. Moreover, if the mass of the spherical detector is increased, a desirable prospect and indeed a requirement in a future experimental full scale device, then the ratio of the resonator mass to the sphere mass would decrease, so that the difference between r and $\eta^{\frac{1}{2}}$ will be even larger and r can be strictly considered of order 1.

It is in this sense that we say ω_{22} is an unisolated resonance frequency -there exists a second frequency of the free sphere, ω_{14}, within a distance of order $\eta^{\frac{1}{2}}$-, and as long as it is in fact a suitable sphere's frequency for the resonator set to be actually tuned to, the effects of such unisolation, which we are going to call *URF effects*, must be accurately determined and analysed to achieve a description of the detector real behaviour.

5.2.2 Modified Responses

One may expect that the presence of a second frequency $\omega_{N'L'}$ near the resonant ω_{NL} alters in a fundamental form the dynamical responses of the device, since that affects an essential hypothesis for the developments of the theory of the ideal system.

In order to evaluate the induced modifications, it is not necessary to change the method used to solve the GRD equations on the basis of our model. It will just suffice to re-examine our expressions searching for new contributions when (5.14) is taken into account.

[1] We explain that for typical planned aluminium spheres $R = 1.50m$, the Poisson ratio is $\sigma = \frac{1}{3}$ and the transversal velocity of normal vibrations in the material has the value $v_t = 3160ms^{-1}$, according to data given in [31].

- **Frequency Splitting**

We start from equation (5.7) for the zeroes of the determinant $\Delta(s)$:

$$\det\left[\delta_{ab}+\eta\,\frac{s^2\Omega^2}{(s^2+\Omega^2)^2}\,\chi_{ab}^{(NL)}+\eta\sum_{nl\neq NL}\frac{s^2\Omega^2}{(s^2+\Omega^2)(s^2+\omega_{nl}^2)}\,\chi_{ab}^{(nl)}\right]=0, \tag{5.16}$$

whose solutions, giving the coupled detector natural resonances around the resonance frequency Ω, were taken as the perturbative series

$$s_0^2=-\Omega^2\,(1+\chi_{\frac{1}{2}}\eta^{\frac{1}{2}}+\chi_1\eta+\ldots). \tag{5.17}$$

For the one associated to first order, $\chi_{\frac{1}{2}}$, determinant $\Delta(s)$ reduces to

$$\det\left[\delta_{ab}-\frac{1}{\chi_{\frac{1}{2}}^2}\chi_{ab}^{(NL)}\right]=0, \tag{5.18}$$

from which $\chi_{\frac{1}{2}}^2$ were found to be the eigenvalues of $\chi_{ab}^{(NL)}$:

$$\chi_{\frac{1}{2}}^2=\frac{2L+1}{4\pi}\,|A_{NL}(R)|^2\,\xi_a^2, \tag{5.19}$$

being ξ_a^2 the J positive or null eigenvalues of matrix $P_L(\mathbf{n}_a\mathbf{n}_b)$, implicitly contained in $\chi_{ab}^{(nl)}$.

$$\chi_{ab}^{(nl)}=\frac{2L+1}{4\pi}\,|A_{NL}(R)|^2\,P_L(\mathbf{n}_a\mathbf{n}_b). \tag{5.20}$$

We face a different situation when there exists a second $\omega_{N'L'}$ neighbouring ω_{NL}. In this case, the contributing term to leading order in $\Delta(s)$ is not only that associated to $\chi_{ab}^{(NL)}$, but also the one related to $\chi_{ab}^{(N'L')}$, what simply arises from the result of substituting (5.14) and (5.17) into (5.16), and just retaining terms of order η^0:

$$\det\left[\delta_{ab}-\frac{1}{\chi_{\frac{1}{2}URF}^2}\chi_{ab}^{(NL)}-\frac{1}{\chi_{\frac{1}{2}URF}(\chi_{\frac{1}{2}URF}-r)}\chi_{ab}^{(N'L')}\right]=0. \tag{5.21}$$

The zeroes of this determinant will provide the URF[2] resonances of the antenna around ω_{NL}:

[2] *URF* on a subscript of a quantity stands for a label indicating that such quantity is calculated for the case of the system having an unisolated resonance frequency.

$$\omega^2_{i,URF} = \omega^2_{NL}\,(1 + \chi_{\frac{1}{2},i,URF}\,\eta^{\frac{1}{2}}) + O(\eta). \tag{5.22}$$

Clearly, the determinant (5.21) is more complicated than its counterpart (5.18) for the situation of isolated resonance frequency, *IRF case*, to which it reduces when r is large, i.e., when ω_{22} can be considered to be isolated. The procedure of diagonalizing $\chi^{(NL)}_{ab}$ developed for (5.18) can also be applied here. $\chi^{(NL)}_{ab}$ and $\chi^{(N'L')}_{ab}$ are hermitian matrices, hence their combination in (5.21) is also hermitian and therefore diagonalizable.

Which one is the correct basis diagonalasing at the same time both $\chi^{(NL)}_{ab}$ and $\chi^{(N'L')}_{ab}$ is not an obvious question, since the simultaneous reduction of a pair of matrices to a diagonal form cannot always be performed.

However, consider the particular situation in which we construct a matrix Q whose columns consist in the common normalised eigenvector of $\chi^{(NL)}_{ab}$ and $\chi^{(N'L')}_{ab}$. From their orthogonality property, $Q^\dagger$ will of course coincide with Q^{-1}, so that

$$\begin{aligned} Q^\dagger \cdot Q &= Q^{-1} \cdot Q = I \\ Q^\dagger \cdot \chi^{(NL)} \cdot Q &= diag\left[\ \chi^2_{1,NL},\ \cdots,\ \chi^2_{J,NL}\ \right] \\ Q^\dagger \cdot \chi^{(N'L')} \cdot Q &= diag\left[\ \chi^2_{1,N'L'},\ \cdots,\ \chi^2_{J,N'L'}\ \right], \end{aligned} \tag{5.23}$$

being $\chi^2_{i,NL}$ the eigenvalues of $\chi^{(NL)}$ and $\chi^2_{i,N'L'}$ those of $\chi^{(N'L')}$:

$$\begin{aligned} \chi^2_{i,NL} &= \frac{2L+1}{4\pi}\,|A_{NL}(R)|^2\,\xi^2_{i,L} \\ \chi^2_{i,N'L'} &= \frac{2L'+1}{4\pi}\,|A_{N'L'}(R)|^2\,\xi^2_{i,L'}, \end{aligned} \tag{5.24}$$

each pair associated to an unique eigenvector $v^{(i)}$.

Then it is easy to see that Q diagonalizes the matrix associated to (5.21):

$$\begin{aligned} Q^{-1} \cdot \left[\delta_{ab} - \frac{1}{\chi^2_{\frac{1}{2},URF}}\,\chi^{(NL)}_{ab} - \frac{1}{\chi_{\frac{1}{2},URF}\left(\chi_{\frac{1}{2},URF} - r\right)}\,\chi^{(N'L')}_{ab}\right] \cdot Q = \\ = \left[\delta_{ab} - \frac{1}{\chi^2_{\frac{1}{2},URF}}\ diag\left[\chi^2_{1,NL},\cdots,\chi^2_{n,NL}\right] - \right. \\ \left. - \frac{1}{\chi_{\frac{1}{2},URF}\left(\chi_{\frac{1}{2},URF} - r\right)}\ diag\left[\chi^2_{1,N'L'},\cdots,\chi^2_{n,N'L'}\right]\right], \end{aligned} \tag{5.25}$$

so that its determinant could be rewritten

$$\prod_{i=1}^{J}\left[\chi^3_{\frac{1}{2},URF} - r\cdot\chi^2_{\frac{1}{2},URF} - (\chi^2_{i,NL}+\chi^2_{i,N'L'})\cdot\chi_{\frac{1}{2},URF} + r\cdot\chi^2_{i,NL}\right] = 0. \qquad (5.26)$$

Therefore, the assumption of the existence of matrix Q simplifies the process of finding the roots of determinant (5.21) in a general case, but, in return, gives rise to the crucial question: when does it happen that there exists a common set of eigenvectors for $\chi^{(NL)}$ and $\chi^{(N'L')}$?.

The following theorem holds [20, 36, 119]:

If two hermitian matrices commute –their product is independent of the order of the factors–, they have a common set of eigenvectors forming an orthogonal basis. The converse of this result, that if there exists a complete set of vectors such that each of them is simultaneously an eigenvector of both matrices, then they commute, can also be proved.

Hence, we have arrived to a certainly simple requirement over $\chi^{(NL)}$ and $\chi^{(N'L')}$, or over P_L and P'_L, which allows us to go further in the interpretation of possible generic conclusions about how any spherical GW antenna is influenced by the URF effect. The requirement is

$$\left[\chi^{(NL)},\chi^{(N'L')}\right] \equiv \chi^{(NL)}\cdot\chi^{(N'L')} - \chi^{(N'L')}\chi^{(NL)} = 0. \qquad (5.27)$$

As we shall see, this is the case for the PHC and TIGA arrangements.

Note that the implementation of (5.27) leads to re-express (5.21) as the product (5.26) of cubic algebraic independent equations having as unknowns $\chi_{\frac{1}{2}}$, once the eigenvalues $\chi^2_{i,NL}$ and $\chi^2_{i,N'L'}$ are fixed. This simplicity allows us to advance, previously to further calculations constricted to specific layouts of resonators, a qualitative *a priori* picture of the new frequency spectrum, where doublets appearing in the splitting of the isolated resonance frequency transform into *triplets* in the unisolated case:

- if P_L does not present null eigenvalues[3], $P_{L'}$ may or may not, then each factor in (5.26) maintains its four terms, so that each will present three non-zero solutions which, in principle, could integrate a triplet containing three strongly coupled frequencies (triplet of the scT type) at most, although the actual classification will depend on the final numerical outcomes;

[3]Of course, this case is only possible if $J \leq 2L+1$.

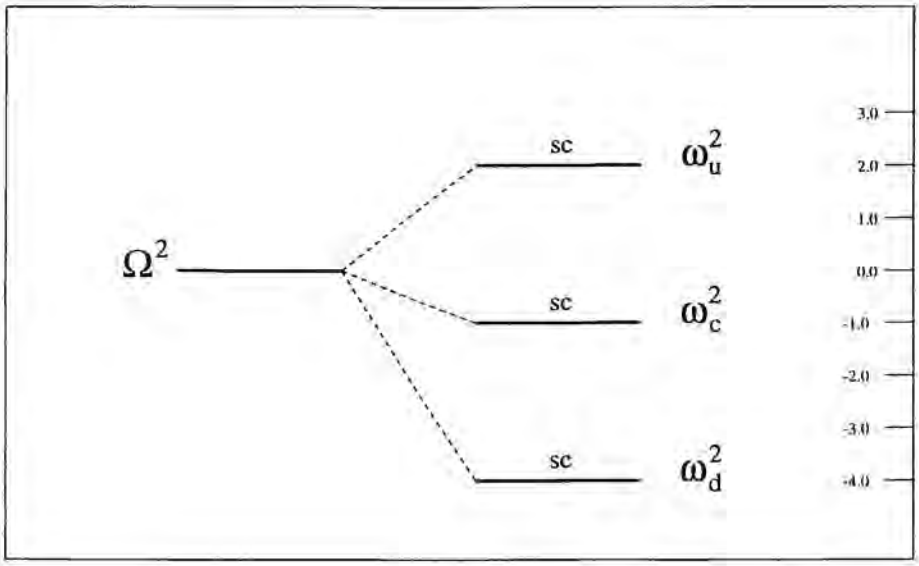

Figure 5.1. *Example of scT type triplet. The three splitted frequencies are strongly coupled. Distances to the original resonance one are represented in the graduated vertical axis on the right, where units are* $\Omega^2\eta^{\frac{1}{2}}$, *and the central value, labelled 0.0, corresponds to* Ω^2.

- if P_L presents a number n of null eigenvalues, sublabelled j, associated to certain eigenvectors of the common basis, whereas the corresponding eigenvalues of $P_{L'}$ are non-null, the cubic equations associated to j will decompose as follows:

$$\chi_{\frac{1}{2},URF}\left(\chi^2_{\frac{1}{2},URF} - r\cdot\chi_{\frac{1}{2},URF} - \Upsilon^2_{j,N'L'}\right) = 0. \tag{5.28}$$

  Among the resulting J triplets n will contain a central weakly coupled value exactly at the resonance ω_{NL} frequency. so that each of them will be constituted at most by a doublet of strongly coupled frequencies (triplets of the $scD{+}wcS$ type);

- if both P_L and $P_{L'}$ present m null eigenvalues, sublabelled j, associated to the same common eigenvector, the cubic equations depending on j will decompose as follows:

$$\chi^2_{\frac{1}{2},URF}\left(\chi_{\frac{1}{2},URF} - r\right) = 0. \tag{5.29}$$

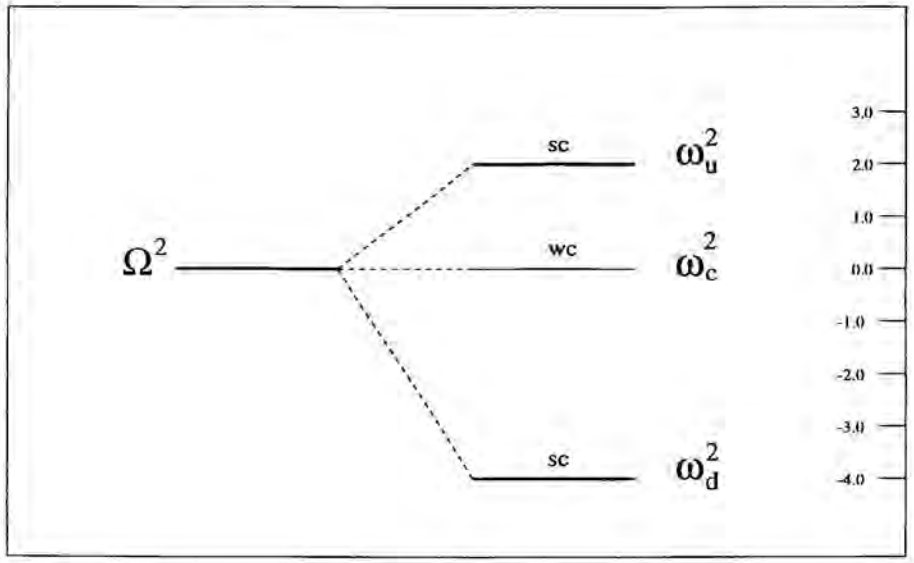

SCD+WCS Triplet

Figure 5.2. *Example of scD+wcS type triplet. The inner frequency ω_c is weakly coupled and exactly occurs at the resonant Ω^2 at order $\eta^{-\frac{1}{2}}$.*

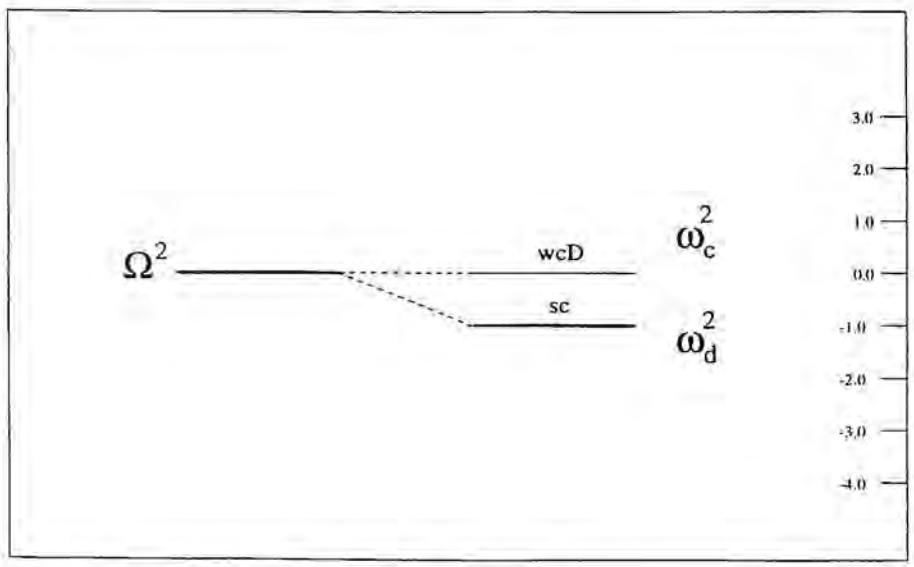

SCS+WCD Triplet

Figure 5.3. *Example of scS+wcD type triplet. There is a degenerate weakly coupled doublet exactly at Ω^2, whereas there is only one strongly coupled frequency at a distance equal to r.*

Of the J resulting sets, m will show at most one strongly coupled frequency and two more weakly coupled forming the triplet ($scS + wcD$ type).

Weakly coupled frequencies are understood here as those at the resonance frequency at leading order, with associated amplitudes smaller than those of the strongly coupled ones by factors of order $\eta^{\frac{1}{2}}$ at least, and which are calculated from the null $\chi^2_{i,nl}$ or $\xi^2_{i,l}$ eigenvalues, so that their expression in powers of η reads

$$\omega^2_{wc} = \Omega^2 (1 + \chi_{1,wc}\eta + \ldots). \tag{5.30}$$

In a given URF triplet, they occur in singlets when it is only one of the matrices, P_2, which presents null eigenvalues, while they appear in pairs when it happens for the two matrices.

In order to clarify this casuistry, let us graphically display an idealised example. Consider a resonator distribution such that P_2 only presents null eigenvalues when $J > 5$, consequently being its number $J-5$, and P_4 only when $J > 9$, so that its number of null eigenvalues will be $J-9$. In other words, consider the layouts for which the ranges of the matrices are as large as possible. Besides, we assume that the number of strongly coupled frequencies in each set is also the maximum allowed by the specification of the eigenvalues in the equations. Then, the former considerations lead to the situation plotted in Figure 5.4 where, as usual, scT stands for strongly coupled Triplets; $scD + wcS$ refers to the triplets including a strongly coupled Doublet and a weakly coupled Singlet, and finally $scS + wcD$ is the label for strongly coupled Singlet and a weakly coupled Doublet. As shown, the number of scT triplets can never exceed 5, while the number of $scD + wcS$ sets is never greater than 4.

In addition to these results, further appreciations can be pointed out. Inspection of orders of magnitude in (5.26), with

$$\begin{array}{ll}
r \approx -0.456 & \\
\mathcal{N}L = 22 & \mathcal{N}'L' = 14 \\
\lambda^2_{i,22} = \frac{5}{4\pi}|A_{22}(R)|^2\xi^2_{i,2} & \lambda^2_{i,14} = \frac{9}{4\pi}|A_{14}(R)|^2\xi^2_{i,4} \\
A_{22}(R) = 0.0745 & A_{14}(R) = -3.6308 \\
\xi^2_{i,2} \approx 1 & \xi^2_{i,4} \approx 1 \\
\lambda^2_{i,22} \approx 0.0022 & \lambda^2_{i,14} \approx 9.4414 \quad i = 1, \ldots, J,
\end{array} \tag{5.31}$$

reveals that it has just two dominant terms in every cubic equation,

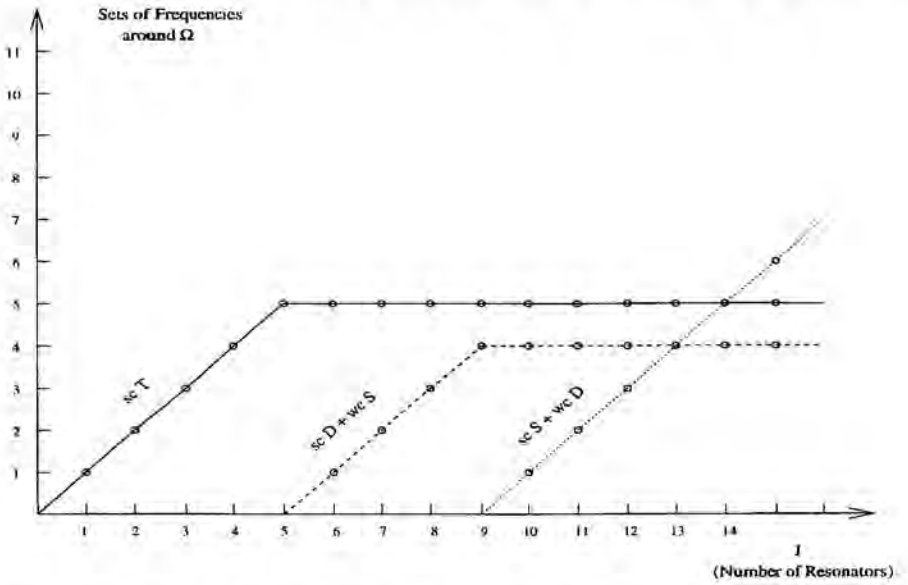

Figure 5.4. *Number of different sets occurring in the splitting of the resonance frequency $\Omega \equiv \omega_{NL}$ if the URF effect is considered in the example described above in the text. For the sake of clarity, we have drawn an imaginary solid, dashed or doted line connecting all the points in the graph for each of the categories of frequency sets.*

$$\chi^3_{\frac{1}{2},URF} - r \cdot \chi^2_{\frac{1}{2},URF} - (\chi^2_{i,NL} + \chi^2_{i,N'L'}) \cdot \chi_{\frac{1}{2},URF} + r \cdot \chi^2_{i,NL} \approx$$
$$\approx \cdot \chi_{\frac{1}{2},URF} \left(\chi^2_{\frac{1}{2},URF} - r\chi_{\frac{1}{2},URF} - \chi^2_{i,N'L'}\right) = 0, \qquad (5.32)$$

from which it becomes clear that one of the frequencies of the triplets will always be located *very close* to the original tuning frequency ω_{NL}. To assess how much near this frequency actually is, one needs to restrict to particular cases and numerical evaluations. This is an important point, because an *excessive nearness* could alter the order of this frequency contribution, turning it weakly coupled. This will happen if the whole product $\chi_{\frac{1}{2}}\eta^{\frac{1}{2}}$ in (5.17) is in fact of the form $\chi_1\eta$, with ξ_1 of order 1 or even smaller, because then its contribution to the vibrational amplitudes will not affect the dominant order but a higher one. The remaining pair will form a *rather symmetric* doublet around it, in good agreement with the idea that the presence of the second frequency must be just a perturbation of the ideal situation, although the strict symmetry of the ideal IRF

doublets will be broken.

Finally, a similar exploration for the effect on the $\omega_{nl} \neq \omega_{NL}$ frequencies of the uncoupled spectrum and their splittings would demonstrate that the presence of $\omega_{N'L'}$ near ω_{NL} does not indeed affect in its essentials the IRF distribution of the J singlets corresponding to each ω_{nl} in the coupled spectrum scheme at leading order.

In conclusion, the configuration of the natural non-tuned-frequencies splittings of the coupled antenna seems to be robust with respect to the *neighbourhood effect*. In contrast, and as expected, the splitting of the tuning mode is influenced so that doublets associated to ideal tuning essentially become triplets, although possibly integrated by strongly coupled doublets, in any case non-symmetrically placed around ω_{NL}, and a third weakly coupled frequency.

- **PHCA and TIGA cases**

As always, let us specify the above presented general analysis for the two spherical GW antennæ proposals: the PHCA and the TIGA arrangements. Our specific purpose will be to solve equation (5.26) for the $\chi_{\frac{1}{2},URF}$ unknowns determining the URF frequencies –see (5.22).

URF-PHCA frequencies around ω_{22}

Let us consider first the neighbourghood effect, or URF effect, for the PHCA antenna.

As usual, the process of application of the general results to certain particular proposals, in which the resonator layout presents specific configurations, begins with the derivation of the eigenvalues and eigenvectors of the $P_l(\mathbf{n}_a\mathbf{n}_b)$ matrices involved in the calculations –see Chapter 4.

Taking the neighbouring frequencies ω_{22} and ω_{14}, the P_l matrices to work with are $P_2(\mathbf{n}_a\mathbf{n}_b)$ and $P_4(\mathbf{n}_a\mathbf{n}_b)$, constructed from the Legendre polynomials of order 2 and of order 4, respectively:

$$\begin{aligned} \mathcal{P}_2(\mathbf{n}_a\mathbf{n}_b) &\equiv \mathcal{P}_2(\cos_{ab}) = \frac{1}{2}(3\cos^2\theta_{ab} - 1) \\ \mathcal{P}_4(\mathbf{n}_a\mathbf{n}_b) &\equiv \mathcal{P}_4(\cos_{ab}) = \frac{1}{8}(35\cos^4\theta_{ab} - 30\cos^2\theta_{ab} + 3). \end{aligned} \tag{5.33}$$

When the positions of the five sensors are fixed in the surface of the pentagonal hexacontahedron at the pentagonal configuration locations with polar angle $\theta = 67.617°$ (see Table 4.1), matrices P_2 and P_4 adopt the same structure:

$$P_2 \equiv P_4 \equiv \begin{pmatrix} 1 & B & C & C & B \\ B & 1 & B & C & C \\ C & B & 1 & B & C \\ C & C & B & 1 & B \\ B & C & C & B & 1 \end{pmatrix} \quad \begin{matrix} B_2 = -0.249 & B_4 = -0.130 \\ C_2 = -0.052 & C_4 = -0.355. \end{matrix} \tag{5.34}$$

This particular arrangement is indeed common to all the P_l associated to the PHCA configuration, for their structure being determined by that of an unique matrix constructed from the angular relative positions between the resonators. Then, it is easy to prove that any pair of these P_l matrices commute:

$$[P_l, P_{l'}] = 0. \tag{5.35}$$

As explained above, it means that there exists a basis of simultaneous eigenvectors for P_l and $P_{l'}$, and in particular it happens for P_2 and P_4, which present the associated eigenvectors arranged in columns of Q:

$$Q \equiv \begin{pmatrix} 0.4472 & -0.5899 & 0.0419 & -0.5525 & .0727 \\ 0.4472 & -0.3992 & 0.6131 & 0.2661 & -0.4281 \\ 0.4472 & 0.3432 & 0.3371 & 0.1220 & 0.6200 \\ 0.4472 & 0.6113 & -0.4048 & -0.4635 & -0.5750 \\ 0.4472 & 0.0346 & -0.5872 & 0.6279 & 0.3104 \end{pmatrix} \tag{5.36}$$

with associated eigenvalues in Table 5.1.

Therefore, eigenvalues of $\chi_{ab}^{(22)}$ and $\chi_{ab}^{(14)}$ appearing in the cubic equations (5.26) for the lowest order coefficient $\chi_{\frac{1}{2}.URF}$ in the frequency series can be calculated from (5.24) -we give the results also in Table 5.1-, so that the only quantity to be eventually fixed in the three final different cubic equations to be solved for the triplets of splitted frequencies is r.

Remember that, once the neighbouring frequencies have been fixed, this is a coefficient depending on the exact value of η -see (5.14). We will work with two possible quantities, the first corresponding to the ratio of the resonator mass to the sphere mass in the TIGA experimental prototype: $\eta = \frac{1}{1762.45}$, hence $|r|$ will be 0.464; and the second a likewise value in a full scale future sphere $\eta = \frac{1}{40000}$, with $|r| = 2.21$. In both cases, the equations will read:

Eigenvalues	P_2	P_4
ξ_0^2	0.3990	0.0295
$\xi_{-1}^2 = \xi_{+1}^2 \equiv \xi_1^2$	0.9298	1.4939
$\xi_{-2}^2 = \xi_{+2}^2 \equiv \xi_2^2$	1.3707	0.9914

Eigenvalues	$\chi_{ab}^{(22)}$	$\chi_{ab}^{(14)}$
χ_0^2	$8.84 \cdot 10^{-4}$	0.2785
$\chi_{-1}^2 = \chi_{+1}^2 \equiv \chi_1^2$	$20.55 \cdot 10^{-4}$	14.1045
$\chi_{-2}^2 = \chi_{+2}^2 \equiv \chi_2^2$	$30.29 \cdot 10^{-4}$	9.3602

Table 5.1. *Eigenvalues of matrices P_2 and P_4 in the left table and of matrices $\chi_{ab}^{(22)}$ and $\chi_{ab}^{(14)}$ in the right table for the PHCA arrangement. As for any pentagonal configuration, the number of different values is 3, in accordance to the expected degeneracy in the ± 1 and ± 2 indexes.*

$$\begin{aligned}
\chi_{\frac{1}{2},URF}^3 - r \cdot \chi_{\frac{1}{2},URF}^2 - 2.794 \cdot 10^{-1} \cdot \chi_{\frac{1}{2},URF} + 8.82 \cdot 10^{-4} \cdot r = 0 \quad (0) \\
\chi_{\frac{1}{2},URF}^3 - r \cdot \chi_{\frac{1}{2},URF}^2 - 14.1066 \cdot \chi_{\frac{1}{2},URF} + 20.55 \cdot 10^{-4} \cdot r = 0 \quad (1) \\
\chi_{\frac{1}{2},URF}^3 - r \cdot \chi_{\frac{1}{2},URF}^2 - 9.3632 \cdot \chi_{\frac{1}{2},URF} + 30.29 \cdot 10^{-4} \cdot r = 0 \quad (2)
\end{aligned} \tag{5.37}$$

with solutions gathered together in Table 5.2.

It happens that solutions in the (1) and (2) sets are doubly degenerate as a consequence of the fact that the eigenvalues of both P_2 and P_4 also are simultaneously degenerate in their indexes ± 1 and ± 2. Therefore, the total number of triplets arising from the splitting of the tuning frequency in the PHCA proposal for the URF case is, as expected, five, although they collapse into three different triplets. The IRF degeneration structure of the resulting sets is maintained again following the spinorial pattern of the gravitational waves, a property that the URF effect does not affect.

The analysis of the URF effect is by itself necessary for a complete study of spherical GW antennæ. However, we are specially interested in it with respect to the PHCA proposal. The reason is that we are able to demonstrate that our model not only gives an accurate account of the coupled spectrum of the detector when it is linked to a first layout of resonators in pentagonal configuration tuned to ω_{12}, but, what is even more

Value of the Mass Ratio	Solution Index	Triplet-Equation Index (0)	(1)	(2)
$\eta_{prototype} = \frac{1}{1762.45}$ $r = -0.464$	1	- 0.8085	- 3.9949	- 3.3006
	2	0.3461	3.5311	2.8369
	3	-0.0015	- 0.0001	- 0.0001
$\eta_{sphere} = \frac{1}{40000}$ $r = -2.210$	1	- 2.3295	- 5.0199	-4.3581
	2	0.1261	2.8102	2.1488
	3	- 0.0066	- 0.0003	- 0.0007

Table 5.2. *Solutions of the three different cubic equations for the PHCA proposal. The solution index indicates a particular frequency in a given triplet, which is labelled as a whole by the equation index.*

interesting, it can also describe the device dynamics when a second group –non cross-interacting at leading order with the first– is tuned to ω_{22}, as we have proposed so to take advantage of the good sphere absorption cross section at the first and the second quadrupole harmonics.

For this coupling, the model considers the effects of the actual presence of ω_{14} near ω_{22}, so that then the understanding of the behaviour of the antenna under the influence of an incoming signal is as complete and as close to reality as possible. The final summarized issues are that our theory predicts the appearance of three different doublets of frequencies, two of them doubly degenerate, around ω_{12} as a result of the coupling of the first layout, whereas ω_{22} will split into three different triplets of the $scD + wcS$ type, being the degeneracy of the sets maintained in all the cases, from which, certainly, different wave amplitudes will couple selectively to different frequencies for the two layouts, and

therefore for the complete antenna.

- **URF-TIGA frequencies around ω_{22}**

With respect to the TIGA, considerations are even simpler. TIGA resonators' arrangement greatly simplifies once more the algebraic mathematical developments, and so the frequency structures of the system's spectrum under the URF effect showing as always a maximum degree of degeneracy.

This is already made evident at the first stages of the analysis. Matrices $P_2(\mathbf{n}_a\mathbf{n}_b)$ and $P_4(\mathbf{n}_a\mathbf{n}_b)$ are identical when the 6 resonators' positions for the TIGA configuration in Table 4.2 are used to fix $\mathbf{n}_a$ and $\mathbf{n}_b$; and not only this, but furthermore all the non-diagonal elements have the same value:

$$P_2 = P_4 = \begin{pmatrix} 1 & A & A & A & A & A \\ A & 1 & A & A & A & A \\ A & A & 1 & A & A & A \\ A & A & A & 1 & A & A \\ A & A & A & A & 1 & A \\ A & A & A & A & A & 1 \end{pmatrix} \quad A = -0.2 \tag{5.38}$$

Eigenvectors read

$$Q \equiv \begin{pmatrix} -0.1796 & 0.7880 & 0.2332 & -0.3543 & -0.0122 & -0.4082 \\ 0.0234 & -0.4376 & 0.2639 & -0.3175 & -0.6861 & -0.4082 \\ 0.0044 & -0.4012 & 0.2527 & -0.2828 & 0.7270 & -0.4082 \\ -0.6929 & -0.0869 & -0.0694 & 0.5834 & -0.0220 & -0.4082 \\ 0.6775 & 0.1377 & 0.1963 & 0.5628 & -0.0067 & -0.4082 \\ 0.1671 & 0.0000 & -0.8768 & -0.1915 & 0.0000 & -0.4082 \end{pmatrix} \tag{5.39}$$

and eigenvalues, that in fact were already calculated in Chapter 4 when studying the TIGA ideal proposal –see (4.31)–, are easily found to be those in Table 5.3, from which one can also derive $\chi^2_{i,22}$ and $\chi^2_{i,14}$.

These quantities enter the two different cubic equations for $\chi_{\frac{1}{2}}$:

$$\begin{aligned} \chi^3_{\frac{1}{2},URF} - r \cdot \chi^2_{\frac{1}{2},URF} - 11.3323 \cdot \chi_{\frac{1}{2},URF} + r1.0106 \cdot 10^{-5} = 0 \quad (1)-(5) \\ \chi^3_{\frac{1}{2},URF} - r \cdot \chi^2_{\frac{1}{2},URF} = 0 \qquad (6) \end{aligned} \tag{5.40}$$

Eigenvalues	P_2	P_4
$\xi_1^2 = \ldots = \xi_5^2$	1.2	1.2
ξ_6^2	0	0

Eigenvalues	$\chi_{ab}^{(22)}$	$\chi_{ab}^{(14)}$
$\chi_1^2 = \ldots = \chi_5^2$	0.0027	11.3297
χ_6^2	0	0

Table 5.3. *Eigenvalues of matrices P_2 and P_4 in the left table and of matrices $\chi_{ab}^{(22)}$ and $\chi_{ab}^{(14)}$ in the right table for the TIGA arrangement. The degree of degeneracy is maximum.*

with solutions given in Table 5.4.

Once again, the frequency shifts in each triplet are all identical among the different sets from (1) to (5), as a consequence of the degeneracy in the eigenvalues. In other words, the quintuplet of degenerate bare sphere-modes associated to ω_{22} has bifurcated into non-symmetrically upshifted, downshifted and central degenerate quintuplets of modes.

For the remaining single triplet (6), that corresponding to the null eigenvalue, we effectively see that it is of the $scS + wcD$ type: a strongly coupled singlet below ω_{22}, plus a weakly coupled doublet just at the original sphere resonance frequency which would not interact with the gravitational wave at leading order.

- **Discussion**

Analysis of the results in Table 5.2 and Table 5.4 for the $\chi_{\frac{1}{2},URF}$ solutions in the PHCA and TIGA cases, which directly yield the coupled frequency spectrum under the URF effect in Table 5.5 for both devices, not only corroborates sensible expectations, such as that of the maintenance of the ideal degeneracy pattern, but also qualitative predictions, in particular the existence of triplets including a central element *very close* to the resonance one and a *non symmetric* doublet around it.

Furthermore, the study reveals some new features. The first set of observations refers to the structure and numerical values of the obtained triplets without a priori weakly coupled components: (0)-(2) for PHCA and (1)-(5) for TIGA.

First of all, the found numbers are comparable to those of the IRF situation (see

Value of the Mass Ratio	Solution Index	Triplet-Equation Index (1) - (5)	(6)
$\eta_{prototype} = \frac{1}{1762.45}$ $r = -0.464$	1	- 3.6062	0
	2	3.1424	0
	3	- 0.0001	-0.464 = a
$\eta_{sphere} = \frac{1}{40000}$ $r = -2.210$	1	- 4.6479	0
	2	2.4384	0
	3	- 0.0005	- 2.21 = a

Table 5.4. *Solutions of the two different equations obtained for the TIGA proposal. The solution index indicates a particular frequency in a given set, which is labelled as a whole by the equation index. For the (6) case constructed from the null eigenvalues, the third order algebraic equation reduces to first order so that it has an unique non-null strong coupled solution, at which the triplet becomes of the* $scS + wcD$ *type.*

PHCA frequencies in (4.25) and TIGA frequencies in (4.35)), although the URF quantities are appreciably larger, and so is the frequency span of the sets.

It also happens that each of them has two downshifted components being the remaining one upshifted, what means that the bifurcation of the degenerate free sphere modes associated to the resonance frequency always follows the same pattern: one frequency above the value of ω_{22}, a second frequency under but near it –we are going to call it central frequency–, and finally a third solution also located under ω_{22}, but *non symmetrically* with respect to the first one.

Hence, each triplet contains a pair imitating the IRF doublets, but it is clearly shown

Proposal	Frequencies around ω_{22}	
	$\eta_{prototype}$	η_{sphere}
PHCA	$\omega_{0,u} = \omega_{22}(1 + 0.1731\,\eta^{\frac{1}{2}})$ $\omega_{0,d} = \omega_{22}(1 - 0.4043\,\eta^{\frac{1}{2}})$ $\omega_{1,u} = \omega_{22}(1 + 1.7656\,\eta^{\frac{1}{2}})$ $\omega_{1,d} = \omega_{22}(1 - 1.9975\,\eta^{\frac{1}{2}})$ $\omega_{2,u} = \omega_{22}(1 + 1.4185\,\eta^{\frac{1}{2}})$ $\omega_{2,d} = \omega_{22}(1 - 1.6503\,\eta^{\frac{1}{2}})$	$\omega_{0,u} = \omega_{22}(1 + 0.0631\,\eta^{\frac{1}{2}})$ $\omega_{0,d} = \omega_{22}(1 - 1.1648\,\eta^{\frac{1}{2}})$ $\omega_{1,u} = \omega_{22}(1 + 1.4051\,\eta^{\frac{1}{2}})$ $\omega_{1,d} = \omega_{22}(1 - 2.5100\,\eta^{\frac{1}{2}})$ $\omega_{2,u} = \omega_{22}(1 + 1.0744\,\eta^{\frac{1}{2}})$ $\omega_{2,d} = \omega_{22}(1 - 2.1791\,\eta^{\frac{1}{2}})$
TIGA	$\omega_{1,\ldots,5,u} = \omega_{22}(1 + 1.5712\,\eta^{\frac{1}{2}})$ $\omega_{1,\ldots,5,d} = \omega_{22}(1 - 1.8031\,\eta^{\frac{1}{2}})$ $\omega_6 = \omega_{22}(1 - 0.232\,\eta^{\frac{1}{2}})$	$\omega_{1,\ldots,5,u} = \omega_{22}(1 + 1.2192\,\eta^{\frac{1}{2}})$ $\omega_{1,\ldots,5,d} = \omega_{22}(1 - 2.3240\,\eta^{\frac{1}{2}})$ $\omega_6 = \omega_{22}(1 - 1.105\,\eta^{\frac{1}{2}})$

Table 5.5. *Strongly coupled frequencies of the spherical antenna spectrum when the URF effect is considered. Calculation have been performed for two different ratios of the resonator mas to the sphere mass –$\eta_{prototype}$, corresponding to the TIGA experimetal prototype at LSU, and η_{sphere}, a theoretical value for a full scale future spherical detector–, and besides for the two existent specific proposals, PHCA and TIGA. Subindex u-(up) labels the values which are above the resonance frequency ω_{22}, whereas d-(down) labels those underneath.*

in the results that their strict symmetry is broken under the URF effect, so that it is always the frequency under ω_{22} the greater in absolute value. Besides, taking into account that the central frequency is also smaller than ω_{22}, it became obvious that the whole set has been influenced by the fact that ω_{14} is smaller than ω_{22}, which explicitly enters the equations for instance through the sign of a. So, each group of coupled frequencies in the IRF case has suffered a displacement approaching ω_{14}. This dragging is always more important for the frequency closer to it: the absolute value of the downshifted frequency is greater than that of the upshifted one in each set.

Summing up, the URF effect results in a dragging effect breaking the symmetry of the IRF doublets, which approach the second disturbing frequency ω_{14}, and moreover induces the appearance of a third component near the resonant ω_{22}.

Near actually means *really near*: we see from the numbers that the central $\chi_{\frac{1}{2},URF}$ in each group is indeed of order $\eta^{\frac{1}{2}}$ itself or even smaller[4], so that the central URF resonances will actually be of the form

$$\omega^2_{i,central} = \omega^2_{NL}(\,1 + \chi_{1,central}\,\eta\,) + O(\eta^{\frac{3}{2}}). \tag{5.41}$$

Reproduction of the process of calculation of residues determining the vibrational amplitudes would demonstrate that the contributions of such modes are not at leading order $\eta^{-\frac{1}{2}}$, but at terms of higher orders; this once more is proved in Appendix D. Therefore, they are referred to as be weakly coupled. The result is that the predicted scT triplets are in fact triplets of the $scD + wcS$ type, possibility which was prudently advanced in the general discussion.

One more remark. When the mass of the detector is increased, or equivalently η decreases, the symmetry breaking of the URF doublets is appreciably more pronounced, and the frequency span of each set is slightly broader; also, the central frequency grows in absolute value, although not enough to become relevant.

5.3 The Suspended Sphere and Axial Symmetry

Our next concern deals with the last of the ideality departures treated in this essay: the breaking of spherical symmetry provoked by the practical requirement of suspension for antennæ in earth-based observatories.

[4] As above indicated, we are not considering the $scS + wcD$ of the TIGA case, which could be understood as a downshifted singlet.

5.3.1 Spherical Symmetry Breaking and New Frequency Splitting

We are not interested in the suspension mechanism *per se*, but in the disturbing effects that it could cause in the detector responses and in their departures from those predicted for the ideal device.

Nevertheless, we explain in a few words that practicality technically requires to select a nodal point of suspension in the sphere which determines, along with the geometrical center of the body, a diameter that is drilled to make a diametral bore across the detector. The hole is then redrilled half way through using a larger drill bit in order to suspend the detector on a wedge at the end of a rod that clears the inside diameter of the large suspension hole but plugs the small hole. The other end is treated so that it can be screwed into a support piece. This has been the procedure followed, for instance, in the mounting of the TIGA prototype support system [95].

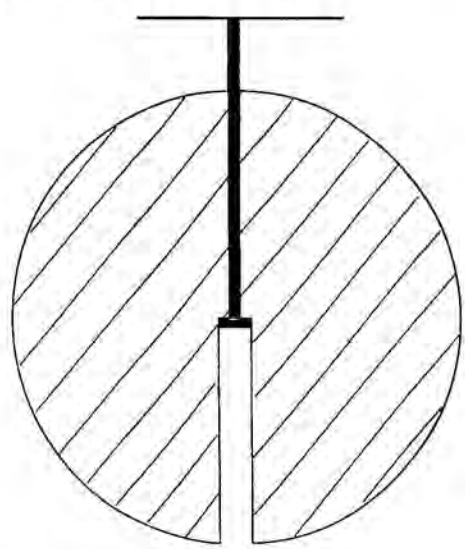

Figure 5.5. *Vertical section of a suspended sphere.*

As a result of those unavoidable manipulations, spherical symmetry is broken, although axial symmetry around the diametral bore is maintained. The most direct consequence of this is that the degeneracy of the spectral frequencies ω_{nl} of the free perfect sphere –each is $(2l+1)$-fold degenerate– is also broken, so that they split up into multiplets ω_{nlm} $(m = -l, \ldots, l)$, with components ω_{nlm} that actually depend on three

different indexes and are associated one to one to the spheroidal oscillation eigenmodes of the suspended sphere (REF).

The question is that, in this case, resonators cannot be tuned to one of the degenerate ω_{nl} as was done for the free sphere.

If we assume that all the transducers on a given layout are identical with natural frequency Ω, one could demand that Ω falls within the span of the multiplet of the $\omega_{NL\{m\}}$, and then we can write the next relations dictated by (5.1) once again:

$$\omega^2_{NL\{m\}} = \Omega^2 (1 + p_m \eta^{\frac{1}{2}}). \tag{5.42}$$

It is obvious that these equations are in complete analogy to that describing the connection between neighbouring free sphere frequencies directly involved in the coupling with resonators, formula (5.14). Hence, the derivation of the new frequency splitting related to the coupled device resonators-suspended sphere naturally follows that of the URF spectrum detailed in the preceding section.

The first step led to find the zeroes of the determinant $\Delta(s)$, although here we must resort to its most general expression due to the removed degeneracy of the ω_{nl}. From (3.72) and (3.75):

$$\begin{aligned} \Delta(s) \equiv \det \Bigg[\delta_{ab} + \eta \sum_{m=-L}^{L} \frac{s^2\Omega^2}{(s^2+\Omega^2)(s^2+\omega^2_{NLm})} \chi^{(NLm)}_{ab} \\ + \eta \sum_{nl \neq NL.m} \frac{s^2\Omega^2}{(s^2+\Omega^2)(s^2+\omega^2_{nlm})} \chi^{(nlm)}_{ab} \Bigg] = 0, \end{aligned} \tag{5.43}$$

being $\chi^{(nlm)}_{ab}$ the matrices

$$\chi^{(nlm)}_{ab} \equiv |A_{NL}(R)|^2 \, Y^*_{lm}(\mathbf{n}_a) Y_{lm}(\mathbf{n}_b). \tag{5.44}$$

We shall exclusively concentrate on the splitting around Ω, so that at leading order $\Delta(s)$ reduces to

$$\Delta(s) \equiv \det \left[\delta_{ab} - \frac{1}{\chi_{\frac{1}{2}}} \sum_{m=-L}^{L} \frac{\chi^{(nlm)}_{ab}}{\chi_{\frac{1}{2}} - p_m} \right] = 0, \tag{5.45}$$

which becomes (5.18) –valid for full degeneracy– when $p_m = 0$.

Solutions to the algebraic equation (5.45) are no longer symmetric pairs. Rather, there are at most $2L + 1 + J$ non identically zero roots with a maximum number of

$2(2L+1)$ if $J \geq 2L+1$ and, as always, modes associated to null roots can be seen to be weakly coupled.

We have applied this theoretical considerations to a real system, the TIGA prototype at LSU, in order to see what are its predictions and how they confront with experimental data.

5.3.2 Experimental Measurements with TIGA

The TIGA prototype at LSU was suspended as described above in the text, so that its first quadrupole frequency split up into a multiplet of five frequencies, with measured values

$$\begin{aligned} \omega_{120} &= 3249Hz \\ \omega_{121} &= 3238Hz \quad \omega_{12-1} = 3236Hz \\ \omega_{122} &= 3224Hz \quad \omega_{12-2} = 3223Hz. \end{aligned} \tag{5.46}$$

All six resonators were equal, and had the following characteristic frequency and mass (with respect the TI mass):

$$\Omega = 3241Hz. \qquad \eta = \frac{1}{1762.45}. \tag{5.47}$$

Substituting these values into (5.42), it is seen that

$$\begin{aligned} p_0 &= \ 0.2075 \\ p_1 &= -0.0777 \quad p_{-1} = -0.1036 \\ p_2 &= -0.4393 \quad p_{-2} = -0.4650. \end{aligned} \tag{5.48}$$

Once these quantities are inserted into equation (5.45) and the resonator positions for the TIGA configurations, in table 4.2 of Chapter 4, are specified in matrices $\chi_{ab}^{(12m)}$, one can calculate the $\gamma_{\frac{1}{2}}$ coefficients which provide the system frequencies by formula:

$$\omega_i^2 = \Omega^2(1 + \gamma_{\frac{1}{2},i}\eta^{\frac{1}{2}}). \tag{5.49}$$

Merkowitz gave a complete account of all the measured system frequencies as resonators are progressively attached to the selected faces, beginning with one and ending with six, in reference [95][5]. In Table 5.8 we include the numerical values of these experimentally reported frequencies along with the calculated theoretically by solving equation (5.45).

[5] We want to express our gratitude to Stephen Merkowitz for kindly handing these data to us.

Item	Measured (Hz)	Calculated (Hz)	Difference %	Item	Measured (Hz)	Calculated (Hz)	Difference %
Tuning	3241	(3241)	(0.00)	4 resonators	3159	3155	-0.12
Free multiplet	3223	(3223)	(0.00)		3160	3156	-0.11
	3224	(3224)	(0.00)		3168	3165	-0.12
	3236	(3236)	(0.00)		3199	3198	-0.05
	3238	(3238)	(0.00)		3236	3236	0.00
	3249	(3249)	(0.00)		3285	3286	0.03
1 resonator	3167	3164	-0.08		3310	3310	0.00
	3223	3223	0.00		3311	3311	0.00
	3236	3235	-0.02		3319	3319	0.00
	3238	3237	-0.02	5 resonators	3152	3154	0.08
	3245	3245	0.00		3160	3156	-0.14
	3305	3307	0.06		3163	3162	-0.03
2 resonators	3160	3156	-0.13		3169	3167	-0.08
	3177	3175	-0.07		3209	3208	-0.02
	3233	3233	0.00		3268	3271	0.10
	3236	3236	0.00		3304	3310	0.17
	3240	3240	0.00		3310	3311	0.03
	3302	3303	0.03		3313	3316	0.10
	3311	3311	0.00		3319	3321	0.06
3 resonators	3160	3155	-0.15	6 resonators	3151	3154	0.11
	3160	3156	-0.13		3156	3155	-0.03
	3191	3190	-0.02		3162	3162	0.00
	3236	3235	-0.02		3167	3162	-0.14
	3236	3236	0.00		3170	3168	-0.07
	3297	3299	0.08		[3239]	[3241]	[0.06]
	3310	3311	0.02		3302	3309	0.23
	3311	3311	0.00		3308	3310	0.06
					3312	3316	0.12
					3316	3317	0.02
					3319	3322	0.10

Table 5.6. *Measured Suspended-TIGA frequencies versus their theoretical predictions from our model. In brackets, calculated values which are taken by definition equal to the measured ones; in square brackets, the weakly coupled central mode in the full 6 resonator TIGA layout.*

As can be seen, coincidence between our theoretical predictions and the experimental data for TIGA is remarkable: the worst error is 0.2%, while for the most part it is below 0.1%. So, *discrepancies between predictions and experiment are of order* η, as indeed expected, what is an encouraging result supporting the correctness of our model. Besides, in reference [98] it is also reported that the 11-th weakly coupled mode of the TIGA has a practically zero amplitude, again in excellent agreement with our general theoretical predictions about weakly coupled modes.

We observe that estimations of next order corrections in the theoretical expressions for the frequencies does not result in a better matching between the compared quantities. This is because the control of the general experimental conditions in which data were obtained had a certain level of tolerance, as Merkowitz and Johnson explicitly stated in [98], and hence the accuracy of these available real outputs is not as refined as to be of order η. As a consequence, those authors showed satisfaction that $\approx 1\%$ of coincidence between theory and measurement is comfortably accomplished. Nevertheless, the evaluation of next order corrections will be necessary in the future as a response to a forseeable enhancement in the control of the system experimental parameters.

5.3.3 Nearly Invariant PHCA Spectrum

Besides the considerations related to TIGA we also add some comments about PHCA. Indeed, they will be suitable for any PHC configuration, those described in section 4.1 of Chapter 4, since the crucial fact consists in having the resonator layout in a pentagonal configuration around a symmetry axis. This axis is taken to coincide with that of the diametral suspension bore in the sphere, so that the coupled-suspended-device will clearly broke the spherical symmetry of the free sphere, but instead will still keep the axial symmetry of the suspended sphere and of the PHC layouts.

One may expect that these axially symmetric distributions give place to suspended-PHC spectrums quite similar to those of the perfect PHC configurations, with like structures of the frequency pairs, even possibly maintaining the degeneracy scheme.

To be specific, we shall particularly speculate over the PHCA configuration, under the hypothesis that the values of its split ω_{12} frequencies and its resonator characteristics are those in (5.46) and (5.47). This will enable comparison with the actual TIGA prototype data. Results are displayed in Figures 5.6 and 5.7.

It is clear that the drilled TIGA pairs, obtained from measured real data, are different from those of the ideal non-suspended TIGA. This is not at all surprising, since the high

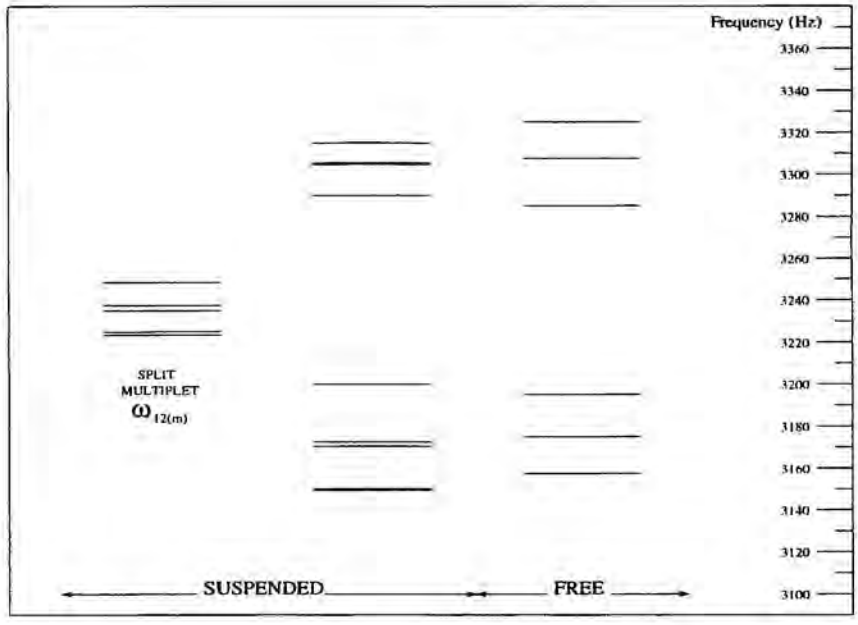

Figure 5.6. *Suspended PHCA spectrum versus that corresponding to the non-suspended device. Clearly, the essential structural characteristics are similar in both cases.*

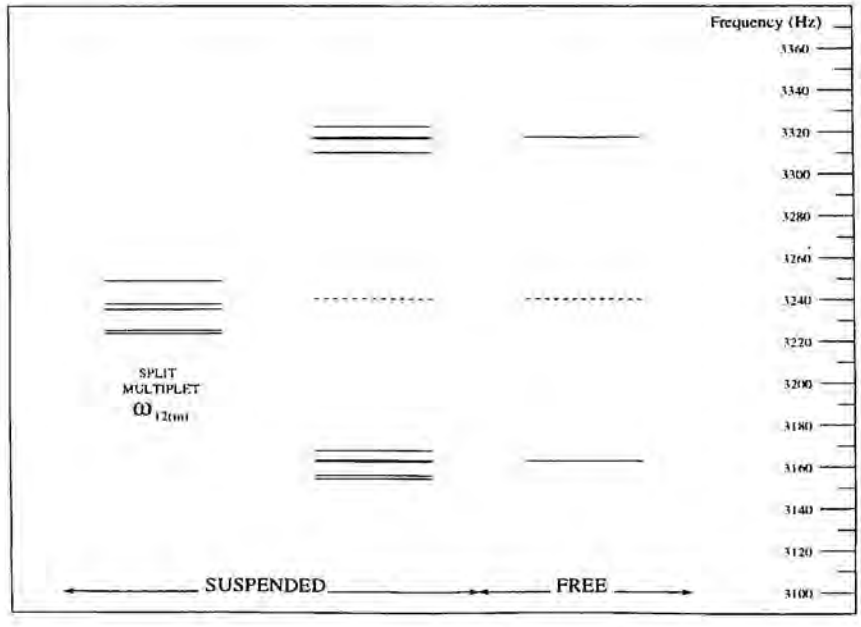

Figure 5.7. *Suspended TIGA spectrum versus that corresponding to the non-suspended device. Degeneracy in the second case in not further maintained in the first.*

symmetry of the ideal device inducing the appearance of an unique pair 5-fold degenerate is no longer maintained when the truncated icosahedron is drilled.

Instead, PHCA pairs effectively remain distributed in agreement to similar schemes in both situations, as an indication that PHC configurations naturally adapt to the suspended device, becoming the alternative to more symmetric proposals in real systems.

Chapter 6

SIGNAL DECONVOLUTION

The previous chapters have been devoted to the investigation of the behaviour of spherical resonant detectors when they are typically influenced by the action of impinging gravitational waves. This is, of course, the first important problem in the resonant GW detection research. As has already been shown, it has been rigorously solved through the implementation of powerful mathematical techniques which have allowed us to determine the antennae's responses in a general case and even more to limit them to particular proposals.

Beyond this first step, there exist some other key questions. One of them, and possibly the next in a series of logical order, is the so-called *Inverse Problem* or *Signal Deconvolution Problem*: determination of the unknown direction, polarization and amplitudes of the incoming GW from the responses and data provided by the antenna.

This specific information is available from the readout of a single spherical detector, an appealing advantage over cylindrical bar detectors. Nevertheless, there are certain other details in the signal deconvolution process which cannot be sorted out with a single sphere. For example, the direction determination is only unique within an hemisphere: the position of a given source and a second one located on its antipode in the sky would be indistinguishable: or nothing could be said about the propagation speed of the wave or the wave form. A two sphere array performing a coincidence experiment will help solving some of these problems, and if a xylophone -a set of detectors for different frequencies- is used the reliability of detection and the amount of achievable information could be further increased.

Let us consider here the basic inverse problem, that solvable from the data that a single detector will produce, exclusively in the case in which:

- we do not know (*a priori* or by other means) anything about the incidence direction, polarization or amplitudes of the gravitational wave, and
- we cannot assume any hypothetical model relatively to the GW source.

The relaxation of any of our hypothesis will induce modifications in the deconvolution procedure, which will be altered if we actually know some properties of the incoming gravitational wave because the source is known from astronomical observations or even a network of other GW antennæ, or at least we are confident about an hypothesis over the GW source to be checked *a posteriori*.

Here, we are facing the most unfavorable deconvolution situation presupposing a high degree of disinformation. Besides, and although Lobo outlined in [80] a procedure that can be used if the valid theory of gravity is unknown, we will always restrict here to accept that General Relativity happens to be correct. So, the viability of our procedure is strongly dependent on GR being true, and any appearance of incompatibilities in the procedure has to be held as vetoes on the hypothesis that GR is correct.

In section 6.1 we will sketch the signal deconvolution procedure for a noiseless spherical antenna, subject which has been extensively treated in literature (see references below), and will continue by introducing for the first time in this essay the problem of noise in section 6.2. We will show that it is also possible to analytically treat the inverse problem using only linear algebra even in the presence of those disturbances [96, 99]. As expected from the omnidirectionality of spherical antennæ, we shall see that error estimations for the incidence direction and the GW amplitude are direction independent. On the contrary, we will demonstrate that the polarization angle or the polarization amplitudes cannot be determined with isotropic sensitivity under the original hypotheses exposed in this introduction.

6.1 Signal Deconvolution in the Absence of Noise

The solution to the inverse problem for a noiseless spherical antenna was partly outlined by Wagoner and Paik in the mid 1970's [133]. More recently, in 1988, Dhurandhar and Tinto published an article [37] where the inverse problem was analytically solved in the case of a network of five detectors (either bars or laser interferometers) by using only their complex amplitudes for monochromatic signals. Since a sphere monitored by n transducers can be thought of as n bar detectors occupying the same space, the solution of Dhurandhar and Tinto has been adapted for spherical antennæ by several authors

[144, 90, 92]. In addition, a more general guideline has been pointed out by Lobo [80] even allowing the possibility of assessment or at least establishment of vetoes on which is the theory or the class of theories compatible with the measures.

All these solutions have the common property of only requiring linear algebra to estimate the unknowns from the detector outputs. Let us expose here an approach.

6.1.1 Detector Outputs and GW Amplitudes

As repeatedly explained through this essay, the standard technique for extracting information from spherical detectors is to position a number of resonant transducers on its surface at specific locations and tuned to a quadrupolar frequency ω_{N2} of the free sphere.

Such a device will indeed measure the quantities $q_a(t)$ representing the resonators' actual elastic deformations, and it has been already seen in Chapter 3 how these functions relate to the spinorial GW amplitudes $g^{(2m)}(t)$ in a general case and in the most interesting particular proposals allowing the construction of mode channels $y^{(m)}(t)$ characterized by a one-to-one correspondence with the quadrupole modes of the sphere and thus with the $g^{(2m)}(t)$ amplitudes of the GW.

Here, a word is in order about how the GW amplitudes $g^{(2m)}(t)$ are related to the spherical GW amplitudes $h_m(t)$ of GR commonly used in the literature.

These spherical amplitudes also provide a complete and orthogonal representation of the cartesian metric deviation tensor $H(t) \equiv h_{ij}(t)$[1],which in the laboratory frame (L-F), with origin at the center of mass of the detector, coordinate axes $(\hat{x}, \hat{y}, \hat{z})$ and the $\hat{z}$ axis aligned with the local vertical. reads:

$$H(t) = \begin{pmatrix} h_1(t) - \frac{1}{\sqrt{3}}h_5(t) & h_2(t) & h_4(t) \\ h_2(t) & -h_1(t) - \frac{1}{\sqrt{3}}h_5(t) & h_3(t) \\ h_4(t) & h_3(t) & \frac{2}{\sqrt{3}}h_5(t) \end{pmatrix}. \tag{6.1}$$

Through the definitions (2.38) for the $g^{(2m)}(t)$ as combinations of the spatial Riemann tensor components,

$$g^{(2m)}(t) = \frac{8\pi}{15} E_{ij}^{*(2m)} R_{0i0j}(t) \tag{6.2}$$

[1] We recall that we restrict ourselves to detectors much smaller than the gravitational wavelength, so only the time dependence of h_{ij} will have significant physical effects.

(the basis of the five-dimensional vector space of three-dimensional, symmetric and traceless matrices $\{E_{ij}^{(2m)}\}$ is given in (2.39)), and in GR

$$R_{0j0k}(t) = -\frac{1}{2} h_{jk,00}(t), \tag{6.3}$$

the following relations are easily found:

$$\begin{aligned}
g^{(2+2)}(t) &= -\sqrt{\tfrac{2\pi}{15}}\,(\ddot{h}_1(t) - i\ddot{h}_2(t)) \\
g^{(2-2)}(t) &= -\sqrt{\tfrac{2\pi}{15}}\,(\ddot{h}_1(t) + i\ddot{h}_2(t)) \\
g^{(2+1)}(t) &= -\sqrt{\tfrac{2\pi}{15}}\,(-\ddot{h}_4(t) + i\ddot{h}_3(t)) \\
g^{(2-1)}(t) &= -\sqrt{\tfrac{2\pi}{15}}\,(\ddot{h}_4(t) + i\ddot{h}_3(t)) \\
g^{(20)}(t) &= -\sqrt{\tfrac{4\pi}{15}}\,\ddot{h}_5(t)
\end{aligned} \tag{6.4}$$

$$\begin{aligned}
\ddot{h}_1(t) &= -\sqrt{\tfrac{15}{2\pi}}\,\left(\tfrac{g^{(2+2)}(t)+g^{(2-2)}(t)}{2}\right) \\
\ddot{h}_2(t) &= \sqrt{\tfrac{15}{2\pi}}\,\left(\tfrac{g^{(2+2)}(t)-g^{(2-2)}(t)}{2i}\right) \\
\ddot{h}_3(t) &= -\sqrt{\tfrac{15}{2\pi}}\,\left(\tfrac{g^{(2+1)}(t)+g^{(2-1)}(t)}{2i}\right) \\
\ddot{h}_4(t) &= \sqrt{\tfrac{15}{2\pi}}\,\left(\tfrac{g^{(2+1)}(t)-g^{(2-1)}(t)}{2}\right) \\
\ddot{h}_5(t) &= -\sqrt{\tfrac{15}{4\pi}}\,g^{(20)}(t).
\end{aligned} \tag{6.5}$$

Therefore, it naturally occurs as it must be that the spherical GW amplitudes $h_m(t)$ can also be obtained as particular linear combinations of the measured $q_a(t)$. We can construct them through formulas (6.5) from our previously achieved results for the GW amplitudes $g^{(2m)}$.

In what follows, and for the sake of simplicity in further results, we will work with the spherical GW amplitudes $h_m(t)$ and will drop the notation of time dependence (t) for brevity.

6.1.2 Deconvolution Procedure

Definitely, the existence of mode channels will no doubt facilitate the calculation of the quantities h_m from the measured q_a. It would be only necessary to substitute each function $g^{(2m)}$ in (6.5) by its correspondent mode channel combination (see section 3. in Chapter 3 or results in Chapter 4 for specific proposals).

Then, in the absence of noise matrix H in (6.1) can be directly constructed from our measurements and so it also coincides with a matrix describing the response of the detector to the gravitational wave. Let us to introduce this matrix as matrix $A(t)$, although

for the moment we are just going to work always with H due to their equivalence[2]. This matrix $A(t)$ is indeed related to what Dhurandhar and Tinto called the detector response [37]. They were also the first indicating that the eigenvector of $A(t)$ with zero eigenvalue points in the propagation direction of the wave. As well as other authors –e.g. [96]–, we will also use this basic concept. The full procedure is as follows.

Once the spherical amplitudes h_m have been determined, it would be now easy to deduce which are the unknown incidence direction, polarization and amplitudes of the incoming GW. The key idea arises when studying the general form of the spatial components of the metric deviation tensor in a second reference frame: the wave frame (W-F). It is a coordinate frame with origin also at the center of mass of the detector and wave axes $(\hat{x}', \hat{y}', \hat{z}')$, with axis $\hat{z}'$ aligned by definition to the propagation direction of the wave and $(\hat{x}', \hat{y}')$ axes of the polarization ellipse. If, as assumed, GR is valid, the strain tensor in the wave frame can be written when working in the TT (transverse traceless) gauge as:

$$H'(t) = \begin{pmatrix} h_+(t) & h_\times(t) & 0 \\ h_\times(t) & -h_+(t) & 0 \\ 0 & 0 & 0 \end{pmatrix}, \tag{6.6}$$

where we recall $h_+(t)$ and $h_\times(t)$ are the wave plus and cross amplitudes for the two allowed states of linear polarization (see section 2.1 in Chapter 2).

It becomes obvious that tensor H' has a particular matrix structure. It makes evident two related properties:

- H' is a canonical form in the sense that rotations of any angle about the $\hat{z}'$ axis leaves its structure invariant;
- H' possess a null eigenvalue with an associated eigenvector pointing in the direction of the z' axis. Due to the fact that, by definition, this axis tells the propagation direction of the wave, this *null* eigenvector is an indicator of the propagation direction.

Indeed, the resolution of the general eigenvalue problem for the strain tensor H' in the wave frame:

$$H' \vec{v}_i = \lambda_i \vec{v}_i. \tag{6.7}$$

[2] In the noisy case A and H will no longer coincide.

leads to the following results:

$$\begin{aligned} \textit{Eigenvalues} \quad & \lambda_1 = -\lambda \\ & \lambda_2 = +\lambda \qquad \lambda = \frac{\lambda_2 - \lambda_1}{2} = \sqrt{h_+^2 + h_\times^2} \\ & \lambda_3 = 0 \end{aligned} \tag{6.8}$$

$$\textit{Eigenvectors}$$

$$\vec{v}_1' = N_1 \begin{pmatrix} h_\times \\ -h_+ - \lambda \\ 0 \end{pmatrix} \quad \vec{v}_2' = N_2 \begin{pmatrix} -h_\times \\ h_+ - \lambda \\ 0 \end{pmatrix} \quad \vec{v}_3' = \begin{pmatrix} 0 \\ 0 \\ 1 \end{pmatrix}, \tag{6.9}$$

with the values for the normalization constants:

$$N_1 = \frac{1}{\sqrt{2\lambda^2 + 2\lambda h_+}} \qquad N_2 = \frac{1}{\sqrt{2\lambda^2 - 2\lambda h_+}}. \tag{6.10}$$

Summarizing, the absolute value λ of λ_1 or λ_2, can be taken as a measure for the wave amplitude, whereas eigenvector $\vec{v}_3' \equiv \hat{z}'$ associated to the null eigenvalue λ_3 points in the propagation direction with a perpendicular plane or polarization plane defined by $\vec{v}_1'$ and $\vec{v}_2'$.

Which are the implications of these properties for the quantities in the laboratory frame? As we have seen, the strain tensor H' in the wave frame is a symmetric traceless matrix and thus it can be orthogonally diagonalized. Its counterpart in the lab frame, tensor H, must maintain these characteristics as shown in (6.1), whereupon it could also take a diagonal form. Even more, it is immediately demonstrated that the eigenvalues of H in the L-F and H' in the W-F have exactly the same value, whereas eigenvectors change as dictated by the matrix R_{WL} which changes the basis from the W-F to the L-F and can be considered the rotation matrix that transforms the metric perturbation H' to the lab frame:

$$H = R_{WL}^{-1} H' R_{WL} \tag{6.11}$$

The proof is as follows. We start from the eigenvalue equation (6.7),

$$H' \vec{v}_i' = \lambda_i \vec{v}_i' \tag{6.12}$$

and introduce the suitable R_{WL} and R_{WL}^{-1} rotations in (6.11). For any rotation, R_{WL} or another, we will use the Euler angles (α, β, γ) in their y-convention form. Generally, the rotation matrix for the y-convention is:

$$R = \begin{pmatrix} \cos\gamma\cos\beta\cos\alpha - \sin\gamma\sin\alpha & \cos\gamma\cos\beta\sin\alpha + \sin\gamma\cos\alpha & -\cos\gamma\sin\beta \\ -\sin\gamma\cos\beta\cos\alpha - \cos\gamma\sin\alpha & -\sin\gamma\cos\beta\sin\alpha + \cos\gamma\cos\alpha & \sin\gamma\sin\beta \\ \sin\beta\cos\alpha & \sin\beta\sin\alpha & \cos\beta \end{pmatrix}, \tag{6.13}$$

made of three diffeent rotations: the first of angle α about the original $\hat{z}$ axis, the second of angle β around the new $\hat{y}$ axis, and the third of angle γ around the final $\hat{z}$ axis.

Going back to (6.12), one finds:

$$R_{WL}^{-1} H' R_{WL} \cdot R_{WL}^{-1} \vec{v}_i' = \lambda_i R_{WL}^{-1} \vec{v}_i' \tag{6.14}$$

which is rewritten

$$H \vec{v}_i = \lambda_i \vec{v}_i, \tag{6.15}$$

so that it has been shown that effectively H and H' possess exactly the same eigenvalues while their respective eigenvectors, $\vec{v}_i$ and $\vec{v}_i'$, are just related through $\vec{v}_i = R_{WL}^{-1} \vec{v}_i'$. Of course, the two sets of eigenvectors describe in fact the same reference system, i.e., that in which the strain tensor is seen to be diagonal (D-F): the set $\vec{v}_i$ is the expression of the diagonal axes (x_D, y_D, z_D) in the laboratory basis whereas in parallel the set $\vec{v}_i'$ represents those same diagonal axes in the wave frame.

Then, results directly involving tensor H in the L-F are the following:

- **Incidence Direction.** In accordance to (6.8) and (6.15), tensor H constructed from the experimental data must have a null eigenvalue with an associated *null* eigenvector which indicates the incidence direction of the incoming GW as seen in the L-F.

  It is possible to finally define the propagation direction on the basis of the corresponding Euler angles, simply recognizing that the matrix, named R_{LD}, which diagonalizes H in the L-F and which is constructed from its eigenvectors $\vec{v}_i$, can once again be understood as a rotation matrix of the general form in (6.13) (it may also include a reflection). It will tell us the angles of rotation by identificating

the *null* eigenvector $\vec{v}_3$ with the last column vector of R_{LD}. Looking at expression (6.13) and dividing the elements of this column we find

$$\begin{aligned} \tan\gamma &= -\frac{\vec{v}_{3y}}{\vec{v}_{3x}} \\ \tan\beta &= \frac{\vec{v}_{3y}}{\vec{v}_{3z}}\frac{1}{\sin\gamma}. \end{aligned} \tag{6.16}$$

- **Wave Amplitude.** Besides, H possess two more eigenvalues, λ_1 and λ_2, which, again from (6.8), are equal in absolute value λ actually giving a determination of the wave amplitude $\lambda = \sqrt{h_+^2 + h_\times^2}$.

- **Polarization Amplitudes and Angle.** The problem of the settling of the polarization amplitudes has been classically solved (see for example [144, 90, 96]) by looking at equation (6.11) stating the relation between the expressions for the strain tensor in the wave frame and in the lab frame:

$$H = R_{WL}^{-1} H' R_{WL}. \tag{6.17}$$

We need only the angles β and γ to rotate H' to H, since the remaining α-rotation only changes the polarization components of the tensor and not its canonical form or the direction relative to the lab frame defining the wave frame. This is the reason why α has commonly been assumed to be zero [133], which has a clear geometrical interpretation involving the relative position between the W-F coordinate axes and the L-F coordinate axes: if α is taken to be zero, the $\tilde{y}'$ axis of the W-F reference system is taken to rest on the $\tilde{x} - \tilde{y}$ plane of the L-F reference system.

The embracement of this criterion has as a consequence that the polarization components of the strain tensor remain fixed at certain values which can be found from our measurements once the propagation direction is known. Reversing relation (6.17) with $\alpha = 0$ in R_{WL},

$$H' = R_{WL}(\alpha = 0)\, H\, R_{WL}(\alpha = 0)^{-1}, \tag{6.18}$$

and selecting the proper elements one arrives to [96]:

$$h_+ = h_1 \frac{1}{2}(1 + \cos^2\beta)\cos 2\gamma - h_2 \frac{1}{2}(1 + \cos^2\beta)\sin 2\gamma - h_3 \frac{1}{2}\sin 2\beta \sin\gamma$$

$$+h_4\frac{1}{2}\sin 2\beta\cos\gamma + h_5\frac{\sqrt{3}}{2}\sin^2\beta$$

$$h_\times = h_1\cos\beta\sin 2\gamma + h_2\cos\beta\cos 2\gamma + h_3\sin\beta\cos\gamma + h_4\sin\beta\sin\gamma, \quad (6.19)$$

equations that can also be directly derived again from (6.17) by taking linear combinations of the resulting spherical amplitudes as functions of the polarization amplitudes and the source direction.

We face now a new possibility more in accord to our general previous line of expressing the unknowns as functions of the eigenvalues and the eigenvectors of H (the importance of this strategy will be clarified in next section where we will analyse the inverse problem in the presence of noise). *Our intention is then that of finding alternative formulas to those in (6.19) for h_+ and $h_\times$, now in terms of λ_i and $\vec{v}_i$.*

This new approach leads again as before to investigate relations between the representations of the strain tensor in different reference frames. In this case, we are interested in the rotation that takes H' -normally not represented by a diagonal matrix- to the diagonal form

$$H_D = \mathrm{diag}[\lambda_1, \lambda_2, \lambda_3]\,. \quad (6.20)$$

It is simply a rotation about the propagation axis, since the wave frame and that in which the strain tensor is diagonal clearly share their $\hat{z}$ axes and thus its perpendicular or polarization plane. In fact, this rotation is characterized only by the Euler angle α as defined above in the text, so that

$$H' = R_\alpha^{-1}\, H_D\, R_\alpha\,, \quad (6.21)$$

with R_α the rotation matrix

$$R_\alpha = \begin{pmatrix} \cos\alpha & \sin\alpha & 0 \\ -\sin\alpha & \cos\alpha & 0 \\ 0 & 0 & 1 \end{pmatrix}, \quad (6.22)$$

Substituting the explicit forms in (6.21) and performing the operations we find

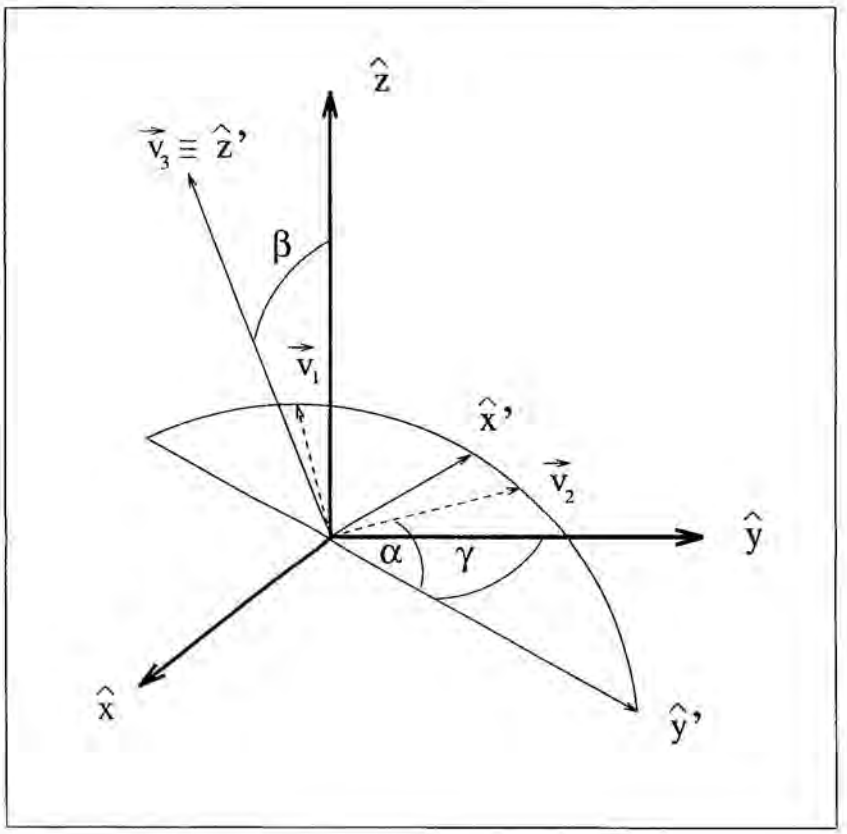

Figure 6.1. *Relative position between the three different reference frames considered. The set* $(\hat{x}, \hat{y}, \hat{z})$ *labels the L-F axes, whereas* $(\hat{x}', \hat{y}', \hat{z}')$ *name those of the W-F.* $(\vec{v}_1, \vec{v}_2, \vec{v}_3)$ *stands for the three eigenvectors of the cartesian strain tensor defining the D-F. Note that* $\hat{y}'$ *rests on the* $\hat{x} - \hat{y}$ *plane of the laboratory frame as a consequence of the* $\alpha = 0$ *criterion fixing the wave frame. Secondly, the W-F axis* $\hat{z}'$ *pointing in the incidence direction of the GW obviously coincides with axis* $\vec{v}_3$ *of the diagonal frame, so that these two systems are just related by a rotation of angle* α *around* $\hat{z}' \equiv \vec{v}_3$*. Finally, the remaining two Euler angles* β *and* γ *indicate the rotations that take the W-F to the L-F.*

$$\begin{pmatrix} h_+ & h_\times & 0 \\ h_\times & -h_+ & 0 \\ 0 & 0 & 0 \end{pmatrix} = \begin{pmatrix} -\lambda\cos 2\alpha - \frac{1}{2}\lambda_3 & -\lambda\sin 2\alpha & 0 \\ -\lambda\sin 2\alpha & \lambda\cos 2\alpha - \frac{1}{2}\lambda_3 & 0 \\ 0 & 0 & \lambda_3 \end{pmatrix}. \quad (6.23)$$

Hence

$$\begin{aligned} h_+ &= -\lambda\cos 2\alpha \\ h_\times &= -\lambda\sin 2\alpha, \end{aligned} \quad (6.24)$$

since we recall that in the noiseless case

$$\begin{aligned} \lambda_3 &= 0 \\ \lambda &= |\lambda_1| = |\lambda_2| = \frac{\lambda_2 - \lambda_1}{2}, \end{aligned} \quad (6.25)$$

and obviously

$$\lambda = \sqrt{h_+^2 + h_\times^2}. \quad (6.26)$$

In accordance to the $\alpha = 0$ criterion fixing the wave frame and its geometrical interpretation explained above, it is not difficult to realize that this new Euler angle α relating the W-F and the D-F appearing in (6.24) is just the absolute value of the quantity that one needs to rotate the $\hat{y}_D$ axis of the D-F around $\hat{z}' \equiv \hat{z}_D$ to take it to coincide with $\hat{y}'$ placed on the $\hat{x} - \hat{y}$ plane of the laboratory frame. Precisely, directly from (6.24) or also from the quotient

$$\frac{h_\times}{h_+} = \tan 2\alpha \quad (6.27)$$

defining the polarization angle, it is found that the Euler angle α is just half the value of the polarization angle or. in other words, the polarization angle is double the angle of rotation around $\hat{z}' \equiv z_D$ which places vector $\hat{y}_D$ of the D-F basis on the plane $\hat{x} - \hat{y}$ of the L-F or, equivalently, it is double the angle between the GW's polarization axes and the eigenvectors $\vec{v}_1$ and $\vec{v}_2$ perpendicular to the incidence direction $\vec{v}_3$.

Now, we have the polarization amplitudes given in terms of the eigenvalues of the cartesian strain tensor H and of the polarization angle. To complete our purpose it is then necessary to express α in terms of the eigenvectors $\vec{v}_i$ of H. For this, we have to take into account that the rotation relating the wave frame and the diagonal frame can also be directly evaluated in an independent form with respect to other rotations in the laboratory frame. Starting from the geometrical view, we actually have to perform the operation

$$R(\vec{v}_3, \alpha) \cdot \vec{v}_2 = \begin{pmatrix} a \\ b \\ 0 \end{pmatrix}, \tag{6.28}$$

where the ij element of $R(\vec{v}_3, \alpha)$ is defined as

$$R(\vec{v}_3, \alpha)_{ij} = \cos\alpha\, \delta_{ij} + (1 - \cos\alpha)\, v_{3i} v_{3j} + \sin\alpha\, \varepsilon_{ijk}\, v_{3k}, \tag{6.29}$$

being ε_{ijk} the Levi-Cività antisymmetric tensor. This is a rotation of angle α around $\hat{z}' \equiv \hat{z}_D$, $\vec{v}_3$ in the L-F, taking vector $\hat{y}_D$, which in its turn reads $\vec{v}_2$, to the plane $\hat{x} - \hat{y}$.

From equalizing the third components of the resulting vectors in both sides of (6.28), we arrive to

$$\tan\alpha = -\frac{v_{2z}}{v_{3y} v_{2x} - v_{3x} v_{2y}} = -\frac{v_{2z}}{v_{1z}} \tag{6.30}$$

or in spherical coordinates

$$\tan\alpha = -\frac{\theta_2}{\theta_1}, \tag{6.31}$$

with θ_1 and θ_2 the polar angles associated to eigenvectors $\vec{v}_1$ and $\vec{v}_2$ of H in the lab frame.

It is timely to point out that if eigenvector $\vec{v}_3$ coincides by chance with the $\hat{z}$ axis or, in other words, the propagation direction of the wave is just that of the vertical axis of the laboratory frame, then $\vec{v}_1$ and $\vec{v}_2$ stay in the $\hat{x} - \hat{y}$ L-F plane perpendicular to $\hat{z}$, or equivalently it happens that $\theta_1 = \theta_2 = \frac{\pi}{2}$. Therefore, $\tan\alpha$ becomes indeterminate an the sense that we cannot fix it from our equations. This is not, of course, an intrinsic inconvenience of the inverse problem , but just a consequence

of the use of a parametrization with anomalous definitions at certain points (e.g., the azimuthal angle associated to vector $(0, 0, 1)$ in spherical coordinates can never be determined).

In short, up to here we have shown how it is possible to extract relevant information about GWs affecting a spherical detector from the eigenvalues and eigenvectors of its measurable response matrix, exactly equal to the cartesian strain tensor H in absence of noise. Let us now analyse all these procedures and results when noise affecting the detector responses is taken into account.

6.2 Signal Deconvolution in the Presense of Noise

The solution to the inverse problem in the presence of noise is more complicated. Zhou and Michelson investigated using a maximum likelihood method [144] applied beforehand by Gürsel and Tinto to the case of noisy interferometers [55]. However, the original transparency of the procedure and results for the noiseless situation was lost, and furthermore exact solutions were not found making it necessary to solve the problem numerically.

In contrast, we will show in this section that it is possible to analytically solve the inverse problem using only linear algebra even in the presence of noise [96, 99]. To fully discuss the effects of those disturbances we would need to introduce a model of the detector that includes noise from several sources such as Brownian motion and noise from the motion sensors (see [97, 124] for a discussion of noise sources in spherical antennæ). However, such a model is beyond the scope of this essay, but it is worthwhile to have a feel for the magnitude of the errors with a simplified model. Its simplicity will result in understandable solutions which will enable the exploration of the errors in the estimated GW parameters to any desired degree of precision using standard techniques.

More specifically, we will examine the isotropic errors on the incidence direction and on the GW amplitude estimations calculated from the mode channels, not only at first but also considered at higher orders. Of course, we will also discuss the errors on the polarization amplitudes and angle estimates, demonstrating that their disturbing direction dependence appears even when they are written as functions of the eigenvalues and eigenvectors of H. Possibly, this problem could be circumvented by using a rotation axis description of the wave, i.e., by accepting an hypothesis over the source able to describes the real situation.

6.2.1 Isotropic Direction and Amplitude Estimation Errors

In the presence of noise, the detector matrix A introduced in section 6.1 is no longer equal to the cartesian strain tensor H in the lab frame. Nevertheless, A will maintain the structure and the properties of symmetry and tracelessness of H since we construct it from the detector responses combined into mode channels y_m having a one-to-one correspondence with the spherical amplitudes of the gravitational wave, so that

$$A(t) = \begin{pmatrix} y_1(t) - \frac{1}{\sqrt{3}}y_5(t) & y_2(t) & y_4(t) \\ y_2(t) & -y_1(t) - \frac{1}{\sqrt{3}}y_5(t) & y_3(t) \\ y_4(t) & y_3(t) & \frac{2}{\sqrt{3}}y_5(t) \end{pmatrix}. \tag{6.32}$$

We insist on the fact that in the absence of noise A was equal to H so that the direction of the gravitational wave could be determined from the detector outputs by finding the eigenvalues and eigenvectors of $A \equiv H$ as described in section 6.1.

In the presence of noise and under ideal conditions referring it, it has been shown that a modified version of the above procedure can be used: the eigenvector of the noisy A with eigenvalue closest to zero is the best approximation to the eigenvector of H that points in the propagation direction of the wave [96]. We will also use this concept to derive the equations of the noisy problem just in the context of linear algebra.

Eigenvalue Errors

Let us start from the idea that noise in the mode channels will change the eigenvalues and eigenvectors of A such that they are no longer equal to those of H.

We assume that the mode channels form a set $y = (y_1, y_2, y_3, y_4, y_5)$ of five independent Gaussian random variables as defined in standard textbooks, for instance [62], with mean $\mu = (\mu_1, \mu_2, \mu_3, \mu_4, \mu_5)$ at their ideal values if there were no noise and variances $\sigma^2 = (\sigma_1^2, \sigma_2^2, \sigma_3^2, \sigma_4^2, \sigma_5^2)$ calculated from the expectation values (represented by the bracket $<>$)

$$\sigma_m^2 = < (y_m - \mu_m)^2 > = < (y_m)^2 > - \mu_m^2. \tag{6.33}$$

Then, any regular function having as arguments the elements of the y set is a random variable itself, although it will generally be non-Gaussian, with an expectation value or mean and a variance represented by:

$$\begin{aligned} \mu_f &= < f > \\ \sigma_f^2 &= < f^2(y) > - < f(y) >^2 . \end{aligned} \tag{6.34}$$

Obviously, eigenvalues and eigenvectors of matrix A are functions of this kind for they being expressed in terms of the mode channel functions y_m, with associated statistical errors that can be evaluated and used to find the direction estimation error.

We start from the eigenvalue equation

$$A\,\vec{v}_k = \lambda_k\,\vec{v}_k \qquad k = 1, 2, 3, \tag{6.35}$$

and write the characteristic polynomial giving the eigenvalues:

$$\lambda_k^3 - y^2\lambda_k - D = 0, \tag{6.36}$$

where we have defined

$$\begin{aligned} y^2 &= y_1^2 + y_2^2 + y_3^2 + y_4^2 + y_5^2 \\ D &\equiv \det(A). \end{aligned} \tag{6.37}$$

Solving this cubic equation we find the eigenvalues of A to be

$$\lambda_k = -\frac{2}{\sqrt{3}}\, y \cos\theta_k \qquad k = 1, 2, 3, \tag{6.38}$$

where

$$\theta_k = \frac{\theta + 2(k-1)\cdot\pi}{3} \quad \text{and} \quad \cos\theta = -\frac{3\sqrt{3}}{2}\frac{D}{y^3}. \tag{6.39}$$

In the absence of noise, these eigenvalues will coincide with those in (6.8) since D will be exactly zero at which $\theta = \pi/2$ and then

$$\begin{aligned} \theta_1 &= \frac{\pi}{6} \qquad \lambda_1 = -y \\ \theta_2 &= \frac{5\pi}{6} \qquad \lambda_2 = y \\ \theta_3 &= \frac{3\pi}{2} \qquad \lambda_3 = 0. \end{aligned} \tag{6.40}$$

However, in the presence of noise λ_3 will no longer be identically null but it will generally be the one closest to zero. Random fluctuations may change this (more likely for low SNR), but we shall always take the corresponding eigenvector $\vec{v}_3$ as the best approximation to the direction of the source. With respect to the other two eigenvalues, their semi-difference $\lambda = (\lambda_2 - \lambda_1)/2$ will give the best estimate for the amplitude of the wave [96], although it can be indeed calculated in many ways from the mode channels (for example, y is an estimate for the amplitude).

Our aim now is to calculate the mean and variance of the eigenvalue functions $\lambda_k(y)$. To this end we Taylor expand it around the mode channels mean μ. Formally:

$$\lambda_k(y) = \lambda_k(\mu) + \lambda_k^i \delta y_i + \frac{1}{2}\lambda_k^{ij} \delta y_i \delta y_j + \dots \tag{6.41}$$

with

$$\lambda_k^{ij\cdots} \equiv \frac{\partial \lambda_k}{\partial y_i \partial y_j \dots}|_{y=\mu} \quad \text{and} \quad \delta y_i \equiv y_i - \mu_i, \tag{6.42}$$

where the usual convention of summation over repeated indexes has been adopted.

Given that y is a set of independent Gaussian variables, it is easy to see that the expectations of the eigenvalues are:

$$\mu_{\lambda_k} = \lambda_k(\mu) + \frac{1}{2}\lambda_k^{ii}\sigma_i^2 + O(\sigma_i^4), \tag{6.43}$$

so that down to first order in the variances of the variables the expectations take in fact their values in the noiseless case, those in (6.8) or in (6.40), as it should be.

From (6.33), (6.34) and (6.41), the lowest order statistical errors are easily calculated by

$$\sigma_{\lambda_k}^2 = \sum_{i=1}^{5} \left(\frac{\partial \lambda_k}{\partial y_i}\right)^2 \sigma_i^2, \tag{6.44}$$

where the derivatives of the eigenvalues must be evaluated from the expressions (6.37), (6.38) and (6.39). If the variances on the mode channels are equal, $\sigma_i^2 = \sigma_y^2 \ \forall i$, the final results are

$$\sigma_{\lambda_k}^2 = \frac{4}{3}\sigma_y^2 + O(\sigma_y^4), \tag{6.45}$$

so that all three eigenvalues show equal variance at first order.

Cross correlations are also easily calculated, and for equal mode channel variances they are again equal for all pairs $(\lambda_k, \lambda_{k'})$:

$$\sigma_{\lambda_k,\lambda_{k'}} = -\frac{2}{3}\sigma_y^2 + O(\sigma_y^4). \tag{6.46}$$

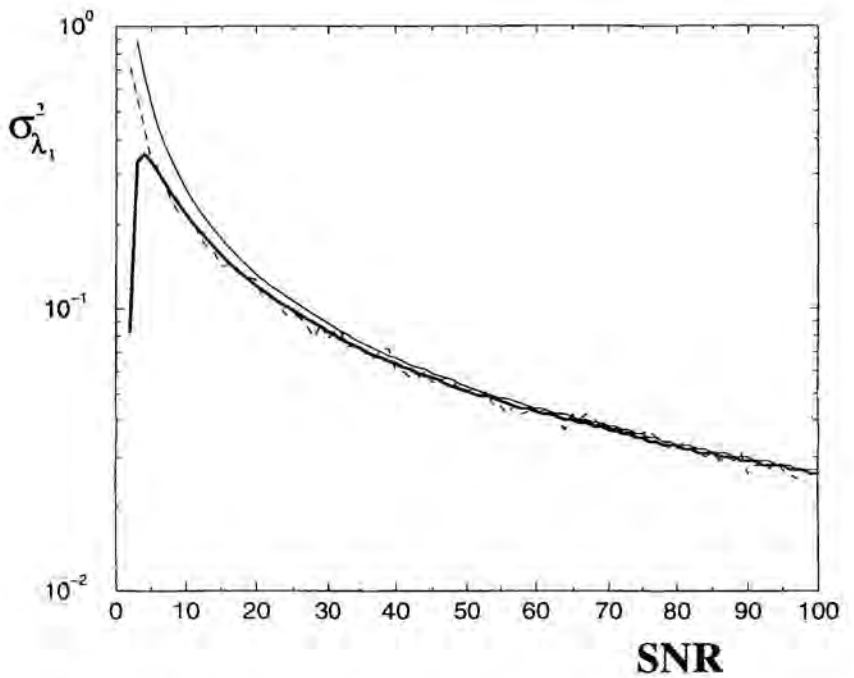

Figure 6.2. *Comparison between numerical simulation outputs and analytic results for the variance of the first eigenvalue. The dashed line was computed by a 1000 trial Monte Carlo simulation for every of 100 given values of SNR. The solid thin line is the error found from the first order analytic expression and the solid thick line includes second order corrections.*

Higher order corrections for the means μ_{λ_k} are easily calculated from (6.43):

$$\begin{aligned}
\mu_{\lambda_1} &= -y - \frac{3}{2}\frac{\sigma_y^2}{y} + O(\sigma_y^4) \\
\mu_{\lambda_2} &= y - \frac{3}{2}\frac{\sigma_y^2}{y} + O(\sigma_y^4) \\
\mu_{\lambda_3} &= 0 + O(\sigma_y^4)
\end{aligned} \tag{6.47}$$

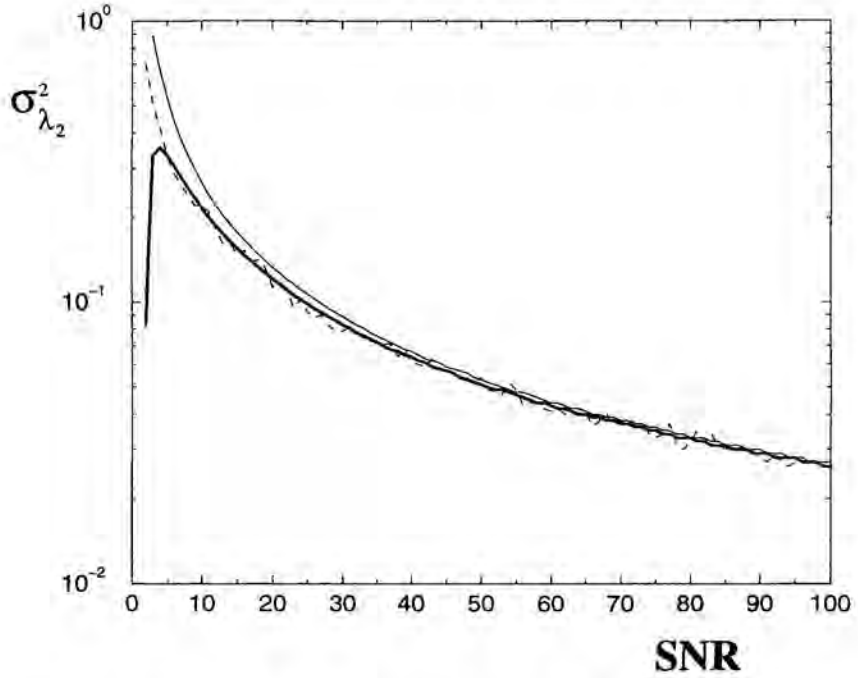

Figure 6.3. *Comparison between numerical silumation outputs and analytic results for the variance of the second eigenvalue. The dashed line was computed by a 1000 trial Monte Carlo simulation for every of 100 given values of SNR. The solid thin line is the error found from the first order analytic expression and the solid thick line includes second order corrections.*

In contrast, the variances require calculations of higher order derivatives for the added terms resulting in complicated general expressions. They somewhat simplify for equal mode channel variances, but are still rather cumbersome:

$$\sigma^2_{\lambda_k} = \frac{4}{3}\sigma_y^2 + \left(\sum_{m,m'=1}^{5} \frac{\partial \lambda_k}{\partial y_m} \frac{\partial^3 \lambda_k}{\partial y_m \partial y_{m'} \partial y_{m'}} + \frac{1}{2} \frac{\partial^2 \lambda_k}{\partial y_m \partial y_{m'}} \frac{\partial^2 \lambda_k}{\partial y_m \partial y_{m'}} \right) \sigma_y^4 + O(\sigma_y^6). \quad (6.48)$$

After long algebra, it is found that

$$\sigma^2_{\lambda_k} = \frac{4}{3}\sigma_y^2 - 2\left(1 + \sin^2\theta_k\right) \frac{\sigma_y^4}{y^2} + O(\sigma_y^6). \quad (6.49)$$

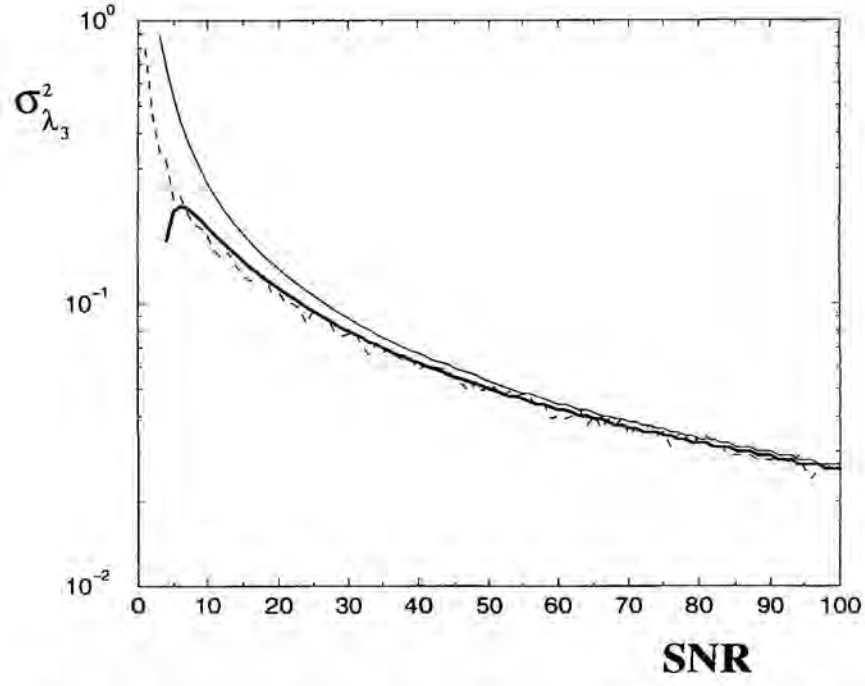

Figure 6.4. *Comparison between numerical silumation outputs and analytic results for the variance of the second eigenvalue. The dashed line was computed by a 1000 trial Monte Carlo simulation for every of 100 given values of SNR. The solid thin line is the error found from the first order analytic expression and the solid thick line includes second order corrections.*

Note also that this formula shows that errors in λ_1 and λ_2 split from the error in λ_3, and reproduces the observed behaviour that for low SNR $\sigma^2_{\lambda_3}$ falls below $\sigma^2_{\lambda_1}$ and $\sigma^2_{\lambda_2}$.

These variances are displayed in graphs 6.2, 6.3 and 6.4 as functions of the SNR= $\frac{y^2}{\sigma_y^2}$, along with the results of a Monte Carlo type numerical simulation of the errors. It turns out that the second order analytic expressions constitutes an evident improvement to the first order analytic values matching the simulated errors for the most of the studied SNR range. For low SNR, discrepancies arise between the analytic and simulated values, which is within expectation since the series for the variances converge very slowly in this zone so that even higher order terms would be required here for a further improvement.

Direction and Amplitude Estimation Errors

We are ready to face now the problem of the determination of the direction estimation error. As explained, we assume that the eigenvector $\vec{v}_3$ points in the propagation direction of the gravitational wave. We want to estimate the fluctuations in the determination of this direction caused by the presence of noisy fluctuations in the mode channels. Allowing fluctuations in (6.35) and retaining only first order terms (high SNR) we arrive to

$$[A - \lambda_3]\, \delta\vec{v}_3 \;=\; -[\delta A - \delta\lambda_3]\, \vec{v}_3, \tag{6.50}$$

where we represent with δ a difference between a given quantity and its ideal value if there were no noise.

As expected, matrix $[A - \lambda_3]$ is not invertible. Hence, we cannot determine the component of $\delta\vec{v}_3$ which is parallel to $\vec{v}_3$ itself, although the orthogonal components parallel to $\vec{v}_1$ and $\vec{v}_2$ can easily be found:

$$\begin{aligned} \vec{v}_1 \cdot \delta\vec{v}_3 &= -\frac{1}{\lambda_1 - \lambda_3}\, \vec{v}_1\, \delta A\, \vec{v}_3 \\ \vec{v}_2 \cdot \delta\vec{v}_3 &= -\frac{1}{\lambda_2 - \lambda_3}\, \vec{v}_2\, \delta A\, \vec{v}_3. \end{aligned} \tag{6.51}$$

An appropriate assessment of the error on a direction measurement is the solid angle error $\Delta\Omega$. Since $|\vec{v}_3| = 1$, this error is

$$\Delta\Omega \;=\; \pi\, |\Delta\vec{v}_3|^2, \tag{6.52}$$

where the quadratic error in the determination of $\vec{v}_3$ is just

$$\begin{aligned} |\Delta\vec{v}_3|^2 &= E\left\{(\vec{v}_1 \cdot \delta\vec{v}_3)^2 + (\vec{v}_2 \cdot \delta\vec{v}_3)^2\right\} = \\ &= E\left\{\left|\frac{\vec{v}_1 \delta A \vec{v}_3}{\lambda_1 - \lambda_3}\right|^2 + \left|\frac{\vec{v}_2 \delta A \vec{v}_3}{\lambda_2 - \lambda_3}\right|^2\right\}. \end{aligned} \tag{6.53}$$

First order calculations only require to take expectations in δA.

$$|\Delta\vec{v}_3|^2 \;=\; \sum_{m=1}^{5} \left[(\vec{v}_1 \cdot A_m \vec{v}_3)^2 + (\vec{v}_2 \cdot A_m \vec{v}_3)^2\right] \frac{\sigma_y^2}{y^2}. \tag{6.54}$$

where matrices A_m are formally defined by $A_m \equiv \frac{\partial A}{\partial y_m}$.

Equal variances on the mode channels lead to

$$|\Delta\vec{v}_3|^2 = 2\frac{\sigma_y^2}{y^2}, \quad \text{so that} \quad \Delta\Omega = \frac{2\pi}{SNR}, \tag{6.55}$$

which is independent of the incidence direction as expected of an omnidirectional antenna. Furthermore, this expression is in perfect agreement with the estimation error of Zhou and Michelson [144]. The advantage of our approach is that, by using unit vectors described by cartesian components, we are free from the anomalously high errors and correlations in intervening calculations related to the Euler angle parametrization used by other authors [144, 96].

The quadratic errors $|\Delta\vec{v}_1|^2$ and $|\Delta\vec{v}_2|^2$ for the remaining two eigenvectors can be analogously calculated. One obtains at leading order:

$$|\Delta\vec{v}_1|^2 = |\Delta\vec{v}_2|^2 = \frac{5}{4}\frac{\sigma_y^2}{y^2}. \tag{6.56}$$

If high order corrections are considered, we will arrive to expressions for the direction errors:

$$\begin{aligned} |\Delta\vec{v}_3|^2 &= 2\frac{\sigma_y^2}{y^2}\left(1+\frac{\sigma_y^2}{y^2}\right)^{-1} \\ \Delta\Omega &= \frac{2\pi}{SNR}\left(1+\frac{1}{SNR}\right)^{-1}, \end{aligned} \tag{6.57}$$

which amounts to be a better approach, although it is important to remind ourselves that for very low SNR the uncertainties on the direction estimation are so large that the measurement is almost meaningless.

The observed isotropy in the estimation of the propagation direction error arising from the isotropy in the estimated quantities referring the eigenvalues and the eigenvectors of the cartesian strain tensor H in the lab frame, is also preserved in the computation of the GW amplitude $y \equiv \lambda = \sqrt{h_+^2 + h_\times^2}$. It has been shown [96] to have a best estimate. $y \equiv \lambda = (\lambda_2 - \lambda_1)/2$, which can clearly be determined with isotropic sensitivity for it being possible for the eigenvalues λ_1 and λ_2 as just seen. Calculations are simple once the eigenvalues' expectations values, their variances and their correlation are known. From (6.47), (6.49) and (6.46), we respectively have:

$$\mu_{\lambda_1} = -\mu_{\lambda_2} = -y\left(1+\frac{3}{2}\frac{\sigma_y^2}{y^2}+\ldots\right)$$

and to evaluate the statistical central moments of the trigonometric functions $\sin 2\alpha$ and $\cos 2\alpha$. These computations referring angle α are quite complicated and are precisely the source of direction dependences as we shall see.

Since we can always express $\sin 2\alpha$ and $\cos 2\alpha$ as functions of $\tan\alpha$,

$$\begin{aligned} \sin 2\alpha &= \frac{2\tan\alpha}{1+\tan^2\alpha} \\ \cos 2\alpha &= \frac{1-\tan^2\alpha}{1+\tan^2\alpha}, \end{aligned} \tag{6.62}$$

we will directly work with $\tan\alpha$ following standard developments in statistical mathematics [62]. We recall once more that

$$\tan\alpha = -\frac{v_{2z}}{v_{1z}} = -\frac{\cos\theta_2}{\cos\theta_1}, \tag{6.63}$$

α defined in accordance to the $\alpha = 0$ criterion as the angle which takes the diagonal frame to the wave frame –both of the frames described in section 6.1– through a single rotation around the incidence direction indicated by eigenvector $\vec{v}_3$. Equivalently, α is also the necessary angle in a rotation of the polarization plane to take eigenvector $\vec{v}_2$ to the L-F $\hat{x}-\hat{y}$ plane.

Now, the action of noise will induce changes in α through fluctuations of the eigenvectors $\vec{v}_1$, $\vec{v}_2$ and $\vec{v}_3$, which we consider vary following an uniform probability density function –the simplest one– in a range inside three respective cones with bases on the spherical surface of radius 1, heights in the directions of the eigenvectors' ideal values $\vec{v}_{01}$, $\vec{v}_{02}$ and $\vec{v}_{03}$ if there were no noise –in fact the eigenvalues of the cartesian strain tensor H–, and aperture angles $\Delta\delta_1$, $\Delta\delta_2$ and $\Delta\delta_3$ clearly fixed by $|\Delta\vec{v}_1|$, $|\Delta\vec{v}_2|$ and $|\Delta\vec{v}_3|$ already known as functions of the mode channels and their variance, see (6.55) and (6.56). We give an schematic representation in Figure 6.5.

Finally, let us obviate the correlation between eigenvectors $\vec{v}_1$ and $\vec{v}_2$, which actually must always be perpendicular for they forming part of an orthogonal basis. Up to this point, this is possibly the stronger supposition assumed referring correlation, but this simplification is unavoidable if one accounts for final analytic results simple enough to be interpreted. Besides, we insist on the idea that we are basically interested in the qualitative pathological dependences, so that we can think that if they already become evident at high SNR, which would imply small values of $\Delta\delta_1$ and $\Delta\delta_2$ and so small correlation effects, they will not disappear at low SNR.

$$|\Delta\vec{v}_3|^2 = 2\frac{\sigma_y^2}{y^2}, \quad \text{so that} \quad \Delta\Omega = \frac{2\pi}{SNR}, \tag{6.55}$$

which is independent of the incidence direction as expected of an omnidirectional antenna. Furthermore, this expression is in perfect agreement with the estimation error of Zhou and Michelson [144]. The advantage of our approach is that, by using unit vectors described by cartesian components, we are free from the anomalously high errors and correlations in intervening calculations related to the Euler angle parametrization used by other authors [144, 96].

The quadratic errors $|\Delta\vec{v}_1|^2$ and $|\Delta\vec{v}_2|^2$ for the remaining two eigenvectors can be analogously calculated. One obtains at leading order:

$$|\Delta\vec{v}_1|^2 = |\Delta\vec{v}_2|^2 = \frac{5}{4}\frac{\sigma_y^2}{y^2}. \tag{6.56}$$

If high order corrections are considered, we will arrive to expressions for the direction errors:

$$\begin{aligned} |\Delta\vec{v}_3|^2 &= 2\,\frac{\sigma_y^2}{y^2}\left(1+\frac{\sigma_y^2}{y^2}\right)^{-1} \\ \Delta\Omega &= \frac{2\pi}{SNR}\left(1+\frac{1}{SNR}\right)^{-1}, \end{aligned} \tag{6.57}$$

which amounts to be a better approach, although it is important to remind ourselves that for very low SNR the uncertainties on the direction estimation are so large that the measurement is almost meaningless.

The observed isotropy in the estimation of the propagation direction error arising from the isotropy in the estimated quantities referring the eigenvalues and the eigenvectors of the cartesian strain tensor H in the lab frame, is also preserved in the computation of the GW amplitude $y \equiv \lambda = \sqrt{h_+^2 + h_\times^2}$. It has been shown [96] to have a best estimate, $y \equiv \lambda = (\lambda_2 - \lambda_1)/2$, which can clearly be determined with isotropic sensitivity for it being possible for the eigenvalues λ_1 and λ_2 as just seen. Calculations are simple once the eigenvalues' expectations values, their variances and their correlation are known. From (6.47), (6.49) and (6.46), we respectively have:

$$\mu_{\lambda_1} = -\mu_{\lambda_2} = -y\left(1+\frac{3}{2}\frac{\sigma_y^2}{y^2}+\ldots\right)$$

$$\begin{aligned} \sigma^2_{\lambda_1} &= \sigma^2_{\lambda_2} = \frac{4}{3}\sigma^2_y - \frac{5}{2}\frac{\sigma^4_y}{y^2} + \dots \\ \sigma_{\lambda_1\lambda_2} &= -\frac{2}{3}\sigma^2_y + \frac{9}{4}\frac{\sigma^4_y}{y^2} + \dots \end{aligned} \tag{6.58}$$

whence

$$\begin{aligned} \mu_\lambda &= y\left(1 + \frac{3}{2}\frac{\sigma^2_y}{y^2} + \dots\right) \\ \sigma^2_\lambda &= \sigma^2_y - \frac{19}{8}\frac{\sigma^4_y}{y^2} + \dots, \end{aligned} \tag{6.59}$$

expressions which evidently are direction independent.

6.2.2 Polarization Amplitudes and Anisotropic Estimated Errors

We come now to discuss errors for the components of λ, the polarization amplitudes h_+ and $h_\times$. We recall that they are obtained as functions of the mode channels and the incidence direction Euler angles β and γ once the $\alpha = 0$ criterion has been adopted, see formulas (6.19), or they can be in parallel computed from the eigenvectors and eigenvalues of the cartesian strain tensor H evaluated in the laboratory frame. From formulas (6.23) and (6.30):

$$\begin{aligned} h_+ &= -\lambda\cos 2\alpha - \frac{1}{2}\lambda_3 \\ h_\times &= -\lambda\sin 2\alpha \\ \text{and} \quad \tan\alpha &= -\frac{v_{2z}}{v_{1z}} = -\frac{\cos\theta_2}{\cos\theta_1}. \end{aligned} \tag{6.60}$$

The term in h_+ containing λ_3 appears here as a consequence of the fact that it is no longer zero once noise is introduced in the developments. These formulas of course reduce to (6.24) when there is no noise.

Anisotropic Estimations and the $\alpha = 0$ criterion

Based on methods including Euler angle parametrizations computing h_+ and $h_\times$ from (6.19), some authors have claimed [144, 124] that it does not appear to be a standard description of the wave polarization that has a direction independent variance. It turns

out that these direction dependent uncertainties seem inherent to the use of Euler angles to describe the wave direction. This is easily visualized in the y-convention of the Euler angles also used in this chapter (see Figure 6.1): it is clear that if β goes to zero, α and γ become indistinguishable, leading to large errors in their estimations, whereupon errors in the polarization angle $\alpha_p = 2\alpha = \tan^{-1}\frac{h_\times}{h_+}$ go to infinity near $\beta = 0$.

On the other hand, the $\alpha = 0$ criterion, commonly used to resolve the arbitrariness in the α Euler angle relating the diagonal frame to the wave frame and also associated to the rotation which takes eigenvector $\vec{v}_2$ to the L-F $\hat{x} - \hat{y}$ plane, is a very much observer dependent criterion, for detectors at different locations would claim different values for h_+ and $h_\times$ even if they agree to be seeing the same source. Consequently, errors based on this criterion have been shown to be strongly direction dependent, which is certainly not surprising.

Here rests indeed the clue to the problem of the anisotropy of the h_+ and $h_\times$ estimated errors since, as we are going to prove immediately, the second parametrization (6.60) of these quantities as functions of the eigenvalues λ_1, λ_2 and λ_3 and their eigenvectors' components also leads to anisotropic estimations of these errors whenever the $\alpha = 0$ criterion (or equivalently any other α fixation) is adopted.

The demonstration begins from (6.60) by understanding that the associated errors will be induced by fluctuations in the eigenvalues λ_1, λ_2 and λ_3, and so also in the GW amplitude λ, along with fluctuations in the polarization angle $\alpha_p = 2\alpha$, and so in the trigonometric functions $\cos 2\alpha$ and $\sin 2\alpha$, all these quantities naturally being in its turn functions of the mode channels. These two categories of fluctuations will be considered uncorrelated (in favour of this supposition we can argue that the GW energy is independent of the GW polarization, and anyway the corrections obtained from taking into account correlation would be just numeric and would not affect the qualitative isotropic or anisotropic behaviour of the results, therefore not being justifiable the complexness which would be introduced in the developments).

Following as always (6.34) and taking fluctuations in (6.60) it is straightforward to find that the variances on the polarization amplitudes will formally read:

$$\begin{aligned} \sigma_+^2 &= \mu_\lambda^2 \cdot \sigma_{\cos 2\alpha}^2 + \mu_{\cos 2\alpha}^2 \cdot \sigma_\lambda^2 + \frac{1}{4}\sigma_{\lambda_3}^2 \\ \sigma_\times^2 &= \mu_\lambda^2 \cdot \sigma_{\sin 2\alpha}^2 + \mu_{\sin 2\alpha}^2 \cdot \sigma_\lambda^2 \end{aligned} \tag{6.61}$$

Previously, it is then necessary to recover the results for the GW amplitude λ and the third eigenvalue λ_3 in (6.49) and (6.59) –we recall all of them showed perfect isotropy–,

and to evaluate the statistical central moments of the trigonometric functions $\sin 2\alpha$ and $\cos 2\alpha$. These computations referring angle α are quite complicated and are precisely the source of direction dependences as we shall see.

Since we can always express $\sin 2\alpha$ and $\cos 2\alpha$ as functions of $\tan\alpha$,

$$\begin{aligned} \sin 2\alpha &= \frac{2\tan\alpha}{1+\tan^2\alpha} \\ \cos 2\alpha &= \frac{1-\tan^2\alpha}{1+\tan^2\alpha}, \end{aligned} \tag{6.62}$$

we will directly work with $\tan\alpha$ following standard developments in statistical mathematics [62]. We recall once more that

$$\tan\alpha = -\frac{v_{2x}}{v_{1x}} = -\frac{\cos\theta_2}{\cos\theta_1}, \tag{6.63}$$

α defined in accordance to the $\alpha = 0$ criterion as the angle which takes the diagonal frame to the wave frame –both of the frames described in section 6.1– through a single rotation around the incidence direction indicated by eigenvector $\vec{v}_3$. Equivalently, α is also the necessary angle in a rotation of the polarization plane to take eigenvector $\vec{v}_2$ to the L-F $\hat{x}-\hat{y}$ plane.

Now, the action of noise will induce changes in α through fluctuations of the eigenvectors $\vec{v}_1$, $\vec{v}_2$ and $\vec{v}_3$, which we consider vary following an uniform probability density function –the simplest one– in a range inside three respective cones with bases on the spherical surface of radius 1. heights in the directions of the eigenvectors' ideal values $\vec{v}_{01}$, $\vec{v}_{02}$ and $\vec{v}_{03}$ if there were no noise –in fact the eigenvalues of the cartesian strain tensor H–, and aperture angles $\Delta\delta_1$, $\Delta\delta_2$ and $\Delta\delta_3$ clearly fixed by $|\Delta\vec{v}_1|$, $|\Delta\vec{v}_2|$ and $|\Delta\vec{v}_3|$ already known as functions of the mode channels and their variance, see (6.55) and (6.56). We give an schematic representation in Figure 6.5.

Finally, let us obviate the correlation between eigenvectors $\vec{v}_1$ and $\vec{v}_2$, which actually must always be perpendicular for they forming part of an orthogonal basis. Up to this point, this is possibly the stronger supposition assumed referring correlation. but this simplification is unavoidable if one accounts for final analytic results simple enough to be interpreted. Besides, we insist on the idea that we are basically interested in the qualitative pathological dependences, so that we can think that if they already become evident at high SNR, which would imply small values of $\Delta\delta_1$ and $\Delta\delta_2$ and so small correlation effects, they will not disappear at low SNR.

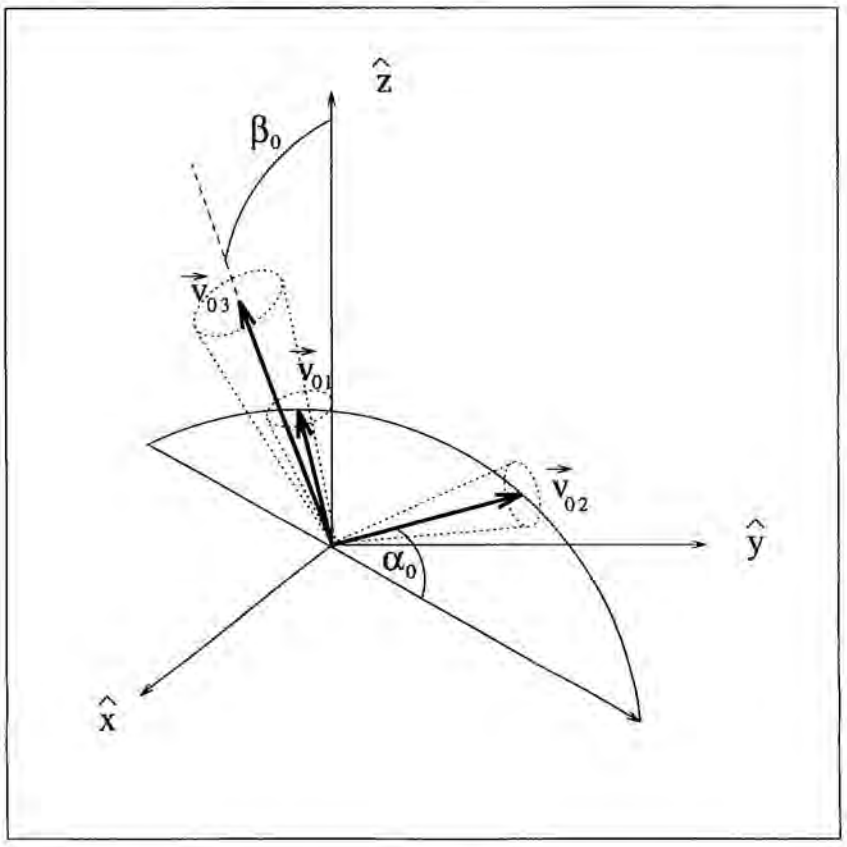

Figure 6.5. *Error cones as seen in the L-F associated to the three eigenvalues* $\vec{v}_1$, $\vec{v}_2$ *and* $\vec{v}_3$ *calculated from the noisy data. As shown in the sketch, the axis of the cones follow the directions of their ideal values* $\vec{v}_{01}$, $\vec{v}_{02}$ *and* $\vec{v}_{03}$ *if there were no noise.*

Under all these conditions, the normalized uniform probability density function will be of the form:

$$p(\Delta\delta_1, \Delta\delta_2; \delta_1, \psi_1, \delta_2, \psi_2) =$$
$$= \frac{1}{2\pi(1-\cos\Delta\delta_1)} \frac{1}{2\pi(1-\cos\Delta\delta_2)} \sin\delta_1 d\delta_1 d\psi_1 \sin\delta_2 d\delta_2 d\psi_2 \qquad (6.64)$$

where the two first quotients are normalization constants, say N_1 and N_2, naturally depending on the aperture angles of the cones, (δ_1, ψ_1) are the spherical coordinates describing the position of the unit eigenvector $\vec{v}_1$ calculated from noisy data in the refer-

ence system S_1 having its $\hat{z}$ axis in the direction of $\vec{v}_{01}$, and respectively (δ_2, ψ_2) are the spherical coordinates associated to $\vec{v}_2$ in the reference system S_2 where the $\hat{z}$ axis follows the direction of $\vec{v}_{02}$.

We will first evaluate the expectation value of $\tan\alpha$. Substituting this function by its expression in spherical coordinates:

$$\mu_{\tan\alpha} = -\int_{cones} \frac{\cos\theta_2}{\cos\theta_1} \sin\delta_1 d\delta_1 d\psi_1 \sin\delta_2 d\delta_2 d\psi_2, \tag{6.65}$$

with θ_1 and θ_2 the polar angles which respectively indicates the separation between $\vec{v}_1$ and $\vec{v}_2$ and the $\hat{z}$ axis of the L-F. To compute the integral, it is essential to express these angles in terms of (δ_1, ψ_1) and (δ_2, ψ_2), what is acquired by resorting to our well known summation formula for spherical harmonics involving the P_l Legendre polynomial (see Appendix C):

$$P_l(\cos\theta) = \frac{4\pi}{2l+1} \sum_{m=-l}^{l} Y^*_{lm}(\rho_1, \zeta_1)\, Y_{lm}(\rho_2, \zeta_2), \tag{6.66}$$

where θ stands for the angle between the two directions (ρ_1, ζ_1) and (ρ_2, ζ_2). For $l = 1$:

$$P_1(\cos\theta) = \cos\theta, \tag{6.67}$$

and that we can take S_1 (S_2) as a common reference system in which (ρ_1, ζ_1) are the spherical coordinates (θ_{01}, ψ_{01}) ((θ_{02}, ψ_{02})) of the L-F $\hat{z}$ axis and (ρ_2, ζ_2) are those named (δ_1, ψ_1) ((δ_2, ψ_2)) for the fluctuating eigenvector $\vec{v}_1$ ($\vec{v}_2$), see Figure 6.6. Once the explicit expressions for the spherical harmonics has been introduced, it is possible to write:

$$\begin{aligned} \cos\theta_1 &= \sin\theta_{01}\sin\delta_1\cos(\psi_1 - \psi 01) + \cos\theta_{01}\cos\delta_1 \\ \cos\theta_2 &= \sin\theta_{02}\sin\delta_2\cos(\psi_2 - \psi 02) + \cos\theta_{02}\cos\delta_2. \end{aligned} \tag{6.68}$$

Then, (6.65) can effectively be split up into the product of two double integrals, one for each cone, as expected from the non-correlation of $\vec{v}_1$ and $\vec{v}_2$ assumed so far:

$$\begin{aligned} \mu_{\tan\alpha} &= N_1 I_1 \cdot N_2 I_2 = \\ &= -N_1 \int_0^{\Delta\delta_1}\int_0^{2\pi} \frac{1}{\sin\theta_{01}\sin\delta_1\cos(\psi_1 - \psi_{01}) + \cos\theta_{01}\cos\delta_1} \sin\delta_1 d\delta_1 d\psi_1 \times \end{aligned}$$

$$\times \quad \frac{\cos\theta_{01}}{1-\cos\Delta\delta_1} \ln \frac{1+\cos\theta_{01}}{\cos\Delta\delta_1 + \sqrt{\cos^2\theta_{01} - \sin^2\Delta\delta_1}}. \tag{6.72}$$

For the variance $\sigma^2_{\tan\alpha}$, we start from the general definition in (6.34):

$$\sigma^2_{\tan\alpha} = <(\tan\alpha)^2> - <\tan\alpha>^2 = \mu_{\tan^2\alpha} - \mu^2_{\tan\alpha}, \tag{6.73}$$

and since

$$\begin{aligned} \mu_{\tan^2\alpha} &= N_1 I_3 \cdot N_2 I_4 = \\ &= N_1 \int_0^{\Delta\delta_1}\int_0^{2\pi} \frac{1}{(\sin\theta_{01}\sin\delta_1\cos(\psi_1-\psi_{01}) + \cos\theta_{01}\cos\delta_1)^2} \sin\delta_1 d\delta_1 d\psi_1 \times \\ &\times N_2 \int_0^{\Delta\delta_2}\int_0^{2\pi} (\sin\theta_{02}\sin\delta_2\cos(\psi_2-\psi_{02}) + \cos\theta_{02}\cos\delta_2)^2 \sin\delta_2 d\delta_2 d\psi_2 \end{aligned} \tag{6.74}$$

one has first to work out two more double integrals:

$$I_3 = 2\pi\left(\frac{\cos\theta_{01}}{\sqrt{\cos^2\theta_{01} - \sin^2\Delta\delta_1}} - 1\right) \quad \cos\theta_{01} \geq |\sin\Delta\delta_1| \tag{6.75}$$

$$I_4 = \pi\left[\frac{2}{3} - \sin^2\theta_{02}\cos\Delta\delta_2 + \cos^3\Delta\delta_2(\sin 2\theta_{02} - \frac{2}{3})\right]. \tag{6.76}$$

Eventually, $\mu^2_{\tan\alpha}$ is

$$\begin{aligned} \mu_{\tan^2\alpha} &= \frac{1}{2}\frac{\frac{2}{3} - \sin^2\theta_{02}\cos\Delta\delta_2 + \cos^3\Delta\delta_2(\sin\theta_{02} - \frac{2}{3})}{1-\cos\Delta\delta_2} \times \\ &\times \frac{(\cos\theta_{01}) / \left(\sqrt{\cos^2\theta_{01} - \sin^2\Delta\delta_1}\right) - 1}{1-\cos\Delta\delta_1}. \end{aligned} \tag{6.77}$$

It is obvious that the expression for the expectation value and even more that for the variance are quite complicated. To gain some insight one could Taylor expand them around the free noise values. From (6.56), one sees that

$$|\Delta\vec{v}_1| = |\Delta\vec{v}_2| \Rightarrow \Delta\delta_1 = \Delta\delta_2 = \Delta\delta, \tag{6.78}$$

and for small apertures of the cones (high SNR) it is found that

$$I = \int_0^{\pi} \frac{1}{a + b\cos\psi_1} d\psi_1, \qquad \begin{array}{l} a = \cos\theta_{01} \\ b = \sin\Delta\delta_1 \end{array} \tag{6.82}$$

I could be evaluated through complex integration and calculation of residues, although it becomes evident directly from (6.82) that:

- if $a > |b|$ the integrand is perfectly regular for every value of ψ_1 in the integration interval;
- on the contrary, if $a = |b|$ the integrand $\frac{1}{1\pm\cos\psi_1}$ is singular in just one point in coincidence with one of the integration limits;
- the case $a < |b|$ also presents singularities of the integrand $\frac{1}{a}\frac{1}{1\pm\frac{a}{b}\cos\psi_1}$, this time in two ψ_1 values between 0 and π.

Then, the not allowed situations $\cos\theta_{01} = |\sin\Delta\delta_1|$ and $\cos\theta_{01} < |\sin\Delta\delta_1|$ correspond to integrals divergent in just one and just two points of the integration interval of which it is not even possible to define its principal value.

These divergences bring about values for the mean and the variance of $\tan\alpha$ divergent in their turn in the sense that they cannot be determined. It is consistent with the geometrical view for such situations: if at the same time that eigenvector $\vec{v}_2$ is actually blended with the $\hat{x} - \hat{y}$ plane the error cone of $\vec{v}_1$ intersects this very plane even in just one of its generatrix, then the error cone of $\vec{v}_3$, with aperture angle $\Delta\delta_3$ wider than those of the error cones of $\vec{v}_1$ and $\vec{v}_2$, will be placed so vertical in the laboratory frame that the angle between $\vec{v}_{03}$ and the L-F $\hat{z}$ axis will be smaller than $\Delta\delta_3$, what means that we cannot distinguish between the two directions in analogy with the case $\beta = 0$ when noise is absent. Notice that the described situation is only possible if originally it is in fact the case, i.e., if before the α rotation it happens that the plane $\vec{v}_1 - \vec{v}_2$ is already confounded with the plane $\hat{x} - \hat{y}$. Hence, we are actually facing the case in which the propagation direction of the GW can be confounded with the L-F vertical axis, whereupon it is not possible indeed to fix the angle α which one needs to rotate $\vec{v}_2$ to take it to the $\hat{x} - \hat{y}$ plane.

This indetermination is completely transferred to the polarization amplitudes through their dependence on the polarization angle $\alpha_p = 2\alpha$. Let us limit to the case $\cos\theta_{01} > |\sin\Delta\delta_1|$ and work with $\mu_{\tan\alpha}$ and $\sigma^2_{\tan\alpha}$. The mean and variances related to the polarization angle entering σ^2_+ and $\sigma^2_\times$ in (6.61) can easily be found. It would be necessary

independent situation.

Isotropic Estimations

The anisotropy in the determination of h_+ and $h_\times$ arises as a disturbing paradox given that a spherical antenna is equally sensitive to waves from all directions and polarizations. It seems that under our assumed hypotheses at the beginning of the chapter, this paradox is unsolvable.

However, if we make suitable reference to the source properties, i.e., if we relax our initial conditions of absolute disinformation about the source and admit that the GW source is known ahead of time or that we can at least base on a hypothesis to be checked *a posteriori* isotropic error estimations could be obtained.

If α is known beforehand, we can use results in (6.45), (6.58), (6.59) and (6.60) to see that

$$\begin{aligned} \sigma_+^2 &= \left(\frac{1}{3} + \cos^2 2\alpha\right) \sigma_y^2 \\ \sigma_\times^2 &= \sin^2 2\alpha \, \sigma_y^2 \\ \sigma_{+\times}^2 &= -\frac{1}{4} \sin^2 4\alpha \, \sigma_y^2, \end{aligned} \tag{6.84}$$

indeed isotropic quantities for they only depend on σ_y^2.

In the second case, α is no longer known. Then, the key idea is that any criterion to resolve its arbitrariness, therefore to estimate h_+ and $h_\times$, should be resolved relatively to the hypothetical GW source.

We finally summarize in a few words the general procedure for solving the inverse problem in the presence of noise. We construct the response matrix A from the mode channels y and compute its eigenvalues λ_1, λ_2 and λ_3 and its eigenvectors $\vec{v}_1$, $\vec{v}_2$ and $\vec{v}_3$. The eigenvector with eigenvalue closest to zero is assumed to point in the propagation direction of the GW, which can be determined with isotropic sensitivity as well as the GW amplitude λ. In return, the polarization angle α –by the sake of its arbitrariness commonly fixed by the imposition of a certain criterion– and so the polarization amplitudes h_+ and $h_\times$ –calculated on the basis of a single α-rotation of the polarization plane relating the wave frame and the diagonal frame or equivalently on the basis of two independent Euler rotations relating the wave frame and the laboratory frame– cannot

be known from the eigenvalues and eigenvectors of A as direction independent estimations. If isotropy is expected, direct reference to the source physical properties, real or hypothetical, must be made.

Chapter 7

CONCLUSIONS

We conclude with a brief summary of our main results and add a few words on some opened questions and prospects for future work.

7.1 Summary of Results

1. The development of a rigorous mathematical frame for the physical description of a resonant spherical GW antenna has been at the core of our investigation, which presents the theoretical scheme for the statement and treatment of the completely general and signal-independent GRD set of equations, indeed applicable to a solid elastic detector of any shape endowed with a set of resonant radial motion sensors in arbitrary locations and which can differ in mass and resonance frequency.

    - We have applied to the ideal case of a perfect spherical detector coupled to an arbitrary layout of J identical resonators for resolving the equations and determining the system responses to an impinging GW when a specific resonator tuning is chosen, with resonance frequency ω_{NL}. The solutions are written as perturbative series expansions in ascending powers of the small coupling constant $\eta^{\frac{1}{2}}$, where $\eta = \frac{m_{resonators}}{M_{sphere}}$.
    - We obtain the frequency spectrum of the coupled device to lowest order in η. It is seen to be structured in J pairs $\omega_{a\pm}$ -although at most only $2L+1$ of them are strongly coupled pairs- split from the tuning frequency ω_{NL} and symmetrically distributed around it.

The amplitudes of the excited modes are also obtained through the quantities $q_a(t)$ representing the actual deformations associated to the linear springs which model the resonators. We find that these amplitudes occur with a mechanical amplification factor of $\eta^{-\frac{1}{2}}$, and their spectral composition is dominated by the symmetric frequency pairs $\omega_{a\pm}$.

- We also show how, under several quite general requirements over the resonator layout, these amplitudes can be arranged in certain linear combinations named *mode channels*, each one coupled only to a single mode amplitude of the uncoupled sphere, and hence to a single amplitude of the gravitational field.
- Our approach allows not only to investigate the responses to a GW, but also to inquire into the dynamical behaviour of the antenna to other external agents such as calibration signals. We show the final results for two specific resonator configurations, those of the TIGA and PHCA proposals.

2. Our model leads to:

   - The analysis and even the suggestion of particular proposals of spherical perfectly ideal antennæ with resonators fixed at specific positions. It is only necessary to calculate for each given distribution the eigenvalues and the eigenvectors of the geometry dependent matrix, which are the only quantities determining the particular distinctive characteristics of the coupled spectrum and of the amplitudes or the mode channels.

     Then, we can reconsider already existent proposals, such as the TIGA of the pioneers Johnson and Merkowitz, but furthermore we are able to present an alternative proposal based on pentagonal layouts keeping axial symmetry. Our PHCA antenna is thought as a complete multi-mode multi-frequency device, so that we propose two sets of supplementary pentagonal layouts respectively tuned to the first and the second quadrupole harmonic frequencies to maximally exploit the possibilities of the detector. An eleventh resonator is also added at the first monopole frequency for monopole sensing.
   - The implementation of realistic assumptions leading to the investigation of departures from the perfectly ideal detector.

     Our model has turned out to be flexible enough to be also valid for the study of small defects –thereby increasing its degree of applicability to real systems– by the use of a generic parametrization for a wide class of ideality departures

consistently with our perturbative expansions, so that we have been able to address the question whether the device is affected or not by those ideality breakings.

The evaluations reveal that the antenna's response is rather robust against some of those small imperfection: non accurate locations in the layout or non identical masses or natural frequencies of the resonators.

In contrast, the existence of a second free sphere frequency $\omega_{N'L'}$ near the resonant ω_{NL} appreciably affects the system's responses even at leading order. The analysis for the TIGA and the PHCA demonstrates that it results in a dragging effect breaking the original symmetry of the ideal doublets, and moreover induces the appearance of a third weakly coupled component near the resonance frequency ω_{NL}. This effect is relevant for our PHCA proposal since, as explained, it considers a second layout of resonators coupled to the second quadrupole harmonic of the free sphere, which in fact has a second free sphere frequency very close to it. Then, we are able to correctly describe the whole PHCA spectrum as composed of two groups of strongly coupled frequency pairs. the first symmetrically distributed around the first quadrupole harmonic frequency whereas the second arises as a non-symmetrical splitting from the second quadrupole harmonic.

The breaking of spherical symmetry by suspension also induces significant changes relative to the ideal perfect device performance. We put to test our model's predictions for the spectrum by confronting them with the reported experimental data obtained in the TIGA prototype experiment, and see that agreement is fully satisfactory in the given experimental conditions.

3. Finally, we are able to handle the ideal antenna's responses to trace back the features of the incoming GW. This is commonly called the inverse or the deconvolution problem. and we show that it is solvable using only linear algebra even in the presence of noise.

   In the noiseless situation, the incidence direction of the GW, its amplitudes and polarization can be worked out from the eigenvalues and eigenvectors of the detector response matrix constructed from the mode channels.

   For the noisy antenna, we implement a modified version of the above procedure which provides isotropic errors on the GW incidence direction and amplitude as

Appendix A
Bare Sphere Radial Eigenfunctions and Spheroidal Spectrum

This is a digest of explicit expressions for the radial components entering the toroidal and spheroidal eigenfunctions describing the normal modes of vibration of a perfect bare sphere (formulas (3.9)). We also present a diagram for the spectrum of spheroidal eigenfrequencies ω_{nl}.

A.1 Bare Sphere Radial Eigenfunctions

Radial eigenmodes $A_{nl}(r)$, $B_{nl}(r)$ and $C_{nl}(r)$ are complicated functions which describe the radial behaviour of spheroidal and toroidal normal modes of vibration in a solid elastic bare sphere. They are rigorously derived in [80] or [103], but we give here their explicit expressions:

$$A_{nl}(r) = C_a(n,l)\left[\beta_3(k^S_{nl}R)\frac{dj_l(q^S_{nl}r)}{d(q^S_{nl}r)} - l(l+1)\sqrt{\frac{\mu}{\lambda+2\mu}}\beta_1(q^S_{nl}R)\frac{j_l(k^S_{nl}r)}{k^S_{nl}r}\right] \quad \text{(A.1)}$$

$$B_{nl}(r) = C_b(n,l)\left[\beta_3(k^S_{nl}R)\frac{dj_l(q^S_{nl}r)}{d(q^S_{nl}r)}\frac{j_l(q^S_{nl}r)}{q^S_{nl}r} - \sqrt{\frac{\mu}{\lambda+2\mu}}\frac{\beta_1(q^S_{nl}R)}{k^S_{nl}r}\frac{d}{dr}\{rj_l(k^S_{nl}r)\}\right] \quad \text{(A.2)}$$

$$C_{nl}(r) = C_c(n,l)j_l(k^T_{nl}r) \quad \text{(A.3)}$$

with

- $C(n,l)$ normalisation constants with dimensions of length,
- $\beta_i(z)$ the auxiliary functions

$$\begin{aligned}
\beta_1(z) &\equiv \frac{d}{dz}\left(\frac{j_l(z)}{z}\right) \\
\beta_2(z) &\equiv \frac{d^2 j_l(z)}{dz^2} \\
\beta_3(z) &\equiv \frac{1}{2}\left[\beta_2(z) + (l+2)(l-1)\frac{j_l(z)}{z^2}\right] \\
\beta_4(z) &\equiv \beta_2(z) - \frac{\lambda}{2\mu} j_l(z),
\end{aligned} \tag{A.4}$$

- $j_l(z)$ the Bessel functions of the first kind [56] defined as:

$$j_l(z) = \frac{z^l}{2^l l!}\left\{1 - \frac{z^2}{2(2l+2)} + \frac{z^4}{2\cdot 4\cdot(2l+2)(2l+4)} - \ldots\right\}, \tag{A.5}$$

- q_{nl}^S and $k_{nl}^{S,T}$ proportional to the eigenfrequencies $\omega_{nl}^{S,T}$,

$$q_{nl}^{2\,S} = \frac{\varrho\omega_{nl}^{2\,S}}{\lambda+2\mu} \qquad k_{nl}^{2\,S,T} = \frac{\varrho\omega_{nl}^{2\,S,T}}{\mu}, \tag{A.6}$$

- superindex S and T denoting the spheroidal and the toroidal families respectively,
- subindex l running from 0 to infinity and n from 1 to infinity for each fixed l.

A.2 Spheroidal Spectrum

In next page, we present in graphical form the free sphere's spectrum for a Poisson ratio $\sigma = 0.33$ associated to its spheroidal normal modes of vibration.

Then, for determining the corresponding frequencies in the usual ω_{nl} form one also needs to fix other sphere's physical characteristics such as its radius R and the speed v_t of transversal elastic waves propagating in it. The relationship is

$$k_{nl}^2 = \frac{\varrho}{\mu}\omega_{nl}^2 = \frac{2+\sigma}{v_t}\omega_{nl}^2. \tag{A.7}$$

In particular, for typical planned aluminium spheres $R = 1.5m$ and $v_t = 3160ms^{-1}$.

Appendix B
Laplace Transform

Chapter 3 was devoted to the presentation and resolution of the GRD equations describing any coupled spherical GW antenna. Previously to resolution, it was necessary to convert the original differential set of equations into a more manageable system, so that the GRD set transmuted first into its integro-differential counterpart by the application of the Green Function Formalism, and finally into an algebraic system on account of Laplace transformations. Here, we summarize some results we have made use of concerning that integral transform: its direct and inverse definitions, and related theorems helpful with respect to its application. All this information can be found more extensively treated in standard textbooks, such as [3] or [79].

B.1 Direct Laplace Transform

The Laplace Transform of a generic function $F(t)$ is defined by

$$\mathcal{L}\{F(t)\} \equiv \hat{f}(s) = \int_0^\infty F(t)e^{-st}\,dt. \tag{B.1}$$

It has two important properties with a central position in its application; for instance, this integral representation allows to convert integral and differential equations into simpler forms that may be solved more easily.

The first one is that it obeys the faltung theorem, also named convolution theorem. In words, it states that the Laplace Transform of a convolution integral product of two functions is the simple algebraic product of the Laplace Transform of each individual function:

$$\mathcal{L}\left(\int_0^\infty F(t)\,G(t-t')\,dt'\right) = \tilde{f}(s)\,\tilde{g}(s), \tag{B.2}$$

which, for instance, will hold for the kernel integral in (3.60).

The second property is that -like Fourier transform- it replaces differentiation with multiplication:

$$\mathcal{L}\{F^{(n)}(t)\} = s^n\tilde{f}(s) - s^{n-1}F(0) - s^{n-2}F'(0)\ldots - F^{(n-1)}(0), \tag{B.3}$$

what could be easily verified by using the integration by parts technique.

B.2 Inverse Laplace Transform

The Inverse Laplace Transform of any given function $\tilde{f}(s)$ is denoted by

$$\mathcal{L}^{-1}\{\tilde{f}(s)\} = F(t). \tag{B.4}$$

Among the several methods to find it. the most powerful is that of the Bromwich integral, also known as the Fourier-Mellin integral or theorem:

$$F(t) = \frac{1}{2\pi i}\int_{\gamma-i\infty}^{\gamma+i\infty} e^{st}\tilde{f}(s)\,ds \tag{B.5}$$

s is a complex variable of the form $s = \gamma + iu$, with γ such that

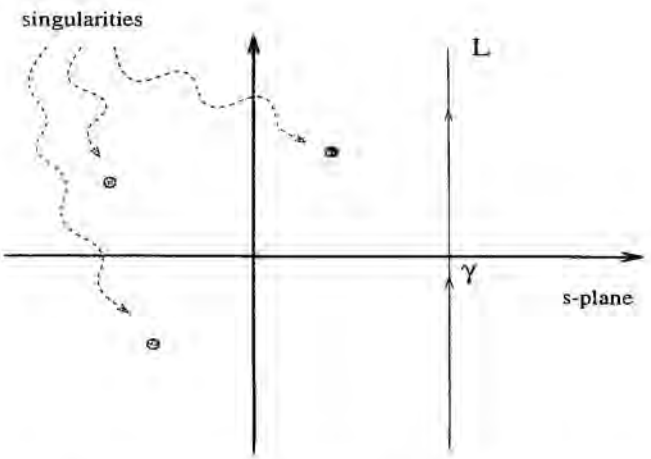

all the possible singularities of $\tilde{f}(s)$ are on the left-hand side of L [79].

The integral in (B.5) may be evaluated by the methods of contour integration. If $t > 0$, as it is for the functions we are concerned with, the integral contour may be closed by Jordan's lemma by an infinite semicircle in the left half-plane, and this does not change the value of the integral. Then, it becomes of the form

$$\oint_C g(s)\,ds \tag{B.6}$$

where C represents the closed integration path, and by the residue theorem [79]

$$\begin{aligned} \oint_C g(s)ds &= 2\pi i\,(a_{-1,0} + a_{-1,1} + a_{-1,2} + \ldots) \\ &= 2\pi i \sum \textit{residues enclosed by } C. \end{aligned} \tag{B.7}$$

This is the *residue theorem*, which replaces the problem of evaluating one contour integral by the algebraic problem of computing residues at the singular points of $g(s)$ enclosed in the region boundered by C.

Hence, for $F(t)$ in (B.5) $g(s) \equiv e^{st}\hat{f}(s)$ and it reduces to a calculation of residues at the singularities of $e^{st}\hat{f}(s)$ included in this region.

Appendix C
$\mathbf{P_l}$ Matrices

P_l matrices are at the core of the mathematical developments describing the dynamical behaviour of GW antennæ. They become the key for the characterization of the system responses. Here, we present a brief survey of their interesting structure and important properties for arbitrary order l, number of resonators J, and resonator's locations $\mathbf{n}_a$.

C.1 Description

P_l matrices are $J \times J$ matrices constructed so that their ab element is the Legendre polynomial

$$\mathcal{P}_l(z_{ab}) = \frac{1}{2^l l!} \frac{d^l}{dz_{ab}^l} (z_{ab}^l - 1)^l, \tag{C.1}$$

where subindex l stands for a given integer value in the range from zero to infinity, and $z_{ab} \equiv \cos\theta_{ab}$ depends on the θ_{ab} angle between the $\mathbf{n}_a$ and the $\mathbf{n}_b$ resonators' locations. Therefore, P_l will be a symmetric matrix of real values with diagonal components always 1, with independence of the number J of resonators and of the order l of the matrix.

It can be represented by

$$P_l = \begin{pmatrix} 1 & \mathcal{P}_l(\cos\theta_{12}) & \cdots & \mathcal{P}_l(\cos\theta_{1J}) \\ \mathcal{P}_l(\cos\theta_{12}) & 1 & \cdots & \cdots \\ \vdots & \vdots & \vdots & \vdots \\ \mathcal{P}_l(\cos\theta_{1J}) & \cdots & \cdots & 1 \end{pmatrix}, \tag{C.2}$$

where the first possible Legendre functions $\mathcal{P}_l(\cos\theta)$ entering it are given in next table:

l	$\mathcal{P}_l(\cos\theta)$
0	$\mathcal{P}_0(\cos\theta) = 1$
1	$\mathcal{P}_1(\cos\theta) = \cos\theta$
2	$\mathcal{P}_2(\cos\theta) = \frac{1}{4}(1 + 3\cos 2\theta)$
3	$\mathcal{P}_3(\cos\theta) = \frac{1}{8}(3\cos\theta + 5\cos 3\theta)$
4	$\mathcal{P}_4(\cos\theta) = \frac{1}{64}(9 + 20\cos 2\theta + 35\cos 4\theta)$
$\vdots$	$\vdots$

It interestingly happens that every $\mathcal{P}_l$ can be decomposed following the summation formula for spherical harmonics products:

$$\mathcal{P}_l(\mathbf{n}_a\mathbf{n}_b) = \frac{4\pi}{2l+1}\sum_{m=-l}^{l} Y_{lm}(\theta_a,\varphi_a)Y^*_{lm}(\theta_b,\varphi_b), \tag{C.3}$$

or in vector form

$$\mathcal{P}_l(\mathbf{n}_a\mathbf{n}_b) = \frac{4\pi}{2l+1}\left(Y_{l,-l}(\mathbf{n}_a), Y_{l,-l+1}(\mathbf{n}_a), \ldots, Y_{l,l-1}(\mathbf{n}_a), Y_{l,l}(\mathbf{n}_a)\right)\cdot\begin{pmatrix} Y^*_{l,-l}(\mathbf{n}_b) \\ Y^*_{l,-l+1}(\mathbf{n}_b) \\ \vdots \\ Y^*_{l,l-1}(\mathbf{n}_b) \\ Y^*_{l,l}(\mathbf{n}_b)\end{pmatrix}, \tag{C.4}$$

so that matrix P_l is in fact the product of two matrices of spherical harmonics:

$$P_l = \mathbf{H}\mathbf{H}^\dagger, \tag{C.5}$$

being $\mathbf{H}$ the $J \times (2l+1)$ matrix

$$\mathbf{H} = \sqrt{\frac{4\pi}{2l+1}} \left(\vec{Y}_{l,-l}, \vec{Y}_{l,-l+1}, \ldots, \vec{Y}_{l,l-1}, \vec{Y}_{l,l} \right), \tag{C.6}$$

where each column has been represented as a whole by $\vec{Y}_{lm}$, the name of the J-vector

$$\vec{Y}_{lm} = \begin{pmatrix} Y_{l,m}(\mathbf{n}_1) \\ Y_{l,m}(\mathbf{n}_2) \\ \vdots \\ Y_{l,m}(\mathbf{n}_J) \end{pmatrix}, \tag{C.7}$$

and $\mathbf{H}^\dagger$ stands for the complex transposed, or the hermitian conjugate, of $\mathbf{H}$.

C.2 Eigenvalues and Eigenvectors

As usual in matrix theory [76], eigenvalues ξ_c^2 of the P_l matrices and their associated eigenvectors $v^{(c)}$ are defined by

$$P_l \, v^{(c)} = \xi_c^2 \, v^{(c)}, \tag{C.8}$$

which is equivalent to

$$\left(P_l - \xi_c^2 I \right) v^{(c)} = 0, \tag{C.9}$$

It has non-trivial solutions if and only if

$$\det \left[P_l - \xi_c^2 I \right] = 0, \tag{C.10}$$

so that ξ_c^2 are commonly calculated as the zeroes of this determinant. Once they are known, one could construct the eigenvectors $v^{(c)}$ from (C.8).

As long as all the P_l matrices follow the same pattern, some general assertions affecting all of them about the properties of their eigenvalues and eigenvectors can be made:

- The first remark is that P_l is real and symmetric and so coincides with its complex transposed counterpart, i.e., it is an hermitian matrix by construction as the product of a matrix times its hermitian conjugate:

$$P_l = \mathbf{H}\mathbf{H}^\dagger = (\mathbf{H}\mathbf{H}^\dagger)^\dagger = P_l^\dagger, \tag{C.11}$$

whereupon it *is diagonalizable and would have real eigenvalues with corresponding eigenvectors forming an orthogonal basis.*

- Secondly, *the maximum number of its non-null eigenvalues is at most* $2l+1$. To prove this, we recall once again that P_l is the product

$$P_l = \mathbf{H}\mathbf{H}^\dagger, \tag{C.12}$$

being $\mathbf{H}$ the $J \times (2l+1)$ matrix in (C.6) and $\mathbf{H}^\dagger$ its $(2l+1) \times J$ hermitian conjugate. It happens that the rank of a given matrix is always equal to the rank of its hemitian conjugate, here

$$\text{rank } \mathbf{H} = \text{rank } \mathbf{H}^\dagger$$

and *at most* it clearly would have the value of $(2l+1)$, of course even if $J > (2l+1)$. Taking into account that for the product of two matrices the rank generally satisfies

$$\text{rank } AB \leq \min(\text{rank } A, \text{rank } B) .$$

it happens in this case that

$$\text{rank } P_l \leq (2l+1) .$$

Since the rank is an invariant property, it must be maintained by P_l even in its diagonal form, so that the number of its non-null eigenvalues can never exceed $(2l+1)$, and consequently, if $J \geq (2l+1)$, there will be a minimum number $J-(2l+1)$ of them identically null.

- Now, it is easy to prove that *the non-null eigenvalues are positive.*

  This can be deduced from the structure of P_l. Products of matrices of the form $AA^\dagger$ or $A^\dagger A$ are always positive semi-definite, and then their rank gives just the number of positive eigenvalues [76]. Matrix P_l has just this form, whence it is positive semi-definite and hence it has at most $(2l+1)$ positive eigenvalues, –this is why we have used the squared notation ξ^2. The rest of eigenvalues of course must be zero for the condition of P_l of being positive semi-definite.

One could also see it from the eigenvalue equation (C.8):

$$P_l\, v^{(c)} = \xi_c^2\, v^{(c)}. \tag{C.13}$$

It would be necessary to multiply its both sides by the hermitian conjugate eigenvector $v^{(b)\dagger}$:

$$v^{(b)\dagger}\, P_l\, v^{(c)} = \xi_c^2\, v^{(b)\dagger}\, v^{(c)}. \tag{C.14}$$

Clearly, the rhs of this formula contains a scalar product of orthogonal eigenvectors (recall that P_l is hermitian) which can be taken to be normalized:

$$v^{(b)\dagger}\, v^{(c)} = \delta_{bc}. \tag{C.15}$$

Whereas, the lhs of (C.14) can be rewritten as

$$v^{(b)\dagger}\, \mathbf{H}\mathbf{H}^\dagger\, v^{(c)} = (\mathbf{H}^\dagger v^{(b)})^\dagger \mathbf{H}^\dagger\, v^{(c)}, \tag{C.16}$$

from which (C.13) reads

$$(\mathbf{H}^\dagger v^{(b)})^\dagger \mathbf{H}^\dagger\, v^{(c)} = \xi_c^2\, \delta_{bc}. \tag{C.17}$$

Here we see that $\{\mathbf{H}^\dagger v^{(c)}\ \forall c\}$ constitutes a set of orthogonal $(2l+1)$-vectors, $\xi_c^2\, N$ appearing as a result of the scalar product providing the squared modulus of each of them, whereupon it would be always strictly positive.

- Furthermore, *all the non-null eigenvalues of* $P_l = \mathbf{H}\mathbf{H}^\dagger$ *are also eigenvalues of* $P_l = \mathbf{H}^\dagger\mathbf{H}$. The proof set out from the eigenvalue equation for $\mathbf{H}\mathbf{H}^\dagger$:

$$\mathbf{H}\mathbf{H}^\dagger \cdot v_i = \xi_i^2 v_i. \tag{C.18}$$

The following and final step consists in multiplying its boths sides by $\mathbf{H}^\dagger$ on the left:

$$\mathbf{H}^\dagger\mathbf{H} \cdot \mathbf{H}^\dagger v_i = \xi_i^2 \cdot \mathbf{H}^\dagger v_i. \tag{C.19}$$

The converse of this result, that *the eigenvalues of* $\mathbf{H}^\dagger\mathbf{H}$ *are also eigenvalues of* $\mathbf{H}\mathbf{H}^\dagger$, is immediately proved by the same procedure:

$$\mathbf{H}^{\dagger}\mathbf{H} \cdot u_i = \xi_i^2 u_i \tag{C.20}$$

$$\mathbf{H}\mathbf{H}^{\dagger} \cdot \mathbf{H}u_i = \xi_i^2 \cdot \mathbf{H}u_i. \tag{C.21}$$

- Finally, the trace is another invariant property of a matrix. For P_l:

$$tr\ P_l = \sum_{a=1}^{J} \mathcal{P}_l(\mathbf{n}_a\mathbf{n}_a) = \sum_{a=1}^{J} 1 = J, \tag{C.22}$$

but in the diagonal form

$$tr\ P_l = \sum_{a=1}^{J} \xi_a^2 = \sum_{\xi_c \neq 0} \xi_c^2, \tag{C.23}$$

so that the sum of the eigenvalues must always result J:

$$\sum_{\xi_c \neq 0} \xi_c^2 = J. \tag{C.24}$$

Appendix D
Calculation of Residues

Results in Chapter 3 for the amplitudes of excited modes in a spherical GW antenna rely on residue calculations. We recall that the concern was the finding of the Laplace inverse transform

$$q_a(t) = \frac{1}{2\pi i}\int_{\gamma-i\infty}^{\gamma+i\infty} e^{st}\tilde{q}_a(s)\,ds \qquad a = 1\ldots, J, \tag{D.1}$$

computing it through the residue theorem:

$$q_a(t) = \sum residues\ of\ e^{st}\tilde{q}_a(s)\ at\ its\ poles\ in\ the\ complex\ s-plane. \tag{D.2}$$

The poles of $e^{st}\tilde{q}_a(s)$ are isolated singularities which happen to be exclusively at the zeroes of the determinant $\Delta(s)$ in (3.86) for the M_{ab} matrix:

$$\Delta(s) = \det\left[\delta_{ab} + \eta\sum_{nl}\frac{s^2\Omega^2}{(s^2+\Omega^2)(s^2+\omega_{nl}^2)}\Upsilon_{ab}^{(nl)}\right] = 0, \tag{D.3}$$

which were given in formulas (3.87) and (3.93) as roots near the tuning frequency Ω and roots near other frequencies $\omega_{nl} \neq \Omega$.

We are going to demonstrate that for first order calculations it will suffice to consider the contributions due to just the first kind of zeroes.

D.1 s_0 Poles

s_0 poles are:

$$s_{0,c\pm}^2 = -\omega_{c\pm}^2 = -\Omega^2 \left(1 \pm \sqrt{\frac{2L+1}{4\pi}} |A_{NL}(R)| \xi_c \eta^{\frac{1}{2}}\right) + O(\eta), \qquad c = 1, \ldots, J, \quad \text{(D.4)}$$

calculated from the determinant

$$\Delta(s) = \det\left[\delta_{ab} + \eta \frac{s^2\Omega^2}{(s^2+\Omega^2)^2} \chi_{ab}^{(NL)}\right] = 0. \quad \text{(D.5)}$$

These roots are arranged in a set of J symmetric pairs around $\Omega = \omega_{NL}$, depending on the eigenvalues ξ_c^2 of matrix $P_L(\mathbf{n}_a\mathbf{n}_b)$. Let us write them in a more suitable form:

$$s_{0,c\pm}^2 = -\omega_{c\pm}^2 = -\Omega^2 \left(1 + b_{c\pm}\eta^{\frac{1}{2}}\right) + O(\eta), \quad \text{(D.6)}$$

and taking the square roots

$$s_{0,poles} = \pm s_{0,c\pm} = \pm i\omega_{c\pm} = \pm i\Omega \left(1 + \frac{1}{2} b_{c\pm}\eta^{\frac{1}{2}}\right) + O(\eta) \qquad c = 1, \ldots, J. \quad \text{(D.7)}$$

When the detector is acted upon by an incoming gravitational wave, the amplitudes $\tilde{q}_a(s)$ in the Laplace domain are written as

$$\tilde{q}_a(s) = \sum_{\substack{L=0 \text{ and } 2 \\ m=-L,\ldots,L}} \tilde{\phi}_a^{(Lm)}(s)\tilde{g}^{(Lm)}(s) \qquad a = 1, \ldots, J, \quad \text{(D.8)}$$

being

$$\tilde{\phi}_a^{(Lm)}(s) = -\sum_{b=1}^{J} M_{ab}^{-1} \frac{s^2}{s^2+\Omega^2} \frac{a_{NL}A_{NL}(R)}{s^2+\Omega^2} Y_{Lm}(\mathbf{n}_b) \quad \text{(D.9)}$$

(formula (3.127) in Chapter 3), and

$$M_{ab}^{-1} = \left[\delta_{ab} + \eta \frac{s^2\Omega^2}{(s^2+\Omega^2)^2} \chi_{ab}^{(NL)}\right]^{-1} \quad \text{(D.10)}$$

for $L = 0$ monopolar response and $L = 2$ quadrupolar response, with $\Omega = \omega_{N0}$ and $\Omega = \omega_{N2}$ respectively.

Hence, one just has to find $\phi_a^{(Lm)}(t)$, since the convolution theorem assures

$$q_a(t) = \sum_{\substack{L=0 \text{ and } 2 \\ m=-L,\ldots,L}} \int_0^t \phi_a^{(Lm)}(t-t')\, g^{(Lm)}(t')\, dt' \qquad a = 1, \ldots, J. \quad \text{(D.11)}$$

In analogy with (D.2),

$$\phi_a^{(Lm)}(t) = \sum \textit{residues of } e^{st}\tilde{\phi}_a^{(Lm)}(s) \textit{ at its poles in the complex } s-\textit{plane}. \tag{D.12}$$

We shall see that these poles are still $s_{0,c\pm}$, those in equation (D.6), and that they are the only appearing. For this, it would be more convenient to express the determinant $\Delta(s)$ in (D.5) like the product of its contributing root monomials *at leading order*:

$$\begin{aligned}\Delta(s) &= (s^2+\Omega^2)^{-2J}\prod_{c=1}^{J}(s^2+\omega_{c+}^2)(s^2+\omega_{c-}^2)\\ &= (s^2+\Omega^2)^{-2J}\prod_{c=1}^{J}(s+i\omega_{c+})(s-i\omega_{c+})(s+i\omega_{c-})(s-i\omega_{c-}),\end{aligned} \tag{D.13}$$

so that the inverse of matrix M_{ab} reads

$$M_{ab}^{-1} = \Delta(s)^{-1}\, M_{ab}^{ADJ} = (s^2+\Omega^2)^{2J}\prod_{c=1}^{J}\frac{1}{(s^2+\omega_{c+}^2)(s^2+\omega_{c-}^2)}\, M_{ab}^{ADJ}, \tag{D.14}$$

where ADJ stands for labelling the adjoint operation which substitutes each of the elements of M_{ab} by its conjugate minor (currently, matrix inversion also requires transposition, but M_{ab} is a symmetric matrix whereupon it and its transposed are equal).

Finally, for $\tilde{\phi}_a^{(Lm)}(s)$:

$$\begin{aligned}\tilde{\phi}_a^{(Lm)}(s) &= -s^2(s^2+\Omega^2)^{2J-2}\prod_{c=1}^{J}\frac{1}{(s^2+\omega_{c+}^2)(s^2+\omega_{c-}^2)}\times\\ &\times\sum_{b=1}^{J} M_{ab}^{ADJ}\, a_{NL}A_{NL}(R)Y_{Lm}(\mathbf{n}_b) \qquad a=1,\ldots,J.\end{aligned} \tag{D.15}$$

Clearly, the only singularities in last equation are $s_{0,c\pm}^2 = -\omega_{c\pm}^2$, even when multiplied by the analytic function e^{st}. Each $\pm s_{0,c\pm}$ appears there in a monomial of unit power, whereupon they are classified as simple poles. Theory of residues [79] establish that the residues associated to such poles are simply calculated as the limits

$$
\begin{aligned}
R_{a,0-pole} &\equiv \lim_{s\to s_{0,pole}} (s - s_{0,pole}) \times \hat{f}(s) \\
&\equiv \lim_{s\to s_{0,pole}} (s - s_{0,pole}) \times e^{st}\hat{\phi}_a^{(Lm)}(s) \\
&= \lim_{s\to s_{0,pole}} -(s - s_{0,pole}) e^{st} s^2 (s^2+\Omega^2)^{2J-2} \prod_{c=1}^{J} \frac{1}{(s^2+\omega_{c+}^2)(s^2+\omega_{c-}^2)} \times \\
&\times \sum_{b=1}^{J} M_{ab}^{ADJ} a_{NL} A_{NL}(R) Y_{Lm}(\mathbf{n}_b). \qquad \text{(D.16)}
\end{aligned}
$$

Let us perform this computation in two stages, always taking into account that we are interested in calculations to the lowest order:

$$
\begin{aligned}
R_{a,0-pole} &= R_{1a,0-pole} \times R_{2a,0-pole} \\
&\equiv \lim_{s\to s_{0,pole}} -(s - s_{0,pole}) e^{st} s^2 (s^2+\Omega^2)^{2J-2} \prod_{c=1}^{J} \frac{1}{(s^2+\omega_{c+}^2)(s^2+\omega_{c-}^2)} \times \\
&\times \lim_{s\to s_{0,pole}} \sum_{b=1}^{J} M_{ab}^{ADJ} a_{NL} A_{NL}(R) Y_{Lm}(\mathbf{n}_b). \qquad \text{(D.17)}
\end{aligned}
$$

- **$R_{1a,0-pole}$**

  In compact notation, $(s - s_{0,pole})$ is substituted by $(s - (\pm\omega_{c\pm}))$, so that in fact one has to undertake only one calculation giving results for the four different cases for a fixed c.

$$
\begin{aligned}
R_{1a,0-pole} &\equiv \lim_{s\to\pm i\omega_{c\pm}} -(s - (\pm i\omega_{c\pm})) e^{st} s^2 (s^2+\Omega^2)^{2J-2} \times \\
&\times \prod_{c=1}^{J} \frac{1}{(s^2+\omega_{c+}^2)(s^2+\omega_{c-}^2)} \\
&= \pm e^{\pm i\omega_{c\pm} t} \omega_{c\pm}^2 \left(\Omega^2 - \omega_{c\pm}^2\right)^{2J-2} \frac{1}{2i\omega_{c\pm}(\omega_{c\mp}^2 - \omega_{c\pm}^2)} \times \\
&\times \prod_{d\neq c} \frac{1}{(\omega_{d+}^2 - \omega_{c\pm}^2)(\omega_{d-}^2 - \omega_{c\pm}^2)} \\
&\approx \pm \eta^{-\frac{1}{2}} e^{\pm i\omega_{c\pm} t} b_{c\pm}^{2J-2} \frac{1}{2i\omega_{c\pm}} \frac{1}{b_{c\mp} - b_{c\pm}} \times \\
&\times \prod_{d\neq c} \frac{1}{(b_{d+} - b_{c\pm})(b_{d-} - b_{c\pm})}. \qquad \text{(D.18)}
\end{aligned}
$$

- $\mathbf{R_{2a,0-pole}}$

  Here, one has to consider the second limit:

$$\begin{aligned} R_{2a,pole} &\equiv \lim_{s\to\pm i\omega_{c\pm}} a_{NL}A_{NL}(R)\sum_{b=1}^{J} M_{ab}^{ADJ}Y_{Lm}(\mathbf{n}_b) \\ &\equiv \lim_{s\to\pm i\omega_{c\pm}} a_{NL}A_{NL}(R)\times \\ &\times \sum_{b=1}^{J}\left[\delta_{ab}+\eta\frac{s^2\Omega^2}{(s^2+\Omega^2)^2}\chi_{ab}^{(NL)}\right]^{ADJ} Y_{Lm}(\mathbf{n}_b). \end{aligned} \tag{D.19}$$

  It would only be necessary to substitute the value $\pm i\omega_{c\pm}$ in place of s, since this expression does not contain singularities at these points.

  In that limit and restricting to the dominant order, matrix M_{ab}^{ADJ} presents the general structure

$$\begin{aligned} M_{ab}^{ADJ} &= -b_{c\pm}^{-(2J-2)}\left[\chi_{ab}^{(NL)}-b_{c\pm}^2\delta_{ab}\right]^{ADJ} \\ &= -b_{c\pm}^{-(2J-2)}\times \\ &\times \det\left[\chi_{ab}^{(NL),ADJ}-b_{c\pm}^2\delta_{ab}\right]\left[\chi_{ab}^{(NL),ADJ}-b_{c\pm}^2\delta_{ab}\right]^{-1}. \end{aligned} \tag{D.20}$$

  Realizing that $b_{c\pm}^2$ is an eigenvalue of matrix $\chi_{ab}^{(NL)}$,

$$b_{c\pm}^2=\frac{2L+1}{4\pi}|A_{NL}(R)|^2\xi_c^2\equiv\chi_c^2, \tag{D.21}$$

  we give matrix $\left[\chi_{ab}^{(NL),ADJ}-b_{c\pm}^2\delta_{ab}\right]$ the name $D_{ab}(\chi_c^2)$, which depends on the eigenvalue χ_c^2 of $\chi_{ab}^{(NL)}$.

Next step will be to introduce these new labels in the multiplication of the two results for $R_{1a,0-pole}$ and $R_{2a,0-pole}$:

$$\begin{aligned} R_{a,\pm i\omega_{c\pm}} &= \mp\eta^{-\frac{1}{2}}e^{\pm i\omega_{c\pm}t}\frac{1}{2i\omega_{c\pm}}\frac{1}{2\chi_c}\prod_{d\neq c}\frac{1}{\chi_c^2-\chi_d^2}a_{NL}A_{NL}(R)\times \\ &\times \sum_{b=1}^{J} D_{ab}^{ADJ}(\chi_c^2)Y_{Lm}(\mathbf{n}_b). \end{aligned} \tag{D.22}$$

The whole process has to be repeated for every c from 1 to J, except for those with associated null ξ_c since they will provide contributions at higher orders, what can be demonstrated just recalculating $R_{1a,0-pole}$ in these cases (the dominant term in $R_{2a,0-pole}$ is always of order η^0). Instead of depending on the amplification factor $\eta^{-\frac{1}{2}}$ appearing in (D.18), this limit depends on η^{J-1} at leading order, where J is the number of resonators in the layout. Hence, its contribution will affect higher order terms, and not just the leading ones.

Following (D.12), all the residues at leading order has to be summed up. To perform this summation we use that

$$\frac{e^{+i\omega_{c\pm}t} - e^{-i\omega_{c\pm}t}}{2i} = \sin\omega_{c\pm}t, \tag{D.23}$$

and then

$$\begin{aligned} R_a &= -\eta^{-\frac{1}{2}} a_{NL} A_{NL}(R) \sum_{\chi_c \neq 0} \frac{1}{2\chi_c} \prod_{d \neq c} \frac{1}{\chi_c^2 - \chi_d^2} \times \\ &\times \sum_{b=1}^{J} D_{ab}^{ADJ}(\chi_c^2) Y_{Lm}(\mathbf{n}_b) \frac{1}{\omega_{c\pm}} \left[\sin\omega_{c+}t - \sin\omega_{c-}t\right], \end{aligned} \tag{D.24}$$

which indeed is the expression for the dominant approximation of $\phi_a^{(Lm)}$ in the time domain. Trivially, in the Laplace domain:

$$\begin{aligned} \phi_a^{(Lm)}(s) &= -\eta^{-\frac{1}{2}} a_{NL} A_{NL}(R) \sum_{\chi_c \neq 0} \frac{1}{2\chi_c} \prod_{d \neq c} \frac{1}{\chi_c^2 - \chi_d^2} \times \\ &\times \sum_{b=1}^{J} D_{ab}^{ADJ}(\chi_c^2) Y_{Lm}(\mathbf{n}_b) \left[\frac{1}{s^2 + \omega_{c+}^2} - \frac{1}{s^2 + \omega_{c-}^2}\right] + O(\eta) \end{aligned}$$

$a = 1, \ldots, J.$ (D.25)

We are going to exploit the possibility of expressing matrices $D_{ab}^{ADJ}(\chi_c^2)$ by means of eigenvectors $v^{(c)}$ of $P_L(\mathbf{n}_a \mathbf{n}_b)$ associated to the non-null eigenvalues ξ_c^2. $D_{ab}(\chi_c^2)$ matrices have the form:

$$D_{ab}(\chi_c^2) = \chi_{ab}^{(NL)} - \chi_c^2 \delta_{ab}. \tag{D.26}$$

When applied to vector $v^{(c')}$:

$$\begin{aligned} D_{ab}(\chi_c^2)v_b^{(c')} &= \left(\chi_{ab}^{(NL)} - \chi_c^2\delta_{ab}\right)v_b^{(c')} = \\ &= \chi_{ab}^{(NL)}v_b^{(c')} - \chi_c^2\delta_{ab}v_b^{(c')} = \\ &= \chi_{c'}^2 v_b^{(c')} - \chi_c^2 v_b^{(c')} = \\ &= \left(\chi_{c'}^2 - \chi_c^2\right)v_b^{(c')}, \end{aligned} \tag{D.27}$$

since $v^{(c')}$ is of course eigenvector of $\chi_{ab}^{(NL)}$ with eigenvalue $\chi_{c'}^2$, and as a result it also will occur to $D_{ab}(\chi_c^2)$, with associated eigenvalue $\left(\chi_{c'}^2 - \chi_c^2\right)$.

Therefore, we can rewrite the matrix term

$$\prod_{d\neq c}\frac{1}{\chi_c^2 - \chi_d^2}D^{ADJ}(\chi_c^2) \tag{D.28}$$

in formula (D.25) by introducing these results and taking the determinant of matrix $D(\chi_c^2)$ in the basis that makes it diagonal:

$$\begin{aligned} \prod_{d\neq c}\frac{1}{\chi_c^2 - \chi_d^2}D^{ADJ}(\chi_c^2) &= \\ = \prod_{d\neq c}\frac{1}{\chi_c^2 - \chi_d^2}\det D(\chi_c^2)D^{-1}(\chi_c^2) &= \\ = \prod_{d\neq c}\frac{1}{\chi_c^2 - \chi_d^2}\prod_{d=1}^{J}\left(\chi_d^2 - \chi_c^2\right)D^{-1}(\chi_c^2) &= \\ = (-1)^{J-1}\left(\chi_c^2 - \chi_c^2\right)D^{-1}(\chi_c^2). \end{aligned} \tag{D.29}$$

Now, we continue in (D.29) by inserting results from (D.27) in the case $c = c'$:

$$\begin{aligned} (-1)^{J-1}\left(\chi_c^2 - \chi_c^2\right)D^{-1}(\chi_c^2) &= (-1)^{J-1}D_{ab}(\chi_c^2)v_b^{(c)}v_a^{(c)*}D_{ab}^{-1}(\chi_c^2) = \\ &= (-1)^{J-1}v_b^{(c)}v_a^{(c)*}. \end{aligned} \tag{D.30}$$

and introducing it and also (D.21) into (D.25), the final result is obtained:

$$\begin{aligned} \tilde{\phi}_a^{(Lm)}(s) &= (-1)^J\eta^{-\frac{1}{2}}\sqrt{\frac{4\pi}{2L+1}}a_{NL}\sum_{b=1}^{J}\left\{\sum_{\xi_c\neq 0}\frac{1}{2}\left[(s^2+\omega_{c+}^2)^{-1} - (s^2+\omega_{c-}^2)^{-1}\right]\right. \\ &\times \left.\frac{v_a^{(c)}v_b^{(c)*}}{\xi_c}\right\}Y_{2m}(\mathbf{n}_b) \qquad a = 1,\ldots,J. \end{aligned} \tag{D.31}$$

The two interesting cases are those corresponding to monopole tuning $\Omega = \omega_{N0}$ and quadrupole tuning $\Omega = \omega_{N2}$. In each situation, it would be necessary to know the eigenvalues ξ_c^2 and the eigenvectors $v^{(c)}$ for achieving the definite form of $\tilde{\phi}_a^{(Lm)}(s)$.

In the quadrupole case, evaluation of

$$\tilde{\phi}_a^{(2m)}(s) = (-1)^J \eta^{-\frac{1}{2}} \sqrt{\frac{4\pi}{5}} a_{N2} \sum_{b=1}^{J} \left\{ \sum_{\xi_c \neq 0} \frac{1}{2} \left[(s^2 + \omega_{c+}^2)^{-1} - (s^2 + \omega_{c-}^2)^{-1} \right] \times \right.$$
$$\left. \times \frac{v_a^{(c)} v_b^{(c)*}}{\xi_c} \right\} Y_{2m}(\mathbf{n}_b) \tag{D.32}$$

requires to fix the distribution of resonators since eigenvalues and eigenvectors depend on it and will be different for each layout.

On the other hand, monopolar $\tilde{\phi}_a^{(00)}(s)$ is independent of the transducer configuration, so that it can be computed in general. From (D.31),

$$\tilde{\phi}_a^{(00)}(s) = (-1)^J \eta^{-\frac{1}{2}} \sqrt{4\pi} a_{N0} \times$$
$$\times \sum_{b=1}^{J} \left\{ \sum_{\xi_c \neq 0} \frac{1}{2} \left[(s^2 + \omega_{c+}^2)^{-1} - (s^2 + \omega_{c-}^2)^{-1} \right] \frac{v_a^{(c)} v_b^{(c)*}}{\xi_c} \right\} Y_{00}(\mathbf{n}_b) \tag{D.33}$$

ξ_c and $v^{(c)}$ are the eigenvalues and the eigenvectors of the $J \times J$ matrix $P_0(\mathbf{n}_a \mathbf{n}_b)$. This matrix presents a simple form: each of its elements has numerical value 1, independently of the number of resonators J or their locations. ξ_c were already found in Chapter 3:

$$\xi_1^2 = J. \quad \xi_a^2 = 0 \quad \forall a = 2, \ldots, J, \tag{D.34}$$

and calculation of eigenvectors is not more difficult. It is easily found that the normalised eigenvector associated to the non-null eigenvalue ξ_1^2 is the J-vector

$$v^{(1)} = \frac{1}{\sqrt{J}} \begin{pmatrix} 1 \\ 1 \\ \vdots \\ 1 \end{pmatrix}, \tag{D.35}$$

so that

$$\sum_{b=1}^{J} v_a^{(1)} v_b^{(1)*} Y_{00}(\mathbf{n}_b) == \frac{1}{\sqrt{J}} \frac{1}{\sqrt{4\pi}} \frac{J}{\sqrt{J}} = \frac{1}{\sqrt{4\pi}} \quad \forall a, \tag{D.36}$$

which simplifies $\tilde{\phi}_a^{(00)}(s)$ to

$$\tilde{\phi}_a^{(00)}(s) = \eta^{-\frac{1}{2}} \frac{(-1)^J}{\sqrt{J}} a_{N0} \frac{1}{2} \left[(s^2 + \omega_+^2)^{-1} - (s^2 + \omega_-^2)^{-1} \right] + O(0). \tag{D.37}$$

D.2 $\mathbf{s_{nl}}$ Poles

In this section we will prove that s_{nl} poles,

$$s_{nl,c}^2 = -\omega_c^2 = -\omega_{nl}^2 (1 + b_{1c}\eta) + O(\eta^2), \qquad c = 1, \ldots, J, \tag{D.38}$$

calculated from the determinant

$$\Delta(s) = \det \left[\delta_{ab} + \eta \frac{s^2 \Omega^2}{(s^2 + \Omega^2)(s^2 + \omega_{nl}^2)} \chi_{ab}^{(nl)} \right] = 0, \tag{D.39}$$

do not give contributions to the residues of $e^{st} \tilde{q}_a(s)$ at leading order $\eta^{-\frac{1}{2}}$.

The procedure runs in parallel with that described in the previous section. From the convolution and the residue theorems, respectively in (D.11) and (D.12), it will suffice to compute the residues of $e^{st} \tilde{\phi}_a^{(lm)}(s)$ at its poles in the complex s-plane. For s_{nl} poles, we saw in Chapter 3 that $\tilde{\phi}_a^{(lm)}(s)$ is, formula (3.29),

$$\tilde{\phi}_a^{(lm)}(s) = - \sum_{b=1}^{J} M_{ab}^{-1} \frac{s^2}{s^2 + \Omega^2} \frac{a_{nl} A_{nl}(R)}{s^2 + \omega_{nl}^2} Y_{lm}(\mathbf{n}_b) \tag{D.40}$$

and

$$M_{ab}^{-1} = \left[\delta_{ab} + \eta \frac{s^2 \Omega^2}{(s^2 + \Omega^2)(s^2 + \omega_{nl}^2)} \chi_{ab}^{(nl)} \right]^{-1} \tag{D.41}$$

for $l = 0$ monopolar response and $l = 2$ quadrupolar response. This inverse matrix can also be expressed as

$$M_{ab}^{-1} = \Delta(s)^{-1} M_{ab}^{ADJ}, \tag{D.42}$$

with $\Delta(s)$ in (D.39). Substituting this determinant by the product of its contributing monomials,

$$\begin{aligned}\Delta(s) &= (s^2+\Omega^2)^{-J}(s^2+\omega_{nl}^2)^{-J}\prod_{c=1}^{J}(s^2+\omega_c^2)\\ &= (s^2+\Omega^2)^{-J}(s^2+\omega_{nl}^2)^{-J}\prod_{c=1}^{J}(s+i\omega_c)(s-i\omega_c),\end{aligned} \tag{D.43}$$

the inverse matrix reads

$$M_{ab}^{-1} = \Delta(s)^{-1}\, M_{ab}^{ADJ} = (s^2+\Omega^2)^J\,(s^2+\omega_{nl}^2)^J \prod_{c=1}^{J}\frac{1}{(s^2+\omega_c^2)}\, M_{ab}^{ADJ}. \tag{D.44}$$

Finally, for $e^{st}\hat{\phi}_a^{(lm)}(s)$ we have:

$$\begin{aligned}e^{st}\hat{\phi}_a^{(lm)}(s) &= -e^{st}s^2(s^2+\Omega^2)^{J-1}\,(s^2+\omega_{nl}^2)^{J-1}\prod_{c=1}^{J}\frac{1}{(s^2+\omega_c^2)}\times\\ &\times \sum_{b=1}^{J} M_{ab}^{ADJ}\, a_{nl}A_{nl}(R)Y_{lm}(\mathbf{n}_b) \qquad a=1,\ldots,J.\end{aligned} \tag{D.45}$$

Hence, $\pm s_{nl,c}$ are the only singularities in last equation and their classification as simple poles leads to the calculation of the residues in the form

$$\begin{aligned}R_{a,nl-pole} &\equiv \lim_{s\to s_{nl,pole}}(s-s_{nl,pole})\times e^{st}\hat{\phi}_a^{(lm)}(s)\\ &= \lim_{s\to s_{nl,pole}} -(s-s_{nl,pole})e^{st}s^2(s^2+\Omega^2)^{J-1}\,(s^2+\omega_{nl}^2)^{J-1}\prod_{c=1}^{J}\frac{1}{(s^2+\omega_c^2)}\times\\ &\times \sum_{b=1}^{J} M_{ab}^{ADJ}\, a_{nl}A_{nl}(R)Y_{lm}(\mathbf{n}_b) \qquad a=1\ldots,J.\end{aligned} \tag{D.46}$$

As for s_0 poles, we compute them to the lowest order in two stages:

$$R_{a,nl-pole} = R_{1a,nl-pole}\times R_{2a,nl-pole}. \tag{D.47}$$

- $\mathbf{R_{1a,nl-pole}}$

$$
\begin{aligned}
R_{1a,nl-pole} &\equiv \lim_{s\to\pm i\omega_c} -(s-(\pm i\omega_c))e^{st}s^2(s^2+\Omega^2)^{J-1}(s^2+\omega_{nl}^2)^{J-1}\times \\
&\times \prod_{c=1}^{J}\frac{1}{(s^2+\omega_c^2)} \\
&= \pm e^{\pm i\omega_c t}\omega_c^2(\Omega^2-\omega_c^2)^{J-1}(\omega_{nl}^2-\omega_c^2)^{J-1}\frac{1}{2i\omega_c}\times \\
&\times \prod_{d\neq c}\frac{1}{(\omega_d^2-\omega_c^2)} \\
&\approx \pm(-1)^J e^{\pm i\omega_c t}b_{1c}^{J-1}(\Omega^2-\omega_{nl}^2)^{J-1}\frac{1}{2i\omega_c}\times \\
&\times \prod_{d\neq c}\frac{1}{(b_{1d}-b_{1c})}. \qquad \text{(D.48)}
\end{aligned}
$$

Therefore, $R_{1a,nl-pole}$ is of order η^0, in contrast to what happens for $R_{1a,0-pole}$ which is responsible for the dominant amplification factor $\eta^{-\frac{1}{2}}$.

- $\mathbf{R_{2a,nl-pole}}$

$$
\begin{aligned}
R_{2a,nl-pole} &\equiv \lim_{s\to\pm i\omega_c} a_{nl}A_{nl}(R)\sum_{b=1}^{J}M_{ab}^{ADJ}Y_{lm}(\mathbf{n}_b) \\
&\equiv \lim_{s\to\pm i\omega_c} a_{nl}A_{nl}(R)\times \\
&\times \sum_{b=1}^{J}\left[\delta_{ab}+\eta\frac{s^2\Omega^2}{(s^2+\Omega^2)(s^2+\omega_{nl}^2)}\chi_{ab}^{(nl)}\right]^{ADJ}Y_{lm}(\mathbf{n}_b) \\
&\equiv -a_{nl}A_{nl}(R)\left(\frac{\Omega^2}{\Omega^2-\omega_{nl}^2}\right)^{J-1}b_{1c}^{J-1}\times \\
&\times \sum_{b=1}^{J}\left[\chi_{ab}^{(nl)}-\left(\frac{\Omega^2}{\Omega^2-\omega_{nl}^2}\right)b_{1c}\delta_{ab}\right]^{ADJ}Y_{lm}(\mathbf{n}_b), \qquad \text{(D.49)}
\end{aligned}
$$

which is $O(\eta^0)$ like $R_{2a,0-pole}$.

From these results, we eventually find

$$
\begin{aligned}
R_{a,\pm i\omega_c} &= \mp e^{\pm i\omega_c t}\frac{1}{2i\omega_c}\omega_{nl}^2\Omega^{2J-2}\prod_{d\neq c}\frac{1}{(b_{1d}-b_{1c})}\times \\
&\times a_{nl}A_{nl}(R)\sum_{b=1}^{J}\left[\chi_{ab}^{(nl)}-\left(\frac{\Omega^2}{\Omega^2\omega_{nl}^2}\right)b_{1c}\delta_{ab}\right]^{ADJ}Y_{lm}(\mathbf{n}_b), \qquad \text{(D.50)}
\end{aligned}
$$

which is $O(\eta^0)$. Therefore, it represents a correction for the $O(\eta^0)$ terms of the tuning mode and does not contribute at leading order $\eta^{-\frac{1}{2}}$, as announced.

D.3 $s_{central}$ Poles

$s_{central}$ poles appear in the coupled frequency spectrum structure when the URF situation is studied, i.e., when there exists a second free sphere's frequency $\omega_{N'L'}$ in the neighbourhood of the resonance frequency $\Omega = \omega_{NL}$, formula (5.14). We recall from Chapter 5 that it then splits into J different triplets containing each a rather symmetric pair $\omega_{c,u}$ and $\omega_{c,d}$ imitating the IRF doublets plus a third component, a *central* frequency $\omega_{c,c}$ very near Ω. Due to their excessive nearness, these central resonances are actually of the form in (5.39),

$$\omega_{i,c}^2 = \omega_{NL}^2(1 + \chi_{1c}\eta) + O(\eta^{\frac{3}{2}}). \tag{D.51}$$

How to demonstrate that the contributions of such modes are not at the leading order $\eta^{-\frac{1}{2}}$ but at superiors? Simply by computing again (D.12), with $\tilde{\phi}_a^{(Lm)}(s)$ in (D.9) and (D.10). With respect to the s_0 poles analysis, we face an unique relevant change. From (5.16) and (5.21), $\Delta(s)$ is here

$$\Delta(s) = (s^2+\Omega^2)^{-2J}(s^2+\omega_{N'L'}^2)^{-J}\prod_{c=1}^{J}(s^2+\omega_{c,u}^2)(s^2+\omega_{c,d}^2)(s^2+\omega_{c,c}^2), \tag{D.52}$$

and so

$$\begin{aligned} o_a^{(Lm)}(s) &= -s^2(s^2+\Omega^2)^{2J-2}(s^2+\omega_{N'L'}^2)^J \prod_{c=1}^{J}\frac{1}{(s^2+\omega_{c,u}^2)(s^2+\omega_{c,d}^2)(s^2+\omega_{c,c}^2)} \times \\ &\times \sum_{b=1}^{J} M_{ab}^{ADJ} a_{NL}\mathcal{A}_{NL}(R)Y_{Lm}(\mathbf{n}_b) \qquad a = 1,\ldots,J. \end{aligned} \tag{D.53}$$

We have repeatedly seen that the order of the dominant contribution is revealed in the computation of just the limit $R_{1a,pole}$ in (D.18) or in (D.48). Here, for central frequencies

$$R_{1a,central-pole} \equiv \lim_{s\to\pm i\omega_{c,c}} -(s-(\pm i\omega_{c,c}))e^{st}s^2(s^2+\Omega^2)^{2J-2}(s^2+\omega_{N'L'}^2)^J \times$$

$$
\begin{aligned}
&\times \prod_{c=1}^{J} \frac{1}{(s^2+\omega_{c,u}^2)(s^2+\omega_{c,d}^2)(s^2+\omega_{c,c}^2)} \\
&= \pm e^{\pm i\omega_{c,c}t}\omega_{c,c}^2\left(\Omega^2-\omega_{c,c}^2\right)^{2J-2}\left(\omega_{N'L'}^2-\omega_{c,c}^2\right)^{J}\frac{1}{2i\omega_{c,c}} \\
&\times \frac{1}{(\omega_{c,u}^2-\omega_{c,c}^2)(\omega_{c,d}^2-\omega_{c,c}^2)} \times \prod_{k\neq c}\frac{1}{(\omega_{k,u}^2-\omega_{c,c}^2)(\omega_{k,d}^2-\omega_{c,c}^2)(\omega_{k,c}^2-\omega_{c,c}^2)} \\
&\approx \pm\eta^{\frac{J}{2}-1}e^{\pm i\omega_{c,c}t}1^{2J-2}a^{J}\frac{1}{2i\omega_{c,c}}\frac{\omega_{c,c}^2}{\chi_{\frac{1}{2}c+}\chi_{\frac{1}{2}c-}} \times \\
&\times \prod_{k\neq c}\frac{1}{\chi_{\frac{1}{2}k,u}\chi_{\frac{1}{2}k,d}(\chi_{k,c}-\chi_{c,c})}.
\end{aligned}
\tag{D.54}
$$

Therefore, the dominant order depends here on the number J of resonators in the layout. For the URF effect, the interesting resonance frequency is always a quadrupolar one. Such tuning demands a minimum number of five resonators to extract the maximum information from the detector's readout. For $J = 5$ we have $\eta^{\frac{3}{2}}$, and hence $s_{central}$ contributions are not at s_0-poles leading order $\eta^{-\frac{1}{2}}$ and can be obviated.

RESUMEN

R.1 Preliminares

R.1.1 Introducción Histórica

Desde su publicación en 1916, se han obtenido confirmaciones ciertamente impresionantes de los fundamentos de la teoría de la Relatividad General de Einstein y también de algunas de sus predicciones y nuevas implicaciones. Inicialmente, los tres tests clásicos propuestos por el propio Einstein ya en 1916 –explicación de las anomalías en el movimiento del perihelio de Mercurio, predicción de la desviación de rayos de luz por campos gravitatorios confirmada por Eddington [38, 107], y el efecto parcialmente demostrado del desplazamiento al rojo de líneas espectrales [107]– pronto conformaron una base exitosa para la Relatividad General. Sin embargo, la experimentación en este campo permaneció letárgica durante un tiempo, al igual que la investigación propiamente teórica, debido a que pese a ser considerada una bella teoría con implicaciones incluso revolucionarias en areas concretas como la Cosmologia, su relevancia potencial con respecto al resto de la Física no había sido universalamente admitida, en parte porque la teoría de Newton llevaba a las mismas predicciones cuando se trataban campos poco intensos, como en el caso de experimentación en condiciones de laboratorio.

No obstante, a finales de los 50 se comenzó a reavivar un fuerte interés, especialmente promovido por el grupo de Princeton encabezado por John Wheeler y el grupo de Londres dirigido por Herman Bondi. Aparte del potencial impacto en otros campos de la Física, la propia teoría de la Relatividad General atrajo mayor atención y este renovado interés, junto con el desarrollo de avances tecnológicos, llevó tanto a la realización de versiones más cuidadosas y precisas de los viejos tests astronómicos como a observaciones previamente inaccesibles de otros efectos[1], de las que la Relatividad General de Einstein

[1] Ver [28, 120, 142] para ampliar referencias.

queda perfectamente establecida como la teoría clásica de la gravitación.

De esta manera, el tercer efecto predicho por Einstein fue cuidadosamente verificado por Pound y Rebka en los 60 [112] y pronto otros experimentos concernientes a los fundamentos de la teoría fueron repetidos otra vez o realizados por primera vez. En particular, consecuencias o partes importantes del Principio de Equivalencia en sus varias formas –desde la unicidad en la caída libre para partículas de prueba, o Principio de Equivalencia de Galileo, hasta la forma muy fuerte– han sido probadas, entre ellas la dilatación temporal gravitacional, la invariabilidad temporal y espacial de constantes como G, la invariabilidad local de Lorentz de las leyes de la Física en los sistemas en caída libre, o la contribución de la energía gravitatoria a la masa inercial de los cuerpos celestes de acuerdo a la forma muy fuerte. También hay que señalar que existe soporte experimental para otras suposiciones básicas de la RG. Por ejemplo, la curvatura del espacio está confirmada por la verificación del efecto de de Sitter (o precesión geodésica), o por medidas en el Sistema Solar de desviaciones en las trayectorias de fotones y de retraso temporal en la propagación de ondas de radio viajando cerca del Sol. Ciertamente, también han sido observados otros efectos que confirman más de un aspecto. Así, se obtiene verificación experimental de las ecuaciones del movimiento y de las soluciones de Einstein para las ecuaciones de campo, por ejemplo, de estudios sobre la dinámica de planetas, naves espaciales o incluso el movimiento de la Luna, u observaciones de algunos sistemas binarios, como el paradigmático pulsar binario PSR 1913+16, que merece especial atención por proporcionar el test observacional que confirma la existencia de otra predicción fundamental de la Relatividad General: las ondas gravitatorias.

Ondas Gravitatorias

Uno de los nuevos fenómenos físicos predichos por la RG, y también por cualquier otra teoría métrica de la gravedad [135, 66, 67, 54], que se encontraba fuera del marco de la gravitación newtoniana fue la existencia de ondas gravitatorias. Como Einstein indicó tempranamente, el campo gravitatorio es una entidad dinámica que permite perturbaciones de la curvatura que se propagan en el espaciotiempo con velicidad finita, análogamente a lo que ocurre en la teoría del electromagnetismo de Maxwell. Einstein demostró [41, 42] que sus ecuaciones para el campo gravitatorio admitían en la aproximación lineal soluciones radiativas que representaban ondas planas y que se dividían en *ondas reales*, que transportaban energía, y *ondas aparentes*, que no lo hacían y podían ser eliminadas mediante transformaciones de coordenadas. Eddington [40] fue el primero

en dar un criterio invariante que las distinguía y era válido en cualquier sistema de coordenadas: la onda era física si el tensor de Riemann calculado de su métrica no era cero. Al igual que las ondas electromagnéticas, en RG las ondas gravitatorias son ondas planas transversales con dos estados de polarización propagándose en el vacío con la velocidad de la luz.

J. Weber fue pionero en los 60 en la tarea de intentar medir ondas gravitatorias. Su método se basaba en el hecho de que partículas libres que se mueven en un campo de gravitación experimentan aceleraciones relativas como se refleja en la ecuación de la desviación geodésica. Si las partículas no se pueden mover libremente sino que están conectadas mediante una pieza sólida rígida, las fuerzas gravitatorias de marea producirán un esfuerzo en el material que lo llevará a un estado de oscilación. La técnica de Weber [136, 137] consistía en medir estas deformaciones en grandes cilindros de aluminio a temperatura ambiente, presumiblemente excitados por un impulso incidente de radiación gravitatoria. Después de trabajar con un único detector en el período 1963-1968, Weber mandó construir un segundo cilindro en el Argone National Laboratory de Chicago para llevar a cabo experimentos coordinados buscando coincidencias en sus resultados.

De hecho, en un laboratorio no se pueden producir ondas gravitatorias intensas, así que Weber las buscó en el espacio. Su trabajo fue pronto respaldado por el descubrimiento en la misma década de una profusión de nuevos objetos astrofísicos tales como quasares, pulsares y fuentes binarias de rayos X [110]. Era entonces posible concebir sucesos altamente relativistas en agujeros negros pulsantes, acrecientes o en colisión, estrellas que colapsan o sistemas binarios emergentes de estrellas de neutrones, que podían ser fuentes intensas de radiación gravitatoria [109]. En este período de entusiasmo por la física y la astrofísica de estos objetos interestelares, Weber anunció la detección de radiación emanando del centro de nuestra galaxia [138, 139]. Él aseguraba que había detectado varias señales por día, aunque su afirmación no era corroborada por otras observaciones tales como las llevadas a cabo por telescopios ópticos. Sin embargo, estas noticias provocaron una oleada de nuevo interés y trabajo en radiación gravitatoria y sus fuentes astrofísicas y la construcción de una *primera generación* de detectores que trabajaban a temperatura ambiente. Todo ello ocurría pese a la considerable controversia que rodeaba las proclamas de Weber, ya que la sensibilidad de su antena era considerada suficiente sólo para detectar radiación emanando de explosiones de supernova en nuestra galaxia que, de acuerdo con sus resultados, debían ocurrir varias veces cada día en la Vía Láctea, una circunstancia increible. Además, también había desacuerdo en la forma

en que los resultados habían sido analizados, y el consenso es que en realidad el equipo probablemente no detectó radiación. Aún así, Weber es reconocido como el pionero que promovió este área de investigación con la invención de la antena resonante capaz de alcanzar una precisión revolucionaria –aunque no suficiente– del orden de $\frac{\delta l}{l} = 10^{-16}$, por debajo de un radio nuclear en una distancia de 1m. También desempeñó la importante función de alertar a los experimentales de la necesidad de acometer esta investigación y así, a finales de los 70, otros investigadores se vieron envueltos en la construcción de una *segunda generación* de antenas gravitatorias [10] que ofrecían mejor respuesta como consecuencia de importantes mejoras tecnológicas en el diseño, tales como criogenia, mayor aislamiento, o sistemas de lectura más perfecionados con transductores resonantes y amplificadores de bajo ruido basados en efectos cuánticos.

En este período de desarrollo de antenas resonantes comenzaron a surgir otros métodos de detección, tales como el seguimiento Doppler de naves espaciales o la interferometría –por ejemplo, en 1972 Forward [48] construyó el primer prototipo a pequeña escala de detector interferométrico de láser. Todas estas técnicas de detección fueron perfeccionadas en los 80 y actualmente se lleva a cabo un esfuerzo continuado como se refleja en varios proyectos ambiciosos, incluso algunos en funcionamiento [28, 111, 45][2].

Pese a todos estos esfuerzos, ningún otro experimento ha confirmado los resultados de las observaciones de Weber. Pero aún así, la existencia de las ondas gravitatorias, y también otras predicciones de la física de radiación gravitatoria, se confirmaron afortunadamente a partir del descubrimiento del pulsar binario PSR 1913+16 por Hulse y Taylor [64] en 1974. Este objeto estelar consiste en un pulsar periódico (59 milisegundos) en órbita elíptica, de periodo 2.79×10^4, alrededor del centro de masas del sistema que está formado además por una estrella de neutrones con una separación máxima de sólo 10^{11} cm ($\approx$ 1 radio solar). Cinco años de análisis de datos llevaron a la observación de cambios seculares en la órbita del pulsar, que se esperaba correspondieran a efectos de emisión de radiación gravitatoria descritos por la fórmula de radiación cuadrupolar. Más concretamente, a partir del análisis de los tiempos de llegada de las señales pulsantes se ha visto que el valor observado del decrecimiento del periodo orbital del sistema está en acuerdo con el predicho por la Relatividad General con un error[3] de aproximadamente un 1% [127, 128].

Esta indudable evidencia experimental sugiere que los resultados negativos propor-

[2]Ver sección R.2 para referencias más detalladas.

[3]En [72], los cálculos dan $\dot{\tau}_{predicted} = -2.4032 \times 10^{-12}$, mientras que $\dot{\tau}_{observed} = -2.409 \times 10^{-12}$.

cionados por las antenas gravitatorias actuales son debidos a una falta de sensibilidad en los dispositivos. El hecho es que las señales que se esperan detectar son extremadamente débiles y pueden ser fácilmente disimuladas por el ruido que emana de diversas fuentes. Por tanto, se necesita mejorar la sensibilidad. En el caso de interferómetros, el futuro prevee proyectos de gran embergadura. Para detección resonante, además de perfeccionamientos tecnológicos se plantea la cuestión de sustituir la geometría cilíndrica de las barras por la geometría esférica. Forward [47] fue el primero en reconocer que la esfera presenta una *geometría natural* para un detector resonante ofreciendo mejores capacidades de detección que las barras cilíndricas. Poco después, otros autores también se interesaron por esta idea y así, en 1975, Ashby y Dreintlein [4] estudiaron la respuesta de una esfera elástica influenciada por radiación gravitatoria. En 1977, Wagoner y Paik [133] encontraron un sistema de ecuaciones de las que se podían hallar la dirección de incidencia de la señal, y así la posición de la fuente en el hemisferio celeste, y las polarizaciones de la onda, y además demostraron que la sensibilidad de la esfera por unidad de masa es superior a la de los cilindros. Los investigadores experimentales ignoraron estos resultados hasta el comienzo de la década actual, momento en el que varios grupos en todo el mundo han comenzado a desarrollar el tema de los detectores esféricos, tanto desde el punto de vista teórico [80, 32, 84, 103] como desde el experimental [49, 69, 97].

R.1.2 Motivación

En vistas a este breve relato sobre la evolución de la investigación de la radiación gravitatoria, no se puede evitar la siguiente pregunta: ¿cuál es de hecho el objetivo final que se persigue? ¿Es la mera resolución, por otro lado desafiante, de medir cuantitativamente tan débiles perturbaciones o es posiblemente la búsqueda de una prueba experimental directa y concluyente de su realidad?

Parece ser que después del descubrimiento del pulsar binario PSR 1913+16 y de los análisis y conclusiones subsiguientes, la existencia de las ondas gravitatorias en la Naturaleza no debe ser ya un asunto polémico. Sin embargo, en ocasiones se dice que estos resultados proporcionan una prueba indirecta y el interés en construir antenas operativas se explica por la intención de obtener una evidencia directa.

No obstante, no sería correcto restringir la respuesta a una motivación tan primaria y concreta. No es en absoluto imprudente afirmar que la intención última recae en un intento de establecer los fundamentos de una nueva astronomía de ondas gravitatorias, una nueva fuente de información para la Astrofísica y la Cosmología. Es más, se cree que

provocaría una revolución en nuestro conocimiento del Universo comparable o incluso superior a la que resultó del descubrimiento de las ondas de radio y la radioastronomía, que transformó nuestra visión de un Universo sereno donde las estrellas y los planetas viajaban suavemente en sus órbitas en un escenario violento con galaxias en colisión, jets emergiendo de núcleos galácticos o quasares con luminosidades que varían en horas. Esta espectacular revolución fue posible debido a que la información que se puede obtener de las ondas de radio es muy diferente de la que proporciona la luz visible. Las diferencias son incluso mayores en la comparación entre radiación electromagnética y gravitatoria, lo que hace que una *Astronomía Gravitatoria* pueda llegar a crear una nueva y más fiable imagen del Universo.

El desarrollo de esta nueva astronomía no sólo requiere esfuerzo experimental, sino también contribuciones teóricas. Por una parte, se deben estudiar más a fondo posibles fuentes de ondas gravitatorias elaborando modelos más apropiados que determinen con mayor precisión la cantidad de radiación emitida, qué tipos de fuentes ocurren realmente y con qué frecuencia. Por otra parte, es obvio que es esencial un estudio completo de las características físicas y del comportamiento dinámico de los detectores para la correcta interpretación de la información que pueden proporcionar.

En el caso de antenas resonantes, los modelos existentes se basan en suposiciones excesivamente simplificadoras que negligen efectos relevantes. En particular, las principales simplificaciones para detectores esféricos –dejando a un lado el problema del ruido– se refieren al problema de los resonadores. La filosofía de utilizar transductores resonantes como sensores del movimiento comenzó con las barras cilíndricas. Son dispositivos que se acoplan a los modos de vibración de la antena, amplificándolos mecánicamente cuando su frecuencia de resonancia se sintoniza cuidadosamente con una del cilindro. En detectores esféricos son igualmente útiles y necesarios, con la única salvedad de que es necesario un conjunto múltiple en lugar de un único resonador para explotar sus capacidades potenciales como sistema multimodo, es decir, para obtener la máxima información sobre la dirección de incidencia de la onda y sus amplitudes. En consecuencia, la dinámica del sistema acoplado debe ser estudiada si se quiere obtener una interpretación adecuada de las lecturas o, en otras palabras, se debe resolver el problema de los resonadores. Corrientemente, el comportamiento predicho para la esfera acoplada se extrapola de los resultados para la esfera libre lo que, por ejemplo, lleva a implementaciones no válidas para las correcciones de segundo orden según la exactitud de los datos expeimentales. Y esta situación resulta ser altamente indeseable bajo la perspectiva razonable de que las antenas esféricas utilizarán en el futuro técnicas de medición extremadamente precisas,

que probablemente requieran análisis más refinados.

Por ello, nuestra intención en este trabajo es la de construir un modelo teórico más sofisticado con el objetivo de determinar la respuesta de la antena a cualquier señal interesante y con precisión ilimitada.

R.1.3 Sumario

En resumen, esta tesis presenta una cuidadosa descripción, tanto física como matemática, del comportamiento dinámico de las antenas esféricas resonantes de ondas gravitatorias cuando son excitadas por radiación gravitatoria o también por señales de calibración[4], centrando especialmente nuestra atención en el problema de los resonadores y desarrollando un procedimiento general aplicable a cualquier propuesta.

El trabajo se ha estructurado en tres partes.

La primera es una introducción que incluye los Capítulos 1 y 2. Después de los preliminares en el Capítulo 1, el Capítulo 2 comienza con una breve supervisión de la teoría de Radiación Gravitatoria según la Relatividad General, aunque los principales argumentos son también válidos para cualquier otra teoría métrica. Se deriva la ecuación de ondas en la aproximación lineal y se discuten sus soluciones de vacío –caracterizadas como ondas planas–, sus polarizaciones y su acción sobre cuerpos extensos, lo que resulta ser del mayor interés en el estudio de detectores resonantes. Las soluciones de las ecuaciones de Einstein de tipo retardado se consideran en conexión con el tema de la generación de ondas gravitatorias y radiación cuadrupolar, y también se hace referencia a algunas de sus posibles fuentes. En la segunda parte del capítulo la atención se centra en otro asunto ya clásico y que es el marco de referencia de este ensayo: la detección de ondas gravitatorias. Para establecer una perspectiva general, se describe primero el estado actual revisando las diversas técnicas de detección: seguimiento Doppler, interferometría y detección resonante especialmente con detectores esféricos. El resto de la tesis se centra exclusivamente en estos últimos.

El Capítulo 3 abre la segunda parte del trabajo. En él se desarrolla una descripción matemática del comportamiento dinámico de las antenas esféricas bajo la acción de ondas gravitatorias o también de señales de calibración. Como introducción necesaria se recogen primero algunos resultados bien conocidos sobre la esfera libre –por ejemplo el hecho de que sólo sus modos cuadrupolares y monopolares pueden ser excitados por las

[4] Este apartado se halla fuera de la línea principal de este trabajo, pero representa un caso interesante tanto desde el punto de vista experimental como teórico.

ondas gravitatorias incidentes– modelizada como un sólido elástico y homogéneo perfectamente esférico, y sobre el conjunto de resonadores que se acoplan en posiciones fijas pero arbitrarias. Estos resonadores se tratan como osciladores armónicos lineales con una frecuencia natural de resonancia cuidadosamente sintonizada a una dada del espectro de la esfera libre, lógicamente una monopolar o cuadrupolar.

El análisis del sistema acoplado comienza con el establecimiento del conjunto de ecuaciones diferenciales, las ecuaciones GRD, que describen el sistema bajo suposiciones generales: el detector es un sólido elástico sin geometría fijada, los resonadores se modelizan como osciladores armónicos lineales que se mueven radialmente, pueden no ser idénticos y se acoplan en posiciones arbitrarias, y por último la fuerza que actúa sobre el sistema es de tipo separable. Inmediatamente, el sistema se transforma en algebraico mediante transformadas de Laplace y se restringe a detectores esféricos perfectos, resonadores idénticos y fuerza de marea gravitatoria -o asociada a señales de calibración–. Su resolución proporciona las resonancias del sistema acoplado, así como las amplitudes vibracionales en las posiciones de los resonadores, aunque no se pueden obtener soluciones exactas sino que se trabaja con series perturbativas para obtener resultados a primer orden en $\eta^{\frac{1}{2}}$ –η es el cociente entre la masa de los resonadores y la masa de la esfera–. Finalmente, se discute la posibilidad de construcción de *canales de modo (mode channels)*, que son combinaciones lineales de las medidas de los resonadores directamente proporcionales a las amplitudes de las ondas gravitatorias con pesos determinados por las frecuencias acopladas.

Nuestra propuesta PHCA o la antena TIGA de Johson y Merkowitz, que se examinan en el Capítulo 4 como aplicaciones de nuestros desarrollos teóricos en el Capítulo 3, presentan distribuciones mínimas de transductores que permiten la implementación de los canales de modo. Debido a exigencias experimentales, las dos propuestas adoptan la sustitución de la esfera por un poliedro regular que la aproxima, y también sugieren configuraciones específicas de resonadores, según simetría axial o máxima isotropía respectivamente. Se ve que sus respuestas no difieren en la estructuración básica explicada por el modelo general, sino en ciertas peculiaridades particulares aunque relevantes.

Después de esta exposición del núcleo de nuestra teoría, en la tercera y última parte de la tesis emprendemos el tratamiento de dos cuestiones más: cómo pequeñas desviaciones de la situación ideal afectan las respuestas del sistema, y el problemas de la deconvlución de señales también cuando se tiene en cuenta el ruido del dispositivo. El primer tema es especialmente interesante por incrementar el grado de aplicabilidad del modelo ideal a sistemas reales. Nos centraremos en desiguladades entre resonadores, en la existencia

de una segunda frecuencia de resonancia que provoca el efecto URF, y en la rotura de simetría esférica debido a la suspensión. Estos dos últimos efectos llevan a cambios significativos con respecto al comportamiento del sistema ideal, e incluso para la antena suspendida la predicción de nuestro modelo ha sido confrontada con resultado satisfactorio con los datos experimentales obtenidos del prototipo TIGA. La deconvolución de señales es el último punto tratado en este trabajo. Se trata de determinar la dirección de incidencia de la onda, sus amplitudes y su polarización a partir de las lecturas de la antena. Se estudian los dos casos de ausencia y presencia de ruido.

La memoria se cierra finalmente con una breve discusión que resume los resultados y algunos comentarios sobre perspectivas para futuros trabajos.

R.2 Teoría y Detección de Ondas Gravitatorias

En este capítulo nos centraremos de forma más concreta en la Detección de Ondas Gravitatorias y más específicamente en Antenas Esféricas. Nuestro principal interés es el de presentar brevemente un panorama general del estado actual de la investigación sobre ondas gravitatorias, concentrándonos en los detectores resonantes para evaluar las posibilidades de las antenas esféricas. Previamente, será necesario repasar la teoría que describe y explica la radiación gravitatoria para asegurar la comprensión de resultados posteriores. Por supuesto, se pueden encontrar presentaciones más completas y extensas en obras clásicas como Kenyon [72], Wald [134] o Weinberg [140].

R.2.1 Generalidades sobre Teoría de Radiación Gravitatoria

Como se ha indicado anteriormente, las ondas gravitatorias no son exclusivas de la Relatividad General de Einstein. Entre las teorías alternativas existe una amplia clase, llamada de las teorías métricas, cuyos miembros son muy similares a la Relatividad General; de hecho ésta es en sí misma una teoría métrica al igual que las teorías de Dicke-Brans-Jordan o de Rosen [141]. Cualquier teoría métrica de la gravedad predice perturbaciones de la curvatura que se propagan con velocidad finita en el espaciotiempo transportando energía. siendo así responsables de cambios en cantidades geométricas y de las fuerzas de marea en la materia. Aquí, nos vamos a restringir a la discusión de ondas gravitatorias en Relatividad General, aunque la perspectiva y los argumentos generales son válidos para cualquier otra teoría métrica.

Nuestro propósito es ver cómo es posible encontrar soluciones radiativas de las ecua-

ciones de Einstein, que describen ondas que no transportan suficiente energía o momento como para afectar su propia propagación. Se trata de soluciones de las ecuaciones de campo linearizadas válidas para campos débiles, de manera que la métrica se puede considerar

$$g_{\mu\nu}(x) = \eta_{\mu\nu} + h_{\mu\nu}(x) \qquad |h_{\mu\nu}(x)| \ll 1, \tag{R.1}$$

donde $\eta_{\mu\nu}$ representa la métrica plana de Minkowski y $h_{\mu\nu}(x)$ es una pequeña perturbación. En esta aproximación las soluciones de vacío se pueden describir por un tensor simétrico, localmente caracterizado solamente por dos funciones debido a la inviancia gauge presente en las ecuaciones. De hecho, se trata de ondas planas transversales con dos estados de polarización. Las diferentes polarizaciones dan lugar a patrones diferentes de deformación del espaciotiempo que pueden ser analizados a partir de la ecuación de la desviación geodésica. Estas perturbaciones no sólo son capaces de cambiar cantidades geométricas como las distancias, sino que también pueden actuar como fuerzas de marea –guardando una estructura monopolar-cuadrupolar según las teorías métricas– capaces de modificar la forma de objetos materiales.

Esta propiedad es fundamental para entender el funcionamiento de los detectores masivos resonantes, que se enfrentan a la difícil tarea de tener que detectar señales extremadamente débiles que no pueden generarse de forma mínimamente apreciable en el laboratorio, como se puede deducir de las estimaciones que se obtienen a partir de la fórmula cuadrupolar que describe las contribuciones a la métrica debidas al movimiento cuadrupolar de la fuente, las más importantes ya que no existe radiación gravitatoria dipolar. Una producción medible en la Tierra requiere masas enormes que sufran dinámicas altamente no uniformes o violentas y por esta razón las ondas gravitatorias deben ser buscadas en el espacio exterior.

Sus fuentes se pueden distinguir según el tiempo de emisión en señales cortas, largas y en el fondo estocástico permanente que baña el Universo. Las más intensas son explosiones de breve duración relacionadas con sucesos astrofísicos catastróficos: estrellas que colapsan, supernovas, binarias coalescentes, etc.. Otros candidatos. tales como los pulsar, producen ondas periódicas que son superposición de sinusoides con frecuencias más o menos constantes en tiempos largos comparados con el de observación. Por último, el fondo estocástico está siempre presente con espectro contínuo. Sucesos tales como colapsos estelares en nuestra galaxia producirían las ondas que se detectarían más fácilmente. Sin embargo, ocurren raramente por lo que es inevitable buscar su procedencia en lugares más distantes.

R.2.2 Detección de Ondas Gravitatorias

Han sido varios los diferentes métodos que se han ideado para medir ondas gravitatorias. Una clasificación a *groso modo* los divide en aquellos que trabajan en el régimen de altas frecuencias, $f \geq 10Hz$, todos terrestres, los que lo hacen a bajas frecuencias, $10Hz \geq f \geq 10^{-5}Hz$, y aquellos a muy bajas frecuencias $f \leq 10^{-5}Hz$ y que deben situarse en el espacio para evitar al máximo cualquier tipo de ruido. Los primeros incluyen detectores masivos resonantes e interferómetros, aunque se ha elucubrado sobre otras posibilidades diferentes [53, 117, 2]. En el segundo grupo se incluirían como más importantes el seguimiento Doppler de naves espaciales y ambiciosos proyectos de interferometría. En el tercer caso, la detección requiere cuerpos astronómicos distantes [35, 143], aunque también son interesantes los detectores resonantes [132].

El seguimiento Doppler [17, 28] constituye el mejor método de detección a bajas frecuencias con periodos de entre unos pocos minutos y unas pocas horas. Se persiguen sensibilidades de entre $\approx 10^{-15}$ y $\approx 10^{-17}$ en el rango de frecuencias $10^{-2}-10^{-4}Hz$. Pero los interferómetros pueden mejorar estos resultados. Desde los 70 se han desarrollado algunos prototipos, por ejemplo ver [102], y varios detectores se encuentran en una fase final de construcctión: TAMA300 [71], GEO600 [88], LIGO [1] y VIRGO [23]. Además, se pretenden llevar a cabo experimentos espaciales de gran escala. Uno de ellos es el proyecto LISA [34] de la Agencia Espacial Europea.

Otra de las técnicas importantes de detección requiere el uso de antenas masivas resonantes. Weber fue el primero en construir antenas de este tipo con forma cilíndrica [136, 137]. Estas barras [130] basan su funcionamiento en la medida de los cambios de longitud asociados a oscilaciones mecánicas que pueden ser potencialmente inducidas por ondas gravitatorias incidentes. A cada antena se le acopla un único sensor en el extremo con una frecuencia natural de resonancia que coincide con la frecuencia fundamental del cilindro. Entonces, se produce una transferencia resonante de energía entre ambos, lo que provoca una amplificación pre-electrónica de las vibraciones.

Tras los primeros experimentos de Weber se construyeron otras antenas similares que también trabajaban a temperatura ambiente, como por ejemplo GEOGRAV [21]. A finales de los 70 surgió una segunda generación más perfeccionada de detectores criogénicos con la construcción del detector ALTAIR [14]. Desde 1990, estas antenas criogénicas han sido las únicas en operación y se han obtenido datos de dispositivos como EXPLORER [101, 7], ALLEGRO [93] o NIOBE [59]. Más recientemente, dos antenas ultracriogénicas han comenzado a trabajar a temperaturas tan bajas como $0.1K$. Finalmente, existe una

última antena con forma no cilíndrica adaptada para la detección de ondas provenientes del pulsar Crab [125].

La sensibilidad que han alcanzado estas antenas ronda por ejemplo $h \approx 10^{-19}$ para ondas de tipo impulsivo, pero este valor puede ser mejorado hasta $h \approx 3 \times 10^{-22}$ si la geometría cilíndrica de las barras se sustituye por la esférica.

Un detector esférico es omnidireccional, pero además la estructura de sus modos de vibración se adapta perfectamente a la estructura del tensor de Riemann de una métrica general, de forma que una onda gravitatoria sólo puede excitar sus modos esferoidales monopolares o cuadrupolares, con amplitudes directamente proporcionales a las amplitudes de la onda [80, 11]. Un único detector se erige así en un sistema multimodo, capaz de proporcionar información sobre la dirección de incidencia de la onda, sus amplitudes o su polarización [133, 90]. Incluso presenta mayor sensibilidad no sólo al primer modo cuadrupolar sino también al segundo, y una sección eficaz superior a la de las barras [133].

R.3 Antenas Esféricas

Como sistema multimodo, un detector esférico requiere todo un conjunto de sensores unidos a su superficie en posiciones adecuadas. Estos sensores transforman las oscilaciones en señales eléctricas que después amplifican, pero se da una conveniente amplificación mecánica previa obtenida por el acoplamiento resonante de sus constituyentes mecánicos denominados resonadores. No todo son ventajas; resulta que éstos ejercen un efecto de retroacción en la esfera que no es negligible en el estudio de la estructura fina del sistema. Un análisis completo del dispositivo acoplado, en otras palabras, la resolución del problema de los resonadores, es por ello esencial para la correcta interpretación de las lecturas de la antena.

En este capítulo presentamos este análisis con rigor y obtenemos una elegante descripción del comportamiento físico de las antenas esféricas resonantes a partir de un robusto esquema matemático basado en el formalismo de las funciones de Green, las transformadas de Laplace, y desarrollos perturbativos. Más específicamente, se obtiene el espectro de frecuencias y las amplitudes de vibración en las localizaciones de los resonadores con precisión teórica ilimitada. A partir de éstas se construirán los *canales de modo* que facilitarán la deconvolución de las señales, típicamente ondas gravitatorias aunque también son interesantes las señales de calibración.

Como paso preliminar, se recuperan algunos resultados bien conocidos sobre la esfera libre y se explica la modelización de los resonadores.

R.3.1 La Esfera Libre

Cualquier sólido elástico presenta vibraciones periódicas características cuando no está sujeto a fuerzas externas o tracciones en su superficie. Estos movimientos reciben el nombre de modos normales de vibración, y son los ingredientes para construir la respuesta del cuerpo a la influencia de una fuerza externa general como por ejemplo las fuerzas de marea gravitatorias.

El estudio de estos modos naturales para cuerpos esféricos es un tema clásico [68, 75, 80, 97, 103] en la teoría clásica de la elasticidad [78]. Se dividen en dos familias: modos esferoidales y modos toroidales, cada uno de ellos dependiendo de armónicos esféricos y funciones de Bessel y caracterizado por un triple subíndice $\{nlm\}$. Para cada uno de éstos con n fija existe un único modo monopolar con $l = 0$, mientras que si $l = 2$ existen 5 modos cuadrupolares degenerados en frecuencia.

El formalismo de las funciones de Green permite expresar la reacción de la esfera libre a una fuerza externa en base a estos modos normales. Para fuerzas gravitatorias de marea que interaccionan con sólidos esféricos homogéneos y elásticos [103, 24, 25. 60, 94, 106, 122] -admitiendo que no van a ocurrir movimientos relativistas a las frecuencias típicas esperadas de $1KHz$ y trabajando en el sistema localmente newtoniano adecuado si las dimensiones del detector son pequeñas en comparación con la longitud de onda de la señal- se demuestra que la respuesta sólo depende de los modos esferoidales con precisamente $l = 0$ y $l = 2$, con amplitudes directamente proporcionales a las amplitudes correspondientes de la onda incidente [80, 103], de manera que la geometría esférica se erige en particularmente conveniente para detectores masivos resonantes. En contraste, la respuesta a una señal de calibración impulsiva involucra todos los modos excepto los perpendiculares a la fuerza [80].

R.3.2 Los Resonadores

Los resonadores constituyen la parte mecánica de los sensores, compuestos básicamente por un transductor que transforma las señales en eléctricas y un amplificador. Los resonadores deben ser diseñados para poseer una frecuencia característica idealmente idéntica a una del espectro de la esfera libre. El acoplamiento producirá en este caso un efecto de resonancia, que resultará en una amplificación mecánica pre-electrónica de las vibra-

ciones. Se considera que estos resonadores son únicamente libres para moverse en la dirección radial, y se modelizan como osciladores armónicos lineales, por ejemplo formados por masas puntuales al extremo de un muelle. Por último, hay que señalar que son mucho más ligeros que la esfera, de manera que el parámetro adimensional $\eta \equiv \frac{m_{resonadores}}{M_{esfera}}$ es pequeño , $\approx O(10^{-4})$.

R.3.3 Detectores Esféricos y el Problema de los Resonadores

El estudio del problema de los resonadores parte del establecimiento del conjunto de ecuaciones generales GRD que describe el sistema acoplado bajo la acción de una fuerza general de tipo separable, y que se plantea en un principio para cualquier geometría del detector y cualquier configuración de J resonadores idealmente sintonizados a una única frecuencia ω_{NL} de la esfera libre.

Mediante la aplicación de la teoría de las funciones de Green, las ecuaciones GRD en derivadas parciales se transforman en un sistema integro-diferencial, del que se obtiene finalmente un sistema de J ecuaciones lineales algebraicas por transformación de Laplace.

R.3.4 Aproximación Ideal: Esfera Perfecta y Resonadores Idénticos

Este último sistema se resuelve en el caso ideal de una esfera pefecta con resonadores idénticos en masa y frecuencia de resonancia. Se puede entender que estos resonadores causan una perturbación con respecto al comportamiento de la esfera libre provocando la correlación entre las deformaciones de la esfera y todos sus modos normales esferoidales. Este hecho se refleja en las ecuaciones a través de un término introducido por la pequeña constante de acoplamiento adimensional η. Esto va a permitir el desarrollo de series perturbativas para las soluciones, que por otra parte no se pueden obtener de forma exacta.

Estas soluciones proporcionan las frecuencias propias del sistema acoplado así como las amplitudes de las deformaciones elásticas de los resonadores, las únicas cantidades medibles. Con respecto a las frecuencias, se observa que la presencia de los J resonadores afecta la estructuración de todo el espectro de la esfera libre, de manera que en principio aparecerán generalmente J dobletes de frecuencias simétricamente distribuidas alrededor de la frecuencia de resonancia ω_{NL} -aunque de hecho serán a lo sumo $2L+1$ los pares fuertemente acoplados a orden $\eta^{\frac{1}{2}}$- y J singletes desplazados por cada una de las restantes ω_{nl}.

La tarea del cálculo de las amplitudes es mucho más laboriosa y requiere la inversión de las transformadas de Laplace que se habían llevado a cabo, lo que a su vez necesita de la aplicación del cálculo de resíduos. Previamente, es conveniente fijar el tipo de fuerza que actúa sobre la antena. Si corresponde a ondas gravitatorias monopolares y los resonadores se sintonizan precisamente a una frecuencia también monopolar ω_{N0}, ocurre que las respuestas de todos los resonadores son iguales ya que el comportamiento dinámico de éstos es el mismo por la simetría esférica de las oscilaciones monopolares de la esfera. Un único resonador será suficiente en este caso. En cambio, para detectar radiación cuadrupolar serán necesarios al menos cinco resonadores con lecturas independientes acoplados a una frecuencia cuadrupolar ω_{N2}. En ambos casos, se da la presencia de un factor de amplificación $\eta^{-\frac{1}{2}}$, y sólo es relevante la contribución de los modos sintonizados que estén fuertemente acoplados; el resto contribuirá a órdenes superiores. Además, la composición espectral de estas amplitudes está dominada por las frecuencias acopladas correspondientes. Para finalizar, se observa que cuando se expresan en el espacio del tiempo tras realizar la transformada de Laplace inversa, estas amplitudes son de hecho pulsos, es decir, sinusoides de frecuencia igual a la frecuencia de resonancia y amplitud modulada por una nueva frecuencia que depende de hecho de las que surgen alrededor de ésta después del acoplamiento.

Los resultados para señales de calibración son totalmente análogos y se obtienen siguiendo estrictamente los mismos procesos.

Por último, para ciertas distribuciones de resonadores se pueden realizar determinadas combinaciones lineales de las amplitudes, cada una de ellas directamente proporcional a una única amplitud del campo gravitatorio. Los primeros en obtenerlas fueron Johnson y Merkowitz en el estudio de su propuesta TIGA [69, 97], y las llamaron canales de modo, (*mode channels*). Su existencia es muy ventajosa ya que su utilización simplifica notablemente los métodos de deconvolución. Hay dos configuraciones con un número mínimo de resonadores que cumplen los requisitos de existencia y permiten la implementación de canales de modo, aunque realmente no son las únicas. Estas dos distribuciones son la base para las propuestas de antena esférica PHCA y TIGA que se estudian en el próximo capítulo.

R.4 Configuraciones Específicas de Resonadores

Vamos a estudiar dos propuestas particulares sobre antenas esféricas, con resonadores fijados en posiciones específicas que permiten la implementación de canales de modo. El núcleo de la antena se sustituye por un poliedro regular que aproxima la esfera perfecta para evitar así complicaciones técnicas como las relacionadas con el montaje y la estabilidad de los resonadores. Presentamos primero nuestra propia propuesta PHCA.

R.4.1 Propuesta PHCA

Para la detección de radiación cuadrupolar se requieren al menos cinco resonadores en posiciones no paralelas. Dado que más de cinco producirían información redundante y complicarían más la resolución de las ecuaciones GRD, nos limitamos a este número y los distribuimos alrededor de un eje según una simetría pentagonal: los resonadores se hallan en el mismo plano marcado por un cierto paralelo y separados cada dos consecutivos por 72°. Estas distribuciones pentagonales muestran un espectro acoplado alrededor de la frecuencia de resonancia ω_{N2} que se distribuye en tres dobletes diferentes, dos de ellos doblemente degenerados, y amplitudes que se acoplan selectivamente a estas diferentes frecuencias de manera que la inspección del espectro ya informa sobre qué amplitudes están presentes.

Los resonadores se montan sobre un hexacontaedro pentagonal. Este es un cuerpo regular convexo de sesenta caras iguales no paralelas con forma de pentágono irregular. Este poliedro encierra una esfera inscrita –siendo la relación de volúmenes de 1.057– tangente en un punto de confluencia a cada cara, lugar en el que los resonadores deben ser acoplados. De entre las distribuciones pentagonales compatibles con la geometría de este poliedro, se elige aquella que mantiene los pares de frecuencias acoplados más equitativamente espaciados para mantener la estructura espectral máximamente diferenciada.

Así que, en definitiva, proponemos la antena PHCA formada por un hexacontaedro pentagonal como núcleo del detector acoplado a una distribución pentagonal alrededor de una eje de simetría con 5 resonadores montados en las caras cuyos puntos de confluencia corresponden al ángulo polar $\Theta = 67.617°$.

Es más, esta antena puede ser sensible no sólo al primer modo cuadrupolar ω_{12}, sino también al segundo ω_{22} –debido a que la esfera posee una sección eficaz interesante también a esta frecuencia– e incluso a radiación monopolar. Por ello proponemos un segundo conjunto de resonadores sintonizados a esta nueva frecuencia ω_{22} distribuidos

una vez más según simetría pentagonal en una posición suplementaria a la primera. Para completar, se puede añadir un onceavo sensor a la frecuencia ω_{10} para la detección de radiación monopolar. Se comprueba que los diferentes grupos de resonadores no interaccionan entre sí.

Un detector esférico como el descrito con 11 resonadores es un dispositivo multifrecuencial y multimodo sin precedentes en cuanto a capacidades como antena indiviual.

R.4.2 Propuesta TIGA

Stephen Merkowitz and Warren Johnson fueron los primeros en sugerir un diseño específico para la construcción de una antena esférica de ondas gravitatorias, TIGA [69, 97, 95, 98].

Se trata de un conjunto de 6 resonadores montados sobre un icosaedro truncado. El icosaedro truncado es un poliedro con una esfera circunscrita asociada –la relación de volúmenes es 1.153– de 32 caras, 20 de ellas hexágonos regulares y 12 pentágonos formando 6 pares de caras paralelas. Merkowitz y Johnson precisamente propusieron los centros de 6 de estas caras no paralelas, también interesantes por ser las posiciones de los centros de la mitad de las caras de un dodecaedro convenientemente orientado.

Encontraron que su distribución simplificaba máximamente el espectro de frecuencias: sólo se obtienen un par quíntuplemente degenerado y un singlete a la frecuencia de resonancia débilmente acoplado. La distribución TIGA es la mínima configuración con tal degeneración, aunque no es única en este sentido [91]. Esta degeneración se hace también extensiva a las expresiones de las seis amplitudes, todas idénticas, y a los cinco canales de modo, todos ellos con el mismo peso frecuencial.

R.4.3 Un Ejemplo Simple: Respuestas a Señales de Calibración

Una forma simple de contrastar los resultados para ambas propuestas PHCA y TIGA es estudiar sus respuestas a señales particularmente simples, como lo son las señales de calibración de tipo impulsivo, lo que reflejará las características más relevantes de las dos configuraciones.

Los resultados muestran que la diferencia fundamental es que las respuestas PHCA son superposiciones de tres pulsos distintos –el espectro de frecuencias contiene tres pares de picos como se ha comentado anteriormente–, en contraste a la componente única para TIGA. Ademaás, los canales de modo para la antena PHCA son cada uno de ellos pulsos simples, pero con diferentes frecuencias de modulación cada uno, mientras

que las frecuencias de modulación de los pulsos simples en el caso TIGA son siempre iguales. Así que los canales de modo son siempre pulsos puros con espectros que contienen pares de picos individuales a las frecuencias que surgen del acoplamiento resonante. Se puede interpretar que la antena PHCA da lugar a una especie de efecto Zeeman de las frecuencias degeneradas de la antena TIGA, lo que se puede atribuir a una rotura axisimétrica del carácter isotrópo de esta última distribución.

R.5 Desviaciones Respecto a la Aproximación Ideal

Nuestro modelo se ha construido para explicar la dinámica de esferas perfectas acopladas a una distribución de resonadores idénticos, idealmente montados en su superficie en posiciones exactas y teóricamente sintonizados a una única frecuencia del espectro de la esfera libre.

Estas son ciertamente suposiciones no muy realistas, por lo que el estudio de los efectos que pequeñas desviaciones de esta situcaión ideal producen en el comportamiento de la antena supone una extensión natural de este trabajo que aumentaría de hecho su aplicabilidad a sistemas reales.

Como vamos a ver, esta evaluación revelará que el sistema es en efecto robusto con respecto a algunas de estas imperfecciones, lo que también ha sido referido en otros trabajos [121, 98], pero sin embargo existen dos casos que merecen especial atención ya que muestran cambios significativos con respecto a la dinámica ideal: la existencia de una segunda frecuencia de la esfera libre $\omega_{N'L'}$ cercana a la frecuencia de resonancia ω_{NL}, y la rotura de simetría esférica debida a la suspensión.

En todos los casos, hay que buscar una parametrización adecuada que describa estas pequeñas divergencias. La clave está en aceptar que si la diferencia entre el valor real de un cierto parámetro y su valor ideal es a priori de orden $\eta^{\frac{1}{2}}$ o superior, el sistema puede quedar afectado por esta diferencia, mientras que si la diferencia es apreciablemente menor el sistema será robusto frente a la desviación al orden dominante, lo que constituye una parametrización consistente con la expansión de nuestras soluciones en series de potencias de $\eta^{\frac{1}{2}}$.

Desarrollemos estas ideas en algunos casos interesantes.

R.5.1 Acoplamiento No Ideal de los Resonadores

En esta sección se estudian desviaciones en tres parámetros referidos a las características y situación física de los resonadores. Primeramente, se examina la situación en la que las posiciones reales de los resonadores se hallan muy cercanas a las localizaciones ideales pero no son exactamente éstas. En segundo lugar, se toleran diferencias entre las masas de los resonadores. En ambos casos, las desviaciones se piensan a orden $\eta^{\frac{1}{2}}$ y es fácil corroborar que el sistema resulta ser robusto en sus funciones características a primer orden.

También se evalúan diferencias a este mismo orden entre las frecuencias naturales de los resonadores. Para éstas, resulta que se deberían apreciar cambios significativos al orden dominante en el espectro de frecuencias del sistema. Sin embargo, es aquí la propia suposición de partida que asume diferencias de orden $\eta^{\frac{1}{2}}$ la que no es realista, al menos para resonadores en transductores capacitativos. Estos errores se asumen inferiores, orden η o superior, por lo que estos pequeños cambios tampoco serán relevantes.

R.5.2 Sintonización No Aislada: el Efecto URF

En constraste a lo analizado hasta ahora, el sistema sí resulta ser sensible a la presencia de una segunda frecuencia $\omega_{N'L'}$ cercana a la de resonancia ω_{NL}. Como siempre, el grado de cercanía debe ser de orden $\eta^{\frac{1}{2}}$, lo que ocurre por ejemplo entre la frecuencia ω_{14} y la segunda frecuencia cuadrupolar ω_{22}, que resulta ser adecuada como frecuencia de resonancia a la que se pueden sintonizar los resonadores. Por ello, los efectos que pueden ser inducidos por esta vecindad, llamados efectos URF, deben ser cuidadosamente determinados para conseguir una descripción acertada del comportamiento real del detector.

Un nuevo examen de las cantidades características de las antenas teniendo en cuenta la proximidad entre $\omega_{N'L'}$ y ω_{NL} deriva en una nueva imagen del espectro de frecuencias acoplado. Para una configuración general de resonadores, resulta que los dobletes simétricos alrededor de ω_{NL} se transforman en tripletes con una, dos o tres frecuencias fuertemente acopladas –tripletes $scS+wcD$, $scD+wcS$ y scT respectivamente–. Ocurre que de las tres componentes una, la *frecuencia central*, se encuentra muy cercana a la frecuencia de resonancia, mientras que el par restante se distribuye de forma no simétrica a su alrededor.

Esto se demuestra en particular para las antenas TIGA y PHCA en las frecuencias ω_{22} y ω_{14}. Sus tripletes contienen una frecuencia central que está realmente cerca de la de resonancia, esto significa a una distancia de orden $\eta^{\frac{1}{2}}$ o incluso menor, por lo que una

reproducción del proceso de cálculo de resíduos que determine las amplitudes de vibración demostraría que las contribuciones de estos modos son a órdenes superiores, de forma que se catalogan como débilmente acoplados. El resultado es que los tripletes son de tipo $scD+wcS$. El par restante imita los dobletes del caso ideal, aunque la estricta simetría que presentaban aquellos se rompe, de manera que es justamente la frecuencia por debajo de la de resonancia ω_{22} la mayor en valor absoluto, siendo mayor esta asimetría cuanto mayor es la masa de la antena. Teniendo en cuenta además que la frecuencia central también es menor que ω_{22}, parece obvio que los tripletes en su conjunto están afectados por el hecho de que ω_{14} es menor que ω_{22}. Se puede entender entonces que cada grupo de frecuencias ideales ha sufrido un desplazamiento que la acerca a ω_{14} y este efecto de arrastre es más importante para las frecuencias más cercanas a ésta.

En resumen, el efecto URF es un efecto de arrastre hacia $\omega_{N'L'}$ que rompe la simetría de los dobletes ideales e induce la aparición de una tercera componente cercana a ω_{NL} y por lo general débilmente acoplada.

El análisis de este efecto es relevante por sí mismo en un estudio completo de cualquier antena esférica, pero es especialmente relevante para la antena PHCA. La razón es que como se ha explicado ya, esta propuesta sugiere un segundo conjunto de resonadores sintonizados precisamente a la frecuencia ω_{22}, de forma que sin la determinación de las consecuencias del efecto URF no podríamos dar una imagen correcta del comportamiento del detector. En particular, vemos que para el espectro de resonancia tendremos en realidad un primer grupo de tres pares simétricos de frecuencias, dos de ellos doblemente degenerados. alrededor de ω_{12} y un segundo grupo de tres tripletes diferentes del tipo $scD+wcS$ y que mantienen la degeneración alrededor de ω_{22}.

R.5.3 Suspensión de la Esfera y Simetría Axial

La última situación que se aparta de la ideal y que se estudia aquí es la rotura de simetría esférica por la suspensión necesaria de la antena en observatorios terrestres.

El mecanismo de suspensión requiere la realización de una perforación a lo largo de un diámetro de la esfera. Como resultado de esta manipulación, la simetría esférica inicial se transforma en simetría axial de la esfera perforada y así de la esfera suspendida. La consecuencia inmediata es que todas las frecuencias de la esfera libre pierden su degeneración dividiéndose en multipletes ω_{nlm}, con $m = -l, \ldots, l$. La cuestión ahora es cómo sintonizar los resonadores. Siguiendo la filosofía de parametrización de todo el capítulo, se puede pensar que la frecuencia natural que los caracteriza se encuentra en la

banda marcada por unas ciertas N y L, con diferencias a las distintas componentes ω_{NLm} que son de orden $\eta^{\frac{1}{2}}$ como siempre. El espectro de frecuencias de la esfera suspendida y acoplada también cambia. Se obtienen $2L + 1 + J$ frecuencias alrededor de la de resonancia, con un número máximo de $2(2L + 1)$ modos fuertemente acoplados.

Cuando estas consideraciones se aplican al prototipo TIGA de Johnson y Merkowitz, para un acoplamiento en la banda ω_{12m} se predicen 11 frecuencias no degeneradas alrededor de la frecuencia natural de los resonadores, de las que 10 corresponderán a modos fuertemente acoplados, una imagen muy diferente de la asociada a la antena no suspendida que presentaba degeneración máxima. La comparación de los resultados numericos teóricos para estas frecuencias y las medidas en TIGA muestran un notable acuerdo, con un error de a lo sumo un 0.2%, siendo en general del 0.1%. Se puede decir que las discrepacias entre la teoría y el experimento son de orden η, un resultado que respalda la validez de nuestro modelo. También se corrobora que el modo débilmente acoplado tiene una amplitud prácticamente nula, en excelente acuedo con nuestras predicciones teóricas sobre estos modos.

Para acabar, hay que subrayar que la consideración de estimaciones de correcciones de orden superior no mejora el acuerdo con las cantidades medidas debido a que las propias condiciones experimentales ya incluyen niveles de tolerancia. No obstante, la necesidad de dicha evaluación cercerá a medida que lo haga el control y la precisión del experimento.

Este efecto de suspensión tiene menos impacto en nuestra antena PHCA, dado que la distribución de resonadores mantiene simetría axial. Si el eje de simetría y el de suspensión coinciden, el esquema de frecuencias de resonancia de la esfera suspendida mantiene la degeneración de las estructuras del sistema no suspendido, una indicación de que las configuraciones pentagonales se adaptan naturalmente a la suspensión convirtiéndose en alternativas a considerar frente a propuestas más simétricas.

R.6 Deconvolución de Señales

El propósito de un experimento de detección no es simplemente la mera corroboración de la ocurrecia del fenómeno físico que se examina, sino también la adquisición de la máxima información con respecto a éste y sus causas.

De acuerdo a esta filosofía, uno debe ser capaz de manipular convenientemente las lecturas que se obtienen de las vibraciones de una antena esférica para determinar las

causas y sus propiedades. Esto es lo que comúnmente se conoce como *problema inverso o deconvolución* [133, 80, 91], cuya resolución debe proporcionar la dirección de incidencia de la onda gravitatoria, sus amplitudes y su polarización.

Vamos a tratar aquí este problema en el supuesto de que no conozcamos ninguna información sobre la fuente por vías externas y ni siquiera podamos admitir ninguna hipótesis sobre su naturaleza. Así que nos enfrentamos a la situación de deconvolución más desfavorable.

Veamos cómo se resuelve este asunto tanto para antenas sin ruido como para detectores ruidosos. En ambos casos, el procedimiento se centra en el álgebra lineal.

R.6.1 Deconvolución de Señales en Ausencia de Ruido

La resolución del problema inverso para una antena esférica ruidosa fue primeramente tratada por Wagoner y Paik a mediados de los 70 [133]. Más recientemente, en 1988, Dhurandar y Tinto publicaron un tratamiento para barras e interferómetros [37] que ha sido después adaptado por varios autores al caso de detectores esféricos [144, 90, 92], para los que se han propuesto también procedimientos más generales [80].

Recordamos que los canales de modo son combinaciones lineales de las lecturas de los resonadores que resultan directamente proporcionales a las amplitudes cuadrupolares de la onda incidente. Por ello, si suponemos ausencia de ruido en los dispositivos, podemos reconstruir en el sistema de referecia del laboratorio, con eje z en su vertical, el tensor cartesiano de desviaciones de la métrica H, que describe la señal y codifica toda la información relevante acerca de la onda, directamente de los canales de modo ya que H coincide en este caso con la matriz respuesta del detector A.

La expresión de este tensor en el sistema de referencia de la onda, cuyo eje vertical coincide por definición con la dirección de propagación de la misma, adquiere su forma canónica que claramente explicita el hecho de que H posee un valor propio nulo con vector propio asociado precisamente en aquella dirección. Por tanto, y debido a que los valores propios no se modifican en un cambio de base, la dirección de incidencia de la onda en el sistema del laboratorio vendrá simplemente dada por el vector propio de H asociado a su valor propio cero.

En cuanto a la amplitud de la onda, se puede definir a partir de los dos valores propios restantes como su valor absoluto que es igual para ambos.

Y finalmente, hay que tratar de averiguar el ángulo y las amplitudes de polarización de la onda. Este problema se ha resuelto a partir de relacionar los elementos del tensor

H en los dos sistemas mencionados hasta ahora [96], asumiendo el criterio $\alpha = 0$ [133] para fijar sin ambiguedad el sistema de la onda. Este criterio se basa en la propiedad de invarianza de la forma canónica de H en el sistema de referencia de la onda bajo rotaciones de ángulo α alrededor de la dirección de incidencia.

Existe una forma alternativa que sigue la tónica de trabajar con los valores y vectores propios de H. Para empezar, mantenemos el mismo criterio $\alpha = 0$ que tiene una interpretación geométrica: el eje y del sistema de la onda está situado sobre el plano x-y del sistema del laboratorio. Podemos expresar las amplitudes de polarización en función de la amplitud de la onda, que se tomaba como el valor absoluto de los dos valores propios no nulos, y del ángulo de polarización, que resulta ser el doble del ángulo de rotación que sitúa el segundo vector propio de H sobre el plano x-y del laboratorio o el doble del ángulo entre los ejes de polarización de la onda y los vectores propios perpendiculares a la dirección de incidencia.

Si por casualidad la onda se propagara en la dirección vertical del laboratorio, el ángulo de polarización no podría ser determinado. Ésto no es un problema intrínseco de la deconvolución. sino de la parmetrización con una definición anómala del ángulo acimutal asociado a la dirección del eje z.

R.6.2 Deconvolución de Señales en Presencia de Ruido

El problema inverso en presencia de ruido es mucho más complejo, ver por ejemplo [144, 55], y las soluciones hasta ahora se solían buscar de forma numérica.

Aquí mostramos que también se puede resolver analíticamente mediante álgebra lineal [96, 99], partiendo de un modelo muy simplificado para el ruido del sistema [97, 124]. Se trata de identificar los canales de modo como variables aleatorias independientes con distribuciones gausianas centradas en los valores del sistema sin ruido. Ahora, el tensor H no coincidirá ya exactamente con la matriz respuesta del sistema A construida a partir de la información que proporciona la antena. pero podemos continuar aplicando una versión modificada de los procedimientos anteriores. Sus valores propios y vectores propios serán también variables aleatorias, si bien no tienen porque ser gausianos. En todo caso, se pueden calcular sus valores esperados y varianzas, que como siempres se expresan como desarrollos perturbativos, aquí en series de potencias de la varianza de los canales de modo o del SNR.

Como ya indicaron Dhurandhar y Tinto, el vector propio de A con valor propio más cercano a cero será el que mejor aproxime la dirección real de incidencia de la

onda. Por supuesto, la determinación de esta dirección conlleva un error asociado que se puede dar en función de su ángulo sólido, y que en nuestros cálculos resulta libre de parametrizaciones inadecuadas , independiente de la dirección de incidencia como se podía esperar de una antena omnidireccional, y además en acuerdo con las estimaciones de otros autores [144].

Esta isotropía también esá presente en la estimación de la amplitud de la onda, que se obtiene de la semidiferencia de los valores propios restantes como mejor aproximación [96].

El punto polémico está en la valoración del ángulo y las amplitudes de polarización ya que, en base a métodos que utilizan parametrizaciones según ángulos de Euler, algunos autores hallan una descripción no isotrópa para las varianzas de estas cantidades. Nosotros las hemos recalculado partiendo de la idea de que el ruido induce fluctuaciones en el ángulo de polarización a través de su definición a partir de los vectores propios. En el caso más simple con distribuciones uniformes, los cálculos revelan que los errores en la polarización y sus cantidades asociadas crecen cuando la dirección de incidencia se acerca al eje vertical del laboratorio, mostrando incluso divergencias o indeterminaciones si las dos direcciones pueden ser confundidas, situación que claramente se delimita en los propios cálculos y que corresponde a la confusión del segundo vector propio con el plano x-y del laboratorio. Así, se ve que estos errores efectivamente dependen de la dirección de incidencia de la onda, y que el problema reside en última instancia en que el criterio $\alpha = 0$, que de hecho fija el ángulo de polarización en el sistema sin ruido y que se admite también en el caso ruidoso y es un criterio fuertemente dependiente del obsevador. Este decreto está rompiendo de alguna manera una simetría presente en el sistema al que se esperarían asociar cantidades isótropas. Entonces, se debe deducir que tal criterio no es adecuado para describir la sitaución física real que debe ser independiente del observador. La forma inmediata de superar esta aparente paradoja es introducir información o hipótesis externas sobre la naturaleza de la fuente de las ondas.

R.7 Conclusiones

R.7.1 Principales Resultados

1. El desarrollo de un marco matemático riguroso para la descripción física de antenas esféricas resonantes ha constituido el núcleo de nuestra investigación, que presenta un esquema teórico para el tratamiento del sistema de ecuaciones GRD aplicable

a un detector sólido elástico de cualquier geometría acoplado a un conjunto de resonadores radiales en posiciones arbitrarias y que pueden diferir en masa y frecuencia de resonancia y que se sintonizan justo a una única frecuencia ω_{NL} del espectro de la esfera libre.

- Nos hemos restringido al caso ideal de un detector perfectamente esférico acoplado a una distribución arbitraria de J resonadores idénticos acoplados a la frecuencia ω_{NL} para resolver el sistema de ecuaciones y determinar las respuestas del sistema a una onda gravitatoria incidente. Las soluciones se escriben como series perturbativas en potencias ascendentes de la pequeña constante de acoplamiento $\eta^{\frac{1}{2}}$, donde $\eta = \frac{m_{resonadores}}{M_{esfera}}$.
- Obtenemos el espectro de frecuencias del sistema acoplado al orden dominante. Se estructura en J pares $\omega_{a\pm}$ –aunque a lo sumo sólo $2L+1$ de ellos serán pares fuertemente acoplados– que derivan de la frecuencia de sintonización ω_{NL} y están simétricamente distribuidos a su alrededor. También se consiguen las amplitudes a partir de las deformaciones asociadas a los osciladores que modelizan los resonadores. Estas amplitudes conllevan un factor de amplificación de orden $\eta^{-\frac{1}{2}}$, y tienen una composición espectral dominada por los pares de frecuencias $\omega_{a\pm}$.
- También demostramos cómo bajo ciertos requisitos sobre la distribución de resonadores estas amplitudes pueden ser ordenadas en ciertas combinaciones lineales, los *canales de modo (mode channels)*, cada uno acoplado a un único modo de la esfera libre y por ello a una única amplitud del campo gravitatorio.
- Los desarrollos no sólo permite investigar las respuestas a ondas gravitatorias, sino también a otros agentes externos tales como señales de calibración. Éstas son interesantes debido a que constituyen un ejemplo simple que refleja todas las características principales del sistema y que también se asocian a las respuestas a señales gravitorias.

2. Nuestro modelo permite:

- El análisis e incluso la sugerencia de cualquier propuesta particular de antena esférica con resonadores fijados en posiciones específicas. Tan sólo será necesario calcular los valores y los vectores propios asociados a la distribución, que son las cantidades que determinan las características distintivas y particulares del espectro acoplado, de las amplitudes y de los canales de modo.

Entonces, no sólo es posible reconsiderar propuestas ya existentes, como la TIGA de Johnson y Merkowitz, sino lo que es más, nosotros presentamos una propuesta alternativa basada en distribuciones pentagonales que mantienen simetría axial. Nuestra antena PHCA se piensa como un sistema multimodo y multifrecuencial, para lo que proponemos dos grupos de distribuciones pentagonales suplementarias respectivamente sintonizadas a la primera y a la segunda frecuencia armónica cuadrupolar para explotar al máximo las posibilidades del detector. Un onceavo resonador sintonizado a la primera frecuencia monopolar se añade también para percibir radiación monopolar.

- La implementación de suposiciones más realistas que llevan a la investigación de desviaciones en los detectores ideales perfectos.

  Nuestro modelo ha resultado ser suficientemente flexible como para ser válido en el estudio de pequeños defectos, de este modo incrementándose su grado de aplicabilidad a sistemas reales, a partir de una parametrización útil para una amplia clase de desviaciones en consistencia con nuestras expansiones perturbativas y su precisión, de forma que hemos sido capaces de tratar la cuestión de si el sistema es afectado o no por estas violaciones de la situación ideal.

  Las evaluaciones revelan que la respuesta de la antena es robusta con respecto a algunas de estas imperfecciones: desviaciones en las posiciones de los sensores o desigualdades en sus masas o sus frecuencias naturales.

  En cambio, la existencia de una segunda frecuencia $\omega_{N'L'}$ cercana a la frecuencia de resonancia ω_{NL} afecta apreciablemente las respuestas del sistema incluso a primer orden. Esto constituye el efecto URF. Su análisis para las propuestas PHCA y TIGA demuestra que provoca un efecto de arrastre que rompe la simetría original de los dobletes ideales, y además induce la aparición de una tercera componente débilmente acoplada y cercana a la frecuencia de resonancia ω_{NL}. Este efecto resulta ser muy importante para la antena PHCA, ya que en ella se incluye una segunda distribución de resonadores sintonizados a la segunda frecuencia cuadrupolar de la esfera libre, que se halla realmente cerca de otra frecuencia del mismo espectro. En esta situación, el estudio del efecto URF permite describir correctamente el espectro completo de la antena PHCA, compuesto por dos grupos de pares de frecuencias fuertemente acopladas, el primero simétricamente repartido alrededor del primer armónico

cuadrupolar, mientras que el segundo surge como una división no simétrica del segundo armónico cuadrupolar.

La rotura de simetría esférica debido a la suspensión también induce cambios significativos en relación al comportamiento ideal. El contraste de las predicciones espectrales de nuestro modelo con datos experimentales del prototipo TIGA ha demostrado un acuerdo satisfactorio bajo las condiciones reales de experimentación.

3. Finalmente, somos capaces de tratar convenientemente las respuestas del sistema para extraer información acerca de la onda gravitatoria incidente. Esto constituye el llamado problema inverso o problema de la deconvolución, y demostramos que es resoluble algebraicamente incluso si se considera ruido en el sistema.

   Cuando se obvia la presencia de ruido, la dirección de la onda incidente, sus amplitudes y su polarización se obtienen de los valores y los vectores propios de la matriz respuesta construida de los canales de modo.

   Para la antena ruidosa, una versión modificada de los desarrollos anteriores da errores isotrópos para la dirección de incidencia y la amplitud de la onda como se puede esperar de un detector esférico. Por el contrario, los errores en el ángulo de polarización y sus amplitudes de polarización son aparentemente anisotrópos. Analizamos esta circunstancia y encontramos que tales dependencias direccionales surgen como consecuencia de la rotura de simetría que introduce el criterio $\alpha = 0$ comúnmente asumido y que fija el sistema de referencia de la onda. También presentamos una interpretación geométrica que permite una discusión más clara y nos lleva a concluir que se debe obtener alguna información externa o se debe asumir alguna hipótesis con respecto al tipo de fuente de las ondas si se persiguen resultados isotrópos para las cantidades relacionadas con la polarización.

R.7.2 Trabajo Futuro

Se planea estudiar al menos dos cuestiones más como extensiones naturales del trabajo teórico presentado en este ensayo.

La primera de ellas deriva directamente de los desarrollos matemáticos perturbativos que se han expuesto. Recordamos que nuestras soluciones no son exactas, sino que son aproximaciones dominantes en series de potencias ascendentes de $\eta^{\frac{1}{2}}$. Si en el futuro se necesitara mayor precisión en las comparaciones con las medidas experimentales o

se pretende un estudio teórico completo se deben calcular los términos de orden superior. La valoración correcta de tales correcciones no es en absoluto una tarea fácil como pudiera parecer a primera vista, y de hecho puede involucrar otras importantes y complicadas cuestiones como el estudio de series divergentes y su posible tratamiento por renormalización.

La segunda línea de acción se refiere más específicamente a la física de las condiciones reales de experimentación. Nuestra intención en este sentido es la de introducir un término de ruido en nuestras ecuaciones que describen el comportamiento dinámico del sistema para obtener así una imagen más fiel de la situación real.

Bibliography

[1] Abramovici A., *et al.*, *Science*, **256**, 325 (1992).

[2] Anandan J., *Physics Letters*, **A105**, 280 (1985).

[3] Arfken G.B. and Weber H.J., *Mathematical Methods for Physicists*, Academic Press, San Diego (1995).

[4] Ashby N., and Dreitlein J., *Phys. Rev.*, **D12**, 336 (1975).

[5] Astone P. *et al.*, *Europhys. Lett.*, **16**, 231 (1991).

[6] Astone P. *et al.*, *Phys. Rev.*, **D47**, 2 (1993).

[7] Astone P. *et al.*, *Phys. Rev.*, **D47**, 362 (1993).

[8] Astone P. *et al.*, *Phys. Lett.*, **B385**, 421 (1996).

[9] Astone P. *et al.*, *Astroparticle Physics*, **7**, 231 (1997).

[10] Bassan M., *Class. Quant. Grav.*, **11**, A39 (1994).

[11] Bianchi M., Coccia E., Colacino C., Fafone V., and Fucito F., *Class. Quant. Grav.*, **13**, 2865 (1996).

[12] Bondi H., *Nature*, **179**, 1072 (1957).

[13] Bonifazi P. *et al.*, *Nuovo Cimento*, **1C**, 465 (1978).

[14] Bonifazi P. and Visco M., *Nuovo Cimento*, **15C**, 943 (1992).

[15] Boughn S.P. and Kuhn J.R., *Astrophysical Journal*, **286**, 387 (1984).

[16] Braginsky V.B. *et al.*, *Uspekhi Fizicheskikh Nauk*, **147**, 422 (1985).

[17] Braginsky V.B. and Gertsenshtein M.E., *Sov. Phys.-JETP Lett.*, **5**, 287 (1967).

[18] Braginsky V.B. and Thorne K.S. *Nature*, **316**, 610 (1985).

[19] Brans C. and Dicke R.H., *Phys. Rev.*, **124**, 925 (1961).

[20] Bransden B.H. and Joachain C.J., *Introduction to Quantum Mechanics*, Longman Scientific & Technical. UK (1989).

[21] Bronzini F. *et al.*, *Nuovo Cimento*, **8C**, 300 (1985).

[22] Carelli P. *et al.*, *Phys. Rev.*, **A32**, 3258 (1985).

[23] Caron B. *et al.*, *Class. Quant. Grav.*, **14**, 1461 (1997).

[24] Carter B., in *Gravitational Radiation, Les Houches 1982*, ed. N. Deruelle and T. Piran, North-Holland. New York (1983).

[25] Carter B. and Quintana H., *Phys. Rev.*, **D16**, 2928 (1977).

[26] Cerdonio M. *et al.*, in *Gravitational Wave Experiments. Proc. of the First Edoardo Amaldi Conf.*, ed. S.T. Ruggiero and D.A. Rudman, Academic Press, Boston (1990).

[27] Cerdonio M., Fortini P., Ortolan A., Prodi G.A. and Vitale S., *Phys. Rev. Lett.*, **71**. 4107 (1993).

[28] Ciufolini I. and Wheeler J.A., *Gravitation and Inertia*, Princeton University Press, Princeton (1995).

[29] Coccia E., in *Les Rencontres de Physique de la Vallee d'Aoste: Results and Perspectives in Particle Physics*. La Thuille, (1994).

[30] Coccia E. and Fafone V., *Phys. Lett.*, **A213**, 16 (1996).

[31] Coccia E., Fafone V. and Frosati G., in *Proc. of the First Edoardo Amaldi Conference on Gravitational Waves Experiments*, ed. E. Coccia *et al.*. World Scientific, Singapore (1995).

[32] Coccia E., Lobo J., and Ortega J., *Phys. Rev.*. **D52**, 3735 (1995).

[33] Crivelli-Visconti V., Ortolan A., Taffarello L., Vedovato G., Cerdonio M., Prodi G.A. and Vitale S., *Phys. Rev.*, **D57**, 2045 (1998).

[34] Danzmann K. and the LISA Study Team, *Class. Quant. Grav.*, **14**, 1399 (1997).

[35] Dautcourt G., in *Proc. of the IAU Symposium. Confrontation of Cosmological Theories with Observational Data*, ed. M.S. Longair, Dordrecht (1974).

[36] Davidov A.S., *Quantum Mechanics*, Pergamon Press, Oxford (1965).

[37] Dhurandhar S.V. and Tinto M., *Mon. Not. R. Astron. Soc.*, **234**, 663 (1988).

[38] Dyson F.W., Eddington A.S., and Davidson C., *Phys. Trans.*, **A220**, 291 (1920).

[39] Eardley D.M., Lee D.L., Lightman A.P., Wagoner R.V.and Will C.M., *Phys. Rev. Lett.*, **30**, 884 (1973).

[40] Eddington A.S., *Proc. R. Soc.*, **A102**, 268 (1923).

[41] Einstein A., *S.B. Preuss. Akad. Wiss.*, 688 (1916).

[42] Eisntein A., *S.B. Preuss. Akad. Wiss.*, 154 (1918).

[43] Einstein A., *Annal. der Phys.*, **49**, 769 (1916). English translation in H.A. Lorentz *et al., The Principle of Relativity*, Dover, New York (1952).

[44] Einstein A., *The Meaning of Relativity*, 5th ed., Princeton University Press, Princeton (1955).

[45] *First International LISA Symposium*, *Class. Quant. Grav.*, **14**, number 6 (1997).

[46] Fock V.A., *Teoriya Prostranstva Vremeni i Tyagoteniya*, Fizmatgiz, Moscow (1955).

[47] Forward R.L., *Gen. Rel. and Grav.*, **2**, 149 (1971).

[48] Forward R.L., *Phys. Rev.*, **11**, A39 (1994).

[49] Frossati G., *J. Low. Temp. Phys.*, **101**, 81 (1995).

[50] Gibbons G.W. and Hawking S.W., *Phys. Rev.*, **D4**, 2191 (1971).

[51] Giffard R.P., *Phys. Rev.*, **D14**, 2478 (1976).

[52] Gradshteyn I.S. and Ryzhik I.M., *Table of Integrals, Series, and Products*, Academic Press, New York (1980).

[53] Grishchuk L.P., in *Proc. of the Ninth Int. Conf. on General Relativity and Gravitation*. ed. E. Schmutzer, Cambrigde University Press, Cambridge (1983).

[54] Grishchuk L.P. and Polnarev A.G., in *General Relativity and Gravitation, One Hundred Years After the Birth of Albert Einstein*, ed. A. Held, Plenum Press, New York and London (1980).

[55] Gürsel Y. and Tinto M., *Phys. Rev.*, **D 40** 3884 (1989).

[56] *Handbook of Mathematical Functions*, ed. M. Abramowitz and I.A. Stegun, Dover, New York (1972).

[57] Har'El Z., *Geometriæ Dedicata*, **47**, 57 (1993).

[58] Helstrom C.W., *Statistical Theory of Signal Detection*, Pergamon Press, Oxford (1968).

[59] Heng I.S. *et al.*, *Phys. Lett.*, **A218**, 190 (1996).

[60] Hernández W.C., *Phys. Rev.*, **D1**, 1013 (1970).

[61] Hobson E.W., *The Theory of Spherical and Ellipsoidal Harmonics*, Chelsea Publishing Company, New York (1965).

[62] Hogg R.V. and Craig A.T., *Introduction to Mathematical Statistics*, The MacMillan Company, New York (1965).

[63] Holden A., *Formes, espace et symétries*, CEDIC (1977).

[64] Hulse R.A. and Taylor J.H., *Astrophys. J.*, **195**, L51 (1975).

[65] Infeld L. and Plebanski A., *Motion and Relativity*, Pergamon Press, London (1960).

[66] Isaacson R.A., *Phys. Rev.*, **166**, 1263 (1968).

[67] Isaacson R.A., *Phys. Rev.*, **166**, 1272 (1968).

[68] Jaerisch P., *J.f. Math. (Crelle)*. **Bd. 88** (1880).

[69] Johnson W.W. and Merkowitz S.M., *Phys. Rev. Lett.*, **70**, 2367 (1993).

[70] Jotania K., Valluri S.R. and Dhurandhar S.V., *Astron. Astrophys*, **306**, 317 (1996).

[71] Kawabe K. and the TAMA Collaboration, *Class. Quant. Grav.*, **14**, 1477 (1997).

[72] Kenyon I.R., *General Relativity*, Oxford University Press, Oxford (1990).

[73] Krolak A., Lobo J.A. and Meers B.J., *Phys. Rev.*, **D 43**, 2470 (1991).

[74] Krolak A., Lobo J.A. and Meers B.J., *Phys. Rev.*, **D 47**, 2184 (1993).

[75] Lamb H., in *Proc. London Math. Soc.*, **13** (1882).

[76] Lancaster P. and Tismenetsky M., *The Theory of Matrices*, Academic Press, Inc. (1985).

[77] Landau L.D. and Lifshitz E.M., *The Classical Theory of Fields*, Pergamon, Oxford (1962).

[78] Landau L.D. and Lifschitz E.M., *Theory of Elasticity*, Pergamon, Oxford (1970).

[79] LePage W.R., *Complex Variables and the Laplace Transform for Engineers*, McGraw-Hill, New York (1961).

[80] Lobo J.A., *Phys. Rev.*, **D52**, 591 (1995).

[81] Lobo J.A., in *General Relativity, Proc. of SUSSP-46*, ed. G.S. Hall and J.R. Pulham. SUSSP Publications & IOP, Bristol (1996).

[82] Lobo J.A., in *Mathematics of Gravitation*, ed. A Królak, Banach Center Publications. Varsaw (1997).

[83] Lobo J.A. and Montero M., *Mon. Not. R. Astron. Soc.*, **301**, 729 (1998).

[84] Lobo J.A. and Serrano M.A., *Europhys. Lett.* , **35**, 253 (1996).

[85] Lobo J.A. and Serrano M.A., *Class. and Quantum Grav.*, **14**, 1495 (1997).

[86] Lobo J.A. and Serrano M.A., *Mon. Not. R. Astron. Soc.*, (1999). Submitted.

[87] Love A.E.H., *A treatise on the mathematical theory of elasticity*, Dover, New York (1944).

[88] Lück H. and the GEO600 Team, *Class. Quant. Grav.*, **14**, 1471 (1997).

[89] Mach E., *Die Mechanik in ihrer Entwicklung Historisch-kritisch dargestellt*, Brockhaus. Leipzig(1912).

[90] Magalhaes N.S. *et al.*, *Mon. Not. R. Astron. Soc.*, **274**, 670 (1995).

[91] Magalhaes N.S., Aguiar O.D., Johnson W.W. and Frajuca C., *GRG*, **29**, 1509 (1997).

[92] Magalhaes N.S., Johnson W.W., Frajuca C. and Aguiar O.D., *Astrophys. J.*, **475**, 462 (1997).

[93] Mauceli E. *et al.*, *Phys. Rev.*, **D54**, 1264 (1996).

[94] Maugin G.A., *Gen. Rel. Grav.*, **4**, 241 (1973).

[95] Merkowitz S.M., *Ph. D. Thesis*, Louisiana State University (1995).

[96] Merkowitz S.M., *Phys. Rev.*, **D 58** (1998) 062002.

[97] Merkowitz S.M. and Johnson W.W., *Phys. Rev.*, **D51**, 2546 (1995).

[98] Merkowitz S.M. and Johnson W.W., *Phys. Rev.*, **D56**, 7513 (1997).

[99] Merkowitz S.M., Lobo J.A. and Serrano M.A., *Class. and Quantum Grav.*, (1999). Submitted.

[100] Misner C.W., Thorne K.S. and Wheeler J.A., *Gravitation*, Freeman, San Francisco (1973).

[101] Montero M., *Ph. D. Thesis*, Universitat de Barcelona (1998).

[102] Niebauer T.M. *et al.*, *Phys. Rev.*, **D47**, 3106 (1993).

[103] Ortega J.A., *Ph. D. Thesis*, Universitat de Barcelona (1997).

[104] Ortolan A., Vedovato G., Cerdonio M. and Vitale S., *Phys. Rev.*, **D50**, 4737 (1994).

[105] Paik H.J., in *Gravitational Wave Experiments. Proc. of the First Edoardo Amaldi Conf.*, ed. E. Coccia, G. Pizella and F. Ronga, Wold Scientific, Singapore (1995).

[106] Papapetrou A., *Ann. Inst. Henri Poincaré*, **16**, 63 (1972).

[107] Pauli W., *The Theory of Relativity*, Pergamon Press, London (1921).

[108] Pizzella G., *Class. Quant. Grav.*, **14**, 1481 (1997).

[109] *Proc. of the 1972 Les Houches Summer School on Black Holes*, ed. de Witt, Notrh-Holland, Amsterdam, New York, Oxford (1973).

[110] *Proc. of the 1975 Varenna School on Physics and Astrophysics of Neutron Stars and Black Holes.* ed. R. Giacconi and R. Ruffini, Notrh-Holland, Amsterdam, New York, Oxford (1978).

[111] *Proc. of the First Edoardo Amaldi Conference on Gravitational Wave Experiments*, ed. E. Coccia *et al.*, World Scientific, Singapore (1995).

[112] Pound R.V. and Rebka G.A., *Phys. Rev. Lett.*, **4**, 337 (1960).

[113] Rapagnani P., *Nuovo Cimento*, **5C**, 385 (1982).

[114] Richard J.P., *Phys. Rev. Lett.*, **521**, 165 (1984).

[115] Riemann G.F.B., Bei die Hypothesen, welche der Geometrie zu Grunde liegen, in *Gesammelte Mathematische Werke*, (1866); reprint of 2nd ed., ed. H. Weber, Dover, New York (1953).

[116] Roland J., Frossati G. and Teyssier R., *Astron. Astrophys.*, **290**, 364 (1994).

[117] Schrader R., *Physics Letters*, **B143**, 421 (1984).

[118] Schutz B.F., *Class. Quant. Grav.*, **6**, 1761 (1989).

[119] Schwartz J., *W^*-Algebras*, Nelson, London (1968)

[120] Shapiro I.I., in *General Relativity and Gravitation*, ed. N. Ashby, Cambridge University Press, Cambridge (1990).

[121] Solomonson N., Johnson W.W. and Hamilton W.O., *Phys. Rev.*, **D46**, 2299 (1992).

[122] Souriau J.M., *Géométrie et Relativité*, Hermann, Paris (1974).

[123] Stakgold I., *Green's Functions and Boundary Value Problems*, Wiley-Interscience Publications, New York (1979).

[124] Stevenson T.R., *Phys. Rev.*, **D 56** 564 (1997).

[125] Suzuki T., in *Gravitational Wave Experiments. Proc. of the First Edoardo Amaldi Conf.*, ed. E. Coccia, G. Pizella and F. Ronga, Wold Scientific, Singapore (1995).

[126] Taylor J.H., Fowler L.A. and McCulloch P.M., *Nature*, **277**, 437 (1979).

[127] Taylor J.H. and Weisberg J.M., *Appl. Journal*, **253**, 908 (1982).

[128] Taylor J.H. and Weisberg J.M., *Appl. Journal*, **345**, 434 (1989).

[129] Thorne K.S., in *Gravitational Radiation, Les Houches 1982*, ed. N. Deruelle and T. Piran, North-Holland, New York (1983).

[130] Thorne K.S., *Three Hundred Yers of Gravitation*, ed. S.W. Hawking and W. Israel, Cambridge University Press, Cambridge (1987).

[131] Tricomi F.G., *Integral Equations*, Interscience Publishers (1957).

[132] Vitale S., Cerdonio M., Coccia E., Ortolan A., *Phys. Rev.*, **D55**, 1741 (1997).

[133] Wagoner R.V. and Paik H.J., in *Proc. of the International Symposium on Experimental Gravitation, Pavia*, Acad. Naz. dei Lincei, Roma (1976).

[134] Wald R.M., *General Relativity*, The University of Chicago Press, Chicago (1984).

[135] Weber J., *General Relativity and Gravitational Waves*, Wiley-Insterscience, New York (1961).

[136] Weber J., *Phys. Rev. Lett.*, **17**, 1228 (1966).

[137] Weber J., *Phys. Rev. Lett.*, **20**, 1307 (1968).

[138] Weber J., *Phys. Rev. Lett.*, **22**, 1320 (1969).

[139] Weber J., *Phys. Rev. Lett.*, **24**, 276 (1970).

[140] Weinberg S., *Gravitation and Cosmology*, Wiley. New York (1972).

[141] Will C.M., *Theory and Experimentation in Gravitational Physics*, Cambridge University Press, New York (1982).

[142] Will C.M., *Theory and Experiment in Gravitational Physics*, Cambridge University Press, Cambridge (1993).

[143] Zeldovich Y.B. and Novikov I.D., *Relativistic Astrophysics Vol.2. The Structure and Evolution of the Universe*, University of Chicago Press, Chicago (1983).

[144] Zhou C. and Michelson P.F., *Phys. Rev*, **D51**, 2517 (1995).